CHEMICAL REVIEWS

REVIEW

pubs.acs.org/CR

Probing Liquid/Solid Interfaces at the Molecular Level

Francisco Zaera*

Department of Chemistry, University of California, Riverside, California 92521, United States

CONTENTS

1. INTRODUCTION

The ability to obtain a molecular-level understanding of the chemistry that takes place at liquid/solid interfaces is key to the development and improvement of many chemical and biological systems, and is arguably the next big challenge for the surface-science community.[1] Liquid/solid interfaces are certainly ubiquitous in nature. The biology of life, for instance, relies heavily on the uptake of molecules from aqueous phases onto surfaces, either onto "soft" bilayers or other membranes, or onto "hard" surfaces such as bones, cartilages, or teeth. Phenomena related to self-assembly, including the formation of micelles and the use of surfactants, are also based on chemistry at liquid/solid interfaces. Environmental issues involving liquid/solid interfaces go from the chemistry of aerosols to the purification of groundwater. The evolution of minerals is greatly affected by their interactions with liquid solutions. The corrosion of many metals is a common problem, and other electrochemical processes are relevant to the development of batteries, fuel cells, catalysts, and many other industrial applications. Lubrication and other tribological problems rely on the use of liquids to improve the performance of solid moving parts. Multiple synthetic processes in industry involve liquid phases and require the use of solid catalysts. A variety of sensors, including a large number of the bioassays used nowadays for the analysis of biological samples in medicine, center on chemistry at liquid/solid interfaces.

It is not easy to investigate the chemistry of liquid/solid interfaces at a molecular level. Already, the study of the chemistry of any interface is hampered by the need to discriminate between the few atoms at that interface and the much larger number of atoms that exist in the two bulk phases involved. A number of modern surface-sensitive techniques were developed in the late 20th century to overcome this obstacle, and with those great advances were made on the understanding of the chemistry that occurs on solid surfaces.[2−4] However, many of those techniques rely on the use of particles such as electrons, ions, or atoms, which work best under a vacuum environment. A second generation of setups has been developed more recently to extend the use of surface probes to cases where the solid is immersed in a gaseous environment,[5,6] and many areas of research have benefited from these advances, heterogeneous catalysis in particular, but systems with interfaces buried between two condensed phases, between a liquid and a solid in particular, can still not be easily probed with the standard surface-science approach developed for operation in vacuum or a gas phase.

New approaches are needed to study liquid/solid interfaces at a molecular level. Some electron-based surface-science

Received: June 6, 2011
Published: January 25, 2012

techniques are being adapted to probe liquid/solid interfaces by minimizing the paths that the probing particles need to travel through the liquid phase. More promising perhaps is the boon seen in the use of techniques based on light or other electromagnetic radiation for surface analysis, since those are less affected by condensed matter. Optical analytical techniques are typically not surface-sensitive; hence their sparse use in surface-science problems in the past, but can be made so by using specific setups or by taking advantage of the uniqueness of the surface chemistry to be investigated. Clearly, the study of liquid/solid interfaces is difficult, but a variety of tools are being developed to rise to the challenge.

Below, we provide a brief overview of the major developments that have occurred in this area in recent years. In this review, we take a broad interpretation of what constitutes a solid surface, and include examples on the study of liquid/solid interfaces involving not only conventional solids but also nanoparticles and membranes such as lipid bilayers and other self-assembled layers used to emulate biological systems. The liquid phases in our discussions include regular solutions, neat liquids, melts, ionic liquids, and liquid crystals. We start with a review of the use of infrared absorption spectroscopy to the interrogation of liquid/solid interfaces, perhaps the technique most used for this purpose, and continue with an overview of other vibrational spectroscopies, in particular Raman scattering spectroscopy and sum frequency generation. Next, we introduce the use of UV−vis spectroscopies, which are employed mainly to obtain electronic information of adsorbates at the interface but can also be employed to quantify coverages. Acoustic-based techniques such quartz crystal microbalances, which are also used for the latter application, are also mentioned. The next section focuses on the use of X-rays and neutrons, both in spectroscopic studies, to extract electronic information about the liquid/solid interface, and in scattering and diffraction modes, to acquire structural details of the interface. The potential use of techniques such as X-ray photoelectron spectroscopy and nuclear magnetic and electron spin resonance spectroscopies for the characterization of liquid/solid interfaces is briefly surveyed. The last chapters are dedicated to the discussion of the approaches available for the acquisition of spatially resolved information on liquid/solid interfaces, including optical and scanning microscopies. We finish our review with some concluding remarks where we provide a brief guideline on the criteria to select the most appropriate techniques for the study of a specific system and give our own assessment of the status and future of the field of surface science as it pertains to liquid/solid interfaces.

2. INFRARED ABSORPTION SPECTROSCOPY

Perhaps the technique most commonly used to date for the molecular-level characterization of liquid/solid interfaces is infrared (IR) absorption spectroscopy. In IR absorption spectroscopy, the sample being studied is exposed to a broad-band infrared beam, typically covering the so-called midrange that encompasses wavenumbers between approximately 400 and 4000 cm^{-1}, and the absorption of that light is analyzed to identify the molecular vibrations that the light excites.[7] Modern IR spectrometers are based on the use of a Michelson interferometer, where the full infrared beam is split, each half is made to travel a separate path, and the two are recombined again before steering the full reconstituted beam into the sample. By varying the difference in path length traveled by the two half-beams with

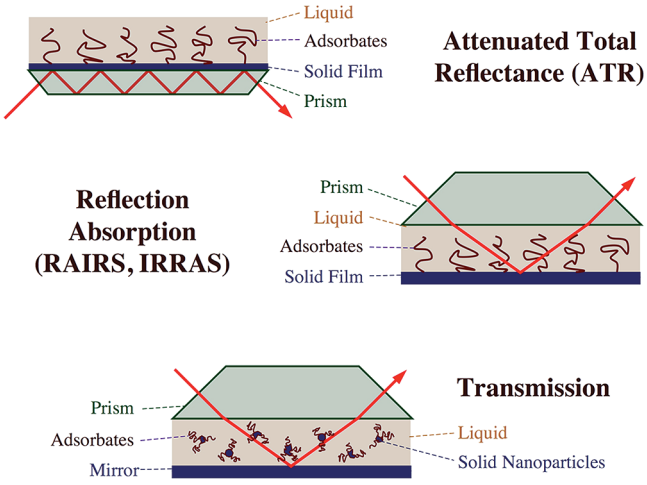

Figure 1. Schematic representation of the different modes available for infrared absorption spectroscopy studies of liquid/solid interfaces. Top: In attenuated total reflectance (ATR) mode, the IR beam travels through a prism while the evanescence wave that extends toward the outside is used to probe the chemical system of interest, typically molecules adsorbed on the prism itself or on a thin film grown on top. Center: In absorption−reflection (RAIRS) mode, the beam is bounced directly off the solid substrate where adsorption takes place, and on metals the surface selection rule that establishes that only p-polarized light can be absorbed at the surface is used to discriminate between molecules on the surface versus in solution. Bottom: Transmission IR absorption spectroscopy can also be performed with the RAIRS setup if the metal is used as a mirror and the solid, typically a powder or another type of nanoparticle, is suspended in solution.

time, by scanning the mirror used in the path of one of them, an oscillating interference pattern is developed for each wavelength; a Fourier transformation (FT) of the intensity of the beam versus time provides a plot of light intensity versus wavelength. The introduction of this FT-IR approach greatly advanced the use of infrared absorption spectroscopy because the new technique enhances performance in two ways: (1) information on the intensity of all wavelengths of light is collected at once, and (2) the throughput of light is not limited by entrance and exit slits, as is the case with the old monochromator-based spectrometers.

Infrared absorption spectroscopy is quite versatile, and with the advent of Fourier-transform instruments, it has become quite easy and cheap to implement; nowadays, FT-IR instruments are found in almost all analytical chemistry laboratories worldwide. IR absorption spectroscopy is also ideal for the study of chemical problems, including those involving surfaces,[8] because it provides information on the vibrational details of molecular structures, which are quite sensitive to local chemical environments.[9] On the negative side, IR absorption spectroscopy is a nonzero background technique, that is, full signal is detected when there is no light absorption at all, a fact that sets a limit on its dynamic range and with that its sensitivity. This is particularly critical in the study of interfacial systems, where the size of the sample is often severely limited (there are only $\sim 10^{13}-10^{15}$ molecules/cm^2 in a typical saturated monolayer of adsorbates). Thankfully, the recent development of highly sensitive, low-noise detectors has minimized this problem. In addition, infrared absorption spectroscopy, like most optical analytical techniques, is not intrinsically surface sensitive, although it can be made so in certain circumstances, as discussed in more detail below. Finally, infrared

radiation is absorbed by almost all solids and liquids, which means that it is not always easy to reach the interface of interest, especially when dealing with liquid/solid. Fortunately, great flexibility is provided to address that problem because of the availability of several arrangements for the performance of IR absorption spectroscopy, which include attenuated total reflectance (ATR), reflection−absorption (RAIRS), and transmission (Figure 1). In the next few subsections, an overview of the use of these arrangements for the study of liquid/solid interfaces is reviewed.

2.1. Attenuated Total Reflectance (ATR)

Perhaps the most established infrared absorption spectroscopy setup for the study of liquid/solid interfaces is attenuated total reflectance (ATR, Figure 1, top).[10−12] ATR takes advantage of the total internal reflection of light that occurs when the beam impinges on an interface at a certain angle; the angle at which total reflection occurs is determined by the difference in refractive index between the two materials forming that interface. Such reflection results in the generation of an evanescent wave that penetrates into the other side of the interface, to a depth of between 0.5 and 2 μm depending on the wavelength of the light, the angle of incidence, and the relevant indices of refraction. Thanks to this property, an IR beam can be made to travel through the inside of an optical element, a prism typically made out of silicon, germanium or another high-refractive-index element, while using its outer surface to carry out the chemistry of interest. The absorption of light from the evanescence wave by the chemical system being probed can be then detected on the beam collected at the exit of the prism. Many research projects based on this approach have involved chemistry on the surface of the prism itself, but others have being directed at the study of other systems such as metal thin films, which may be deposited on the surface of the prism, or powders or nanoparticles, which may be placed in a suspension within the liquid right above the ATR optical element. ATR infrared absorption spectroscopy has been extensively used for the study of problems related to general adsorption, mineral chemistry, environmental chemistry, biology, surfactants, sensors, electrochemistry, catalysis, and materials science.

The simplest studies of liquid/solid interfaces with ATR-IR have been those on the characterization of adsorption processes. This application already has a relatively long history, in particular in terms of the quantitation of the uptake of adsorbates to estimate adsorption isotherms.[13,14] As with most optical spectroscopies, IR absorption can be linearly related to concentration, and chemical specificity can be obtained by following a particular vibrational feature in the spectra associated with the compound of interest. One example illustrating this type of application is the ATR-IR study of the adsorption of ethyl acetate and 2-propanol on silica sol−gel films in contact with n-heptane solutions, which was focused on extracting information related to solute retention and elution in normal-phase chromatography.[15] The nonlinear isothermal behavior observed in those systems was explained by differences in adsorption behavior on silanol groups free on the surface versus covered with water. ATR-IR has also been recently implemented to monitor the concentrations of solutes in solutions flowing through the microfluidic channels of lab-in-a-chip systems.[16] Spectra could be acquired in those cases for the chemical characterization of the system at the same time as concentration measurements were carried out, affording independent measurements of concentrations of solutes with distinct spectral features in mixed solutions.

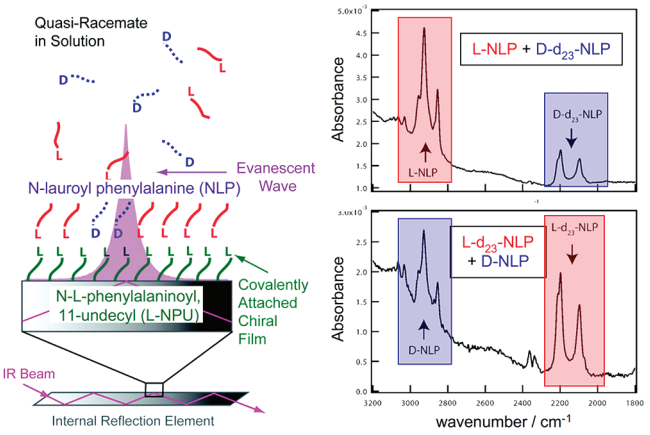

Figure 2. Example of the use of infrared absorption spectroscopy in ATR mode to probe liquid/solid interfaces.[17] In this study, the enantioselective uptake of *N*-lauroyl-phenylalanine (NLP), a surfactant, on a silicon surface modified with a chiral *N*-L-phenylalaninoyl-11-undecyl (L-NPU) layer is tested. The left panel shows schematically the experimental setup, in which an ATR prism derivatized with a L-NPU monolayer is exposed to a quasi-racemate solution of NLP in carbon tetrachloride in which one NLP enantiomer (the D isomer in the right-top panel, the L form in the right-bottom panel) was fully deuterated to differentiate it from its normal-hydrogen-labeled NLP counterpart (L in the top, D in the bottom). Preferential adsorption of the L-NLP enantiomer is evidenced by the larger signals for the C−H (C−D) stretching modes in L-NLP (D-NLP) seen around 3000 (2200) cm^{-1} in the IR spectra compared to those for the C−D (C−H) peaks around 2200 (3000) cm^{-1} because of D-d_{23}-NLP (L-d_{23}-NLP) in the data on the right-top (right-bottom) panel. Reprinted from ref. 17 with permission. Copyright 2010 American Chemical Society.

More sophisticated adsorption uptake ATR-IR experiments can be designed by taking advantage of unique characteristics of the surface chemistry to be investigated. Figure 2 shows key results from an example where the enantioselectivity of adsorption was tested on chirally modified surfaces.[17] Specifically, the enantioselective adsorption of the chiral *N*-lauroyl phenylalanine (NLP) surfactant onto a chiral monolayer consisting of *N*-L-phenylalaninoyl, 11-undecyl-silicon (L-NPU-Si) was demonstrated by using deuterium labeling in one of the enantiomers of the pseudoracemic NLP mixture used in solution. Another very different recent application where the uniqueness of the chemistry involved was used in the experimental design was for the characterization of the electronic properties of a photocatalyst.[18] In that case, the photogeneration of charge carries in a Pt/GaN photocatalyst developed for hydrogen evolution under light irradiation was investigated by following the vibrational frequency of adsorbed carbon monoxide, used here as a probe: it was determined that after irradiation the C−O stretching frequency first shifts to higher values, indicating that the Fermi level of the metal particles is positively shifted by the photogenerated holes, but then reverts toward lower frequencies as hydrogen is produced. This is a clever way of using local bonding information as a proxy for changes in local electronic properties.

ATR-IR can also be used to determine adsorption geometries.[12] This has often been reported in connection with the characterization of adsorbed surfactants and self-assembled monolayers, but the same approach can be easily extended to other systems. In fact, when thin metal film are added to the ATR surface, the electric field distribution of the evanescent wave at the substrate−sample

interface is modified so only the p-polarized light, which is oriented perpendicular to the surface, penetrates into the adsorbed phase.[19] This effectively gives rise to a surface selection rule similar to that more usually associated with reflection−absorption experiments (see Section 2.2) by which only IR vibrations with dynamic dipoles with a component perpendicular to the plane of the surface are detected.[20−23] An example on how this selection rule can be used to determine adsorption geometry is provided by the in situ ATR-IR report on the average orientation of the methylene tail of cetyltrimethylammonium bromide adsorbed from solution onto a silica surface as a function of coverage and pH, where it was found that the equilibrium orientation of the surfactant was larger at higher pH values.[24] This was interpreted as the result of an increase in packing density with increasing surface excess. No preferred orientation of the surfactant was seen during the initial stages of adsorption, but a rapid reorientation to a direction normal to the surface was observed after higher surface excesses as time evolved. In another example, the adsorption of a related surfactant, dodecyltrimethylammonium bromide, was followed as a function of uptake to correlate structural transitions with changes in the properties of the interface determined from contact angle, zeta potential, and force measurements.[25] The data indicated that initially the molecules adsorb in random orientations, but that they then form hemimicelles (two-dimensional aggregates) above a certain critical concentration, presumably because of hydrophobic association between the surfactant tails, and rearrange again into randomly oriented spherical aggregates at even higher coverages.

In terms of mineral and environmental chemistry, Cwiertny et al. provided an example where the adsorption of oxalate on α-FeOOH was used to represent the way the surfaces of mineral aerosol dust dissolve by complexation with organics in solution.[26] Particularly interesting in that study was the identification of a possible dependence of the dissolution on particle size and/or surface orientation. In another report, Strongin's group characterized the photodissolution of ferrihydrite in the presence of oxalic acid.[27] They found that the oxalate displaces the original carbonate endings on the surface and slowly produces a new type of carbonate. In a third example involving ionic species, Lefèvre et al. followed the IR absorption frequencies of sulfates, phosphates, and carbonates adsorbed on metal oxy-hydroxides to determine bonding modes and to distinguish between outer-sphere and inner-sphere complexes.[28] These examples illustrate the great chemical specificity of IR absorption spectroscopy, which can be used to obtain information about the chemical nature of new adsorbed species.

Another interesting application of ATR-IR is in the study of systems of biological interest. In one example related to the biocompatibility of proteins and aminoacids with materials used in prostheses, an in situ ATR-IR study of the adsorption of glutamic acid on titania led to the identification of fairly complex chemistry, with several spectroscopically distinct structures and maximized adsorption at pHs where electrostatic interactions between the surface and adsorbate are unfavorable.[29] In another case, the selection rules described above were used to contrast the adsorption geometry of bovine serum albumin on hydrophilic naked silicon-oxide/silicon surfaces versus hydrophobic lipid-covered substrates.[30] On the original silicon surfaces the protein was found to adsorb in a side-on geometry but with some flattening due to either unfolding or denaturation, whereas on the hydrophobic surface the adsorption was shown to lead to a film about half as thick but with the same contact angle, indicating more protein unfolding. A third, more recent example of the use of ATR-IR in biological chemistry has shown how the choice of buffer solution can affect protein uptake on solid surfaces in terms of both adsorption kinetics and the evolution of the secondary structure.[31] The adsorption of most proteins exhibits a short period of rapid adsorption involving large secondary structural changes that is followed by a long period of quasi-linear adsorption, but competitive adsorption between the buffer and the protein sometimes depresses the adsorption in the latter kinetic region. One last biological example is that of the study of the setting reaction of calcium phosphate cements, use as bone substitutes, in aqueous citric acid solutions. Citric acid is typically used as a retardant, to increase setting times and mechanical strength.[32] The ATR-IR data in this case provided evidence for the formation of an intermediate dicalcium phosphate-citrate complex, the concentration of which increases with the concentration of citric acid in solution. It was proposed that the reduction in strength of the final material may be related to the formation of that intermediate at the early stages of setting of the cement. All together, these examples show how ATR-IR absorption spectroscopy can be used to identify new surface species and surface chemistry, establish adsorbate structural information, and collect adsorption kinetics at the liquid/solid interfaces of biologically relevant systems.

ATR-IR can also provide information on the chemistry that occurs at the surface of electrodes. For this, the electrodes are typically deposited as thin films or pressed in close contact against the ATR prism. In a recent example, the adsorption of adenine on gold electrodes was proposed, based on such IR studies, to involve two nitrogen atoms, a sp^3-hybridized amino nitrogen and the N_7 atom of the five-member ring, and to require a tilted geometry.[33] In another study, it was concluded that, during the oxidation of methanol on Pt−Ru electrodes, the platinum sites are responsible for the dehydrogenation of adsorbed methanol to CO whereas the ruthenium sites adsorb water preferentially and promote oxidation between the CO and H_2O adsorbed species.[34] Yet another example of ATR-IR studies of electrochemical systems is that of the electrooxidation of ethanol on Pt electrodes, where the IR spectra indicated the formation of acetaldehyde and/or acetyl reaction intermediates on the surface and provided a correlation between the rate of acetate formation and the current seen in voltammetry.[35] Again, these examples illustrate the power of ATR-IR as a way to identify surface species and their adsorption sites and geometries, and as a means to isolate elementary steps in the mechanism and measure the kinetics of surface electrochemical reactions.

ATR-IR can also be setup to study adsorption on powders and nanoparticles. Typically, this is done by placing a suspension of the particles directly above the surface of the prism used as the optical element. Commercial devices are available for the characterization of such samples under flowing liquids and/or while heating to moderate temperatures. Being able to study powders with ATR-IR is quite useful in catalysis, because heterogeneous catalysts are typically comprised of metal particles or other solid active phases finely dispersed on high-surface-area supports. An illustration of this type of application is that from the group of Williams, who have reported on the adsorption of species such as CO and formaldehyde on Pt/Al_2O_3 catalysts from aqueous and ethanolic solutions.[36] In their investigation on the hydrogenation of butyronitrile in hexane in particular, they were able to detect the presence of a new adsorbed imine species with the CN group in a tilted configuration that, once formed, can be converted into amine products.[37] ATR-IR studies of catalytic systems have been particularly useful for the determination in situ of reaction

mechanisms.[12,38−40] For example, several adsorbed intermediates have been identified during the hydrogenation of nitrites over Pt/Al_2O_3 in water, including NO, HNO, and HNO_2^-, the conversion of which was determined to result mainly in the production of NH_4^+ (although traces of N_2O, a potential intermediate for the formation of N_2, was also observed).[41] In another study, by Ferri et al., on the oxidation of benzyl alcohol over a Pd/Al_2O_3 catalyst, selective blocking of adsorption sites was carried out using bismuth and probed with CO.[42] It was determined that open terraces favor product decomposition. The group of Baiker have also carried out extensive in situ studies of chiral catalysis in liquid phase.[38] For instance, regarding the enantioselective hydrogenation of 4-methoxy-6-methyl-2-pyrone promoted by Pd/TiO_2 powder catalysts modified by cinchonidine, they were able to establish that carboxylate species are formed on the titania surface via alcoholysis of the lactone, which is obtained by a second hydrogenation step, and that the adsorption of those carboxylates follow different kinetics than adsorption of the primary hydrogenation product.[43] In one last example, the catalytic esterification of 1-octanol and hexanoic acid in either cumene or *n*-decane solvents was tested in situ using a Nafion/silica catalyst in an open reflux configuration at atmospheric pressure.[44] One interesting result in that case was the detection of Si−O−R bonds during reaction, presumably associated with the covalent bonding of octanol to the silica surface.

To conclude this subsection, it is worth mentioning the early extensive ATR-IR characterization work performed on surfaces of interest to the microelectronics industry. Those have taken advantage of the fact that the most common materials used for the optical prism in ATR-IR are silicon, germanium, and other semiconductor elements, the same components used in microelectronics fabrication, so the investigation in those cases can be performed directly on the naked optical element. Much has been learned this way about the surface chemistry of etching of the native silicon dioxide layer that grows on silicon wafers, which is typically carried out by using aqueous HF or NH_4F solutions.[45,46] IR spectra has been used to follow and characterize the disappearance of the oxide, the formation of new single and geminal Si−H bonds, and the formation of silicic acid associated with hydrogen-bonded water molecules. More recent studies by Chabal et al. have established that the $SiO_2/Si(100)$ interface that is revealed as the overlying oxide is stripped away is structurally distinct from the rest of the SiO_2 film.[47]

2.2. Reflection−Absorption Infrared Spectroscopy (RAIRS)

Another common arrangement for the performance of infrared absorption spectroscopy studies on liquid/solid interfaces is in single reflection mode. In that type of setup, the IR beam is directed through the liquid onto a mirror-finished surface, and collected after reflection. The catch is that, because of the high density and strong absorption in the IR region of most liquids, this approach requires the use of thin liquid films, down to a few micrometers in thickness, to minimize the path length of the beam through that media. This is commonly achieved by sandwiching the liquid in between the solid surface being studied and the prism used to guide the light in and out of the liquid/solid interface (Figure 1, center). The advantage of using this setup is that it affords the characterization of small (∼1 cm^2) flat surfaces, although the technique requires that those are polished and highly reflective.

This single-reflection IR absorption spectroscopy approach is typically referred to as either reflection−absorption infrared spectroscopy (RAIRS) or infrared reflection−absorption spectroscopy (IRRAS). Because it requires a reflecting surface, it has been most commonly used for systems involving metals. In fact, the use of metals brings the added advantage that a surface selection rule applies according to which only p-polarized light can be absorbed by the adsorbed species.[20,22,23,48] By contrast, light absorption by species in solution is isotropic, which means that the contribution to the IR spectra from adsorbed species can be separated via the subtraction or ratioing of the traces obtained with p- versus s-polarized light. Several optical arrangements have been developed to obtain such p/s ratio directly, the most common of which is the use of a photoelastic modulator (PEM) to modulate the polarization of the light.[7,49−52] The surface selection rule can also be used to extract adsorption geometries, as already mentioned in connection with ATR and as discussed in more detail below.

By and large, the most common application of RAIRS has been in the study of electrochemical systems involving metal electrodes. Perhaps disappointedly, those have so far focused mainly on the characterization of only a handful of simple adsorbates.[53−56] Quite extensive RAIRS work has been published on the adsorption of carbon monoxide,[57,58] from which the pioneering work by Weaver's group aimed at the identification of the effects of electrode potential on the C−O stretching frequencies and local adsorption geometries deserves special mention.[59,60] Those were interpreted in terms of alterations in both the local electrostatic field and the coordination of the adsorbate on the surface, which are influenced in great part by the solvent (via electrostatic interactions and because of competition for adsorption sites). RAIRS characterization studies are also available on other small molecules, including NO,[61] and even on small organics such as indols.[62] In all these, the adsorbates have usually been chosen because they exhibit at least one vibrational mode with a large absorption cross section and a frequency in a relatively clean region of the IR spectrum, ideally between approximately 1500 and 2200 cm^{-1}. That makes their detection easier, given that the sensitivity of RAIRS in liquid/solid is limited and the elimination of contributions from the solvent in practice incomplete.

RAIRS has also been used extensively to follow the evolution of the intermediates that may form on electrode surfaces during electrocatalysis. Much of that work in recent years has been directed to the study of fuel cell reactions, which are ideally suited for this technique because they usually involve the simple, high dynamic dipole, molecules (CO, carboxyl-containing organics, alcohols) that best behave for RAIRS detection; many reports have centered on the characterization of hydrogen oxidation/evolution and oxygen reduction reactions and on the electrooxidation of carbon monoxide, formic acid, and methanol.[63,64] In terms of the electrooxidation of alcohols in particular, a number of surface intermediates have been repeatedly identified with RAIRS, including CO, COH, HCOH, and H_2COH, and two reaction pathways have been confirmed, one involving the oxidation of adsorbed CO and a second involving the formation of an organic intermediate such as an aldehyde or an organic acid.[65,66]

RAIRS studies of oxidation and reduction reactions under electrochemical conditions can in principle be extended to other types of systems. In polymer electrochemistry, for instance, the redox processes of aminophenols on a platinum electrode in aqueous acid solutions were shown to differ markedly depending on the isomer used as reactant.[67] It was established that while *p*-aminophenol undergoes hydrolysis to hydroquinone/*p*-benzoquinone, *m*-aminophenol grows a blocking polymeric

film; phenoxazine units are produced during the oxidation/reduction of poly(*o*-aminophenol). Moreover, with poly(*o*-aminophenol), the redox chemistry was determined to occurs via two consecutive reactions involving a charged intermediate.[68] In a different example, with 2,5-dihydroxybenzyl mercaptan, electrochemical oxidation on a gold electrode was determined to involve a quinone-type moiety.[69] One interesting side conclusion from this latter work is the fact that the performance of RAIRS was found to be quite similar to that of ATR. RAIRS studies with these types of polymers are helped by the strong signals associated with the breathing modes of their aromatic rings and the fact that the corresponding vibrational frequencies appear in a relatively clean spectral range (>1500 cm^{-1}).

The identification of adsorbed species in electrochemical systems can be enhanced by light polarization modulation, as indicated above, but also by potential modulation, a technique known as subtractively normalized interfacial Fourier transform infrared spectroscopy (SNIFTIRS). For instance, SNIFTIRS (and other potential-dependent IR techniques) have been used to investigate the reaction mechanism of the electrooxidation of ethanol on PtSn electrodes.[70] Those studies have help determine that the presence of tin on the surface allows ethanol to adsorb dissociatively and to be activated via scission of its C−C bond at lower potentials and with a higher selectivity than on pure Pt, to form acetic acid. A potential modulation approach has also been used to explain that the anomalous peaks seen in the cyclic voltammetry of Pt(111) in sulfuric acid are associated with the adsorption of bisulfate anions.[71] In connection with the electrooxidation reactions seen in lithium batteries, SNIFTIRS has been used to establish that, in general, the Li insertion processes include the migration of Li ions through surface films but with surface chemistry that is highly dependent on the solution used: in $LiAsF_6$, for instance, the chemistry is dominated by solvent reduction, whereas in either 1−3-dioxolane or tetrahydrofuran the products from salt anion reduction are the major constituents in the surface films formed.[72,73] In these battery related studies, the most characteristic species, the easiest to identify by RAIRS, are carbonates, although signals from other moieties such as trifluoromethyls are also observable.

By using single crystals, RAIRS can also afford the identification of structural factors in the chemistry of electrodes. For example, in a study on the reduction of nitrate anions on a series of single-crystal platinum electrodes in sulfuric and perchloric acid solutions, it was found that there are noticeable differences in reactivity among different exposed facets, but that those are essentially controlled by other species (hydrogen, sulfate) interacting strongly with the electrode surface, not by a structure-sensitive nitrate adsorption, dissociation, or reduction.[74] That type of information may be lost if polycrystalline surfaces are used instead, but in exchange, an enhancement in IR signal may be gained. Indeed, a surface enhancement has been reported on rough metal electrodes, mainly on coinage metals (Au, Ag, Cu), and may occur on other late transition metals as well.[75,76] This phenomenon, which also applies to ATR setups, has been explained by an electric field enhancement because of collective electron resonances associated with the island nature of the thin metal films.[77,78] In a recent example involving a Pt electrode/Nafion interface in $HClO_4$ aqueous solutions (a relevant system in polymer electrolyte fuel cells), SO_3^- groups were identified in the ionomer membrane, with their geometrical orientation driven by the electric field.[79] It was inferred that the SO_3^- groups act like counterions at the Pt/ionomer interface to form the electric double layer. However, full acceptance and utilization of this IR surface enhancement is yet to be reached.

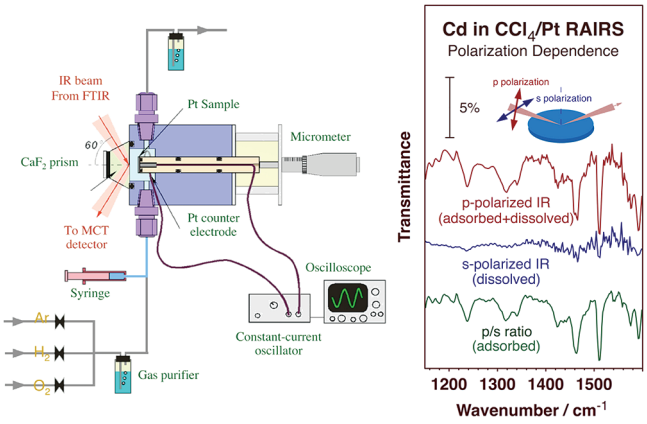

Figure 3. Illustration of the use of RAIRS to characterize the adsorption of molecules from solution onto metal surfaces.[81] Left: Schematic representation of the RAIRS setup used in this study. The cell consists of a calcium fluoride prism and a manipulator for holding, moving, and applying voltages to the platinum solid surface; the liquid samples are pressed in the small volume between those two elements. Right: Spectra obtained by using this instrument for the characterization of the adsorption of cinchonidine, a chiral modifier, from a carbon tetrachloride solution onto the platinum surface. The data provided here illustrate the use of a surface selection rule to discriminate between signals from adsorbates on metals and species dissolved in solution: since the species in solution absorb light isotropically, similar spectra are obtained with s- and p-polarized light, whereas for the adsorbed molecules only the p component is absorbed. Therefore, a ratio of the traces obtained with p- versus s-polarized light (the two top traces) yields a spectrum due exclusively to cinchonidine adsorbed on the platinum surface (bottom trace). Reprinted from ref. 81 with permission. Copyright 2003 American Chemical Society.

More recently, the use of RAIRS has been extended to the study of the adsorption of species involved in catalysis. For instance, in a study by Baiker's group, the selectivity of the liquid-phase oxidation of benzyl alcohol to benzaldehyde on a Pd film was contrasted between anaerobic conditions, where toluene was the major side product, and aerobic conditions, where large quantities of CO_2 and benzoic acid were also observed.[80] CO formation by decarbonylation of benzaldehyde was also observed on a Pd(111) surface under anaerobic conditions, delayed with respect to the formation of benzaldehyde. We in our laboratory have worked extensively on the use of RAIRS to characterize the adsorption of chiral molecules on metal surfaces, by using a system derivative from those developed for electrochemical studies (Figure 3, left).[81,82] In catalysis-relevant RAIRS studies, as in the electrochemical work, discrimination between adsorbed species and species dissolved in solution can be achieved by using polarized light (Figure 3, right),[81] and geometrical information can be extracted from polarization dependent measurements by using the surface selection rule mentioned before.[83−86] Particularly noteworthy from the example illustrated in Figure 3 is the correlation that was identified between the adsorption of cinchona alkaloids with their aromatic ring flat on the surface, which occurs at intermediate coverages and disappears at higher solution concentrations, and their ability to promote enantioselective hydrogenations.[83] It was also possible to establish in that work the role that adsorbed gases[87] and the nature of the solvent[88] play in the uptake of the cinchona, and to characterize the adsorption

under competitive conditions[89] and measure adsorption equilibrium constants.[85] Unfortunately, examples such as these where RAIRS has been used to study catalytic reactions at liquid/solid interfaces are quite scarce.

2.3. Transmission

A much less common arrangement in the infrared absorption spectroscopy study of liquid/solid interfaces is in transmission mode. First, many solids are opaque to the infrared radiation, and that renders them nonviable for the use of this setup. In addition, IR signal intensity is easily lost in transmission because of absorption by the solvent. In spite of those difficulties, however, there are a few examples of the use of transmission IR absorption spectroscopy for the characterization of the adsorption of molecules from a liquid phase onto the surface of catalysts or nanoparticles. For instance, if the solid samples are transparent, as in the case of some thin-layer electrochemical cells, a simple transmission cell can be easily devised.[90] Baiker's group has published some reports on the feasibility of an alternative design involving thin liquid films, which they have used for the study of the heterogeneously catalyzed hydrogenation of ethyl pyruvate over Pt/Al_2O_3 under high pressures.[91] In their arrangement, however, the surface chemistry is still followed by ATR; transmission IR absorption spectroscopy is used for the simultaneous recording of changes in the liquid phase. Another reported example of the use of transmission IR in liquid/solid systems involves the extraction of chemicals (i.e., CpMn(CO)) by a polymer (polyethylene) in a CO_2 supercritical fluid.[92]

In our laboratory, we have adapted our RAIRS setup (Figure 3) to be used in transmission mode by employing the back metal surface as a mirror and by suspending the solid sample in a liquid thin film trapped between the prism and the mirror. This arrangement is shown schematically in the bottom panel of Figure 1. That transmission IR setup has been used to investigate the adsorption of carbon monoxide on dendrimer-encapsulated platinum nanoparticles (Pt-DENs) immersed in different solvents (Figure 4).[93] It was found that while only limited, weak, and reversible adsorption is possible in the gas phase, extensive and stronger adsorption occurs in the liquid phase. It was speculated that the dendrimer structure may collapse in the gas phase, blocking access to the Pt surface, but may expand and open up in the presence of a proper solvent.

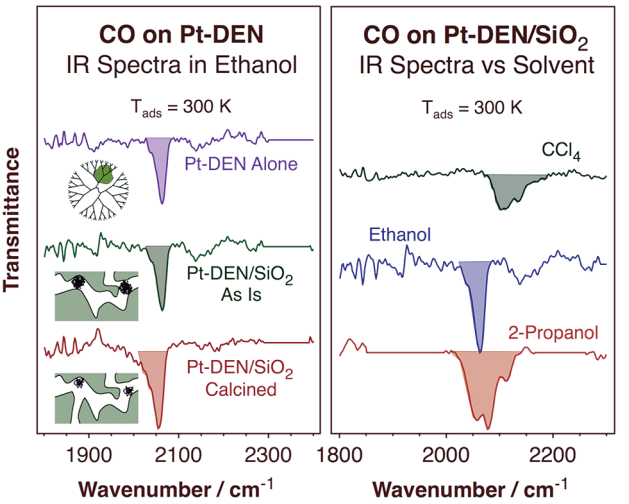

Figure 4. IR absorption spectra for CO adsorbed on Pt dendrimer encapsulated nanoparticles (Pt-DENs) dispersed on a sol−gel silica support.[93] This provides an example on how the setup in Figure 3 can be used to characterize liquid/solid interfaces in transmission mode. Left: Data for CO adsorption on three samples suspended in ethanol: the Pt-DENs by themselves (top); the Pt-DENs dispersed onto a high-surface-area silica support, as prepared (center); and the same supported Pt-DENs after calcination of the organic matter (bottom). Access of CO to the Pt surface is virtually unhindered even before any pretreatment of the catalyst on Pt-DENs where the dendrimer structure is still intact. Right: Spectra for the silica-supported Pt-DENs suspended in three different solvents (carbon tetrachloride, top; ethanol, center; and 2-propanol, bottom). CO adsorption is greatly affected by the nature of the solvent. Reprinted from ref. 93 with permission. Copyright 2010 American Chemical Society.

3. OTHER VIBRATIONAL SPECTROSCOPIES

Vibrational information can also be obtained by using visible or ultraviolet light, via the detection of the Raman scattering or by using nonlinear laser-based optical spectroscopies such as sum-frequency generation (Figure 5). Often, light in the visible and ultraviolet ranges is absorbed less efficiently by condensed matter than infrared radiation, and can therefore travel better through thin liquid films. In addition, the high energy of visible and ultraviolet photons affords their individual detection, a fact that makes the associated spectroscopy quite sensitive. A third advantage to the use of visible or UV radiation for vibrational studies is that most of the spectroscopies in this category are such that signals are detected on top of a zero (or negligible) background. On the negative side, vibrational information can only be extracted from visible or UV excitation indirectly, by relying on low-probability secondary or multiphoton processes. This means that intense beams may be required to increase signal intensity, leading to a high risk of sample damaging. The latter problem is exacerbated by the possible promotion of decomposition photoreactions by the visible or UV radiation. Also, high-beam intensity can in many instances be obtained only with specialized high-power lasers, adding to the cost of the experiment, although laser technology has progressed much in recent years so cheap lasers are now available for many photon energies. In spite of their limitations, vibrational spectroscopies based on the use of visible or UV light have become quite popular, and have in some instances been adapted to address issues associated with liquid/solid interfaces.

3.1. Raman Scattering Spectroscopy

In Raman spectroscopy, the light scattered from the sample is energy-analyzed to detect quantum gains or losses due to energy excitations within the molecules being probed (Figure 5, right). This technique is widely used to obtain vibrational information on many types of samples, not only liquid/solid interfaces. The main shortcoming is the fact that the Raman scattering signals are weak and difficult to separate from the much more intense signal due to the elastically (Rayleigh) scattered photons and also from any possible fluorescence that may emanate from the sample upon laser excitation. This makes the general use of Raman spectroscopy for the analysis of surfaces difficult. Some signal augmentation can be achieved by resonantly exciting a particular electronic transition of the sample being probed, but that requires the use of tunable lasers, limits the range of accessible vibrational modes, and increases the probability of sample damage by the laser radiation. Instead, for the study of interfaces, Raman spectroscopy is most commonly set to take advantage of the signal enhancement that comes from excitation of surface plasmons in rough surfaces.

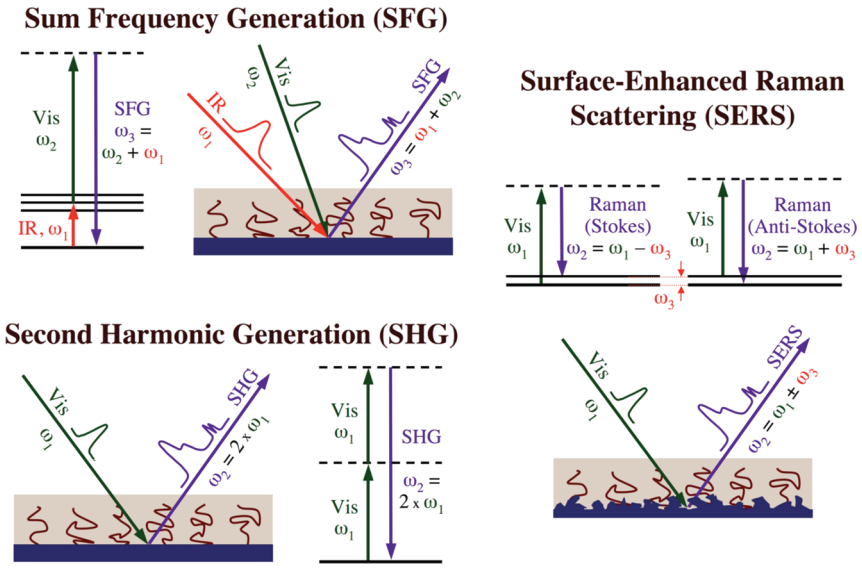

Figure 5. Schematic representation of the laser-based spectroscopies discussed in this review for the characterization of liquid/solid interfaces using UV−vis light. Right: Surface-enhanced Raman scattering (SERS), a technique where the scattered light from a laser illuminating the liquid/solid interface is analyzed for gains and/or losses in energy due to molecular vibrations. Left, Top: Sum frequency generation (SFG), where a tunable infrared laser beam, used as the probe, is combined with a fixed-energy visible laser at the liquid/solid interface in order to up-convert and individually count the reflected IR photons. A vibrational spectrum is obtained by recording the intensity of those versus the energy of the IR beam. Left, Bottom: In second harmonic generation (SHG), two photons from the same laser are added at the liquid/solid interface, and detected. The intensity of the outgoing beam is recorded as a function of the energy of the incident photons to follow changes in electronic properties at the interface.

Surface-enhanced Raman spectroscopy (SERS), as the technique is known, has long been employed to characterize a variety of molecules, in particular organic species, on gold and silver surfaces.[94−98] Those studies have afforded the determination of chemical identities, structures, and adsorption orientation, and also to follow chemical and electrochemical reactions of anions, surfactants, environmental pollutants, biomolecules, and dye molecules. Raman surface enhancement occurs mainly on silver and gold substrates, a fact that makes its application somewhat limited, but by electrodepositing other metals on top of gold nanoparticles, it has been possible to extend the use of SERS to other solid surfaces.[99,100]

To date, the main use of SERS has been for the characterization of bulk samples, which are deposited on rough metal surfaces or on metal nanoparticles only to take advantage of the signal enhancement afforded by those.[101] Many particularly interesting developments have been reported on the analytical use of SERS for the study of biomedical samples,[102−107] including live cells.[108−110] It has been possible, for instance, to detect self-assembled Au−imidazole structures formed in vivo in tumor-bearing mice.[111] Sensors have also been developed in which target-specific SERS probes are prepared by derivatizing appropriate metal surfaces or nanoparticles with labels displaying a characteristic vibrational signature (mercaptobenzoic acid, Rhodamine 6G) and specific binding sites (biomolecules such as antibodies) for the corresponding target molecule (proteins or a nucleic acid).[112]

Analytical applications of SERS have also been advanced for environmental uses such as for the detection of aqueous or airborne contaminants.[107] One example in this category is the SERS-based detection of perchlorate ions in groundwater.[113] Several studies have also focused on the detection and identification of trace elements and compounds,[114] in some instances in combination with electrochemistry to tune the cell potential for maximum adsorption.[115] More recently, SERS has been implemented as a detection tool in chromatography and in capillary electrophoresis schemes.[116] In one example, silica sol−gels were used for the dual purpose of acting as the stationary phase in liquid chromatography and of immobilizing the metal particles needed for SERS detection.[117] Another detection scheme combined SERS with thin-layer chromatography, using silica-gel coupled with citrate-reduced Ag colloids, to analyze the composition of natural dyes on works of art.[118] In a third case, SERS was used as the detection method in a microflow, lab-on-a-chip, cell for the detection of TNT.[119] In all these examples, however, the interest was to selectively detect and quantify specific compounds in solution; no attention was directed in any of those cases to the study of the adsorption of the molecules probed on the surface of the solid.

Although less common, there are also reports on the use of SERS for the characterization of liquid/solid interfacial chemistry,[120] many of them related to electrochemistry.[99,121] One of the early examples of this use of SERS is that of Pemberton and Buck, who combined the advantages of the surface enhancement obtained by using silver rough surfaces with the resonant effect afforded by tuning the excitation source to obtain adsorption isotherms and determine adsorption geometries during the uptake of diphenylthiocarbazon anions from an alkaline aqueous solution onto a silver electrode at the potential of maximum uptake.[122] Another early example of the use of SERS in electrochemistry is that of Shi et al., who followed the time evolution of the oxidation of p-nitrobenzoic acid on a Ag electrode.[123] In addition to three stable intermediates, *p*-nitrosobenzoate, hydroxylamine, and azoxy compounds, a transient *p*-nitrosobenzoate free-radical anion intermediate was detected. The voltage required to decompose methanol on platinum electrodes could be followed by SERS as well; a strong dependence on surface roughness was identified.[97] In all those cases, unique information has been extracted from SERS data about the kinetics and thermodynamics of the adsorption processes and

dx.doi.org/10.1021/cr2002068 |*Chem. Rev.* 2012, 112, 2920–2986

about the chemical and structural details of the adsorbates. Time-resolved SERS has also afforded the measurement of the kinetics of electrochemical processes upon either step changes in potential[124] or fast voltage ramping, as done in cyclic voltammetry.[125]

Applications of SERS to other fields involving liquid/solid interfaces are sparser. In those, SERS has typically been used to provide molecular information on the interaction of adsorbates with the solid surface, and also on adsorption geometry. For instance, SERS was recently used to aid in the identification of the mechanism by which iodine ions enhance the effect of benzotriazole as an inhibitor in iron corrosion.[97] It was concluded that the electrostatic interaction induced by adsorbed I^- facilitates the adsorption of a protonated version of benzotriazole, and that the resulting mixed layer can protect the iron substrate from corroding agents. In an earlier study, SERS was use to evaluate the effectiveness of self-assembled monolayers of alkanethiols adsorbed on the surface of a polycrystalline bulk copper against corrosion in an aerated Na_2SO_4 solution.[126] It was determined that the alkanethiols chemisorb via the formation of strong bonds between Cu and S atoms following cleavage of the S−H bond and form densely packed, water-repellent, monolayers on the surface. Other self-assembled monolayers, based on benzenethiol, benzenemethanethiol, *p*-cyanobenzenemethanethiol, diphenyl disulfide, and dibenzyl disulfide, were also determined by SERS to adsorb dissociatively as thiolates on rough gold electrodes.[127] The aromatic rings in those cases were found to adopt a tilted geometry, but a reduction in surface coverage was seen upon switching of the applied potential to positive or negative extremes. In terms of the formation of colloidal particles, pyrazinamide and 2-mercaptopyridine were shown to form Ag colloid−adsorbate films at the interface between the silver colloid aqueous and dichloromethane-adsorbate solutions, in contrast to 4-mercaptopyridine, which forms Ag organosol aggregates via the transfer of adsorbate-covered Ag colloidal particles from the aqueous to the organic phase.[128] The differences between the two latter systems confirmed that the formation of Ag colloid−adsorbate films is an adsorbate specific process.

In a more complex study of biological relevance, a SERS characterization of the uptake of cytochrome c (Cyt c) on self-assembled monolayers of mercaptoalkanoic acids on colloidal silver indicated that the adsorption is selective on negatively charged surfaces, on a second layer on top of a SAM directly attached to the Ag.[129] Previous SERS studies had indicated that adsorption of heme proteins on aqueous silver sols occurs with formation of surface-bound hemin μ-oxo dimers, implying that the heme prosthetic groups are extracted from their binding pockets in at least some of the protein molecules, and that heme extraction is facilitated under oxidizing conditions, perhaps via increased surface charge on the Ag surface.[130] SERS has also been used to look into the adsorption of aminoacids in silver colloidal solutions, to determine the geometry and orientation of the adsorbates and to identify their specific interactions with the surface.[131] In most instances, with L-methionine, L-glycine, L-leucine, L-phenylalanine, and L-proline as well as with their homodipeptides, it was found that the majority of the C−C bonds adopt an almost parallel orientation with respect to the surface. In the case of L-cysteine, however, the SERS spectra indicated a potential-induced reorientation of the molecules adsorbed from a KCl solution onto a polycrystalline silver electrode, from bonding with the protonated amino group pointing toward the surface at positive potentials to the carboxylate group becoming closer to the surface at negative potentials.[132] Again, in these examples, key information was extracted from SERS experiments about adsorption affinity and adsorption geometry.

In materials chemistry, SERS can also be used to investigate adsorption processes. A SERS study of the adsorption and acidity of the highly fluorescent anthraquinone-based pigment alizarin on Ag colloids, for instance, indicated that the order of deprotonation of the two OH groups reverses on the metal in comparison with the way it happens in the aqueous solution.[133] Other SERS studies have been directed at the characterization of interfaces between solids and nonaqueous liquids.[134] In some instances SERS can be used to characterize photochemical reactions, as in the case of methylviologen adsorbed on a roughened silver electrode, which was determined to undergo a reduction step at its cation radical position upon irradiation with the blue spectral region of laser excitation light even at liquid nitrogen temperature.[135] It was also established in that study that the dication form of methylviologen interacts more strongly with the surface than the monocation. SERS can provide information about the collective vibrational characteristics of solids as well. For instance, SERS was used to map the phonon characteristics of mixed CdS/CdSe layers on gold, a system with potential applications in electronics.[136] A phonon band associated with CdS was found to soften with increasing thickness because of the crystallographic strain caused by expansion to match more closely the adjacent CdSe layer. It has even been possible to record SERS data from nanomaterials without the aid of any signal-enhancing metals, as in the case of the study of the adsorption of pyridine on InAs/GaAs quantum dots.[137] It was suggested, based on the SERS data, that adsorption occurs via coordination of the lone-pair-electrons of the N atom to the semiconductor surface. Only a few examples are available to date on SERS applications to materials problems, but those illustrate the range of both molecular and solid-state information that can be extracted from such studies.

Next, a couple of examples are provided of applications of SERS to problems of heterogeneous catalysis involving liquid/solid interfaces. In one, Heck et al. looked into the time dependence of the hydrodechlorination of 1,1-dichloroethene in water catalyzed by Pd−Au nanoshells.[138] They identified a sequence of dechlorination and hydrogenation steps involving several intermediates, including π and di-σ bonded species, vinylidene, and other oligomeric moieties (Figure 6). In another report, from our laboratory, the adsorption of cinchonidine was tested by SERS on a thin film of platinum deposited on a rough gold surface.[84] Clear features could be identified in the SERS spectra because of the adsorbed molecule, including the ring-breathing mode at close to 1600 cm^{-1}, even if some interference from the solvent could not be completely avoided (Figure 7), and those could be used to establish a change in adsorption geometry with the concentration of cinchonidine in solution. One important conclusion from our work was that the information obtained with SERS is complementary to that extracted from RAIRS experiments because of the different selection rules that apply to each technique, the different cross sections of the different vibrational modes to both types of excitation, and the different experimental setups needed.

New ideas have been advanced to attempt to improve on the performance of Raman spectroscopy for the study of liquid/solid interfaces. One approach is the use of high-energy visible or ultraviolet light for the excitation, as a way to shift the Raman signals out of the spectral range of the fluorescence of the solid and also to increase signal intensity, since the Raman scattering

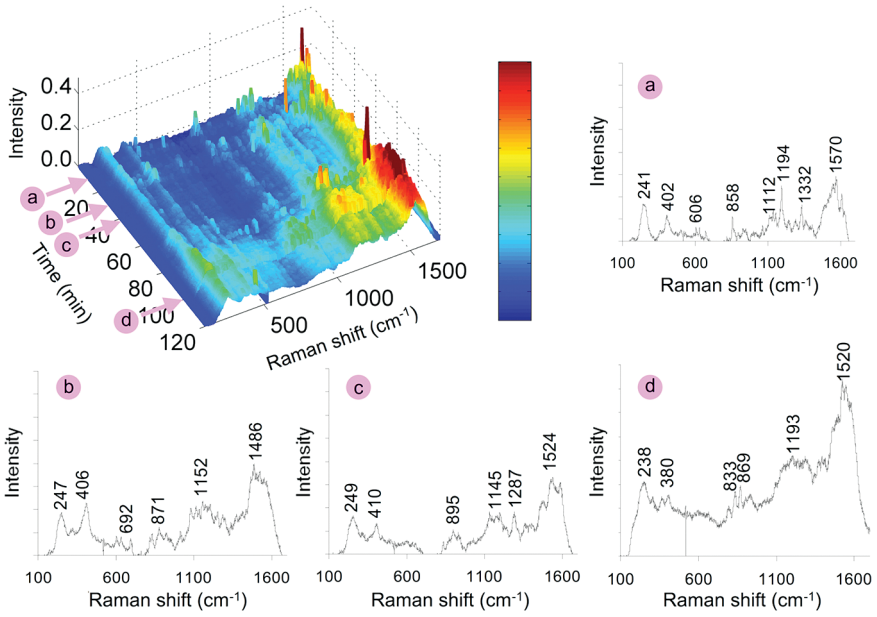

Figure 6. Illustration of the use of SERS to probe liquid/solid interfaces, in this case to follow the kinetics of a hydrodechlorination catalytic process.[138] Shown are time-resolved spectra for the reaction of 254 μM 1,1-dichloroethane with 81.9 mM H_2 on a catalyst made of a palladium film deposited on gold nanospheres and suspended in water. Also shown are individual scans obtained after 12, 30, 41, and 100 min of reaction (a, b, c, and d, respectively) to highlight the changes that occur on the surface with time. Evidence is provided for the formation of a number of surface species, including the reactant bonded in both π (1500−1600, 1220−1290, and 1000−1100 cm^{-1}) and di-σ (954, ∼1160, 1430 cm^{-1}) modes, and vinylidene (∼1500, ∼390, 230 cm^{-1}) and other oligomeric intermediates (∼1500 cm^{-1}). Courtesy of Michael S. Wong. Reprinted from ref. 138 with permission. Copyright 2008 American Chemical Society.

intensity is proportional to the fourth power of the excitation frequency. One problem with UV−vis excitation is that it can lead to faster degradation of the sample. To date, only a couple of examples are available on the use of UV−vis Raman on liquid/solid interfaces. In one, a dye adsorbed on the surface of alumina particles suspended in solution was used as an indicator of the pH of the solution.[139] In another, the adsorption of pyridine was studied on silver films grown over nanospheres, modified by subsequent deposition of alumina ultrathin films to improve their thermal and solvent stability.[140] These reports do not themselves add much insight into the chemistry of the systems studied, but do point to the potential of UV−vis Raman for the study of liquid/solid systems.

Another possibility for enhancing signal intensity in Raman spectroscopy is to use coherent anti-Stokes Raman scattering (CARS), a third-order nonlinear optical process where a pump beam (ω_p), the generated stokes photon ($\omega_s = \omega_p - \omega_{vib}$), and a third photon from a second probe laser (ω_{pr}), are combined to generate a coherent optical signal at the antistoke frequency ($\omega_{as} = \omega_p - \omega_s + \omega_{pr} = \omega_{pr} + \omega_{vib}$). The CARS signal is orders of magnitude stronger than spontaneous Raman emission, but the experiment requires two tunable lasers, so it is significantly more complex and difficult to set up. Very few examples can be cited on the use of CARS for the study of chemistry at liquid/solid interfaces. In one recent case in analytical chemistry, CARS was used to detect specific analytes in a microfluidic chip.[141] The wavenumber difference between the pump and Stokes lasers was tuned to the C−D stretching vibration of deuterated toluene, and the signal imaged throughout the cross section of the chip to obtain a chemical contrast map of the flow of that specific solvent. In another report, on a CARS imaging experiment of a biological sample, chemical sensitivity was attained by tuning to the aliphatic CH_2 stretching vibrational band present in most organic matter.[142] In a third study, of the in vivo behavior of cancer cells in mice exposed to an excess of lipids in the bloodstream, CARS imaging revealed intracellular lipid accumulation induced by excess free fatty acids leading to membrane phase separation, a reduction in cell−cell contact, an increases in surface adhesion, and a promotion of tissue invasion.[143] In all these examples, however, the goal was to obtain spatial images of particular molecules within the samples of interest, not to characterize any chemistry occurring at the liquid/solid interface.

The potential of using surface-enhanced CARS (SE-CARS) as a way to probe liquid/solid interfaces was recently tested in the case of the adsorption of pyridine on silver colloidal particles.[144] Disappointingly, while conventional SERS experiments were shown to display enhancement factors of up to 4 orders of magnitude compared to regular Raman spectroscopy, an enhancement of only a factor of 10 was seen for the SE-CARS signal, even though the technique requires a complex setup with three laser beams. Nevertheless, other advantages, including temporal resolution, may make SE-CARS useful for specific applications in liquid/solid interface characterization in the future.

3.2. Sum Frequency Generation

Another spectroscopy that has received significant attention in recent years in connection with the vibrational characterization of solid surfaces is sum frequency generation (SFG). In this nonlinear optical technique, two photons are added at a surface, an infrared photon from a tunable IR laser, used to excite the vibrational modes of the interface, and a second photon in the visible region, from a second (frequency-fixed) laser, used to energy up-convert the IR photons (Figure 5, left, top). Vibrational transitions in SFG are identified by an increase in signal of the resulting outgoing photon because of the resonant

dx.doi.org/10.1021/cr2002068 |*Chem. Rev.* 2012, 112, 2920–2986

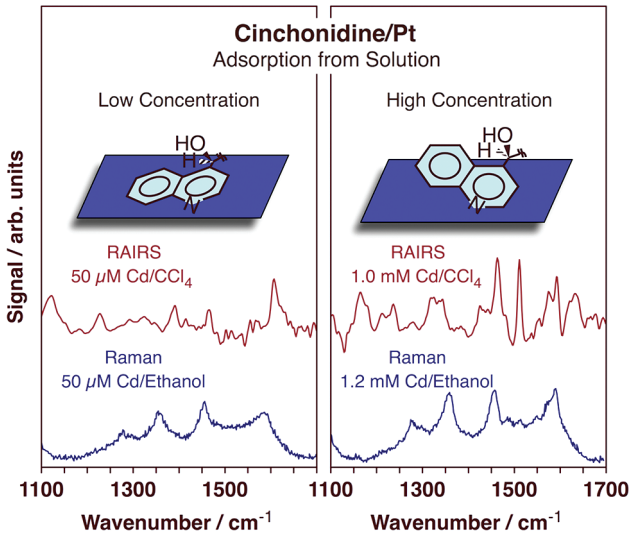

Figure 7. Comparison of the use of RAIRS vs SERS in the characterization of adsorption at liquid/solid interfaces.[84] The SERS data correspond to the uptake of cinchonidine from ethanol solutions onto a sample prepared by electrochemical deposition of platinum on an electrochemically roughened gold electrode, whereas the RAIRS spectra were obtained by using a carbon tetrachloride solution and an electrochemically cleaned platinum foil. The RAIRS and SERS data, which are here reported for two different concentrations to highlight the changes in adsorption geometry with surface coverage, are complementary. The SERS data appear to be less rich in information and contain many interfering peaks from the solvent (882, 1051, 1095, 1276, and 1456 cm^{-1}), but similar interferences were observed in RAIRS experiments with ethanol. Interestingly, the most prominent peak in the SERS traces is that at 1357 cm^{-1}, which is assigned to a quinoline ring-stretching mode of cinchonidine adsorbed on Pt; that feature is quite weak in RAIRS. Reprinted from ref. 84 with permission. Copyright 2003 American Chemical Society.

component of the second order susceptibility, $\chi^{(2)}$.[145,146] The uniqueness of SFG is the fact that $\chi^{(2)}$, a third rank tensor, becomes zero in centrosymmetric media, and that SFG intensity is only generated from noncentrosymmetric media, which means that interfaces can be probed selectively in the presence of isotropic media such as the bulk of liquids and solids. The upconversion of the IR photons to the visible range also affords the use of single-photon counting, which greatly increases sensitivity. On the negative side, SFG is an expensive and difficult-to-implement technique (only one commercial company offers SFG instrumentation at present),[147] and the data analysis, which requires the separation of the resonant and nonresonant components of $\chi^{(2)}$, is not trivial. Moreover, SFG experiments can only cover the range of frequencies available from the tunable IR laser used, typically around 3000 cm^{-1} (to probe C−H stretching frequencies). SFG experiments are most often carried out on flat, reflecting surfaces, to facilitate the collection of the SFG photons, and that usually limits its use to small model surface systems such as single crystals and polished films. Nevertheless, experiments with colloidal particles can also be designed, as discussed below. Finally, high laser intensities are needed, and that can lead to surface damage.

SFG, like IR absorption spectroscopy, can be used to characterize many types of liquid/solid interfaces. The vibrational information extracted by using SFG can be used to identify specific adsorbates on those interfaces. In addition, SFG follows a set of selection rules that, although complex, can be used to extract molecular geometry information by employing different combinations of polarizations of the incoming IR and visible light beams. An example of the use of this approach is provided in a recent report on the behavior of hydrocarbon chains covalently anchored to alumina via silane linkers in different environments.[148] The authors of that work found that, in general, tethered alkanes and cycloalkanes align at liquid/solid interfaces with the hydrocarbon backbone parallel to the surface, in contrast to their behavior at vapor/solid interfaces, where they adopt a tilted orientation. On the basis of the SFG data in the C−H stretching region, they also observed an increase in ordering of the alkyl tails of 1-hexanol in mixtures with cyclohexane over alumina surfaces with increasing surface coverage, and a correlated orientational change of the cyclohexane solvent from flat to tilted.[149]

In the early years of SFG, the technique was used extensively to study the interaction of water molecules with solid surfaces by focusing on the information that could be extracted from the behavior of the O−H stretching signals. In one study on fused quartz, it was seen that all the dangling OH bonds of the silica surface are eliminated upon the addition of water because of an hydrophilic interaction at the interface, and that the other OH bonds that are present in disordered and ordered water structures undergo changes in their interfacial structure with pH.[150] In a second study it was reported that, on sapphire, the water dipoles at the liquid/solid interface flip by 180° when the pH of the aqueous solution crosses the isoelectric point of the surface.[151] The structure of water molecules at water/electrode surfaces was found to also depend on the electrode potential: variations were seen in the relative SFG intensities for the symmetric O−H stretching bands associated with tetrahedrally coordinated, that is, strongly hydrogen-bonded "ice-like", water, versus water molecules in a more random arrangement, that is, weakly hydrogen-bonded "liquid-like" water.[152] Significant perturbations of the interfacial water structure were reported on silica upon the addition of small amounts of NaCl, because the cations electrostatically interact with the surface and perturb the hydrogen-bond network of water molecules at the water/silica interface.[153] A couple of recent reviews nicely summarize the knowledge extracted from SFG experiments on the ordering of water molecules at solid surfaces in terms of the main contributing factors, namely, hydrogen-bonding, electrostatic and dipolar interactions, and specific interactions with the surface.[154,155] Studies on the adsorption of surfactants and carboxylates on fluorite (CaF_2) have shown behavior similar to that reported for water on quartz.[156]

SFG reports are also available on liquid/solid interfaces involving neat liquids other than water. For instance, an early SFG study on the interaction of acetonitrile with zirconia suggested the formation of dimers and clusters on the surface,[157] and a more recent SFG (and theory) investigation with silica indicated an interfacial acetonitrile structure reminiscent of a lipid bilayer, with an ordering that persists for tens of angstroms into the bulk liquid.[158] An interesting aspect of the first study is its use of a low-frequency IR laser, covering a frequency range between approximately 2210 and 2270 cm^{-1}, to access the information about the C≡N stretching vibrational mode. Following a slightly different approach, by focusing on the behavior of the solid surface rather than the adsorbate (the changes in O−H stretching frequencies of surface hydroxide groups), another study reported estimates for the interaction energies of sapphire with several polar and nonpolar liquids and polymers.[159] It was determined that molecular rearrangements at the sapphire interface to maximize bonding of the acid−base groups play a dominant role in these interfacial interactions.

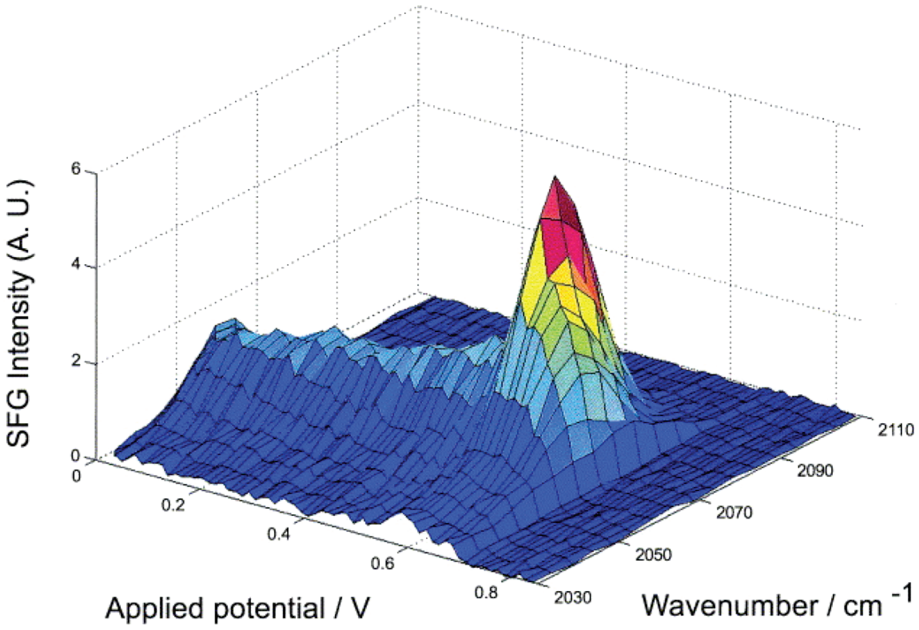

Figure 8. Evolution of the SFG spectra of CO on a platinum electrode during an electrochemical sweep at 0.5 mV/s toward more positive potentials.[162] Several pieces of information can be extracted from this in situ spectroscopy study. First, the trends seen in the SFG data correlate well with results from CO striping current measurements, which indicate that oxidation peaks at 0.684 V and stops by 0.690 V. Second, shifts in C−O stretching frequency are observed as a function of applied potential: for potentials below 0.50 V a vibrational Stark effect is seen, with the C−O stretching frequency increasing at a rate of about 30 cm^{-1}/V, but at higher potentials a red shift is seen due to a decrease in CO coverage. Courtesy of Gabor A. Somorjai. Reproduced from ref. 162 with permission. Copyright 2003 Elsevier.

SFG is quite suitable for the characterization of electrochemical systems. For instance, Tadjeddine et al. have reported on the adsorption behavior of CN^- on silver electrodes, on the identification of intermediates from the dissociative adsorption of methanol on Pt-$HClO_4$, and on the sensitivity of the deposition of hydrogen from acid media on the structure of the platinum surface.[160] Bozzini et al. have recently identified an acetate intermediate using SFG in situ during the electrooxidation of ethanol on Pt-black supported on tungsten carbide.[161] Somorjai and co-workers have shown how acetonitrile reorients on a Pt(111) surface as a function of applied potential, and how the C−O stretching SFG peak can be used to follow the oxidation and stripping of CO from platinum electrodes (Figure 8).[162]

A related application of SFG is in the study of corrosion. For instance, an SFG study by Leygraf and co-workers designed to establish the mechanism of the corrosion of Cu and Zn with acetic acid in a humid environment afforded the detection of the metal acetate species believed to initiate the oxidation of the surface.[163] SFG data were used in a second example to show that the corrosion of gold by cyanide ions starts with the formation of linearly bound cyanide but evolves over time to generate higher-coordinated gold-cyanide complexes.[164] Regarding the adsorption of the corrosion-inhibitor benzotriazole in the presence of acidic solutions, ordered adsorbate layers with the benzotriazole anion either coordinated to the surface only or to both the surface and metal ions in solution, were observed on Cu(100) surfaces at all potentials probed and on Cu(111) at positive potentials (a disordered layer forms at negative potentials).[165] The examples in the last two paragraphs illustrate the type of chemical, structural, kinetic, and mechanistic information that can be obtained by SFG in electrochemical systems. Details about the nature and geometry can be easily extracted in situ as a function of electrode potential, the nature and acidity of the solvent, and the concentration of the solute and other agents.

Some interest has arisen recently on the characterization of the interfaces between electrodes and ionic liquids, and SFG has provided a convenient way to fulfill that need. In one case, a clever methodology was developed by which surface potentials were measured via the observation of vibrational Stark shifts in coadsorbed carbon monoxide, a molecule used as a probe. Since those measurements rely on the behavior of the SFG C−O stretching frequency in coadsorbed CO, however, a laser that can reach frequencies as low as 1900 cm^{-1} was required. It was determined by using this approach that the ions in ionic liquids organize in a Helmholtz-like layer at the interface, with a potential drop extending 3−5 Å from the metal surface.[166,167] The authors of those studies also found that the structure of the ion-liquid layer depends on the applied potential: with 1-butyl-3-methylimidazolium tetrafluoroborate on platinum, for instance, the anions adsorb on the surface and the imidazolium rings orient normal to the surface at positive potentials, but the same anions are repelled from the surface, and the rings adopt a more parallel configuration, at negative potentials. A double layer of the ions has been identified by SFG with 1-butyl-3-methylimidazolium trifluoromethanesulfonate, a similar ion liquid, in a adsorption/desorption process that displays significant hysteresis.[168,169]

Several examples are available for the use of SFG in the characterization of the adsorption of polymers and surfactants, typically to establish adsorption geometries and their changes upon variations of parameters such as the nature of the solvent, the pH of the solution, the addition of ionic species, or the application of electrical potentials to the surface, or even to follow the formation of self-assembled bilayers in aqueous solution. For instance, the group of Shenhave has shown that saturated monolayers of octadecyltrichlorosilane adsorb on fused silica

with the alkane chains normal to the surface regardless of the nature of the solvent.[170] In contrast, the same group proved that, in dioctadecyldimethyl ammonium chloride adsorbed at liquid/quartz interfaces, the hydrocarbon chains can assume different conformations depending on the solvent used: an all-trans configuration in alkanes with chains of similar length, a bent form with significant trans−gauche defects in CCl_4, $CDCl_3$, or short-chain alkanes, and a highly contracted form in water or alcohol.[171] Cremer's research team has shown similar ordering and chain alignment changes with polydiallyldimethylammonium chloride at the water/quartz interface as a function of pH.[172] Ion-induced interfacial structural changes in Langmuir−Blodgett films of stearic acid on hydrophilic (fused quartz or Au) solid substrates have been reported as well.[173] Somorjai and co-workers have provided SFG results on the changes in wettability of (16-mercapto)hexadecanoic acid self-assembled on Au(111) in response to an electrical potential, presumably because of conformational transitions between hydrophilic and moderately hydrophobic states.[174]

As mentioned at the beginning of this subsection, some SFG studies have been carried out to characterize chemistry on the surface of colloidal particles. This requires a change in both the experimental setup and the data processing[175] because, due to the nature of the surfaces involved, scattered rather than reflected light needs to be collected. The signals in this case are weaker, and the data analysis rather complex, especially if adsorption geometry is to be extracted. As a consequence, not many SFG studies have been reported in this area to date. In one of the few examples available, the calcium-induced ordering of phospholipids was shown to depend on surface pressure.[176] In another, where stearyl molecules were used to coat silica particles dispersed in CCl_4, the high ratio observed of the CH_2 symmetric versus the CH_3 symmetric stretching amplitudes was used to conclude that the surface displays a large amount of disorder.[177,178]

SFG has recently proven quite powerful for the identification of interfacial chemistry associated with biological systems, to establish bonding modes and adsorption geometries on biomimicking solids. An SFG study of the adsorption of aminoacids from water solutions onto titania surfaces, for instance, has shown that aspartic acid and glutamic acid both form ordered layers, the first by bonding via both carboxylic groups, whereas other amino acids with nonacidic side chains exhibit little affinity toward TiO_2.[179] In another instance, Chen et al. used SFG to distinguish among different secondary structures of proteins and peptides adsorbed from liquids onto polystyrene surfaces.[180] In a third case, SFG data were used to demonstrate that the antimicrobial peptide Cecropin P1 chemically immobilized on a polymer adopts a more ordered orientation than when physically adsorbed on the surface.[181] On the basis of the observation of prominent SFG C−H resonances, the adsorption of LK14 (a 14-amino acid amphiphilic peptide) was shown in a fourth study to occur via the hydrophobic (nonpolar) leucine side chains on hydrophobic polystyrene surfaces; electrostatic bonding via the lysine (charged) groups was suggested on hydrophilic silica because of the sole detection of N−H stretching modes instead (Figure 9).[182,183] Further correlations between the orientation of the leucine side chains of LK14 on polystyrene and its dynamic trends, observed by solid-state NMR, were derived by combining SFG with selectively isotope labeling of individual isopropyl groups.[184] Recently, chiral SFG vibrational spectra were obtained for fibrinogen bonded on a calcium fluoride surface by using a novel method based on the interference between normal achiral and chiral data; it was found that the chiral SFG signal originated

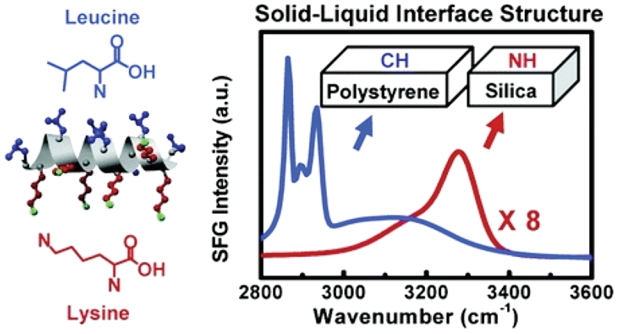

Figure 9. Example of the application of SFG to the study of biology-relevant systems. In this case, the adsorption of a 14-aminoacid amphiphilic peptide, LK14, which is composed of leucine (L, nonpolar) and lysine (K, charged) units, was contrasted on hydrophobic polystyrene versus hydrophilic silica surfaces.[182] Adsorption was probed in situ from a pH 7.4 phosphate-buffered saline solution. The spectra indicate a different ordering on the two surfaces. On the hydrophobic surface, the data are dominated by C−H resonances, 2869 (ν_{s,CH_3}), 2895 (CH or CH_2 Fermi resonance), and 2935 (CH_3 Fermi resonance) cm^{-1}, all corresponding to the hydrophobic leucine side chains, suggesting strong adsorption mediated by the hydrophobic (leucine) side of the peptide. On the hydrophilic substrate, on the other hand, only the N−H stretching modes from lysine (3294 cm^{-1}) are observed, and a different, and weaker, surface bonding is operative. Courtesy of Gabor A. Somorjai. Reprinted from ref. 182 with permission. Copyright 2006 American Chemical Society.

mainly from the β-sheet structure, which adsorbs with its tachyplesin I peptide in an ordered fashion.[185] It is worth pointing out that, in the two last examples, special experimental approaches (selective isotope labeling, an interference enhancement method) were added to the SFG studies to collect specific and hard-to-obtain molecular information (regiospecific binding, chirality).

An additional advantage of SFG (and other laser-based spectroscopies) is that the pulsed nature of the lasers can be used to add a temporal dimension to these experiments, to follow the kinetics or dynamics of the systems being studied.[186] In one example, the lifetime of the C−N stretching excitation in CN^- was found to increase from a few picoseconds on platinum to tens of picoseconds on silver, an effect that was determined to correlate with the onset of interband transitions in those metals.[187] The authors of that work also proved that this vibrational lifetime can be controlled by tuning the Fermi level, by changing the applied potential in the electrochemical cell. In a second example, it was determined that water molecules exchange vibrational energy at the liquid/glass interface on a subpicosecond time scale.[188] A more recent example on the use of SFG for the study of dynamics is that of the incoherent transfer of heat, generated via infrared-laser excitation near the interface, between membrane-bound water and a lipid monolayer; energy transfers both from the excited CH_2 groups to the terminal CH_3 moieties within the lipid molecules and between water and lipids were also found to occur within 1 ps.[189] Particularly noteworthy in the latter study is the selective study of energy transfer from specific vibrational modes, a possibility afforded by the tunability of the SFG signal. In a slower time frame, kinetic parameters have been measured by SFG on the exchange of CO ligands within an oxo-centered triruthenium cluster attached to a self-assembled monolayer on the surface of a gold electrode in both aqueous and nonaqueous solutions.[190]

4. OTHER UV−VIS AND ACOUSTIC TECHNIQUES

Because of the relatively large depths that ultraviolet and visible (UV−vis) light can penetrate into liquids, spectroscopies based directly on absorption, scattering, or reflectance of such light should in principle be suitable for the characterization of liquid/solid interfaces. The large mean-free-path of UV−vis photons through liquids is certainly one of the advantages of Raman and SFG spectroscopies when applied to the study of liquid/solid interfaces, as mentioned above. The simplest conceivable way to use UV−vis light for the characterization of liquid/solid interfaces is via the acquisition of absorption spectra, to obtain information about the electronic structure of the relevant species at the interface. Other optical spectroscopies in this family include fluorescence emission spectroscopy, which does require the use of flourophores, and second harmonic generation (SHG), a nonlinear spectroscopy based on a simplified version of SFG involving only one excitation source. Techniques based on wave propagations and/or optical transducers such as surface plasmon resonance (SPR) and ellipsometry are also popular in some fields involving liquid/solid interfaces, and equivalent approaches based on acoustic resonators, quartz crystal microbalances (QCM) in particular, have proven fairly insightful as well. Most of these techniques lack the molecular-level information available from IR absorption, Raman, or SFG spectroscopies, but are nevertheless quite useful to follow electronic changes and also adsorption kinetics in liquid/solid interfaces. A brief discussion of these is provided next.

4.1. UV−vis Absorption Spectroscopy

UV−vis radiation covers energies on the order of a few electronvolts, a range typically associated with the excitation of electrons from valence bands or shallow molecular electronic levels into the conduction bands or unoccupied orbitals of solids or molecules. Accordingly, UV−vis absorption spectroscopy typically probes those electronic transitions. Multiple absorption bands may be observed within the signal associated with excitation between a given pair of electronic levels, because those may be coupled with the vibrational motions of the solid or molecule being probed. Detection of such vibronic bands could add much detailed molecular information about the system being studied, but, unfortunately, they can usually be well resolved into separate sharp peaks only in the spectra of gas-phase molecules, and tend to broaden and merge into a single broad and structureless feature in condensed phases. In spite of the loss of vibrational information due to this broadening of vibronic peaks, UV−vis absorption spectroscopy is still used extensively to study chemistry in solutions. In contrast, and perhaps surprisingly, it is not commonly employed for the study of liquid/solid interfaces. One possible reason for this may be that weak UV−vis absorption signals from species at liquid/solid interfaces are easily obscured by the much more intense broad bands due to the liquid phase. To bypass this limitation, many studies of adsorption kinetics using UV−vis absorption spectroscopy rely on the indirect measurement of the concentration of the adsorbate molecules in solution before versus after the uptake. There are also many reports where UV−vis absorption spectroscopy has been used to characterize solids ex-situ after exposure to given solutions. Only in a few instances UV−vis absorption spectroscopy has proven viable as a way to characterize adsorption processes in situ, usually with systems where strong chromophores or where high surface-area solids are involved.

One area where UV−vis absorption spectroscopy has been often used is to follow the kinetics of layer-by-layer organic film growth at liquid/solid interfaces. For instance, in one study, the alternating adsorption of monolayers of anionic and cationic polyelectrolytes, of polystyrenesulfonate and poly-4-vinylbenzyl-(*N*,*N*-diethyl-*N*-methyl-)-ammonium iodide, on charged surfaces (the native surface of a silicon wafer) were monitored by measuring the optical absorbance of the phenyl chromophores at 225 nm.[191] A similar approach was also used to follow the kinetics of adsorption of poly(*o*-methoxyaniline) on hydrophilized glass, tetrafluorethylenepropylene, and indium tin oxide substrates.[192] This example is particularly interesting in that it shows how UV−vis absorption spectroscopy can be used to unravel complex kinetics: adsorption was shown to occur in two stages, an initial first-order uptake followed by a second stage with much longer characteristic times and an exponential behavior typical of diffusion-controlled processes involving the small domains formed during the first. Layer-by-layer growth has also been established during self-assembly of colloidal systems, as in the case of a hydrogen-bonding-based assembly of CdSe nanoparticles.[193] More recently, UV−vis absorption spectroscopy has been employed to obtain adsorption kinetics on the layer-by-layer buildup of protein layers on electrodes for biosensing applications.[194,195] For instance, linear film growth was established in studies on the alternate adsorption of negatively charged clay platelets (from aqueous dispersions) and positively charged hemoglobin (from pH 4.5 buffers) based on the fact that the Soret absorbance at 412 nm increases linearly with increasing number of protein layers.[194] In contrast, no significant shifts in that Soret absorbance were observed upon adsorption of the related cytochrome $P450_{cam}$, indicating that the colloidal clay particles exert no influence on its heme or secondary structure.[196]

It has been established that, with many chromophores, their adsorption on solid surfaces leads to red shifts in their energy of maximum UV−vis absorption. One example of this, from a study aimed to understand the incorporation of nitroaromatic compounds (fertilizers, explosives) in soils, is the 10 nm red shift of the $\pi-\pi^*$ band of the aromatic ring that occurs upon the uptake of 1,3,5-trinitrobenzene on K^+- and Cs^+-hectorite clays, indicative of an electron donor−acceptor adsorption mechanism.[197] In a separate study, the adsorption of tetramethylpyridylporphyrin onto Laponite was shown to lead to a ∼30 nm red shift in the UV−vis absorption maximum for molecules on the outside surfaces and to a ∼60 nm shift in the dyes trapped in the interlamellar galleries.[198] Past reports had justified those shifts in terms of diprotonation of the porphyrin, but in this work an additional contribution from sterically induced hindrance was highlighted. Perhaps even more interesting is the work by Gautier and Bürgi on the protection of gold nanoparticles with adsorbed chiral *N*-isobutyryl-cysteine.[199] They found that those systems display absorption spectra with well-quantized electronic structures, the onset of which is controlled by the metal core of the particle, and that the adsorption of thiols modifies the frontier orbitals and leads to considerable deformation of that core. In yet another case, in connection with the recent interest in the development of solar cell, the red shifts seen in the UV−vis absorption spectra from several ruthenium colored complexes adsorbed on titania films have been interpreted as due to covalent anchoring of the dye via its carboxylate group.[200,201] The resulting ester linkage is presumed to lead to the desired increase in photoenergy conversion efficiency. Similar red shifts associated with stronger bonding to titania surfaces have also been seen with porphyrins.[202]

UV−vis absorption spectroscopy can also be used to obtain more detailed kinetics, or even fast dynamic, information.

For, this, the absorption of light of a fixed energy, often from a pulsed laser, is followed as a function of time; the use of picosecond lasers affords the study of the dynamics of fast electronic transitions this way. In an example involving photoactive systems, the time constant of the forward electron transfer in 9-anthracenecarboxylic acid bound to titania nanoparticles was determined to be less than 350 fs, whereas the reverse electron transfer in absolute ethanol solutions was measured to occur on a 33 ± 2 ps time scale.[203] Interestingly, it was also observed that the addition of small amounts of water to the TiO_2/ethanol solutions leads to a red shift in the absorbance spectrum and increases the overall rate of back electron transfer. The authors attributed that behavior to the reoxidation of the Ti(III) oxygen vacancy defect sites originally present at the surface of the titania nanoparticles.

4.2. Fluorescence Emission Spectroscopy

A closely related technique to UV−vis absorption is fluorescence emission spectroscopy. In this case, what is followed is not the direct absorption of the incoming photons but rather the emitted light emanating from the sample as it returns from the excited state to its ground electronic state. The detected fluorescence (or phosphorescence) is usually proportional to the concentration of the fluorophore being probed, a relationship that can be used to quantitatively measure concentrations at liquid/solid interfaces. The most common uses of fluorescence emission spectroscopy are for the detection of adsorption and for kinetic measurements of adsorption processes. One advantage of the use of fluorescence emission is that, since those photons are emitted in all directions, they can be detected away from the incident excitation beam to help minimize the background signal. They can also display specific energy and/or angular patterns, a fact that can be used to discriminate the fluorescence originating from specific chromophores against other sources of light. Nevertheless, these advantages are not always sufficient to selectively obtain information on adsorbates in liquid/solid interfaces. Moreover, fluorescence emission spectroscopy is limited to the characterization of fluorescent molecules, otherwise a fluorescent dye needs to be added to the system. All together, it can be said that, like UV−vis absorption spectroscopy, fluorescence emission spectroscopy has not been widely used for the study of specific chemistry at liquid/solid interfaces. In the next paragraphs a few examples are provided to illustrate the range of information that has been acquired with this technique.

Fluorescence emission spectroscopy has been particularly useful to probe the size, polarity, viscosity, and aggregation number of surfactant assemblies such as micelles, reverse micelles, and colloids.[204] It has also been used to characterize the interaction of micelles and other membrane-like systems with proteins, drugs, and other biologically relevant molecules. One example of this is provided by the study of the aggregation and adsorption of sodium dodecyl sulfate in water-acetamide mixtures, where thermodynamic parameters were estimated as function of the composition of the liquid phase: a switch from ionic to nonionic behavior was observed in the surfactant as the percentage of acetamide was increased beyond 30% in the liquid media.[205] In another study, the role of electrostatics on the adsorption of proteins to both negatively charged and neutral small unilamellar vesicles was monitored as a function of the pH of the solution.[206] In that case, the fluorescence emission of positively charged proteins was found to increase after adsorption on negatively charged vesicles, and neutralization of the charge of the vesicles was determined to be the controlling factor in the adsorption. In a third case, the arrangement of the local anesthetic tetracaine within unilamellar vesicles was determined, by measuring the saturating blue shifts of fluorescence emission at high lipid:tetracaine ratio as a way to estimate depth of penetration, to involve the tertiary amine of the drug near the phosphate of the headgroup of the vesicles, its ester bond in the region of the lipids, and the aromatic moiety near the fatty acyl carbons labeled 2 to 5.[207] A fourth, even more biologically relevant, example is that where fluorescence emission was used to determine that bacterial rproSP-$B_{\Delta C}$, a model for the human SP-B protein required to maintain the lungs open after birth, is properly folded (after which it can be dissolved in buffers, the way it was detected) and interacts strongly with zwitterionic or anionic phospholipids vesicles, as required to produced mature SP-B.[208]

Fluorescence detection has also become popular as a way to detect large molecules anchored or adsorbed on solid surfaces, many of them of biological relevance. The detection of fluorescence emission can be used to quantify specific binding to surfaces, assess surface homogeneity at the micrometer scale, or detect protein aggregation.[209] Most applications follow the same format described above, where the intensity of the fluorescence signal is used to quantify the concentration of the fluorophores at the interface and that information then used to acquire uptake kinetics. This is also true in the examples provided in the previous paragraphs; the complex conclusions reported there on other aspects of the interfacial chemistry of interest were reached by combining clever experimental designs with some degree of speculation. However, fluorescence lifetime and anisotropy measurements within short time scales can provide additional information on molecular dynamics, and, with that, knowledge on the direction and specificity of protein adsorption onto solid surfaces.[210] In one example, fluorescent probes were attached to different areas of the surface of the protein human carbonic anhydrase II to resolve the direction in which it binds to negatively charged silica nanoparticles: it was shown that the adsorption of the native protein is specific to limited regions of the external N-terminal domain of the protein, and that the adsorption direction is strongly pH-dependent.[211] Many recent setups of fluorescence emission spectroscopy have also been designed for the detection of single molecules, and are often used in microscopy mode; a few examples of fluorescence-based microscopy will be provided later in Section 7.1.

Time-resolve fluorescence emission spectroscopy studies can be used to extract information about the photophysical behavior of the system.[210] One of the earlier and best know fluorophores developed for time-resolved studies of biological systems is the green fluorescent protein (GFP) derived from the jellyfish *Aequorea victoria*.[212,213] In a study involving aerated aqueous polymer gels, it was determined that excitation of the anchored protein with 488-nm light leads to repeated cycles of fluorescent emission on a time scale of several seconds until reaching a long-lasting dark state, from which the protein can be switched back to the original emissive state by irradiation at 405 nm.[214] This behavior has been extensively exploited since by using GFP as a fluorescent marker for time-dependent cell processes.

Fluorescence emission spectroscopy is also ideal to probe photophysical properties of polymers and other solids in materials science problems such as those associated with the making of electro-luminescent optoelectronic devices. In one case, the behavior of *para*-phenylene vinylene and *para*-phenylene

ethynylene luminescent polymers was contrasted in solid thin films on fused silica substrates versus dissolved in liquid tetrahydrofuran.[215] It was found that the absorption spectra peaks are red-shifted and broadened in the solid compared to those obtained in THF solution, and that the film absorption spectra are more structured in the long-wavelength region. In another example, connected to the development of solid-state tunable lasers using molecular dopants, the spontaneous-emission (fluorescence) cross section of Eu^{3+} ions embedded into a silica gel matrix was shown to increase by several orders of magnitude via chelation.[216] In general, though, the focus in these studies has been on detailing the luminescence properties of materials, not on following their interfacial chemistry. One fluorescence spectroscopy study in which chemical information was extracted is that where the conformational behavior of pyrene-labeled poly(maleic acid-co-propylene) was characterized at an alumina surface: the degree of coiling on the surface was determined to change to a more stretched conformation upon adsorption at low pHs.[217] A fluorescence emission spectroscopy study of liquid crystals, specifically of tetraphenylpyrene, highlights the difficulties of predicting the self-organization of building blocks in liquid-crystalline fluorescent columns: structure forming principles such as microsegregation were found not to apply.[218] In connection with electrochemistry, fluorescence emission spectroscopy was used, for instance, to determine that the adsorption/desorption and oxidation of vitamin B6 at a polycrystalline gold electrode in the presence of an aqueous KOH solution is accompanied by a strong electrogenerated fluorescence emission peaking at 443 nm when excited at 360 nm.[219] That observation helped established that the adsorption and desorption of the oxidation product occur in the double layer region.

Another useful application of fluorescence emission has been as a detection method in chromatography. In most cases fluorescence has been used as a way to detect and quantify different molecules as they are eluted from the chromatographic column, but in some instances the adsorption/desorption process itself has been investigated with this technique. For instance, molecularly imprinted polymers have been evaluated as potential solid-phase adsorbents for the quantitative enrichment of polycyclic aromatic hydrocarbons in coastal sediments, atmospheric particulates, and industrial effluents.[220] Hemimicelle-capped carbon nanotubes have also been tested with the help of fluorescence emission spectroscopy as solid-phase extraction adsorbents in environmental analysis, specifically for the detection of low concentration of arsenic in water samples.[221] A third example is a study on the mechanism of unfolding of calcium-depleted bovine α-lactalbumin adsorbed on methyl- and ethyl-polyether phases bonded to porous silica, which were used as weakly hydrophobic chromatographic surfaces: a slow change in emission maximum from 330 to 350 nm and a 4-fold increase in intensity were seen for the protein adsorbed on the two supports.[222] In all these examples fluorescence emission spectroscopy has provided a convenient way to assess and quantify adsorption on the stationary phase of the chromatographic columns but not much insight on the actual chemistry of adsorption. It should also be said that in these examples the systems studied do not always display significant interactions at the liquid/solid interfaces.

Applications of fluorescence emission spectroscopy to other fields are scarcer. In one interesting application, Nile red was used for the visualization of the adsorption behavior of two immiscible liquid fluids within a pore network containing a homogeneous array of pillars in silicon oxide surfaces, one that wets and another that does not.[223] Taking advantage of the fact that the fluorescence emission spectra are sensitive to the solvent environment, the two phases could be distinguished by the color of the fluorescence emission band: a network of obstacles defining a tortuous flow path for the nonwetting phase was observed.

Fluorescence emission experiments can be set up in total internal reflection (TIRF) mode, in an arrangement where the evanescent wave generated by the total reflection of the incident light off a liquid/solid interface is used to selectively illuminate fluorophores up to the intrinsic penetration depth of the wave. This approach is similar to that used in ATR IR absorption spectroscopy, only the penetration depth with visible or UV light is on the order of a hundred nanometers. The advantage of TIRF over the regular fluorescence emission spectroscopy experiments is that the light does not need to travel through the liquid phase, a fact that tends to attenuate the total signal. On the other hand, a more complex optical setup is required. Although TIRF is not as commonly used as the direct arrangement, it is similarly viable for the in situ study of protein adsorption and time-dependent protein reorientations at liquid/solid interfaces, and can also be set up in microscopy mode. Most of the examples available in the literature on the use of TIRF for the characterization of liquid/solid interfaces involve biological systems. In one example, TIRF measurements of the adsorption kinetics of fibrinogen onto unmodified and aminopropylsilane-modified quartz glass surfaces indicated only simple first-order kinetics at low initial concentrations of the protein but two first-order kinetic regimes at higher concentrations.[224] In another study, the reversible adsorption kinetics of a cationic dye molecule at a silica surface modified with a C-18 self-assembled layer was measured by using a fluorescence correlation spectroscopy experiment.[225] In that case, the rate at which spontaneous fluctuations in the population of dye molecules within the interfacial volume occurs was used to establish the rate of transport of molecules to the interface and their adsorption kinetics. Regarding correlations of adsorption and reorientation kinetics, a TIRF study on the uptake of the chicken egg lysozyme on silica surfaces identified a two-stage adsorption process, the first involving a reorientation to optimize lysozyme interaction with the charged surface and reduce lateral repulsions between adsorbed protein molecules, and a second of slow restructuring as the adsorbed layer approaches saturation via the filling of the surface vacancies made accessible by the first reorientation.[226]

Fluorescence emission can also be detected and analyzed simultaneously during Raman spectroscopy experiments, in particular when using UV or visible excitation sources. In an UV−Raman (λ = 244 nm) spectroscopy investigation of the host−guest interactions of benzene molecules adsorbed within the pores of MFI zeolites, for instance, the fluorescence spectra displayed well-resolved vibronic benzene bands, suggesting that the adsorbed molecules are not clustered.[227]

4.3. Second Harmonic Generation (SHG)

Second harmonic generation (SHG) is a two-photon process where both photons are provided by the same laser (Figure 5, left, bottom). It is a simplified version of SFG, and shares many of the properties of that technique, including its dependence on the second order susceptibility $\chi^{(2)}$ that makes the technique sensitive to noncentrosymmetrical interfaces (the reason why both SFG and SHG are well-suited to probe liquid/solid

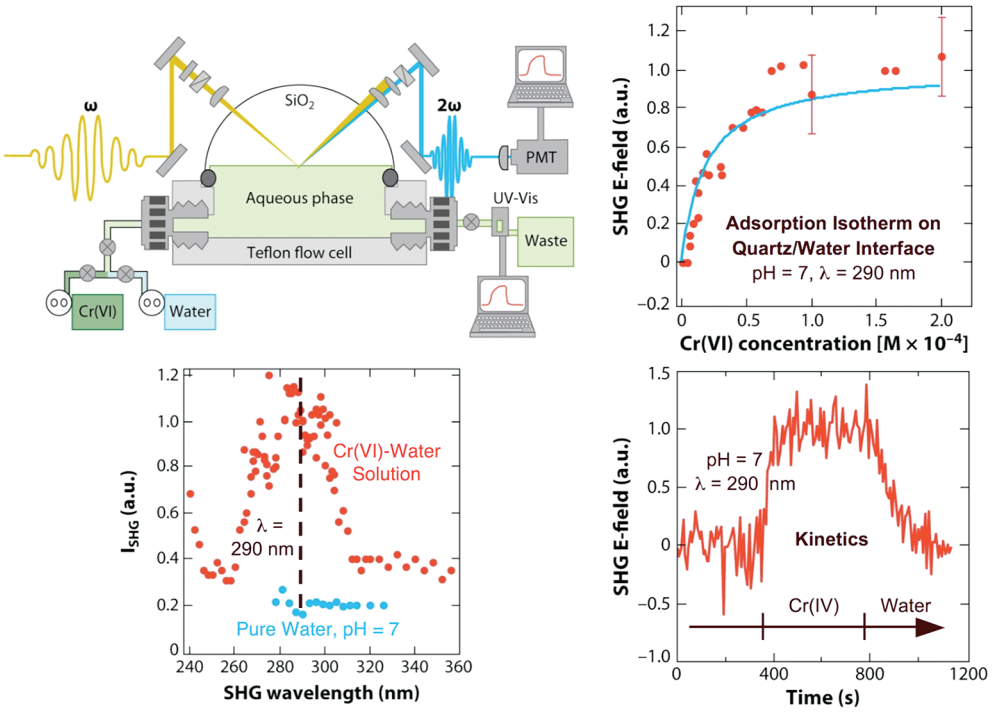

Figure 10. Example of the use of in situ SHG to study adsorption at liquid/solid interfaces.[982] Top, Left: Experimental setup. This instrument was used to acquire the thermodynamic and kinetics data on the adsorption of chromate ions at the water/fused quartz interface shown in the rest of the figure. Bottom, Left: SHG spectra versus wavelength for clean (blue circles) and chromate-covered (red circles) quartz samples, reflecting the absorption spectrum of the adsorbed Cr(VI) ions. The maximum in absorption at λ = 290 nm was used for further characterization. Top, Right: Adsorption isotherm for Cr(VI) on the water/quartz interface as a function of concentration in solution, showing Langmuir behavior. Bottom, Right: Kinetics of adsorption, indicating monolayer saturation and full reversibility. Courtesy of Franz M. Geiger. Reprinted from ref. 982 with permission. Copyright 2003 American Chemical Society.

interfaces).[228] However, because the excitation light used in SHG is typically in the visible range, most of the information extracted from the data is related to electronic (rather than vibrational) properties of the system. Additional knowledge can usually be extracted from results of SHG experiments on related properties such as adsorbate coverages and adsorption geometries (by using polarized light). Like SFG, expensive lasers (one in this case) and optics may be required, and the use of flat surfaces may be preferred, to collect the signal in reflectance mode.

Similarly to UV−vis absorption and fluorescence emission spectroscopies, SHG is most often used as a way to follow the kinetics of uptake of adsorbates at liquid/solid interfaces. One example is provided by the data from the group of Geiger reported in Figure 10, which shows kinetic and isothermal data on the uptake of chromates on alkyl-esters-derivatized quartz surfaces.[229] The results proved the good chelating properties of the anchored ester groups for the removal of Cr(VI) species from solution. Similar adsorption isotherms have also been measured with SHG for the uptake of Ca, Zn, and Cd ions from water onto a fused quartz interface,[230] and for zinc ions on silica-anchored glucose; adsorption in the latter case proved stronger than with carbohydrates in solution.[231]

In some instances, SHG data can be used to draw inferences on the chemical changes induced by adsorption at liquid/solid interfaces. This was the case, for example, in the study of the reductive desorption of self-assembled monolayers dispersed on a Au(111)/mica film into a KOH solution as a function of the length of the aliphatic spacer chain and of the preparation temperature.[232] Sandwich dimerization and in-plane association have also been reported, based on SHG data, on Rhodamine dyes upon adsorption at hydrophobized silica/water interfaces.[233] A phase shift in the SHG signals from the thiol and nitroaniline ends during the uptake of *p*-nitroanilino-dodecane thiol onto a polycrystalline gold film was explained by repulsive intermolecular interaction.[234]

SHG has been used to evaluate the acidity of oxides and derivatized surfaces immersed in solution. For instance, in one study, the acidity of organic acid-functionalized silica surfaces in water was followed by SHG versus the pH of the solution to obtain a titration curve from which K_a constants were extracted.[235] SHG has also been used to determine the extent of protonation on titania (110) single-crystal surfaces immersed in water.[236] Related electrical properties can be extracted from SHG measurements too: the electrostatic surface charge has been estimated this way on single-crystal surfaces of alumina,[237] the pH and ionic strength dependence of the point of zero charge of the interface between a corundum flat surface (a prism) and water has also been determined by SHG,[238] and the dielectric constants of trans-4-[4-(dibutylamino)styryl]-1-methylpyridinium iodide and trans-4-[4-(dibutylamino)styryl]-1-(3-sulfopropyl) pyridinium has been measured with SHG at a acetonitrile/silica interface as a function of interfacial density.[239]

In electrochemistry, structural information may be obtained about the surface of the electrode, as in the early SHG study that focused on the formation and lifting of a surface reconstruction in Au(111) single-crystal electrodes as a function of applied potential and the adsorption of ions or small organic molecules.[240,241]

dx.doi.org/10.1021/cr2002068 |*Chem. Rev.* 2012, 112, 2920–2986

In terms of electrochemical reactions, correlations have been identified between SHG signals and the catalytic performance of molybdenum[242] and platinum[243] electrodes for the production of hydrogen, presumably because of free electron-mediated changes in surface conditions. The structure sensitivity of the anodic oxidation of carbon monoxide has been investigated by contrasting the voltage dependence of its coverage on Pt(111) versus Pt(997) single-crystal electrodes in a CO-saturated $HClO_4$ electrolyte.[244]

One use for which SHG is particularly appropriate is to characterize the effect of localized interactions of solvents on the electronic structure and polarizability of adsorbates in liquid/solid interfaces. For instance, it has been shown that the first allowed electronic transition for *N*-methyl-*p*-methoxyaniline adsorbed on silica surfaces remains almost constant in non-hydrogen-bonding solvents regardless of solvent polarity but shifts to longer wavelengths in hydrogen-bond-accepting solvents such as dimethylsulfoxide and to shorter wavelengths in hydrogen-bond-donating solvents such as water.[245] In another case, resonance-enhanced SHG was used to study the effect of solvent polarity on the adsorption of 4-aminobenzophenone, a chromophore, onto a hydrophilic silica surface: weakly associating systems consisting of polar substrates and nonpolar solvents were found to be more polar than bulk solutions.[246] In a third investigation on interfacial polarity, the SHG signal of *p*-nitroanisole showed a dependence on solvent structure, in contrast to indoline, which proved insensitive to solvent identity and reliant on the hydrogen-bond donating properties of the polar silica substrate instead.[247]

The anisotropy of the SHG signal can be used to obtain geometrical information from liquid/solid interfaces involving crystalline solids. This is commonly achieved by choosing appropriate combinations of linear polarizations for the incident and outgoing beams. In one of the first examples of the application of SHG to the study of liquid/solid interfaces, the group of Shen already contrasted the average arrangement and orientation of *p*-nitrobenzoic acid adsorbed at air-silica versus ethanol-silica interfaces.[248] More recently, the increase in SHG signal to certain orientations was used to follow the removal of the native amorphous silicon oxide layer present on Si(111) single-crystal electrodes.[249] In a *n*-GaAs electrode in a sulfuric acid solution, the rotational anisotropy in the nonlinear response of the second harmonic signal using a *p*-in/*p*-out polarization configuration was found to depend both on the doping level and the applied potential and to be closely relate to the population of surface states.[250] Perhaps a more interesting version of this approach is the use of differential SHG detection from right and left circularly polarized incident light to extract chiral information from the surface. This scheme has been used to study the adsorption of cytochrome c at the interface between a liquid and various self-assembled mono- and bilayers,[251] and to follow the enantioselective adsorption of chiral naphtols on lipid bilayers.[252,253] Another chiral SHG study, on the adsorption of bovine serum albumin at aqueous/silica interfaces, indicated slow conformational changes within the protein layer after adsorption consistent with protein denaturation.[254]

SHG has also been implemented to probe nonflat surfaces, especially nano- and microparticles.[255] The scattered, rather than the reflected, SHG light is collected in these cases, a change that typically results in much weaker signals. This problem has been addressed in some instances by relying on the use of a dye molecule with strong hyperpolarizability such as malachite green. Experiments with aqueous colloidal particles consisting of malachite green adsorbed on spherical polystyrene beads have been useful to better understand the angular dependence of the second harmonic generation,[256] and additional studies on similar systems have added knowledge on the effect of particle size and concentration on adsorption.[257] Studies contrasting the uptake of malachite green on chemically homogeneous plain polystyrene beads versus more heterogeneous carboxylated and hydroxylated polystyrene surfaces identified only one single type of adsorption site on the former but multiple adsorption sites on the latter.[258] On carbon black microparticles in aqueous solution, results from the monitoring of the SHG signal of adsorbed malachite green were used to establish that there is a strong correlation between the uptake of the dye and the oxygen-to-carbon ratio of the surfaces, with particle surfaces with higher O/C ratios appearing to be more hydrophilic.[259] Similar adsorption uptake SHG experiments have been carried out for malachite green on gold nanoparticles.[260] Note, however, that the results obtained with malachite green are not always extendable to other more relevant systems, a serious limitation of this approach.

SHG studies are sometimes viable without requiring the use of particular dyes in systems involving nonflat surfaces. In a chemically relevant study, for instance, SHG was used to measure the pK_a for the protonation of the carboxyl functional groups at the surface of polystyrene carboxylate microspheres dispersed in aqueous medium: a decrease in the acidity at the interface compared to that of the same carboxylate groups in bulk aqueous solution was observed.[261] In work with metal nanoparticles, much effort has been place on using SHG to understand the effect of electrolytes on the electronic properties of the colloidal metal nanoparticles themselves.[255] For instance, with gold, it was found that the concentration of the electrolyte in solution affects the aggregation of the colloids and leads to the formation of a noncentrosymmetric entity that enhances the SHG intensity.[262] Another issue amenable to studies using SHG is how the size and structure of the particles affect their interfacial properties. In an interesting contrasting study, SHG data as a function of pH in aqueous media showed two distinct pK_a values on flat silica surfaces but only one discernible type of silanol site on silica nanoparticles.[263] In another investigation, SHG was used to selectively follow the uptake of 4-(2-pyridylazo)resorcinol onto the edges, but not the basal planes, of disk-shaped montmorillonite clay particles.[264] Regarding adsorption energetics, the free energy of the adsorption of catechol on colloidal TiO_2 was extracted from SHG data,[265] and the adsorption of poly L-lysine from an aqueous solution onto biopolymers terminated with negatively charged sulfonate groups and attached to the surface of micrometer-size polystyrene particles was determined to occur with only a small difference in adsorption free energies as a function of chain length and in a relatively flat conformation under acidic conditions.[266]

Finally, SHG can also be used to measure time-dependent phenomena, both on flat surfaces and in nanoparticles or self-assembled layers. For instance, time-resolved SHG studies have been carried out to follow the dynamics of solvation of the flat and polished surface of a silica prism in the picosecond time domain.[267] In electrochemistry, isotropic and one-fold SHG transients have been used to measure the dynamics of surface charge and surface reconstruction, respectively, upon repetitive step voltage application during metal electrodeposition on gold or platinum (111) single-crystal electrodes (in the millisecond

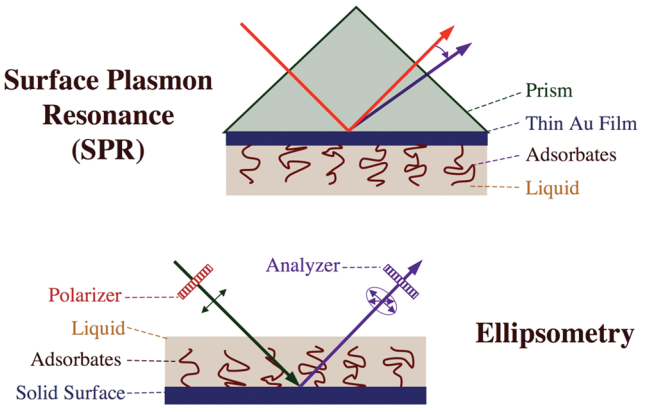

Figure 11. Schematic diagrams of the setups used for surface plasmon resonance (SPR) and ellipsometry. Top: In SPR, a laser beam is used to excite the surface plasmons of a thin gold (or another metal) film deposited on the outer surface of a prism, where adsorption from the liquid phase is to be probed. The exit angle of the reflected beam depends on the plasmon frequency, and that frequency is affected by the adsorption process. Bottom: In ellipsometry, a linearly polarized beam is reflected off the liquid/solid interface, and the elliptical polarization that results from interaction with the film at the interface is analyzed to extract information about its thickness.

range in this case).[268] A time-resolved SHG study of the photochemistry of azobenzene at the interface between an alkane solvent and a pyridinium-modified glass surface highlighted the electrostatic interactions between azobenzene and viologen at the solid/liquid interface.[269]

One problem that has been well studied using time-resolved SHG is the crossing of molecules through liposome bilayers, which has been followed by the flipping in orientation expected upon the switch in adsorption from the outer to the inner surfaces of the liposome. The idea was initially tested with malachite green, in a study that showed that diffusion across the bilayer is relatively fast, taking place in less than one second.[270] However, another study with a neutral styryl dye and a neutral dioleoylphosphatidylcholine liposome showed that the diffusion there takes place over a period of hours.[271] It has been suggested that the difference between the two cases may be accounted by the different charges involved or the differences in size of the liposome; other systems have display intermediate time ranges for this diffusion.[272] The dynamics of adsorption has also been probed for surfactants by following their displacement of dye molecules on solid surfaces, in particular for a methacrylate polymeric surfactant on latex and talc particles in an aqueous solution,[273] and the dynamics of the formation of reverse micelles in oil/surfactant/water interface system has been reported as well.[274] Time-resolved SHG studies involving small particles usually required the use of monodispersed samples, but have been recently extended to polydispersed colloidal particles as well.[275]

4.4. Surface Plasmon Resonance (SPR)

An alternative way of following adsorption processes on surfaces using optical methods is by measuring the accompanying changes in refractive index at the liquid/solid interface. The most common techniques that rely on this approach are surface plasmon resonance (SPR) and ellipsometry (Figure 11). In SPR, the conditions for maximum (resonant) excitation of surface plasmons are followed as a function of wavelength and/or incident angle. A typical SPR setup involves a glass prism with a surface covered or in close contact with a thin film of the metal to be probed, typically gold or silver (because they can support surface plasmons) but sometimes other metals such as copper, titanium, or chromium. The light is totally reflected off the inner surface of the prism, and the outward evanescent wave at the interface used to excite the plasmon of the metal. For resonance excitation the change in momentum of the incoming beam has to match that of the surface plasmon, and the SPR technique is based on the fact that adsorbing molecules change the local index of refraction and with that the resonance conditions of the surface plasmon waves. SPR experiments are commonly carried out in one of three modes: (1) by using light of a fixed wavelength and measuring the angle of minimum reflection (maximum absorption), which can change by approximately 0.1° during thin film adsorption (Figure 11, top); (2) by following the changes in absorption wavelength with adsorption; or (3) in imaging mode. Additional new modalities have been developed in recent years, including, for instance, surface plasmon fluorescence spectroscopy.[276]

The need to use a film of a metal that can support surface plasmons does represent a limitation in terms of the types of liquid/solid interfaces that can be studied with SPR. Also, the surfaces need to be flat, or at least able to make good contact with the prism; they need to be placed within the penetration depth of the evanescent wave, typically less than one micrometer. Finally, only limited information, and not much molecular detail, can be extracted from the data. On the positive side, SPR is reasonably easy to implement, and it is quite sensitive to small changes at the liquid/solid interface. SPR is sensitive to nanometer changes in thickness, density fluctuations, or molecular adsorption on the metal film, and has typically been used to measure uptakes from liquid solutions onto solid surfaces.

One use of SPR is for the characterization of the chemistry of Langmuir−Blodgett and other self-assembled films in coexistence with a liquid phase, mainly to determine their thicknesses. SPR data from such systems may also be used to estimate adsorption geometries, although that requires comparison with appropriate modeling (to match measured film thicknesses with the number of monolayers present at the liquid/solid interface). An early illustration of this use is given by a study where a molecular tilt angle of 26° was deduced for monolayers of behenic acid deposited on a thin silver film.[277] In a second report, SPR data were used to conclude that valinomycin molecules in Langmuir−Blodgett films lie nearly parallel to the silver substrate surface, and also that they can reversibly complex with potassium ions when in the presence of stearic acid.[278] Another systematic SPR study on the uptake of a series of cationic and anionic polymer combinations into Langmuir−Blodgett films showed linear adsorption uptake in terms of thickness versus number of layers, except were deviation occurred because of poorly charged initial layers.[279]

As it pertains to liquid/solid interfaces, SPR has been used mostly in connection with the development of biosensors and bioassays based on probing the interactions between an analyte in solution and a biomolecular recognition element immobilized on the surface of the SPR element.[280,281] In bioassays, thin organic or biopolymer films are prepared in a spatially resolved manner at the metal interface, and interrogated either by rastering of the beam used for SPR or by optically imaging the full surface.[282] SPR sensor architectures have been used for the characterization of supported lipid bilayer films, for monitoring antibody−antigen interactions at surfaces, and for the

study of DNA hybridization adsorption and protein−DNA interactions.[281,283−286] This field has grown considerably within the last decades, and many commercial biosensors have been developed based on this technology. A full survey of that work is outside the scope of our review,[287−289] and only a few representative examples are provided below to illustrate the range of the information obtained by SPR in these applications.

In terms of the development of the binding-specificity knowledge needed for the design of simple sensors, much work has focused on the specific interaction of either peptides or proteins with receptor sites at the self-assembled layers used to mimic membranes.[290,291] One early report showed specific recognition reactions between either streptavidin or a biotinylated monoclonal antibody and interfaces functionalized with different types of receptors, self-assembled biotinylated alkane thiols or adsorbed streptavidin monolayers.[292] It was found that, in general, the binding properties are inversely related to the packing density of the receptors: good accessibility is only possible with diluted surface coverages of the receptors. Binding specificity has also been proven for recombinant proteins tagged with the stretch of the six histidines commonly used to simplify their purification, where preferential adsorption occurs via interaction of the histidines with the two vacant sites on Ni(II) ions chelated to the surface nitrilotriacetic acid group of a thiol self-assembled monolayer but not to a second thiol terminated with a tri(ethylene glycol) group.[293] Selective uptake on specific surface groups can be easily assessed by SPR within mixed self-assembled layers as well. For instance, SPR helped determine that the amount of RNase A, lysozyme, fibrinogen, or pyruvate kinase that adsorbs on mixed self-assembled monolayers of gold-supported alkanethiolates terminated in methyl and hexa(ethylene glycol) correlate well with the molar fraction of the methyl-terminated thiolates on the surface.[294] Similar resistance to adsorption on the hydrophilic glycol groups has been reported with a number of other surfactants.[295]

As mentioned above, bioassays can be designed in imaging mode. For instance, Corn and co-workers have developed sensors based on two-dimensional surface arrays made of covalently bonded thiol-DNA strands on gold surfaces, and have used SPR imaging to follow hybridization adsorption of unlabeled DNA and RNA oligonucleotides, relying on the fact that the changes in reflectivity measured by SPR depend linearly on the surface coverage of the adsorbed DNA oligonucleotide (Figure 12).[282,296] In another application, SPR in imaging mode has been combined with microfluidic device design to provide easy spatial patterns for antibody capturing.[297] More sophisticated SPR sensors have also been designed to rely on the multiplexing of sensing channels to acquire full spectroscopic information for each spatial position as a function of wavelength or angular spread.[298] Interferometry to detect the phase of a beam reflected under SPR has been incorporated to bio and chemical sensing to increase sensitivity and spatial resolution at the micrometer scale as well.[299] In all these cases, however, the basic information extracted from SPR is still the same, usually quantitative knowledge on coverages or film thicknesses in a selective way for particular chemical interactions at the liquid/solid interface.

SPR can also be used in time-resolved mode to follow the kinetics of adsorption and desorption at liquid/solid interfaces.[300] In one example, the use of SPR led to the finding that the total uptake of thiolated dextrans from solution onto a gold surface increases with decreasing molecular weight and degree of thiol substitution even if the rate of adsorption appears to be similar in all cases.[301] A kinetic approach has also been used to study the

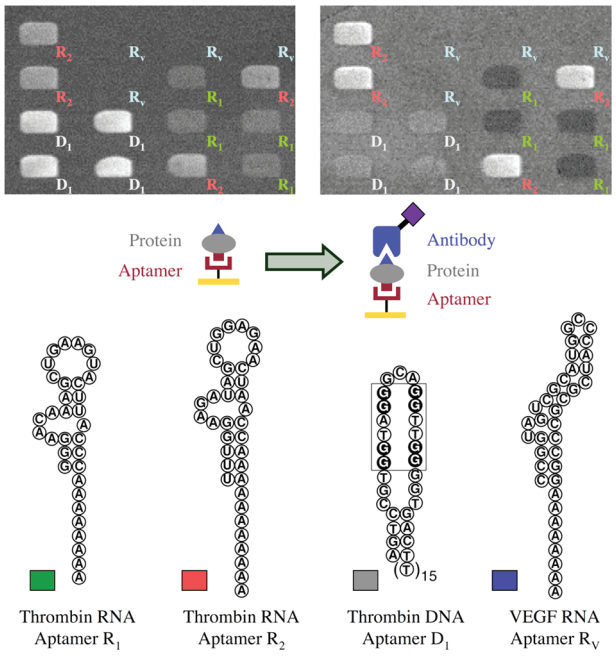

Figure 12. Design of bioassays based on SPR imaging. In this example, measurements are shown for the formation of surface aptamer−protein−antibody sandwich structures.[983] Four different aptamers were first anchored on the surface, the structures of which are shown schematically in the bottom half of the figure: R_1, an RNA aptamer for human thrombin; R_2, an RNA aptamer that was selected for bovine thrombin but can also bind to human thrombin; D_1, a DNA aptamer for human thrombin; and R_V, an RNA aptamer for human vascular endothelial growth factor. These aptamers were made into a bioassay by distributing them in rectangular patches as indicated in the images on the top. The images correspond to the SPR signals obtained after sequential exposure of the bioassay to (Left) human thrombin (hTh), a serine protease commonly used to enhance clot formation in blood samples; and (Right) a monoclonal antibody for hTh. The intensity of the signals in these images indicate that all three thrombin aptamers showed some binding affinity to hTh, with the D_1 aptamer being the highest, but that the antibody can only bind to the hTh-R_2 aptamer surface complex. Courtesy of Robert M. Corn. Reprinted from ref. 983 with permission. Copyright 2007 American Chemical Society.

relative affinities of proteins to different terminal groups within anchored self-assembled monolayers.[300,302,303] For instance, the nonspecific binding of human immunoglobulin G and bovine serum albumin on gold surfaces modified by self-assembled alkyl thiol monolayers with different terminal groups was found to exhibit a complex kinetic behavior that could only be explained in terms of multiple adsorption sites involving different hydrophobic, electrostatic, and hydrogen-bond protein−surface interactions as well as additional lateral interactions due to unfolding of the adsorbed proteins.[304] Another SPR investigation, on the kinetics of the binding reaction between fibrinogen and purified human platelet glycoprotein IIb−IIIa immobilized on the surface of a sensor, led to the identification of the early formation of a reversible low-affinity complex before the development of a second more stable pair.[305]

Interestingly, SPR has, to date, not been used nearly as widely in other fields involving liquid/solid interfaces. In terms of self-assembly processes, the kinetics of formation of thiol films onto gold surfaces has been followed as a function of chain length and concentration.[306] Complex behavior has sometimes been seen, as

in the case of ethanol, for which at least three distinct kinetics steps were identified, the first and third following Langmuir behavior and the second a zeroth order process that depends on alkanethiol chain length, concentration, and partial film thickness.[307] With polymers, SPR has been helpful mainly in following the kinetics of their adsorption on solid surfaces, but in some instances it has also been used to characterize their reactivity in the presence of a liquid phase. One illustration here is the study of the hydration of a series of polyurethanes with poly(ethylene oxide)/poly(propylene oxide) soft segments.[308] The data proved that as the poly(ethylene oxide) content of the polymer, and with that its hydrophilicity, increases, the extent of polymer hydration increases. SPR has also been applied to systems of tribological interest, in one case to determine the uptake kinetics of the perfluoropolyether lubricant Fomblin ZDOL onto a silver surface.[309] In electrocatalysis, the alternated electrostatic layer-by-layer assembly of negatively charged citrate-stabilized platinum nanoparticles and positively charged [tetrakis(*N*-methylpyridyl)porphyrinato] cobalt on a 4-aminobenzoic acid-modified glassy carbon electrode was studied with SPR.[310] In all these examples the main information derived from the SPR experiments is kinetic data on adsorption uptake.

Finally, SPR has also been used in some instances to directly explore chemistry at the liquid/solid interface of metal nanoparticles, for which those need to be deposited on top of the outside surface of the optical element (prism). One example is provided by the study of the effect of exposing silver colloidal nanoparticles to either iodine or iodide solutions, where SPR data were used to conclude that, in the range of small concentrations, surface oxidation leads not to the formation of bulk AgI but rather a new $Ag^{\delta+}I^{-}$ surface structure.[311] However, the use of SPR with nanoparticles has by and large concentrated on sensing, as with the more common thin-film SPR arrangement. In one report, a general discussion is provided on the effect of the morphology of metal nanoparticles on their sensing response.[103] In a more specific application, an SPR nanosensor based on Ag nanotriangles was used to follow the interaction between amyloid β-derived diffusible ligands and their antibody, a chemistry of relevance to the development of Alzheimer's disease.[312] Another study proved the usefulness of recoding scattered SPR signals from gold nanoparticles in imaging mode as a way to develop biosensors in living whole cells.[313] In that case, the specific binding of gold nanoparticles conjugated to monoclonal anti-epidermal growth factor receptor antibodies to the surface of malignant epithelial cell lines in cell cultures was used to provide anatomic labeling information on cancer type cells. To note is the fact that in most of these uses of SPR, the nanoparticles used are mainly made out of gold or silver, the preferred metals for plasmon excitation.

4.5. Ellipsometry

Like SPR, ellipsometry monitors the refractive index at the liquid/solid interface. In this case, though, what is followed is the change of polarization of the light reflected off the sample (Figure 11, bottom). The most common use of ellipsometry is to measure film thickness, the same as SPR, which in this case can be followed in a range from a few angstroms to several micrometers. Nevertheless, the complex refractive index measured by ellipsometry can sometimes be related to other sample properties, including morphology, crystal quality, chemical composition, and electrical conductivity. Because of its lack of chemical specificity, however, ellipsometry cannot typically differentiate among contributions from different adsorbates. In addition, proper analysis of the raw ellipsometry data requires some knowledge of the optical properties of the samples being studied. In terms of the experimental setup, ellipsometry can be considered complementary to SPR (and QCM, see Section 4.6).[145] It does not require the use of gold or silver films, like SPR does (although a reflective surface is still needed), but it does need for the beam of light to travel through the liquid phase, which can attenuate its intensity or even interfere with the polarization measurements.[314]

Much of the work regarding liquid/solid interfaces using ellipsometry has been directed at systems of biological interest, as with SPR.[315,316] Although more data are available in this area from SPR studies than from ellipsometry work, the conclusions derived from both are closely related. Early ellipsometry studies focused on the detection and quantitation of protein adsorption patterns on self-assembled alkanethiolate monolayers, to extract information about specific binding of antibodies to surfaces. For instance, in studies on antifibrinogen binding to adsorbed fibrinogen, it was shown that in simple cases the deposited amount of antibodies correlates well to the true amount of adsorbed antigen but that when proteins are adsorbed from serum, plasma, or other complex solutions, that relationship may be compromised.[315] In experiments involving complement activation on mercapto-glycerol/gold surfaces, it was found that immunoglobulins from human serum bind extensively to the surface but that the ellipsometrically measured thickness decreases with time.[317] Another early example illustrates the use of ellipsometry in the determination of dissociation constants for the adsorption of prothrombin from a buffer solution onto the different binding sites of phosphatidylserine layers stacked on chromium slides.[318] More recently, an ellipsometry study on the adsorption and formation of DNA and cationic surfactant complexes at aqueous/silica interfaces indicated no uptake on negatively charged hydrophilic surfaces for DNA but measurable adsorption when there is an excess of cationic surfactant, just below the point of phase separation.[319] In an ellipsometry investigation of the structure of salivary films in conditions similar to those found in the oral cavity, two sublayer structures were identified in which an inner dense layer is decorated by large aggregates; it was concluded that large mucins may be responsible for the increased resistance of those films on hydrophobic substrates and may protect the intraoral surfaces against surface-active components present in oral health care products.[320]

In terms of nonbiological applications related to liquid/solid interfaces, ellipsometry is perhaps more commonly used than SPR, in particular for the characterization of self-assembled monolayers.[321,322] One classic report identified distinct differences in structure between long- and short-chain *n*-alkyl thiol monolayers when assembled on gold surfaces, with only the long-chain thiols forming densely packed, crystalline-like assemblies with fully extended alkyl chains.[323] Another ellipsometry study, on the removal of ferrocenylalkanethiol self-assembled monolayers deposited from perchloric and sulfuric acid solutions onto a gold electrode by anodic oxidation, showed an increase in thickness at potentials lower than that required for oxide formation, presumably because of oxidation of the ferrocenyl tail group to a ferricinium cation and the simultaneous uptake of anions from the electrolyte.[324] It should be pointed out, though, that in these and many other examples, the use of ellipsometry has been complemented with that of other techniques to reach some of the

molecular-level descriptions associated with the conclusions, since the information derived from the ellipsometry characterization alone is often limited to film thicknesses.

Another use of ellipsometry has been in the study of liquid crystals, to obtain information about ordering, phase transitions, and film thicknesses, both in static and kinetic modes.[325] In one case, it was shown that the ellipsometry signal from liquid-crystal films can in some instances follow characteristic oscillations as a function of temperature, a reflection of different temperature-dependent behavior of each component in mixed anticlinic and azimuthal-helix layers.[326] In another example, ellipsometry was used to identify a wall-induced orientational ordering of a liquid crystal in its isotropic phase.[327] An interesting feature of this work is the fact that it was carried out by using an attenuated total reflection absorption optical setup analogous to those more commonly used in IR absorption spectroscopy or SPR. In a third study, the thickness, dielectric constants, and tilt angle of the principal dielectric axis of the molecularly oriented upper layer of rubbed polyimide films in liquid crystal display devices could be determined by analyzing the anisotropic polarization of the reflected light.[328]

Less common but still useful is the application of ellipsometry to the characterization of the deposition of chemical layers via covalent bond-forming reactions on simple surfaces, oxides in particular. One illustration in this category is an investigation on the deposition of thin films of nonfunctional silane layers on aluminum, where modeling of the ellipsometry signals led to the conclusion that the film thickness was not uniform across the solid surface.[329,330] That case highlights one of the main limitations of ellipsometry, that it relies on the proper analysis of the raw measurements, but also points to the possibility of extracting additional information beyond average film thickness from the data. Another example is the ellipsometry kinetic study of the chemistry of a cyclopentadienone ruthenium complex grafted onto a self-assembled primer layer on a native silicon dioxide/silicon substrate, where a similarity in the rates of uptake of tertiary phosphines between the anchored and solution complexes was interpreted as due to the inaccessibility of the metal center and to preferential bonding to the cyclopentadienone site.[331]

In electrochemistry, rapid scanning spectroscopic ellipsometry with optical multichannel detection was developed to monitor the electropolymerization of pyrrole on a gold electrode. Monolayer adsorption and Au interface reordering was observed in the first 10 Å, followed by sequential two-dimensional nucleation, coalescence, and gradual densification and layer-by-layer growth.[332] This example illustrates one common characteristic of electrochemistry studies that ellipsometry shares with other techniques, that is, the ability to use cell potential as an additional parameter to extract chemical information out of nonchemical-specific data such as film thickness. In corrosion, an in situ ellipsometry study showed that pure iron and zinc surfaces become easily covered with 6−15 nm thick native (hydr)oxide films in near-neutral sodium chloride solutions, and that further deposition can occur upon the addition of rare-earth metal salts, presumably via precipitation induced by cation hydrolysis proximal to the substrate-solution interface driven by increased interfacial pH resulting from cathodic oxygen reduction.[333]

Ellipsometry, like SPR, can also be used in imaging mode. Most imaging experiments rely on the scanning of millimeter-sized light beams, which can provide lateral resolution down to 50 μm. Alternatively, a large diameter beam can be combined with CCD cameras to acquire full images at once; resolutions down to ~5 μm are possible this way. The feasibility of both approaches has been illustrated in antigen−antibody binding studies for the development of biosensors.[334,335] The use of ellipsometry has also been extended to the characterization of molecular structures at the solid/liquid interface.[336] It should be noted, however, that in those cases structural information is extracted from angle-resolved ellipsometry measurements only after significant modeling; the information is quite limited, and heavily reliant on the validity of the theoretical analysis.

Another important new development in ellipsometry has been the use of infrared rather than visible light to be able to acquire, noninvasively, structural, and chemical information simultaneously at the liquid/solid interface, the latter by recording vibrational information.[337] In an in situ infrared spectroscopic ellipsometry with mixed polyelectrolyte brushes, for instance, measurements using the intense carboxyl group and carboxylate ion absorptions at 1718 and 1565 cm^{-1}, respectively, afforded an assessment of the ionization of the thin film as a function of pH.[338] In another example, the pH-dependent adhesion of mucin to a bovine submaxillary mucin/poly(acrylic acid-block-methyl methacrylate) copolymer surface was determined to involve hydrogen bonding preferentially via its carboxyl group; no evidence was obtained that the amide groups of the mucin participate in that bonding.[339] The use of IR light can also address one of the main drawbacks of ellipsometry, that it is applicable only to interfaces in which there is a step or gradation in the refractive index.

4.6. Quartz Crystal Microbalance (QCM)

An alternative way to follow changes in surfaces during the uptake of adsorbates is by using a quartz crystal microbalance (QCM). QCM is a member of a wider class of sensing instruments based on acoustic waves at surfaces, mass-sensitive resonators based on piezoelectric sensors. These are well-know devices, but their use has been extended to the characterization of liquid/solid interfaces only recently. The main limitation has been the need to develop high-gain oscillator circuits to overcome the viscous damping of the shear oscillation under liquid loading.[340−342] The performance of QCM and SPR in adsorption uptake measurements are comparable, and can be complementary.[343,344] The key differences to note are the fact that the starting surface in QCM is that of the quartz crystal (although that can be modified to accommodate the particular application of interest), and that what is followed in QCM are changes in mass, not optical properties. The detection of weight changes in particular can be quite useful in determining absolute uptakes if the molecular weight of the adsorbate is known. Mass differences can sometimes also be used to differentiate among different adsorbates, a way to add some chemical specificity to QCM measurements.

QCM has often been used to follow biomolecular recognition processes such as antigen−antibody binding or ligand−receptor interactions.[344] The approach in these applications has been similar to that followed in SPR and ellipsometry studies, namely, either the ligands or the receptors are immobilized on the quartz surface, and the corresponding counterpart is offered from solution. Also like with SPR and ellipsometry, many examples of the use of QCM include studies of the interaction of DNA or RNA with complementary strands, specific recognition of protein ligands by immobilized receptors, detection of virus capsids,

bacteria and mammalian cells, and the development of complete immunosensors.[345,346] In one report, QCM was used to quantify associated coagulation of human blood plasma on four surfaces, those of Heparin (an active inhibitor of clot formation), titanium (known to activate the intrinsic pathway), polystyrene, and poly(urethane urea).[347] A peculiar initial plasma-protein interaction phenomenon was identified on the titanium surfaces by an early and rapid change in both frequency shift and viscoelastic properties of the coagulating plasma. QCM has also been used to monitor the binding of estrogen receptor α to specific and nonspecific DNA; the complexes formed were found to adopt a more compact conformation (the uptake to be more extensive) in the case of the specific DNA.[348] In a third case, QCM was used to show that laminin forms a highly hydrated protein layer with different characteristics depending on the underlying substrate: a higher amount of laminin was found to adsorb on a thicker layer of a lower effective density in nanopatches compared to equivalent homogeneous surfaces.[349] In a QCM study on the binding behavior of the cyclic peptide STB1 and its linear version LSTB1 on TiO_2 and SiO_2 surfaces, LSTB1 was determined to bind in a similar fashion on both surfaces, whereas STB1, in spite of its weaker affinity, was found to be able to distinguish between the two.[350] In all these cases, the QCM data on mass changes over time during adsorption, derived from changes in oscillator frequency and damping, have been used to infer some specific chemical behavior in the systems studied.

For biosensor applications of QCM, biointerfaces need to be designed to reduce nonspecific binding and to suppress denaturation of the immobilizing proteins, if those are the detecting elements.[351] Those interfaces are typically prepared via self-assembly or by using polymers. One example is a piezoelectric sensor developed for the detection of genetically modified organisms using single-stranded DNA probes immobilized on the surface of a QCM.[352] Designs have also been advanced for the fabrication of immunosensors for the detection of pesticides,[353] such as the QCM-based immunosensor developed for the determination of the insecticide carbaryl and 3,5,6-trichloro-2-pyridinol (TCP), the main metabolite of the insecticide chlorpyrifos and of the herbicide triclopyr, based on a competitive conjugate-immobilized immunoassay format using monoclonal antibodies.[354] Other QCM sensors have been designed to detect bacteria. For instance, *Bacillus anthracis* spores can be selectively detected by utilizing monoclonal antibodies anchored on the surface of the electrode via self-assembled monolayers.[355] In sensing applications QCM provides quantitative measurements of mass uptake, but chemical specificity originates from the design of the bioorganic layer deposited on the surface of the sensor. A few examples exist for nonprotein based sensing elements as well. For instance, a model sensor was constructed by the immobilization of cobalt(II) phthalocyanine and glucose oxidase onto a gold-quartz electrode for the detection of glucose.[356] Analysis of frequency and dissipation plots indicated covalent attachment of glucose oxidase onto the metallophthalocyanine layer.

QCM has also been used for the characterization of micellar systems and self-assembling monolayers. In a straightforward early application, the rates of adsorption and desorption of several long-chain alkyl thiols on gold electrodes were measured this way. Differences were observed as a function of the solvent used: while in acetonitrile an initial multilayer was seen to form and then slowly evolve into a stable self-assembled monolayer, no multilayer growth at all was seen in dimethylformamide.[357] In another project, pK_a values were measured with QCM for carboxylic acid-terminated self-assembled monolayers by quantifying the shifts in resonance frequency as a function of the pH of the solution.[358] Those pK_a proved quite different, with transition region widths significantly greater, than the values for the same carboxylic acids in solution, a difference that was justified in terms of an increase in tensile stress with increasing pH. The role that the counterion plays in the adsorption−desorption process of self-assembled monolayers of alkanethiols and mercaptoalkanoic acids on gold was also examined in various alkaline solutions and supporting electrolytes with this technique.[359] More recently, in a study on the use of amphipathic viral peptides to create lipid bilayer on gold and TiO_2 solid substrates, the results from changes in QCM resonant frequency and dissipation as a function of time led to the conclusions that the peptide destabilized the vesicles (via electrostatic interactions) in the first stages of adsorption.[360] By following the uptake kinetics, the surface bilayers formed via the rupture of such vesicles was also shown to incorporate measurable amounts of water.[361,362] Adsorption of surfactants using QCM have been reported as well.[363]

In tribology, QCM can be used to study the uptake of liquid lubricants on solid surfaces. For instance, a QCM characterization of the adsorption of soybean oil and methyl oleate from an hexadecane solvent onto a steel surface indicated that, at full surface coverage, both substances form rigid films.[364] An interesting extension in this work is that, by assuming uniform and rigid film formation, additional information was extracted about film thicknesses: it was inferred that the soybean oil adsorbs nearly perpendicular to the surface, whereas the methyl oleate adopts an adsorbate geometry nearly parallel to the surface.

In some instances, QCM has also been used to characterizing the film properties of electroactive polymer films.[365] For instance, the deposition of poly(aniline) by electrochemical oxidation from phosphoric acid has been monitored by QCM to determine the optimal concentration for most effective electropolymerization.[366] In situ electrochemical studies are possible with QCM as well.[367] In one report, the electrochemical resistant of methanofullerene films toward dissolution into an acetonitrile solution was found to be associated with the length of the alkyl chains introduced into the C_{60} cage, and to be strongly dependent on the nature of the cation of the supporting electrolyte.[368] In research relevant to the design of batteries, a QCM study on the proton intercalation performance of thin $Ni(OH)_2$ films, the redox mechanisms were shown to differ in whether H^+ or OH^- is transferred, the reactants and/or products are hydrated, and if cations from the solution take part in the reaction.[369] Co^{2+} and Fe^{2+} were also shown to replace Ni sites in the hydrous oxide lattice, thereby forming dense structures with higher stability. A QCM study of a different electrochemical system showed that, in weakly acidic media, nickel electrodissolution and nickel passivation occur simultaneously.[370]

Lastly, QCM studies have on occasion been extended to cover properties other than mass changes, such as viscoelasticity, hydrophobicity, or surface roughness; the additional information has been useful to infer physical and structural information about biological layers immobilized at sensor surfaces such as film thickness, shear viscosity, and elastic modulus.[371,372] These new approaches have been used to investigate the adhesion of cells, liposomes, and proteins onto surfaces, to determine the morphological changes of cells in response to biologically relevant or pharmacological substances, and even to distinguish DNA molecules with the same molecular mass but different structures.[346,372] In one example, the resonance frequency decreases and energy

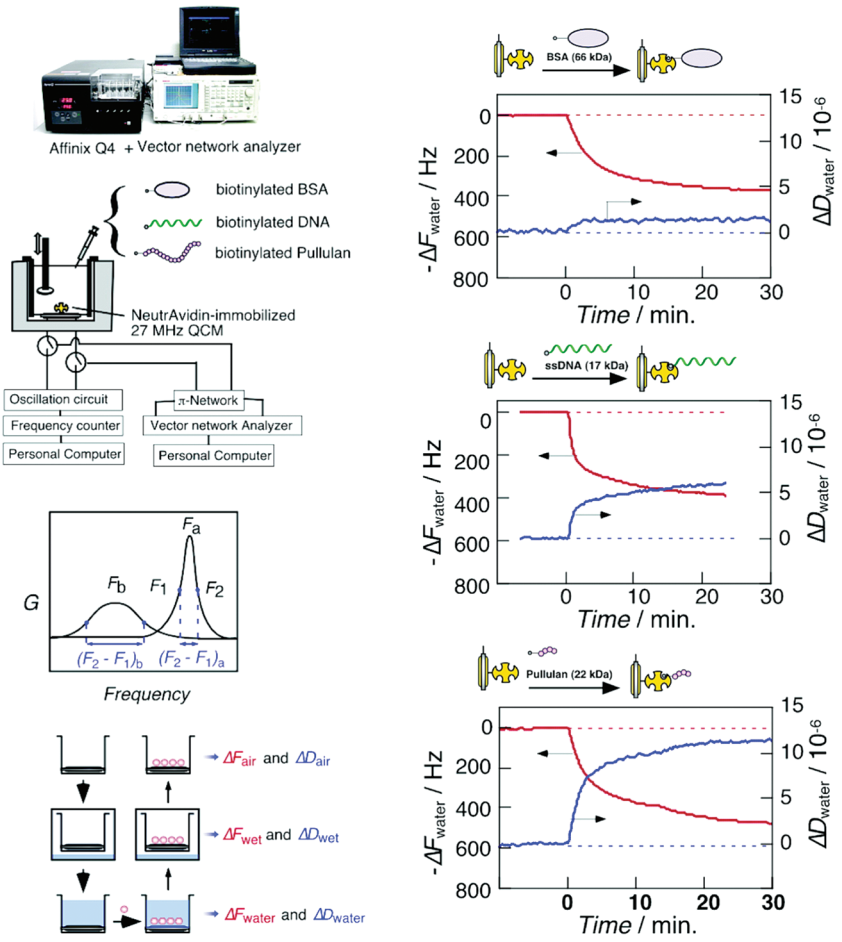

Figure 13. Example of the use of a quartz crystal microbalance (QCM) for the study of adsorption at liquid/solid interfaces.[373] Left, Top: Schematic illustration of the QCM setup, designed to follow both resonance frequencies (F) and energy dissipation (D) by frequency sweep measurements. Left, Bottom: When an elastic mass is added to the piezoelectric crystal oscillator, via molecular adsorption, the frequency of resonance shifts from F_a to F_b, and when additional viscous mass (from the liquid) is added, the peak also broadens from $(F_2 - F_1)_a$ to $(F_2 - F_1)_b$. Right: Examples of measurements carried out with this instrument for the study of the capture of different biologically relevant molecules by the NeutrAvidin protein immobilized on the quartz surface of the QCM. Changes in both ΔF_{water} and ΔD_{water} were followed versus time for the binding of biotinylated bovine serum albumin (BSA, top), biotinylated ssDNA (center), and biotinylated pullulan (bottom) from buffer solutions (20 °C, 10 mM Tris, 200 mM NaCl). Particularly noteworthy is the minimum energy dissipation (ΔD_{water}) seen in the first case. Courtesy of Yoshio Okahata. Reprinted from ref. 373 with permission. Copyright 2006 American Chemical Society.

dissipation increases observed during binding of biotinylated bovine serum albumin, biotinylated ssDNA, biotinylated dsDNA, and biotinylated pullulan to an immobilized NeutrAvidin layer suggested that protein energy dissipation is mainly caused by hydration (Figure 13).[373]

5. X-RAY- AND NEUTRON-BASED TECHNIQUES

With the advent of synchrotron facilities all over the world, the use of intense and tunable X-rays for the characterization of chemical and biological systems has become quite feasible. Several spectroscopy- and diffraction-based techniques have been developed as a result, from which the best known include X-ray absorption (XAS) and X-ray emission (XES) spectroscopies, X-ray reflectivity (XRR), grazing-incidence small-angle (GISAXS), and resonant inelastic (RIXS) X-ray scattering, X-ray standing-wave measurements, surface (grazing-incidence) X-ray diffraction (SXRD, GIXD), and coherent diffraction imaging (CDI) (Figure 14). All these are relatively new techniques. One great advantage of the use of X-rays as probes is that they can penetrate deep into liquid, and even solid, phases, and can therefore easily reach buried interfaces. On the other hand, most X-ray-based techniques are not intrinsically surface sensitive, and special schemes are typically required to discriminate between the signals originating from interfaces and the much more intense signals due to the bulk phases. In most X-ray absorption experiments, this is accomplished either by using high-surface-area solids or by taking advantage of unique compositions or chemical features at the interface, whereas in diffraction experiments the experimental geometry may be used for selective surface probing. In any case, because high-intensity and focused X-ray beams are required, these techniques are difficult to implement: synchrotron sources may be required, and provisions may need to be made to avoid sample damage. Not much research is available in the literature on the use of techniques based on tunable X-rays at present, especially in connection with systems involving liquid/solid interfaces, but pioneering work already points to their potential. Some examples of how these have been applied to problems involving liquid/solid interfaces are discussed below.

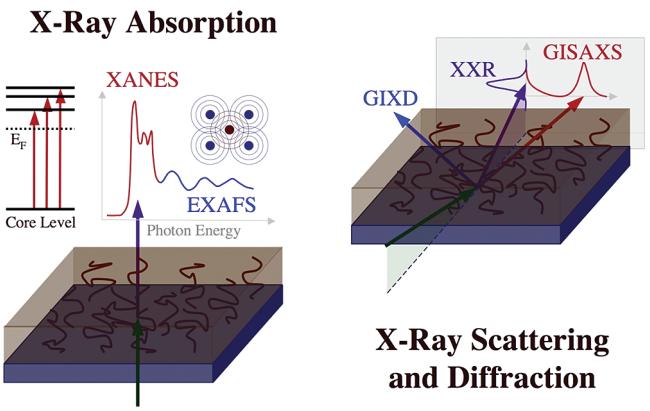

Figure 14. Schematic diagrams of the typical setups used for surface-sensitive X-ray-based experiments. Left: X-ray absorption spectroscopies (XAS), including X-ray absorption near-edge spectroscopy (XANES, NEXAFS, red trace), where excitation from an atomic core level to the molecular or solid empty states is detected, and extended X-ray absorption fine structure (EXAFS, blue trace), which originates from interference with the waves reflected from neighboring atoms and provides local structural information. Right: Most common surface X-ray scattering and diffraction techniques, X-ray reflectivity (XRR), grazing-incidence small-angle X-ray scattering (GISAXS), and grazing-incidence X-ray diffraction (GIXD, SXRD).

5.1. X-ray Absorption (XAS) and Emission (XES) Spectroscopies

X-ray absorption spectroscopy has become a commonly used technique for the characterization of materials.[374−376] Spectra from measurements of absorption of X-ray radiation by the material being studied versus photon energy around the excitation energy of a specific core level of a particular atom can provide information about the electronic properties of that atom. This technique is known as X-ray absorption near-edge spectroscopy (XANES), near-edge X-ray absorption fine structure (NEXAFS), or X-ray absorption fine structure (XAFS). In addition, intensity oscillations are seen farther away from the absorption edge due interference of the forward-propagating waves with electron backscattered from neighboring elements, the so-called extended X-ray absorption fine structure (EXAFS), and Fourier-transform analysis of those oscillations can yield information about the local structure around the element being probed in the form of bond distances and average coordination numbers. Data for both techniques can be collected in one single experiment (Figure 14, left panel). Measurement of the absorption of the X-rays is typically done in transmission mode, by comparing the intensities of the beam before versus after traveling through the sample,[377,378] but other arrangements are possible, including some where X-ray absorption is measured indirectly via the detection of the induced X-ray fluorescence[379,380] or the reflected beam.[381]

XAS, in both XANES and EXAFS modalities, is already fairly popular in studies to follow the progress of catalytic processes in situ, mostly in cases where the reactants and products are in the gas phase but in some instances also to look at liquid/solid interfaces. In terms of XANES studies, an early example for the latter is the study of the oxidation state and structural properties of Al_2O_3-supported PdCu bimetallic catalysts during the reduction of KNO_3 in aqueous solution; the X-ray absorption data were instrumental in determining that only the copper becomes partially oxidized under reaction conditions.[382] In situ XAS experiments were also used to corroborate that the silver in the supported catalysts used for the selective liquid-phase oxidation of benzyl alcohol remains mainly in its metallic state during reaction.[383] In XAS experiments with supported catalysts made out of gold and an oxide of a second metal for the selective oxidation of 1-phenylethanol (dissolved in toluene) with molecular oxygen, metallic gold was shown to be the main active species.[380] Similar in situ XAS experiments on the catalytic oxidation of alcohols were carried out earlier with Pd catalysts.[380,384] In all these examples, the XANES data provided key electronic information on specific metals within the catalysts that was then correlated with catalytic performance assessed by separate means.

Structural information on catalytic systems can also be obtained in situ at liquid/solid interfaces, via the analysis of the EXAFS data. An EXAFS study on the selective aerobic oxidation of cinnamyl alcohol promoted by a Pd/C catalyst, for instance, indicated a small degree of particle growth that correlated with a large drop in catalytic activity.[385] Another in situ EXAFS study, on the performance of a Rh−Sn/SiO_2 bimetallic catalysts during the liquid-phase hydrogenation of citral, showed that the selective production of unsaturated alcohols starts only after an induction period during which the catalyst surface restructures and tin oxide patches form on the surface of the rhodium particles.[386] Time-resolved EXAFS studies on a Heck-type C−C coupling reaction between phenyl bromide and styrene on a supported palladium catalysts indicated the rapid formation of soluble Pd species at temperatures above 150 °C, in the form of colloidal Pd^0 clusters with a size of ∼2 nm.[387]

The use of XAS in catalysis involving liquid/solid interfaces is particularly common with electrocatalytic systems, specifically with fuel cells.[388] Knowledge on the oxidation states of platinum or palladium electrodes both during reaction and upon alloying is critical to the understanding of the redox chemistry of such cells, and XANES is one of the few techniques available to get at that information in situ during electrochemical reactions. In one example, in situ XANES spectra at the Pt edge, obtained for different platinum-based catalysts, indicated that the changes in electronic structure induced by alloying with a second metal leads to an inhibition of the adsorption and dissociation of methanol.[389] In another case, in a study on the oxidation of ethanol on carbon-supported Pt, PtRu, and PtSn anodes, it was found that such oxidation correlates with the formation of O and OH species on the surface, which was also found to depend on the potential applied and to vary with the nature of the surface.[390,391] One key element of that study was the careful analysis of differential XANES spectra obtained by comparing with reference systems to extract information about the nature and configuration of intermediates, oxygen containing species in particular. A third example is a study on the reduction of oxygen on carbon-supported Pd_3Fe nanoparticles in $HClO_4$ solutions, where the downshift observed in the d-band center of the Pd overlayer was suggested to lead to a weaker interaction between the Pd surface and the oxygen-containing species and therefore to an enhancement in activity.[392] Finally, regarding the tolerance of Pt-based proton-exchange membranes in fuel cell anodes to CO poisoning, XANES results showed an increase in the Pt 5d-band vacancies upon the addition of a second metal, leading to a weakening of the Pt−CO bond.[393]

Like with other types of catalysts, EXAFS can also be used in electrocatalysis to extract structural information around individual atoms of specific elements. For instance, based on the different Pt−O bond lengths measured by EXAFS, several oxygen-containing species, including OHH and/or OH groups,

have been identified on platinum nanoparticles at potentials around 1.4 V (referenced to the reversible hydrogen electrode), all of them converting over time into adsorbed atomic oxygen and then into platinum oxide.[394] In another study, EXAFS was used to follow structural and compositional changes in PtRu catalysts for methanol fuel cells by measuring average coordination numbers: those catalysts were determined to restructure into a core−shell distribution, with the size of the Pt core increasing via reduction of its oxide.[395]

In other electrochemical systems, XANES has been useful to follow the oxidation state of key ions at the liquid/solid interface. In one case, the group of Salmeron has developed a convenient electrochemical cell for the simultaneous XAS characterization of the surface in situ during cyclic voltammetry experiments, and demonstrated its performance by following the corrosion behavior of copper in aqueous $NaHCO_3$ versus applied potential.[396] A similar time-dependent in situ XAS experiment involving the monitoring of the solution/surface interface of corroded copper in a sodium sesquicarbonate solution identified a local atomic environments for the copper in solution similar to that on the surface, indicating that chlorine-containing corrosion products are released into the solution and that a thin cuprite layer is left on the original metal surface.[397] Another recent in situ XANES set of experiments indicated that the manganese ions in the electrodes of $MnO_2 \cdot nH_2O$ supercapacitors with a potassium polyacrylate gel electrolyte are present in a higher oxidation state and are subjected to greater valence variations upon charging/discharging over the same potential range than those in the liquid electrolyte counterpart.[398] XAS data also helped in concluding that hydrogen permeation leads to the reduction of oxide films grown on iron electrodes, stabilizing the iron surface at a potential close to that required for hydrogen evolution.[399] In terms of structural studies, recent XAS work on the characterization of nickel batteries indicated that the $Ni(OH)_2$ layers in a brucite structure undergo a contraction during oxidation to NiOOH.[389] In another report, average coordination-numbers extracted from EXAFS data were used to follow the growth of electrochemically deposited copper nanoparticles on p-GaAs(100) from a H_2SO_4 solution.[400] Complementary XANES spectra showed that a metallic state is retained throughout the electrochemical deposition.

XAS has in a few instances been used to study the chemistry of mineral surfaces immersed in liquids.[401] For instance, it was determined by in situ EXAFS experiments that, on water/α-FeOOH(goethite) interfaces, selenate ions form a weakly bonded outer-sphere complex with hydration sphere retention, whereas selenite ions form a strongly bonded, inner-sphere bidentate complex.[402,403] The stability of Fe_2O_3 films in corrosive environments has been characterized as well.[389] One great advantage of X-ray based spectroscopies is that they can be used in situ to study samples under extreme conditions such as the high temperatures and pressures often encountered in geological systems. For example, a study aimed at the in situ XAS mapping of antimony speciation and partitioning in the Sb_2O_3−H_2O−NaCl−HCl system at 673 K and 270−300 bar, conditions typical in magma, reported that hydroxy-chloride complexes are dominant both in the vapor and liquid phases in this salt-water system under acidic conditions.[404] The monitoring of the behavior of fayalite (an iron silicate) and of siderite (an iron carbonate) under temperatures between 323 and 370 K and pressures of 30 MPa pointed to an enhancement in dissolution rate with acetate versus HCl buffered solutions, a result that was explained by ion solvation and nucleophilic attack at the silicate surface.[405,406] An XAS study of the reductive dissolution of MnO_2 by Fe(II) under conditions simulating acid mine drainage suggested that the reaction mechanism changes as MnO_2 is reduced, with Fe(III) precipitating, primarily as ferrihydrite, and an additional passivating phase, jacobsite ($MnFe_2O_4$), forming.[407]

In terms of the growth of nanoparticles, XAS can be used to both characterize chemical environments and determine average coordination numbers around individual atoms, fundamental parameters to follow the initial stages of nucleation in these systems. For instance, the photodeposition of Rh metal nanoparticles from a $RhCl_3$ aqueous solution onto a TiO_2 photocatalyst in the presence of methanol as a sacrificial oxidant has been followed by in situ time-resolved energy-dispersive X-ray absorption fine structure studies, by calculating the fractions of Rh metal particles and of the Rh^{3+} precursor via deconvolution of the XANES spectra using reference traces for Rh^0 and Rh^{3+}.[408] The coordination number for the metallic rhodium was also evaluated, by EXAFS, and was found to increase linearly with photoirradiation time until reaching a constant value of ten. In another case, Salmeron's group has used a combination of XAS, XES, and RIXS to study the electronic structure of cobalt nanocrystals suspended in liquid as a function of size.[409] They found that in the initial stages of growth the strongest interactions of the nanocrystals are with the $C_6H_4Cl_2$ solvent, whereas interactions with the oleic acid surfactant dominate at the later stages of growth. A XANES structural characterization of SiO_2/ZrO_2 nanosol particles indicated that the Zr ions are stabilized in an octahedral symmetry, with each Zr atom initially coordinated to six oxygen atoms, two forming Si−O−Zr linkages and four from water molecules.[410] The number of bridging oxygen atoms increases as the condensation reaction proceeds, suggesting a gelating model based on octahedrally coordinated but distorted zirconium species bonding on the SiO_2 sol surface. Another EXAFS study, on the growth of MnO_3 nanofibers, failed to detect any intermediates, and led to the conclusion that the growth must be solution, not surface, mediated.[411] An EXAFS analysis of iridium nanoparticles made by reduction of [Ir(1,5-cyclooctadiene)Cl]$_2$ dissolved in 1-*n*-butyl-3-methyl tetrafluoroborate, hexafluorophosphate and trifluoromethane sulfonate ionic liquids highlighted coordination to the iridium atoms at distances too short to correspond to Ir−Ir bonds, implying interactions of the ionic liquid with the metal surface because of the formation of an ionic-liquid protective layer surrounding the iridium nanoparticles.[412] Finally, in an example related to environmental remediation, based on a XANES study on the sorption and reduction of aqueous Cr(VI), it was determined that clays containing Fe(II) can remove soluble Cr(VI) efficiently from solution and reduce it to Cr(III), immobilizing the Cr at the water/clay interface.[413]

One limitation of XAS is that light elements such as carbon, nitrogen, and oxygen, the prevailing elements in organic adsorbates, require soft X-rays (E < 600 eV) for the excitation of even their deepest core electronic levels. Because most other elements absorb in that energy range, they interfere significantly with XAS measurements in liquid/solid interfaces. In this, XAS of light element faces similar limitations to those seen in XPS and other UHV-based surface-sensitive techniques (see Sections 6.1 and 10) and requires similar solutions: design of experiments to be carried out under vacuum, with only a thin layer of the liquid on top of the solid. There are a few examples where these technical difficulties have been dealt with and the behavior of compounds

with light elements has been characterized at the liquid/solid interface with XAS. In the study of the melting of ice reported by Salmeron et al., for instance, the thickness of the liquid-like layer present on top was followed as a function of temperature by integration of the signal at 535.0 eV due to an electronic transition from the O 1s orbital of unsaturated donor H-bonds, which increase with the solid-to-liquid conversion during melting, to the 4a1 molecular orbital of water (Figure 15).[414] It was determined from those experiments that liquid water forms on the surface several degrees before reaching the bulk ice melting point.

A technique related to XAS is resonant inelastic X-ray scattering (RIXS) spectroscopy, used to investigate the electronic structure of molecules and materials. In RIXS, high-energy X-ray photons are inelastically scattered off matter, and both the energy and the momentum change of the scattered photon, due to losses to intrinsic excitations of the material under study, are measured. The energy of the incident photon is matched to resonate with one of the atomic X-ray absorption edges of the system to enhance the scattering cross section. The RIXS signal provides convoluted information about both occupied and empty electronic states, also perturbed by the core-hole potential in the intermediate state created by excitation of the core level with which the X-ray resonates. As a source of electronic information, RIXS is sometimes used in conjunction with XAS.

RIXS has been applied to liquid/solid interfaces only in a handful of cases, mostly in connection with corrosion-related processes. In one example, the combined results from a XAS and RIXS characterization of the corrosion of oxidized copper surfaces promoted by Cl^-, SO_4^{2-}, and HCO_3^- ions in aqueous solutions indicated that the main parameters that affect the rate of corrosion are pH and the concentration of Cl^-.[415] In another combined XAS-RIXS study, on the chemistry of oxidized polycrystalline copper surfaces during exposure to sodium sulfate aqueous solutions, an apparent contradiction was observed between the XAS spectra, which showed that sodium sulfide effectively reduces Cu(II) oxide to Cu(I) compounds, and RIXS data, which resembled those of Cu_2O.[416] This pointed to the possibility of the formation of a more complex compound containing both oxygen and sulfur.

5.2. X-ray Reflectivity and Scattering

Surface sensitivity with X-ray-based techniques can be obtained by using grazing incidence. Several approaches are available depending on the direction of detection: if looking in the forward direction, changes in reflectivity (in plane) and scattering (out of plane) of the original X-ray beam can be followed, whereas analysis of the interference patterns away from the plane of the incident and reflected beams provides diffraction information. These are the basis for X-ray reflection (XRR), grazing-incidence small-angle X-ray scattering (GISAXS), and grazing-incidence X-ray diffraction (GIXD, SXRD) studies, respectively. All these techniques share the common need of an intense and focused X-ray beam, almost always from a synchrotron source, and are often combined in a single experiment (Figure 14, right panel). The main type of information extracted is structural, as in studies on bulk samples but about the surface of the solid in contact with the liquid and also on any monolayers adsorbed at the interface. In the case of XRR (also known as X-ray specular reflectivity or X-ray reflectometry), a beam of X-rays is bounced off a flat liquid/solid interface and the intensity of the reflected beam in the specular direction measured; deviations from

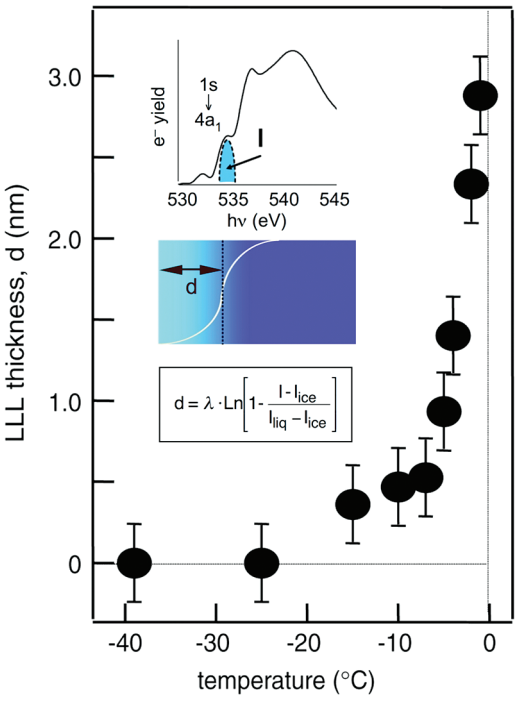

Figure 15. Example of the use of XAS for the characterization of liquid/solid systems, in this case to follow the surface melting of ice. The thickness of the liquid-like layer on ice was followed as a function of temperature by integration of the signal at 535.0 eV due to an electronic transition from the O 1s orbital to the $4a_1$ molecular orbital of water, the peak highlighted in the spectrum shown in the inset.[414] This feature is due to unsaturated H-bonds, the number of which increases with the solid-to-liquid transition during melting. The thickness of the liquid-like layer was calculated using a mean free path of the collected electrons (at 500 eV) of 2.3 nm according to the formula provided. The key observation here is that liquid water forms on the surface several degrees before reaching the melting point of bulk ice. Courtesy of Robert Schlögl. Adapted from ref. 414 with permission. Copyright 2008 Elsevier.

Fresnel's law of reflectivity are analyzed in terms of the presence of imperfections at that interface to obtain a density profile of the interface normal to the surface. In GISAXS, the scattering of X-rays is analyzed at small angles (<1°) in all directions around the beam reflected from the surface: the data reflect inhomogeneities at or near an interface on the same scales, approximately 1 to 100 nm, as those in structures probed by their SAXS bulk counterpart, and provide morphological information in those length scales.[417]

The advantages of these X-ray-based techniques include the fact that they are nondestructive (provided that the sample can withstand the high intensity of the X-rays used), that the probed depth can be varied by varying the incident angle of the radiation, and that the chemical contrast of a given element can be enhanced by using radiation of an energy close to that of an absorption edge of that element; for instance, elemental sensitivity can be attained by techniques based on resonant reflectivity or the detection of X-ray fluorescence.[418] The use of synchrotron radiation offers the additional advantage of wavelength tunability, the same as in X-ray absorption spectroscopy experiments.[418] Among the main disadvantages is the fact that synchrotron-based techniques are difficult to set up, and require samples sturdy enough to withstand the high-intensity X-rays used. Also, like most diffraction and scattering techniques, the structural information is

in reciprocal space and has to be translated into real coordinates, which requires certain assumptions in terms of phase information. Because of the need to use glancing angles, to enhance the signal from the interface being investigated, they have limited sensitivity. Reflectivity measurements also require the use of highly reflective surfaces, single crystals in many instances, and diffraction techniques require long-range order. Finally, complications may arise during the study of organic materials and other low-Z films when the incident angle is below the critical angle for total reflection, in which case scattering from the reflected beam can give rise to a doubling of scattering features in the perpendicular direction. Over all, these X-ray-based scattering and diffraction techniques are still in their infancy and have been used only in a limited number of cases, very few when considering liquid/solid interfaces.

XRR and GISAXS have already been successfully used in several instances to characterize the ordering of organic self-assembled monolayers as they form on liquid/solid interfaces.[419] For instance, GISAXS has been employed to characterize the growth of ordered mesoporous organosilica thin films via co-condensation of tetraethylorthosilicate and organotriethoxysilane in the presence of cetyltrimethylammonium bromide as a structure directing agent under acidic conditions.[420] It was shown that the introduction of chloropropyl groups strongly affects the structure of those films, whereas cyanopropyl groups weakly perturb it. A second XRR and GISAXS study, with liquid octamethylcyclotetrasiloxane films confined in between two flat silicon substrates, showed that the size of the gap between the two surfaces cannot be changed continuously with changing pressure; that gap is quantized due to ordering effects of the surfactant molecules.[421] A combination of XRR and GISAXS has also been used to characterize the structure of Langmuir films of gold nanoparticles stabilized with carboxylic-acid-terminated alkylthiols as a function of area and type of particle on the water surface.[422] The reflectivity data showed an initial particle aggregation into two-dimensional short-ranged hexagonally packed monolayer domains followed by the formation of a laterally homogeneous monolayer near the onset of the monolayer/bilayer coexistence plateau. XRR data obtained in situ at the liquid/solid interface was also useful in showing the periodicity obtained during the decoration of layer-by-layer structures by heavy metal ions.[423] These self-assembly systems are ideal for X-ray scattering studies because they display the long-range order needed to extract structural information from the XRR and GISAXS data.

XRR and GISAXS techniques have been used in biomimetics as well, to look into the structural properties of lipid bilayers.[424] In one example, in a study on highly charged lamellar phases of didodecyldimethylammonium halides, the bilayers were shown to align on a flat solid surface into periodicities going from a few nanometers up to several tens of nanometers in size by means of direct immersion in the osmotic stressor reservoir.[425] The structures of similar supported monolayers in bulk water were characterized with a combination of XRR and small- and wide-angle X-ray scattering.[426,427] The wide-angle patterns in particular reflected a distorted chain−chain correlation.[427] In another XRR and GISAXS study, on the influence of LiCl solutions on lipid bilayers supported on silicon wafers, none of the investigated samples displayed the osmotically stressed liquid-crystalline phase typical of liposomal dispersions.[428] It was concluded that low to medium concentrations of Li^+ ions partially screen the attractive van der Waals forces that are typical between adjacent membrane layers. An X-ray scattering study of the conformation of the antimicrobial fungal peptide alamethicin in highly aligned stacks of model lipid membranes yielded results that were explained by assuming a wide distribution of helix tilt angles with respect to the membrane normal and a partial insertion of the N-terminus into the membrane.[429]

Additional structural information can also be extracted from XRR and GISAXS studies about the effect of the adsorption of proteins and other biological molecules onto lipid bilayers. For instance, an XRR study on the adsorption of monodispersed double-stranded DNA molecules on a positively charged surface based on a layer of *N*-(2-aminoethyl) dodecanamide deposited on a Si(111) wafer showed that the uptake involves the embedment of the DNA into the soft monolayer, which is deformed in the process.[430] An X-ray scattering study of the association between the amyloid-β peptide related to Alzheimer's disease and lipid monolayers have shown an induced crystalline ordering with anionic lipid surfaces, suggesting an in vivo mechanism of templating and aggregation to drive the pathogenesis of the disease.[431] A dynamic XRR study on the adsorption of streptavidin and avidin bound to biotinylated lipid bilayers showed a reduction in lipid mobility due to a small fraction of immobilized lipids bound to the protein layer, and also that a water layer separating the protein layer from the bilayer allows the latter to retain its fluidity and stability.[432]

The scattering and reflectivity of X-rays has also been used for the structural characterization of the interfaces formed between water or aqueous solutions and mineral surfaces. For instance, ordering in both vertical and lateral directions has been observed within the water placed at the interface next to several solid oxides (quartz, ruthenium oxide, rutile, calcite, barite, fluorapatite, muskovite, orthoclase), extending one to a few layers in thickness in the vertical direction.[433] A comparative study using different crystallographic facets of hematite and corundum highlighted the key role that the structure of the surface of the solid plays in defining the ordering adopted by water at such interfaces.[434] In another investigation, the protonation constant of a Ti(110) single-crystal surface in the presence of water was measured by XRR.[435] Structural information has also been reported from in situ XRR and X-ray standing-wave measurements on the adsorption of many small cations (Na^+, Rb^+, Ca^{2+}, Sr^{2+}, Zn^{2+}, Y^{3+}, Nd^{3+}) on the (110) surface of rutile-TiO_2.[436] All those ions were found to bond as "inner sphere" species directly to surface oxygen atoms, but with specific binding geometries and stoichiometries that depend on their ionic radius. In alkaline electrolytes, the polar ZnO(0001) surface was shown by XRR to be covered with a defect-containing hydroxide/oxygen adlayer at hcp hollow sites and a water film that is ordered within the first few layers but not in an ice-like structure.[437] Additional information on ion adsorption at liquid/solid interfaces has been extracted by using resonant anomalous X-ray reflectivity.[438] In a few cases, interactions at liquid/solid interfaces have been studied with liquids other than water. For instance, ordering of liquid squalane near a SiO_2/Si(100) surface has been identified by XRR.[439] In a somewhat different type of system, XRR was used to show strong interfacial layering in the adsorption of ionic liquids in contact with a charged sapphire substrate.[440]

Some applications of X-ray scattering techniques have involved electrochemical systems, to determine the roughness of electrode surfaces and their potential relaxation or reconstruction with changing conditions, to characterize the adsorption and desorption at electrode surfaces, including the deposition of metals, oxides, and other compounds, to obtain structural details

about the electrochemical double layer, and to follow the kinetics and mechanisms of charge-transfer, corrosion, and electrocatalytic reactions.[389,441] For instance, in one XRR study, a lifting of Pt atoms off the surface layer was seen upon electrochemical oxidation, indicating a place-exchange mechanism.[442] Similar experiments were designed to address the submonolayer-level oxidation/reduction of ruthenium dioxide single crystals: the surface structure of the (100) facet was found to display significant changes with applied potential.[443] During the growth and reduction of passive films on copper from borate buffer solutions, X-ray reflectivity measurements showed intensity variations that correlated well with the peaks seen in voltammetry, indicating changes in both Cu layer thickness and roughness.[443] XRR measurements as a function of dissolution pulses during the formation of anodic porous silicon indicated the formation of a steady-state interfacial region about 300 Å in thickness displaying a gradual density gradient.[443] Ordered structures have been documented by in situ surface X-ray scattering for CO adsorbed from aqueous electrolytes onto Pt(111) electrodes.[63,444,445] On gold single-crystal electrodes, CO was found to stabilize surface reconstructions over a wide range of potentials.[446]

X-ray-scattering-based techniques also afford the investigation of dynamic processes.[418] In one example, the use of partial coherence in GISAXS was used to follow fluctuations in the height of lipid bilayers, which can be related to membrane tension and rigidity.[418] In another, a time-resolved GISAXS in situ characterization of the self-assembly of cetyltrimethylammonium bromide onto a homogeneous silica surface identified the formation of a highly ordered surfactant-templated mesostructure, a two-dimensional hexagonal thin-film mesophase with cylinder axes oriented parallel to the substrate surface which forms from an incipient lamellar mesophase by going through a correlated micellar intermediate.[447] In terms of the influence of relative humidity on the self-assembly of amphiphilic molecules from an ethanol/hydrochloric acid solution onto Si(100), a number of transformations were observed with GISAXS over the time of the uptake, including an initial transition from disorder to a 2-D hexagonal network and then to a cubic phase (induced by penetration of water into the thin film).[417] In a fourth example, involving the growth of gold nanoparticles via a reduction reaction at a toluene/water interface, the formation of three-layer clusters 12 Å in diameter was observed, with an electron density profile as a function of depth that evolves with time.[448]

5.3. X-ray Diffraction

Surface X-ray diffraction (SXRD, GIXD) can also be used to provide structural information on buried interfaces. Typically, the data obtained with these techniques are analyzed in a way analogous to that used in 3-D X-ray diffraction studies, but with the goal of extracting structural information about the topmost layers of the solid, to a depth on the order of a few nanometers. For that, GIXD relies on the use of small incident angles. Since below the critical angle of the surface material studied an exponentially damped evanescent wave is established for a short distance, Bragg reflections originate from the surface structure exclusively. An advantage of GIXD is that the electric field at the critical angle is amplified locally by a factor of 4, making the signal stronger. Diffraction information can also be obtained by using a standing wave technique. This is a sensitive method based on the interference between the incident and the Bragg diffracted beams from a perfect crystal: the nodal and antinodal planes of the standing waves are parallel to the planes in the crystal and move as the angle of incidence of the beam is changed, so the fluorescence emission yield from atoms in an overlayer above the crystal are modulated in a way dependent on its structural details. Among the main disadvantages of these standing wave experiments is the fact that they require the use of perfect single-crystal samples and that the periods of the standing wave generated from that single crystal are too short to investigate structures extending far beyond the interface.[389]

Diffraction studies with X-rays, to determine structural information at liquid/solid interfaces, have been applied most often to characterize self-assembled and biological (membrane) layers. It has been shown that GIXD allows for the determination of both in-plane and vertical structures in such monolayers with a resolution approaching the atomic level. GIXD has also been successfully applied to the elucidation of the structure of crystalline aggregates of amphiphilic molecules such as alcohols, carboxylic acids and their salts, aminoacids, and phospholipids at the water surface, and to monitor the growth and dissolution of the crystalline self-aggregates as well as structural changes associated with phase transitions.[449,450] In one example, GIXD experiments with mixtures of phytosterol and sphingomyelin highlighted the nonideal mixing between those lipids in the resulting monolayers, and also the existence of strong interactions between them, with the sterol incorporated into sphingolipid film helping condense the monolayer and order their chains.[451] In another GIXD study, with mixed tetramyristoyl cardiolipin and dipalmitoylphosphatidylcholine Langmuir monolayers, it was found that initially the molecules of the first compound are in a liquid-condensed phase whereas those of the second appear disordered, but that, as the surface pressure is increased, the cardiolipins rearrange into a solid phase with their aliphatic chains perpendicular to the interface and the dipalmitoylphosphatidylcholine into a liquid-condensed phase.[452] In these examples, structural information was obtained for the adsorbed monolayers. Complementary, GIXD may also be used to provide information on the structure of the attached solvent or solute ionic layers.[449]

In bilayer systems involving peptide/lipid and protein/lipid interactions, details on both their thermally induced structural disorder and the folding of membrane proteins have been obtained by X-ray-based techniques.[453,454] In one project involving GIDX, the discrimination of lipid monolayers by the ovine antimicrobial peptide SMAP-29 versus the human LL-37 peptide were compared by following the changes in the phospholipid structure after injection of peptide under the monolayer.[455] The data showed that SMAP-29 discriminates against negatively charged phospholipids in a similar way to LL-37, but that, despite the higher concentration and greater charge of SMAP-29 near the monolayer, the amount of SMAP-29 required to observe monolayer disruption was around three and a half times the number of molecules of LL-37 used to see similar changes. In another example, a GIXD study on the structural changes of phospholipid monolayers indicated changes in phase sequences, from oblique to rectangular and to hexagonal, upon binding of human serum albumin: for instance, with L-α-dipalmitoylphosphatidyl-L-serine and zwitterionic L-α-distearoyl-phosphatidylcholine, the oblique-to-rectangular phase transition disappears and the rectangular-to-hexagonal phase transition shifts to a lower surface pressure.[456] Importantly, all these studies rely on the detection of some degree of ordering in the liquid/solid interface, the same as in X-ray reflectivity and scattering experiments.

GIXD has also been applied to electrochemical systems, mostly in connection with the behavior of batteries. GIXD data have been used to show surface and bulk structural changes in $LiNi_{0.8}Co_{0.2}O_2$ during electrochemical reactions, confirming lithium diffusion through the (110) surface, which is perpendicular to the 2-D edges of the layered structure.[457] In addition, contact with the liquid electrolyte was seen to cause an abrupt deformation of the surface crystal lattice, followed by restructuring upon application of a cell voltage. In another X-ray diffraction study, on the electrochemical delithiation of $LiCoMPO_4$ (M = Mn, Fe, Ni), the oxidation−reduction of 3d elements was determined to proceed via a two-phase mechanism leading to two-phase regions, corresponding to the Co/Co and M/M reactions, while preserving the olivine-like structure of the cathode characteristic of this type of materials.[458] Separate projects have addressed the structural changes in layered $LiCoO_2$ positive electrodes upon battery charging and the effect of cointercalation of ionic liquids into the graphite negative electrode.[459] In situ GIDX experiments have also been performed to follow the electrochemically driven alloying and dealloying of Au substrates with Li ions from organic electrolytes,[460] and also the intercalation of ions into graphite from acetonitrile- and propylene carbonate-based supercapacitor electrolytes.[461] In connection with other electrochemical systems, one GIXD study showed that a $p(1 \times 1)$ adlayer of chloride ions on a Cu(100) surface serves as a structural template for the coadsorption of monovalent potassium and hydronium cations from the acidified supporting electrolyte, and that a layer of interfacial water is formed as a part of the remaining solvation shell of potassium cations in the outer Helmholtz layer.[462] A comparative in situ surface X-ray scattering study of Cu underpotential depositions on Au(111) versus Pt(111) surfaces in the presence of bromide anions established that two different ordered structures form on Au(111), whereas no ordered adlayer grow on Pt(111).[463]

Other uses of GIXD are much less common. GIXD has been used in a few instances to investigate the structure and orientation of liquid crystals. Planar alignment with the liquid crystalline columns parallel to the substrate has typically been found, but it has also been shown that, upon specific thermal processes, homeotropic anchoring with the columns normal to the interface may be stabilized.[464] GIXD has also been used to find the thin-film morphology of an extended molecule with an irregular alternating fluorene−thiophene structure, which has a room-temperature nematic glassy phase and is uniaxially aligned in the plane of the film.[465] Two distinct intermolecular separations were identified, showing that the molecules are lamellar but with stacks exhibiting only local order; the two short axes of the lamellae showed no preferred orientation at the surface or bulk of the film. Another application of GIXD has been to follow the crystallization of calcite templated by calix[4]arene monolayers, in which case uniform (012)-oriented CaCO (calcite) single crystals were seen to grow underneath the monolayers at low compressions, and more randomly oriented single crystals at higher surface pressures.[466] The GIXD data provided no indication of any two-dimensional lattices of the alkyl chain of the calix[4]arene, ruling out any possible epitaxial correlations with the growing calcite. A surface X-ray diffraction determination of the structure of the liquid/Si(111) interface during etching using diluted aqueous potassium hydroxide and ammonium fluoride indicated that the crystal surface is hydrogen terminated and is not reconstructed at open circuit potential, and that a two-monolayers-thick partially ordered liquid film forms, because of a weak interaction with the hydrophobic, hydrogen-terminated surface.[467]

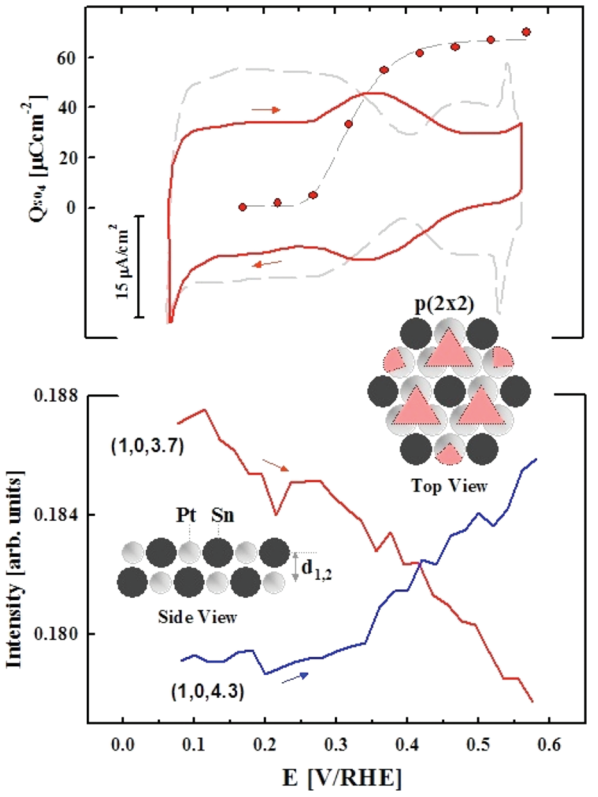

Figure 16. Results from in situ X-ray diffraction experiments designed to probe the changes induced on the surface of a solid electrode, a $Pt_3Sn(111)$ single crystal, immersed in a 0.5 M H_2SO_4 liquid solution, by the applied voltage.[470] Data from X-ray intensity measurements at the (1,0,3.7) and (1,0,4.3) reciprocal lattice point as a function of the electrode potential, shown in the bottom panel, are contrasted with cyclic voltammograms for both the Pt/Sn alloy (solid red line) and a reference pure Pt(111) single crystal (dashed gray line), shown at the top. Potential-dependent integrated charges for the adsorption of bisulfate anions on the $Pt_3Sn(111)$ surface are represented by the circles in the top panel. On the basis of these data, the tetrahedral bisulfate anions (triangles in the schematic model on the right, center) are proposed to adsorb on Pt atoms (gray circles), but not on Sn atoms (black circles), via the three oxygen atoms. A structural change is also observed in the $p(2 \times 2)$ unit cell of the alloy upon adsorption of the bisulfate ions, a contraction of the interatomic $d_{1,2}$ distance (see black and white model on the left, bottom). Courtesy of Nenad M. Marković and Philip N. Ross. Reprinted from ref. 470 with permission. Copyright 2003 American Chemical Society.

An interesting application of GIXD is in dynamic measurements, where the scattered X-ray intensity is measured at a particular reciprocal lattice position as the system is cycled through a particular perturbation.[468] A time-resolved in situ X-ray surface diffraction study on the electrochemical dissolution of Au(001) in a Cl-containing solution indicated that Au etching proceeds via a layer-by-layer mechanism.[469] Electrochemical systems are particularly amenable to dynamic studies induced by changes in the applied potential, in a technique known as X-ray voltammetry. Figure 16 shows data from one example where an expansion of the lattice of a $Pt_3Sn(111)$ electrode was detected because of sulfate adsorption upon an increase in the

dx.doi.org/10.1021/cr2002068 |*Chem. Rev.* 2012, 112, 2920–2986

applied potential.[470] In situ time-resolved energy dispersive X-ray diffraction was also applied to investigate the effect of hydration on the structure of 1,2-dioleoyl-3-trimethylammonium-propane oriented membranes in terms of the evolution of the lamellar spacing, the membrane thickness, and the size of the interbilayer water region.[471] The data provided important information on the central role of free water molecules on the structure and fluidity of the lipid bilayer.

Finally, when using high-surface-area (porous) solids, structural information on the liquid/solid interfaces may be extracted from experiments using regular X-ray diffraction setups. In one example, the X-ray and neutron diffraction characterization of water in mesoporous silica showed that the local order of confined water molecules in the region between 3 and 6 Å on top of the sol−gel network of the solid is significantly different from that of the bulk water, and also different when in hydrophilic versus hydrophobic environments.[472]

5.4. Neutron Scattering and Diffraction

Neutron reflectivity and scattering measurements can in principle also be used to characterize buried interfaces, but those experiments are quite difficult to carry out: there are only a limited number of neutron sources available in the world, and the experimental setups are complex and the data analysis often not straightforward. In addition, it is not trivial to conceive experiments where the scattering can be made specifically sensitive to liquid/solid interfaces. Because collimation of neutrons is more or less impossible, the sample volume must be relatively large, and, compared to the intensity of X-rays, the neutron flux is very low even at the best neutron sources. For all these reasons, only a handful of experimental groups are capable of performing this type of experiments at present.[419,473−475] On the positive side, because the scattering process occurs at the atomic nuclei, light elements, including hydrogen, can be detected. Also, since the scattering power of neighboring elements differs significantly, neutron-based techniques are sensitive to isotopic substitutions. The low absorption of neutrons by most elements means that using neutron-based techniques only minimally perturb the sample being studied, and that they afford the in situ investigation of samples in special environments such as autoclaves, cryostats, or pressure cells.

To date, there are only a few examples of the use of neutron-based techniques for the characterization of liquid/solid interfaces, mostly based on measurements of neutron reflectivity (NR). In NR experiments, the intensity of the specular reflection is measured as a function of the angle of incidence, which relates in a cosine way to the wave vector transfer perpendicular to the reflecting surface. That reflectivity can then be related to the Fourier transform of the scattering length density across an interface. The two relationships combined show that there is a direct relation between reflectivity and structure. Analysis of the data is typically done by the so-called optical matrix method, where the measured data are compared with calculated reflectivity profiles using different model density profiles.[476] The input parameters include the film thickness and roughness, which can be specified as a function of film depth.

Much NR characterization work of liquid/solid interfaces has involved self-assembled layers, some in connection with the behavior of surfactants.[419,449,453,477,478] In an early example, a NR study of the adsorption of nonionic surfactants from aqueous solution onto a self-assembled monolayer highlighted the formation of a new layer with the molecules tilted by about 60° away from the surface normal and some penetration of the alkyl chains of the surfactants into the self-assembled structure.[479] In a second study, involving contrast-variation NR experiments, the structure of an adsorbed layer of hexaoxyethylene glycol monododecyl ether on quartz was found to consist of a bilayer with the ethylene oxide chains forming the layers adjacent to the quartz and the bulk solution.[480] In a third case, stable adsorbed layered structures of the *N*,*N*-didodecyl-*N*,*N*-dimethylammonium bromide surfactant and the corresponding diundecyl compound at the water/silicon interface were determined to display a high sensitivity to temperature, with the repeat spacing decreasing approximately reversibly by about 50% with an increase of temperature of about 40 K.[481] A pronounced off-specular scattering was also seen in that case indicative of a degree of lateral structure or dynamic fluctuation and consistent with two to four correlated layers, which could arise from adsorbed monodispersed unilamellar vesicles, a lamellar phase, or a structured bicontinuous phase. In another report, an ordering of the surfactant membranes of cetylpyridiniumchloride−hexanol in heavy brine sponge phase solutions in the proximity of a quartz surface was identified by a combination of NR and GISANS experiments.[482] The reflectivity results indicated a surface ordering that decays exponentially with distance away from the liquid/solid interface. Neutron-based techniques have been useful in some instances for the study of other types of membranes and polymers as well.[475]

Additional examples of the use of NR to characterize liquid/solid interfaces involve lipid assemblies, used as models of biomembranes to understand hydrocarbon chain packing, structural changes due to headgroup modification, and water penetration.[474] A NR study on the stability of oligolamellar lipid coatings on silicon surfaces against an aqueous liquid phase as a function of applied pressure and temperature indicated a transition in the lamellar structure upon reducing the applied pressure from 90 to 45 MPa, as manifested by detachment from the support, presumably because of a transition from a gel-like to a liquid-like phase.[483] NR was also used to probe the structure of supported lipid bilayers in situ at the liquid/solid interface during the early stages of UV-induced oxidative degradation.[484] It was found that interrupted exposures of the membranes to the light lead to a substantial decrease in membrane coverage but to the preservation of its total thickness, indicating that the initial phase of the UV-induced membrane degradation involves the formation of hydrophilic channels whereas continuous illumination produced a graded interface of continuously varied scattering length density extending into the liquid phase. An advantage of neutron reflectometry in this type of applications is that it allows for the variation of the refractive index of the specific sample by isotope exchange, a method that has been shown to afford the visualization of the adsorption of phospholipid layers to different liquid/solid interfaces and to resolve structural details at the molecular level.[485]

Recent NR projects have also focused on the structural characterization of the response of model biological membranes to exposure to adsorbates or other external stimuli.[486] An in situ NR study of the uptake of DNA on cholesterol-based bilayers showed the formation of a compact DNA sublayer, beneath the cholesterol monolayer, indicating that the adsorbed DNA penetrates into the headgroup region of the charged lipids.[487] Another NR study, on the interactions of lipid-based cubic liquid crystalline nanoparticles (dispersed in glycerol monooleate and stabilized by a nonionic block copolymer) with surface-supported dioleylphosphatidylcholine membranes, showed that the process is dynamic, with the nanoparticles initially adsorbing at the bilayer surface and undergoing interfacial lipid exchange.[488] The attractive interaction between the cubic nanoparticles and

the lipid bilayer proved to be unstable: a subsequent release of the adsorbates could be triggered by an increase in solution concentration. NR has also helped in the evaluation of the effect of applied electrical fields on surface coverage, thickness, roughness, and the relative positions of the aggregates of organic surfactant molecules at liquid/solid interfaces.[489]

Neutron reflectivity is also useful in studies of systems involving mass transport. For instance, NR measurements on the foaming properties of water-soluble complexes of pectin highlighted that, although the foam stability is improved in samples containing soluble complexes, no effect is seen on the foam film thickness.[490] A time-resolved NR study on the penetration of water into thin sulfonated polyphenylene ionomer films pointed to a nonuniform distribution of the water molecules at the air−polymer interface and an excess of water at the polymer−silicon interface.[491] In an example related to tribology, a NR study on Si(100) surfaces in contact with flowing hexadecane identified density depletion of the liquid at the interface.[492] Significantly, the data also showed that while a shear load alters the structure of the depletion layer above the bare Si substrate, no effect of shear is observed upon coating with octadecyltrichlorosilane. In a final example, high-resolution neutron radiography was used to image an operating proton-exchange membrane in a fuel cell in situ, and to quantify the cross-sectional liquid water profile of the cell as a function of cell temperature, current density, and anode and cathode gas-feed flow rates.[493]

A rare example of the application of NR to problems of materials chemistry is the in situ characterization of the composition and structure of the interfaces between a single-crystal sapphire surface and liquid Sn−V alloys at high temperature: a thin (10−25 nm) AlV_2O_4 layer was detected at the liquid/solid interface at 900 °C, with possibly a vanadium-richer thinner layer adjacent to the liquid to promote wetting.[494] An earlier similar study had been reported with Sn−Ti alloys.[495] In situ neutron reflectivity measurements have also provided some insights into the nanometer-scale composition profile of photoresist layers in nanolithography applications.[496]

Most of the studies discussed above are based on neutron reflectivity measurements, but neutron scattering and diffraction techniques have been employed in some instances as well. Again, the majority of the reported work here has been in relation to self-assembled systems. In a grazing-incidence small-angle neutron scattering (GISANS) study of the crystallization of spherical polymer micelles in the vicinity of a flat solid interface, a face-centered close-packed structure with a random orientation perpendicular to the normal of the interface was identified for an attractive surface potential, whereas suppression of crystallization was determined for a repulsive potential.[497] Time-resolved neutron diffraction has also been used to follow the dynamic of the hydrothermal synthesis of many solids from solution, including zeolites and layered calcium silicate hydrates.[498−501] A small-angle neutron scattering (SANS) characterization of the interactions of benzene with a porous silica glass showed that benzene condenses within the pores upon a sudden increase in P/Ps from 0.74 to 0.84, in fair agreement with the prediction of the Kelvin equation for open-ended cylindrical pores with a nominal diameter of 77 Å.[502]

6. OTHER SPECTROSCOPIES

6.1. X-ray Photoelectron Spectroscopy (XPS)

As mentioned in the introduction, many modern surface-sensitive techniques are not well suited to probe buried interfaces, liquid/solid interfaces in particular. This is mainly because the particles used as probes, electrons, ions or atoms, interact strongly with matter and therefore cannot easily travel through liquids or solids. As an example, X-ray photoelectron spectroscopy (XPS), a technique routinely used for the characterization of the surfaces of many solid samples, relies on the detection of the photoelectrons ejected upon X-ray excitation, and therefore is typically operated under ultrahigh vacuum (UHV) conditions. XPS is quite often used to identify the atomic composition of solid surfaces (via the detection of signals for the appropriate photoelectrons) and to characterize their local chemical environment, in particular their oxidation state (based on the specific binding energies measured for a particular type of photoelectron).[2,503] By varying the detection angle, or, if in a synchrotron, the initial photon excitation energy, a compositional profile can also be developed as a function of depth from the interface. A few UHV surface-sensitive instrumental setups have been adapted recently to investigate surface systems under nonvacuum conditions,[504,505] but most of that research has, to date, addressed gas/solid interfaces.[414] The interrogation of liquid/solid interfaces using these techniques require clever arrangements, and those have not yet been developed except for a very few special cases.

Perhaps the first attempts to use XPS to investigate chemistry at liquid/solid interfaces in situ were those directed at the development of a better understanding of electrochemical systems. An electrode emersion technique was developed for this purpose, a quasi in situ approach where the electrochemical cell is removed from the electrolyte in the ideally polarizable region, to preserve the double layer intact, and then transferred to the XPS instrument for analysis.[506,507] Proof was provided early on that the double layer does stay intact during the transfer and immersion in vacuum of the sample, a key assumption for this procedure to work.[508] On the basis of such an approach, systematic XPS binding energy shifts have been correlated with electrode potential due to the so-called electrochemical shift, an apparent shift in binding energy because of the potential drop in the electric double layer.[509] The initial studies have been performed ex situ, but this electrochemical shift was recently confirmed by true in situ XPS analysis of an electrochemical system consisting of a platinum electrode and 1-ethyl-3-methylimidazolium tetrafluoroborate, an ionic liquid.[510] In an alternative approach, the liquid layer above the solid may be prepared ex-situ and cryogenically frozen prior to introduction to the XPS chamber. This methodology has been used in the study of the adsorption of Na^+ and Cl^- ions from an aqueous solution onto a single crystal of TiO_2 in which the electrolyte ions were found to be distributed within at least two to three monolayers above the solid.[511]

XPS and other UHV-based techniques can also be used to study systems involving a liquid phase as long as that liquid exhibits a low vapor pressure. For instance, the melting of $AgNO_3$ was followed in situ by XPS by heating the substrate to temperatures slightly above its melting point, to follow any possible decomposition to silver oxide.[512] A similar approach was used to follow the behavior of tin on an aluminum-alloy powder surface during heating above its melting point, in which case alumina reduction by the manganese was observed,[513] and also the freezing of Ga−Bi alloys, where the thickness of the liquid films were estimated based on the relative composition changes that occur upon melting.[514]

Ionic liquids, a family of compounds that have garnered some interest in recent years, are fit for this type of studies as well.[515,516]

With respect to the adsorption of ionic liquids on solid surfaces, only physisorption has been detected in some instances, with no significant features visible in the XPS spectra that may be identified with the interaction of the liquid and solid phases at the interface.[517] However, in several other cases, chemisorption and strong interactions have been evidenced by XPS data. In a study on the formation of thin films of 1-ethyl-3-methylimidazolium bis(trifluoromethylsulfonyl)imide on a glass substrate, for instance, in situ XPS data were used to demonstrate that the first layer grows in a two-dimensional bilayer structure with the imidazolium cation in contact with the surface and the imide anion pointing toward the vacuum side, and that subsequent layers grow in three-dimensional fashion.[518] Similar ordering of the first layer at the liquid/solid interface of ionic liquids has been seen in other systems.[519] In those cases, the exponential attenuation of XPS signals with respect to the depth of the atoms probed from the interface was used to estimate the compositional profile of the layers.

New instrumental designs have also been implemented to study the chemistry of ionic liquids in electrochemical systems by XPS, in particular to follow charge transfer processes as a function of applied potential.[510,520] In addition to the example provided a few paragraphs back, the voltammetric characteristics of polycrystalline Au and W electrodes immersed in a $AlCl_3$/1-ethyl-3-methylimidazolium chloride melt were characterized under UHV (by using a different design).[521] The underpotential and bulk deposition of Al on Au were found to be very similar to those reported under 1 atm of an inert gas in a glovebox, whereas with W surfaces new voltammetric features ascribed to the stripping of underpotential-deposited Al were observed. In a study on the pseudocapacitive characteristics of manganese oxide in the aprotic butylmethylpyrrolidinium dicyanamide ionic liquid, it was confirmed by in situ XPS studies that the dicyanamide anion rather than the bigger butylmethylpyrrolidinium cations is the working species that compensate the Mn valent state variation upon charging and discharging of the electrode.[522] XPS has been used to follow charge transfers from self-assembled ionic liquid layers adsorbed on electrodes as well. In one case, XPS data were used to follow selective electron transfers toward positively- or negatively charged redox species in boron-doped diamond electrodes modified with an imidazolium-based ionic liquid.[523] Other self-assembled layers with ionic liquids that exhibit selective electron-transfer toward redox-probe molecules according to in situ XPS include 1-alkyl-3-(3-silylpropyl)imidazolium ion-terminated monolayers on Si/SiO_2 surfaces (to control wettability)[524] and thiol-functionalized ionic liquids layers on gold electrodes.[525] Not all XPS studies of ionic liquids on electrodes relate to charge transfer determinations: in one study, the diffusion coefficient of Cu^+ ions generated electrochemically across the surface of the ionic liquid was estimated in situ by XPS.[526]

Some in situ XPS studies have been carried out to identify the nature of the interaction of ionic liquids with the surfaces of nanoparticles.[527] In fact, nanoparticles of the ionic liquids themselves have been seen to precipitate on solid surfaces, and their composition as a function of size estimated from XPS data.[528] In the case of iridium nanoparticles immersed in 1-ethyl-3-methylimidazolium ethylsulfate, for instance, the formation of a N-heterocyclic carbene species derived from the imidazolium cation was identified, suggesting a basic behavior for the ethylsulfate anion.[529] In a more complex study, in situ XPS was used to characterize the interaction of ionic liquids with a model catalytic system consisting of small palladium nanoparticles dispersed on a thin alumina film.[530] It was determined that the ionic liquids adsorb molecularly on both Pd and Al_2O_3 surfaces at room temperature, but that while molecular desorption from the latter can be easily promoted upon heating of the substrate, surface decomposition, mostly from the cation moiety, occurs on the palladium instead. Another intriguing article reports on the use of XPS to prove the addition of metal nanoparticles stabilized by functionalized ionic liquids on carbon nanotubes.[531] Other cases where immobilization of ionic liquids onto solid surfaces has been determined by XPS include the anchoring of a metal-triflate ionic liquid onto a mesoporous MS41 material (a new and efficient catalysts for N-acylation),[532] the modification of carbon nanotubes with ionic liquids (to switch solubility between aqueous and organic solvents),[533] and the synthesis of ionic-liquid-functionalized, gold-nanoparticle-decorated, carbon nanotubes (for oxygen reduction by electrocatalysis).[534]

Another way to keep a thin liquid layer on top of a solid under the conditions required to acquire XPS data is to adjust the vapor pressure to values close to condensation. This does require an arrangement where reasonably high pressures can be maintained right above the sample, but instruments for such experiments are now available in a couple of synchrotron facilities.[414] As an example of the potential of this approach, data are shown in Figure 17 from an in situ XPS study on the dissolution of an ionic salt in water: a thin water film was deposited on a KBr crystal by increasing the water pressure until reaching the deliquescence point, at which point an enhancement in the concentration of the Br^- anions was detected.[535]

A final approach is based on the collection of the photoelectrons from X-ray excitation as current between two electrodes to which a variable potential is applied, in an arrangement known as spectrally resolved internal photoemission (IPE) spectroscopy.[536] This setup was used to characterize the photochemical attachment of 10-amino-dec-1-ene molecules protected with a trifluoroacetic acid group on hydrogen-terminated diamond surfaces, a reaction that was found to occur upon photoexcitation below the optical gap of diamond because of a negative electron affinity.

6.2. Nuclear Magnetic Resonance (NMR)

NMR is one of the most versatile and useful spectroscopies available to chemists. It provides much chemical and structural information, and can be used with a wide variety of atomic nuclei. Since NMR is a well-known technique,[537,538] no details of its general principle or its common applications need to be provided here. Unfortunately, a number of factors have kept this technique from becoming widely use in surface science, in particular for the characterization of liquid/solid interfaces.[539] First, NMR signals are weak, which means that large samples are required. Moreover, NMR is not intrinsically surface sensitive, and in the case of studies of liquid/solid interfaces, discrimination of the surface species against those in the bulk liquid and solid phases is necessary. This limits the use of NMR in surface-related systems to samples with high surface areas, typically involving porous or nanostructured materials. Moreover, the lack of molecular mobility in solids means that the acquisition of NMR spectra for samples involving solids require the use of magic angle spinning (MAS), in order to average out possible spatial anisotropies, and the resolution in MAS NMR is typically not as good as in regular NMR. Other experimental difficulties may arise in connection with sample handling. Finally, some NMR signal is lost with increasing temperature.

There have nevertheless been a few interesting applications of NMR to the study of liquid/solid interfaces. For one, surface

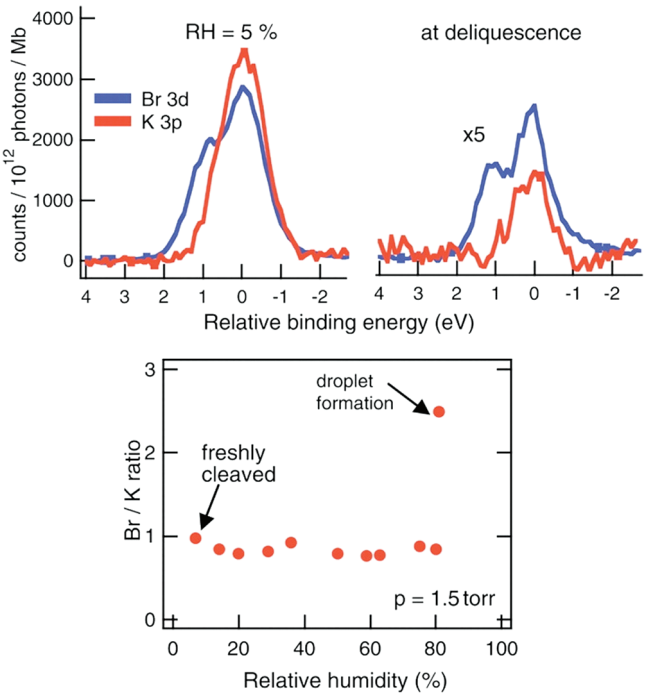

Figure 17. Example of the use of X-ray photoelectron spectroscopy (XPS) for the study of liquid/solid interfaces.[535] Top: Br 3d (blue traces) and K 3p (red traces) core-level photoemission spectra acquired in situ for a KBr solid exposed to an environment with a relative humidity of 5% (left) and at the deliquescence point (right). The photon energy use for excitation was adjusted so that both peaks correspond to the same kinetic energy, 160 eV, and the count rate was normalized by the incident photon flux and photoemission cross section for each element. Bottom: Br/K ratios estimated from spectra like those shown at the top as a function of water-vapor relative humidity. That ratio is approximately 1:1, the value expected from the stoichiometry of the solid, at all values of relative humidity up to the deliquescence point, at which point it more than doubles because of a significant enrichment in Br^- ions at the surface. Reproduced from ref. 535 with permission. Copyright 2005 AAAS.

discrimination may be obtained if the nucleus probed is only present in species present at the interface. Taking advantage of this idea, ^{195}Pt NMR was used to follow the deposition of platinum from H_2PtCl_6 solutions onto alumina surfaces, in which case adsorbed $[PtCl_6]^{2-}$ and $[PtCl_5(OH)]^{2-}$ species were identified.[540] The platinum nucleus was also used in another investigation to follow the extraction of mixed halide complexes of Pt(IV) by a diethylenetriamine-modified silica-based anion exchanger.[541] In a biological application, binding and mobility were quantified in situ by using one-dimensional and pulsed-field-gradient ^{19}F and ^{1}H multinuclear solution NMR for the anticancer drug 5-fluorouracil on the large unilamellar vesicles of egg phosphatidylcholine.[542] It was shown that the mobility of the drug is slowed down by almost 2 orders of magnitude upon binding to the membrane, to values similar to those of the lipids in the membrane around room temperature but somewhat larger at 313 K because of a looser binding. Surprisingly, though, there are not many examples for the use of this approach to study interfacial chemistry.

The use of regular liquid-phase NMR is also suitable for the study of systems where interfaces are prevalent, and some NMR experiments have been reported on systems where neat liquids interact or coexist with high-surface-area solid surfaces. In terms of physical phenomena such as phase changes, the freezing of water was followed in one instance in hydrated powders by taking advantage of the broadening (and disappearance) of the narrow ^{1}H NMR peaks due to water upon the formation of ice.[543] The thickness of the nonfreezing layer of water could be followed by quantifying the intensity of the liquid water signal in the ^{1}H NMR spectra during the freezing and thawing processes. More recent experiments have identify additional dynamic phenomena associated with water inside the pores of solids,[544] and NMR measurements of the depression in melting point of confined liquids has been used to determine pore size distributions in porous media.[545] There have also been reports of in situ characterization of simple adsorption processes on minerals, as in the case of the study of the interaction of cements with water to determine the areas of the surface available for adsorption and the thickness of the resulting adsorbed layers.[546] Another common nucleus probed in cases where organic matter is involved is ^{13}C. Wang et al., for instance, used both liquid and solid-state ^{13}C NMR to follow the adsorption of humic acid and phenanthrene on clay mineral surfaces.[547] They found evidence for fractionation during adsorption, with preferential adsorption of the aliphatic compounds at the expense of the aromatic fractions, which are left in the solution. The hydration of aluminate cements have been followed by recording the NMR signal of ^{27}Al.[548] One interesting application of this liquid NMR approach to the study of adsorbates in liquid/solid interfaces is in connection with the characterization of immobilized stationary phases in liquid chromatography, to evaluate the effects of ligand morphology and mobile-phase composition and temperature on alkyl-chain mobility and conformation.[549,550]

NMR can also be used to obtain atomic-level information on molecules adsorbed on nanoparticles. Indeed, in situ liquid-phase NMR studies have contributed much knowledge to the understanding of the interaction of the organic surfactants used to make colloidal particles with the underlying solid surface.[551] Examples here include the characterization of the stabilizers used to grow cadmium sulfide and cadmium selenide quantum dots, as in the case of thiophenol, which was found, by following transverse and longitudinal relaxation times versus particle size and versus temperature, to bind on top of a single Cd atom.[552] With 2-ethylhexanoate ions, two-dimensional ^{1}H NMR was used to establish that the long hexyl chain spreads over the surface of the nanoparticles while the short ethyl end is primarily surrounded by the DMSO solvent.[553] With n-butanethiolate, a catalytic dimerization to n-butyl disulfide was observed.[554] In a more recent example, on the growth of tin oxide nanoparticles using 2-carboxyethanephosphonic acid, ^{1}H MAS and ^{1}H-to-^{31}P cross-polarization NMR experiments indicated the loss of the protons upon binding of the organic acid to the solid surface, presumably because of the formation of covalent P−O−Sn bonds.[555] Even characterization of organic ligands on a paramagnetic solids such as Fe_2O_3 nanoparticles has been possible with regular liquid ^{1}H NMR; oleic acid was found to lose its allyl and vinyl NMR peaks during nanocrystal synthesis, suggesting the reduction of its double bond.[556]

Changes in peak shape, broadening in particular, can be used to establish changes in the freedom of motion of specific moieties within organic chains (in surfactants, for instance), which can in turn be associated with adsorption or other type of self-assembly into solid-like structures. For instance, in one article, the broadening of specific ^{1}H NMR peaks was used to infer that dendritic-linear amphiphilic block copolymers self-assemble into micelles

dx.doi.org/10.1021/cr2002068 |*Chem. Rev.* 2012, 112, 2920–2986

in aqueous solution and incorporate as templates to prepare dispersed silver nanoparticles in water; that peak broadening presumably indicates the dendrimer chains adopting a solid-like structure.[557] In the case of the formation of alkanethiol-stabilized gold clusters, high-resolution NMR spectra of solutions of the clusters displayed well-defined resonances except for the methylenes nearest the gold interface, a behavior that was attributed to a combination of broadening mechanisms based on the discontinuous change in magnetic susceptibility at the metal-hydrocarbon interface and residual dipolar interactions.[558] On the basis of the line broadening seen in temperature-dependent solid-state ^{13}C NMR studies of those systems, a cooperative chain melting process in the alkylated metal colloids was proposed.[559]

The dynamics of surfactants bonded to nanoparticles can be followed by NMR as well. For example, specific ^{13}C labeling has been combined with variable-temperature solid-state ^{13}C NMR spectroscopy to follow the structural and dynamical behavior of alkanethiols of different chain lengths adsorbed onto gold nanoparticles.[560] For long-chain thiols, it was found that, in solution, they loose the extended all-trans conformation they acquire in the solid state and display large-amplitude motions about their long axes, but a significant increase in conformational order was also observed, because of hydrogen bonding, upon the addition carboxylic acid terminal groups.[561] Magnetically nonequivalent sites were identified, and their rate of exchange measured, by ^{13}C NMR on gold nanoparticles as a function of their charge.[562] In octanethiol-protected gold nanoparticles, it was found that the ^{13}C NMR signal on the first carbon of the chain downshifts, the spin−spin relaxation time increases, and the spin−lattice relaxation time decreases with increasing metal core size, presumably because of changes in the electronic properties of the gold nanoparticles.[563] NMR has also been used to follow chemical reactions on such colloidal nanoparticles. For instance, derivatization of the 11-bromo-1-undecanethiol surfactants used to grow gold nanoparticles by triazole formation via a 1,3-dipolar "click" cycloaddition with a series of alkynyl-derivatized small molecules in nonpolar solutions was confirmed by solution ^{1}H NMR.[564]

NMR experiments can be carried out under high pressures. In one high-pressure NMR spectroscopy investigation of microemulsions of water in supercritical carbon dioxide using a family of anionic perfluoropolyether ammonium carboxylate surfactants, micelles formation was observed even in the absence of mechanical stirring.[565] A highly specific negative nuclear Overhauser effect (NOE) indicated an ordered arrangement where the PF_6^- and carboxylate anions are close to one another, suggesting that those may be concentrated within the electric double layer that forms at the micellar interface. In another in situ high-pressure ^{1}H NMR relaxation and diffusion study on water-in-CO_2 microemulsion systems, in this case formed with phosphorus fluorosurfactants, it was found that although there is rapid exchange of water between the bulk CO_2 and the microemulsion droplets, the entrapped water displays restricted motion.[566]

One limitation in the regular liquid-NMR characterization of nanoparticle surfaces in situ is that those particles need to be soluble in the solution being used, and that is in many systems not the case. Also, when bonded to solid particles, individual molecules may not be able to tumble rapidly enough to average spatial anisotropies and give sharp NMR signals. In those cases, the magic angle spinning (MAS) typically used in solid-state NMR studies may be required. The limitations identified above are not unique to nanoparticles, and may also apply to other adsorbates on other solids. For instance, some of those issues have been identified in studies related to catalysis, in the characterization of the adsorption of small molecules such as hydrocarbons on high surface-area solids such as zeolites and other aluminosilicates. NMR studies of those types of systems have, to date, been done only with gas/solid interfaces,[567] but there are no strong reasons why such work cannot be extended to liquid/solid interfaces, apart perhaps from some technical difficulties with the handling of the sample in the rotors used in MAS NMR. This may be an area where future growth is warranted.

Some in situ MAS NMR studies have been developed to follow the formation of the different solid-state structures (polymorphs) produced during the crystallization of solids from the liquid phase. In the case of the solid formation of glycine from water, for instance, a ^{1}H-to-^{13}C cross-polarization scheme was designed to follow the growth of the solid particles without interference from the liquid phase.[568] A one-dimensional ^{1}H and ^{31}P and multidimensional MAS NMR spectroscopy study of the structural properties of the phase of the molecular glass triphenyl phosphite resulting from annealing the supercooled liquid indicated the formation of a nano- or microcrystalline material at $T >$ 223 K, from the homogeneous and disordered phase present at lower temperatures.[569] If kinetic experiments are to be carried out, suitable NMR nuclei with good sensitivity must be present in the sample, and even then the rates need to be reasonably slow, on the order of minutes to hours, to allow for the proper acquisition of NMR spectra. For this reason, most of the crystallization experiments have focused on zeolites and other alumino-silicates,[570−573] alumino phosphates,[574] or silico-alumino phosphates.[575]

A number of MAS NMR experiments have also been designed to obtain information on structural and conformational changes in proteins upon binding to high-affinity receptors within lipid layers. A particular additional limitation needs to be consider in such systems, the relative size of the signal from the ligand compared to that from the background from all the organic matter present in the system, a problem particularly significant in ^{13}C NMR experiments because of the ∼1% of ^{13}C naturally present in carbon-containing samples. Special techniques such as double-quantum filtering have been advanced to afford the analysis of samples beyond this limit, though. In one example, the binding of the high-affinity peptide agonist (neurotensin) to its G protein-coupled receptor (which mediates the perception of smell, light, taste, and pain) was characterized in buffer/protein solutions by two-dimensional solid-state ^{13}C MAS NMR.[576] It was found that the peptide remains largely unstructured in the absence of the receptor, but that it adopts a β-strand arrangement when in complex with its receptor. Rotational-echo double-resonance solid-state MAS NMR was also recently used to identify and characterize the binding sites for amantadine in the proton channels of the M2 protein of influenza A viruses and in lipid bilayers.[577] These are fairly sophisticated examples on how NMR may be used to provide detailed structural information on the ligand and adsorbate sites, even if the interfaces discussed may not be strictly between liquids and solids.

One way to use MAS NMR to characterize liquid/solid interfaces is by maintaining a certain amount of liquid with the solid samples as they are placed in the rotor in order to retain a local "wet" environment around the solid surfaces. One example that illustrates the effect of the addition of the solvent in such experiments is a study designed to mimic the degradation of the polymer electrolyte membranes in fuel cells caused by the cross-leakage of H_2 and O_2.[578] In that case, a comparative solid-state

^{19}F NMR study produced spectra with sharper peaks with wet samples (as compared to similar dry ones), suggesting more rotational and configurational freedom of the hydrocarbon chains in the former case. Another interesting example of the use of MAS NMR in the presence of some added liquid to look into liquid/solid interfaces, in this case for a system of biological relevance, is the recent characterization of the structure and binding of the indoline quinonoid intermediate that forms during the enzymatic activity of tryptophan synthetase.[579] In that report, solid-state NMR experiments were carried out with the enzyme in microcrystal solid form but exposed to the mother liquid, a solution of L-serine in a triethanolamine buffer, in order to retain its catalytic activity. Various charge and protonation states were identified for the substrate and nearby catalytic residues as a function of time by the NMR chemical shifts seen at specifically ^{13}C- and ^{15}N-labeled positions on the substrate (Figure 18).

An interesting extension of the use of NMR in liquid/solid systems is by taking advantage of its imaging capability. For example, Lysova et al. have used magnetic resonance imaging (MRI) to follow the impregnation of alumina pellets with either Ni^{2+} or $(NH_4)_6Mo_7O_{24}$ in solution as a function of time.[580] They also reviewed the dynamics of redistribution of the liquid phase in a single catalyst pellet during an ignition event triggered by the exothermic hydrogenation of α-methylstyrene to cumene on a Pt/alumina catalyst, and a similar liquid-phase distribution study in Pd/Al_2O_3 catalyst beads was carried out during 1-octene hydrogenation. NMR imaging has also been used to study the flow of liquids in problems associated with membrane filtrations.[581]

6.3. Electron Spin Resonance (ESR, EPR)

A less common technique related to magnetic resonance measurements, electron spin resonance (ESR, also known as electron paramagnetic spectroscopy, EPR), probes the spin of the electrons instead of the nuclei (as done in NMR).[582,583] ESR spectra are typically generated by varying the magnetic field applied to the sample, used to split the spin states of the unpaired electrons, to match the fixed photon frequency used for the excitation from the lower energy to the higher energy level resulting from that split. The magnitude of the field needed for resonant excitation depends linearly on the electron magnetic dipole moment, which in turn depends on the chemical environment surrounding the electron, in a similar way as the nuclear magnetic dipole moment depends on its surrounding and is probed by NMR. The one significant difference between ESR and NMR from the experimental point of view is that because the magnetic moment of an electron is substantially larger than the corresponding quantity for any nucleus, a much higher electromagnetic frequency is needed to bring about a spin resonance with an electron than with a nucleus at identical magnetic field strengths.

ESR suffers from the same limitations discussed for NMR. Like NMR, the signals are weak, which means that only abundant species are detectable. Also, ESR is not intrinsically surface sensitive; discrimination of signals from liquid/solid interfaces needs to be accomplished by other means, either by studying species only present at those interfaces and/or by using high surface-area samples. One additional limitation unique to ESR is that it is a technique only suitable for the characterization of paramagnetic species with one or more unpaired electrons; because most stable molecules have all their electrons paired, only a handful of examples are available on the use of ESR for the interrogation of liquid/solid interfaces. On the other hand, the same requirement makes the technique very sensitive to the paramagnetic centers. In many ESR-based studies, a spin labeling group, often a nitroxide free radical, is added purposely to follow specific localized chemistry.

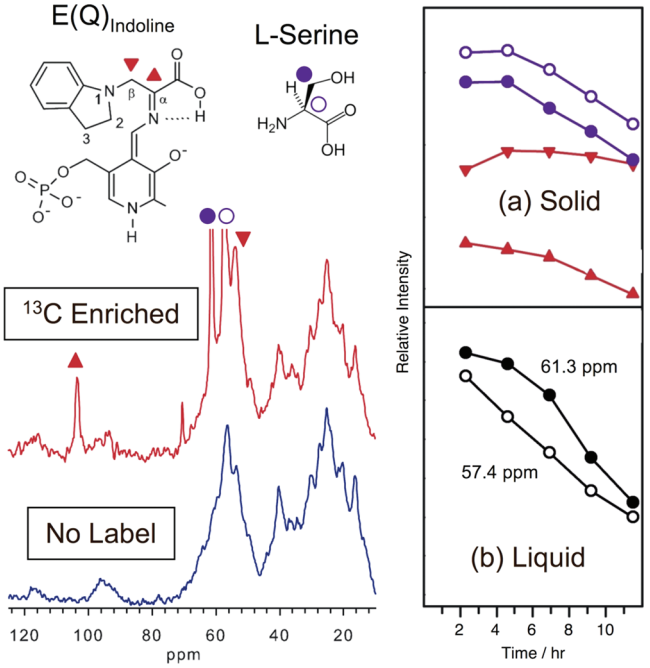

Figure 18. Example of the use of NMR as a way to follow specific reactions in situ at liquid/solid interfaces in biological systems.[579] Left: ^{13}C solid-state cross-polarization magic-angle-spinning (CPMAS) NMR spectra of tryptophan synthase microcrystals in contact with a solution of either 2,3-^{13}C-labeled (red spectrum) or unlabeled (blue spectrum) L-serine mixed with indoline. The signals from the specific labeled carbon atoms within the indoline and L-serine molecules are indicated by the (up and down) red triangles and (filled and open) purple circles, respectively. Right: Time dependence of the evolution of the ^{13}C NMR signals for the ^{13}C-enriched positions indicated above in the bound solid state (top) and mother liquid (bottom). The changes in relative intensities in the signals for the α and β carbon atoms in the indoline indicate a change in binding with time of reaction. Courtesy of Leonard J. Mueller. Reprinted from ref. 579 with permission. Copyright 2011 American Chemical Society.

The spin-labeling method has been used in several occasions for the study of polymers at liquid/solid interfaces. The effects of varying polymer architecture, solid surface, and solvent on the structure of polymers have been studied in some detail this way. For instance, an early study proved that ESR measurements of the bound fractions of poly(vinyl pyrrolidone) on pyrogenic silica adsorbed from two solvents, water and 1,4-dioxane, is a reliable way to determine the amount of polymer in trains, that is, in close contact with the surface of the solid and therefore less mobile than the original random-coil polymers in solution.[584,585] The differences in mobility cause a difference in the magnetic relaxation time of atoms attached to the backbone of the polymer, and that is reflected in differences in the ESR spectra. More recently, in a study on the deposition of random copolymers of dimethylacrylamide and glycidyl acrylate from chloroform onto silica, the different chains were shown by ESR to interact strongly, repelling each other and extending into the solution, so the cross-linking freezes the whole structure without major changes.[586] In both cases, the polymer needed to be

dx.doi.org/10.1021/cr2002068 |Chem. Rev. 2012, 112, 2920–2986

derivatized with a paramagnetic label, 4-isothiocyanato-2,2,6,6-tetramethylpiperidinoox in the first case (one label per five polymer units) and 4-amino tempo in the second. Studies were carried out using other techniques to ensure that this modification does not affect the chemistry of the polymer.[587,588]

Some articles in the literature report on the use of ESR for the characterization of liquid crystal systems. In one case, the intracolumnar order in bis(phthalocyaninato)lutetium, estimated from the line widths of the ESR signals, was shown to determine the dependence of conductivity on frequency.[589] In a study with a different type of system, a discotic liquid crystal radical was found to display an enantiotropic ordered hexagonal columnar mesophase above room temperature with magnetic interactions among molecular spins.[590] In this example, changes in effective magnetic moment were seen to correlate with the phase transitions observed as a function of decreasing temperature because of the collective effect of the alignment of the spins, going from liquid to a glassy solid state and then to an antiferromagnetic phase. The samples in these two cases were intrinsically magnetic, and therefore ideal for ESR studies: no paramagnetic labeling was required in either case.

Molecular dynamics, structural information, and phase states of self-organized bilayers and micelles systems can also be probed with ESR, typically by coadsorbing a paramagnetic probe within the structure of the self-assembled layer. This is in fact the field that has perhaps taken the most advantage of the use of ESR as a characterization technique. Here we reference the work of Zhang et al., who looked into the structural changes of sodium dodecyl sulfate during its uptake on the surface of an alumina solid.[322] They chose to follow the splitting and shape of the ESR signal from nitroxide spin labels coadsorbed with the surfactant on the alumina surface to identify clustering, aggregation, and other phenomena. A second ESR study on micellar systems concluded that the local mobility of cationic long-chain detergents vary little as the length of a chain is increased, but that the order parameter increases noticeably and a phase change takes place from solid to a micellar state.[591] 5-Doxylstearic acid and 16-doxylstearic acid, which have low solubility in water and tend to be localized in the hydrophobic parts of complex systems, were used there as spin probes; those molecules build themselves into the micellar system so that their paramagnetic fragment is located in the hydrocarbon core of the micelle at a fixed distance from the interface and their motion is correlated with that of the surrounding surfactant molecules. In a third example, in a study of model membranes based on phospholipid multilamellar vesicles containing oxidized n-doxylstearoyl spin-labeled lecithin species, the degree of mixing and the rigidity of different bilayers could be assessed in a similar way.[592] It was concluded that the addition of carboxyacyl lecithins to the vesicles tends to disrupt their structure, whereas conjugated dienes lecithins are more likely to affect the physical properties of the bilayer. In a fourth study, related to the performance of stationary phases in liquid chromatography, the structure of an octadecyl chain layer attached to a silica surface was seen to change with the composition of binary solvents (acetonitrile/water; methanol/water): it was determined that high concentrations of acetonitrile help the chains adopt a highly ordered structure, whereas with water or ethanol a poorly ordered interface is the norm.[593] 4-hydroxy-tempo was used in the mobile phase to provide the paramagnetic label for ESR.

In connection with biological systems, several dynamic ESR studies have been reported on systems mimicking the behavior of membranes. For instance, membranes made from binary mixtures of egg sphingomyelin and cholesterol were investigated using conventional and saturation-recovery ESR to estimate the effects that the cholesterol exert on membrane order and oxygen transport, specifically the bimolecular collision rate of molecular oxygen with the 5-doxylstearic acid nitroxide spin label.[594] Discrimination was possible among the liquid-ordered, liquid-disordered, and solid-ordered phases, a fact that helped establish that the addition of cholesterol causes a selective large decrease in the oxygen transport parameter around the nitroxide moiety in the liquid-ordered phase. In another case, a water-soluble lipophilic oligonucleotide, tagged with the spin label group oxyl-2,2,5,5,-tetramethylpyrroline-3-carboxylate, was found to be isotropically mobile not only as a free molecule but also when inserting into vesicular lipid membranes: an increase in the correlation time of motion for the spin label was seen, indicating that the membrane-bound oligonucleotide is still quite mobile at that stage.[595]

Self-assembly has also been studied with ESR in cases related to the preparation of solids with particular structures, specifically mesoporous oxides. For instance, the formation mechanism of a cubic mesoporous KIT-6 solid using Pluronic P123 as a templating agent was followed with ESR by using a series of specially spin-labeled Pluronic molecules. Five main stages were resolved: (1) condensation of the silica oligomers at the water/micellar interface, which reduces the mobility of the ends of the Pluronic chains located at the water/corona interface, (2) a transition from spheroidal to threadlike micelles, (3) their aggregation, precipitation and reorganization, (4) formation of a hexagonal phase through accelerated condensation of silica oligomers in the corona, and (5) formation of the cubic phase.[596] The mechanism of formation of aluminum-containing silicas using alkyltrimethylammonium bromides as a template was also investigated by in situ ESR, by using 4-alkyldimethylammonium-2,2,6,6-tetramethyl-piperidine-1-oxyl as the probe.[597] It was found that the kinetics of the silicoalumina formation is strongly dependent on the surfactant chain length, larger micelles inducing a faster growth, and that the fraction of the probe interacting with the polar sites on the silica surface increases with increasing chain length. The motional heterogeneity of organic−inorganic nanocomposite gels comprising poly(ethyleneoxide) chains grafted between silica particles was investigated as a function of gelation and of drying by paramagnetic probes dissolved in the organic phase or grafted onto the inorganic nodes.[598] The organic phase exhibited marked variations in dynamic behavior, with the liquid-like mobility of the polymer chains strongly hindered at the silica nodes. Like in the examples in the previous paragraphs, extensive knowledge on the dynamics of the systems studied was derived in these cases from the ESR spectra. Those do display multiple lines with splittings and line shapes that are quite sensitive to the local environment of the paramagnetic probe, but some degree of modeling and/or speculation is often also required to associate particular peaks or group of peaks with the states described in the conclusions.

ESR spectroscopy has proven to also be a versatile tool for the online monitoring of catalytic reactions that include paramagnetic species either within the catalyst, as, for instance, in the case of transition metal ions or defects in oxides, or among reaction intermediate radicals.[599] In one example, in a study of the use of titania hollow nanotubes in photocatalysis, ESR was used to identify the formation of the hydroxyl radical species that presumably participate in the catalytic degradation of a textile azo dye, acid orange 7, upon UV excitation.[600] Also, because stable free radicals such as nitroxides may be good catalysts,

several groups have attempted to immobilize those on solid surfaces. An ESR characterization study based on measurements of rotational correlation times indicated that the radicals anchored to silica surfaces retain their properties even after several months, and that polar solvents induce a fast motion of the spin-label.[601]

Finally, a couple of examples for the use of ESR in the characterization of other systems are provided. In terms of the liquid/solid chemistry associated with minerals, the potential for the release of free radicals from iron-containing particulate in asbestos fibers, iron-exchanged zeolites, and iron oxides was measured by using 5,5′-dimethyl-1-pirroline-*N*-oxide as a spin trap in aqueous suspensions of the solids.[602] In another study, restrictions in mobility of aqua complexes of transition metal ions in aqueous solutions by solid surfaces or narrow pores were assessed by ESR.[603] Hydroxyl and carboxylate radicals have been used to model by ESR the potential for hydrogen abstraction in biological compartments and for the formation of hydrogen peroxide in the phagosome during phagocytosis as well. In a materials science project connected with biological applications, ESR was utilized to evaluate the feasibility of surface radical chemistry in γ-sterilized orthopedic materials, including ultrahigh molecular weight polyethylene and the hybrid diurethane dimethacrylate-based RHAKOSS.[604] The failure of those materials to competitively chelate catalytic ferrous ions or readily reduce ferric ions directly was used as an indication of lack of cytotoxicity.

7. MICROSCOPIES. A. OPTICAL

In addition to following adsorption from the liquid phase or characterizing the changes in the chemical and structural details of the solids and adsorbates, some experiments have been designed to obtain spatial resolution during processes occurring at liquid/solid interfaces. Several microscopies have been developed for this purpose based on either optical arrangements or scanning probes. Their adaptation to the study of liquid/solid buried interfaces is briefly surveyed next.

The simplest way to obtain spatial resolution when using optical techniques is via the use of conventional optical microscopes. However, the spatial resolution in such arrangements is limited to dimensions on the order of the wavelength of the light used, micrometers for infrared spectroscopy and hundreds of nanometers for visible light. Those dimensions are several orders of magnitude larger than what is required for the determination of molecular details. Another consideration when implementing microscopy to optical studies of liquid/solid interfaces is that the thickness of the sample must be smaller than the depth of field of the objective of the microscope, typically less than $\sim$1 μm, otherwise there may be some interference from molecules within the liquid or solid bulk phases.

In spite of these limitations, optical microscopies have been extensively used to study liquid/solid interfaces.[605] Some examples have in fact been provided already in previous sections on the use of microscopy in conjunction with several optical spectroscopies to add spatial resolution to the characterization of liquid/solid interfaces. Specifically, studies were discussed above in connection with SPR (Figure 12) and with fluorescence emission spectroscopy. In many of those examples, however, the imaging capabilities are used mainly as a secondary tool to facilitate detection, as in the case of the design of bioassays; no additional chemical information on the liquid/solid interface is acquired by the added spatial resolution capabilities.

7.1. Fluorescence Microscopies

In terms of more specific chemical studies concerning liquid/solid interfaces, fluorescence microscopy is perhaps the most common approach used. In fluorescence microscopy, a fluorophore is added to the system and used as a probe to identify specific spatial locations on the system or to highlight the sites where specific chemistry takes place.[210,606] Much of the use of conventional fluorescence microscopy has been aimed at mapping specific chemical environments in biological systems such as defined intracellular and organellar pHs or threshold concentrations of reactive oxygen species or certain ions within living cells.[209,607,608] In those cases, again, no specific knowledge has been developed on the chemistry that takes place at liquid/solid interfaces. Nevertheless, there are a few fluorescence microscopy studies where chemical interactions have been investigated at the molecular level.

Many fluorescence microscopies studies can be carried out by using regular optical microscopes. In a study of the interactions of annexin A1 with a zwitterionic phospholipid monolayer, for instance, a vibrationally isolated microscope was used to show a strong dependence on the domain structure of the lipid bilayer.[609] It was also shown that annexin A1 forms networks in the presence of the domain structures; interesting fluorescence patterns were detected with features of dimensions on the order of a few micrometers and fluctuating times on the order of minutes. In a second study, it was shown that adsorption of single-stranded DNA to an interface laden with octadecyltrimethylammonium bromide, a surfactant, modifies its interfacial structure via a reorientation from homeotropic (nontilted) alignment to an intermediate tilt angle, and that exposure of the resulting DNA/surfactant complex to its DNA complement induces additional nucleation, growth, and coalescence of lateral regions.[610] The spatial resolution of the microscopy, which in this case focused on the observation of birefringment domains (using polarized light), showed that the uptake of the DNA complement was localized in the same regions as the homeotropic domains.

Confocal microscopes can be used in fluorescence microscopy to add control over the depth of imaging, to afford the selective collection of signal from the liquid/solid interface while reducing background fluorescence originating from sections away from the focal plane. Confocal fluorescence microscopy has been used to study the same sort of systems investigated by regular fluorescence microscopy. For instance, a comparative confocal laser scanning fluorescence microscopy study of the adsorption of a number of proteins and enzymes, including albumin, immunoglobulin G, C3a, interleukin-1β, interleukin-6, human neutrophil elastase, and tumor necrosis factor α, on three membranes (cellulose triacetate, polymethylmethacrylate, and polyacrylonitrile) revealed marked differences that pointed to the importance of membrane biocompatibility in the blood levels of those proteins.[611] In a second example, involving human ovarian carcinoma cells expressing a cyan fluorescent protein-tagged ATP7B, confocal fluorescence microscopy revealed that cisplatin interacts directly with ATP7B to trigger its relocalization and that ATP7B mediates resistance to cisplatin by sequestering it into vesicles of the secretory pathway for export from the cell.[612] Similar colocalization was identified in studies on the interaction between the fluorescent yellow- and fluorescent cyan-tagged protein γ-aminobutyric acidA receptor interacting factor-1 and the kinesin-1 family member KIF5C.[613] It should be indicated that the depth resolution obtained in the images reported in these examples was in the submicrometer range, a range ideal for

biological samples but too large for molecular level chemical studies.

A third setup for fluorescence microscopy is in total internal reflection mode, in ATR arrangements similar to those used in IR absorption spectroscopy or SPR. Because of the exponential decay of the intensity of the evanescent wave as a function of the distance away from the prism in ATR, this arrangement is particularly suited to quantify the separation distance between the surface of that optical element, which can be bioderivatize at will, and cells and other biological samples supplied from solution.[614−620] In one example, total internal reflection fluorescence microscopy was used to determine that the initial adhesion of cells on self-assembled monolayers of alkanethiols depends on the surface functionalities of the latter.[621] Specifically, selective adherence was observed on COOH- and NH_2-terminated monolayers, whereas almost null adhesion was seen on CH_3- and OH-terminated monolayers. In a separate study, on the ligand−receptor interactions between pentameric cholera toxin B subunits and the corresponding membrane ligand ganglioside GM_1, it was determined that binding weakened with increasing GM_1 surface density, presumably because of clustering.[622]

Fluorescence imaging can also be achieved by using near-infrared (NIR) multiphoton microscopy.[623−625] Similar fluorophores and detection schemes as those in regular fluorescence microscopy experiments are used here; only the mode in which the fluorophore is excited changes. One major drawback of this techniques is that its nonlinear nature, where two or three photons are required to match the photon energy of excitation of the fluorophore, implies the need to use high-power lasers, a fact that adds significant complexity to the experimental setups.[626] It could be thought that the use of high-power lasers may lead to increased damage of the sample as well, in particular in biological applications, but in fact the opposite is usually the case: the wavelength range used in NIR multiphoton fluorescence microscopy, between approximately 700 and 1100 nm, is considered an "optical window" for cells and tissues, so radiation can penetrate to a depth of several millimeters in most tissues.[624] Thanks to this property, NIR multiphoton imaging has proven particularly useful in experiments in vivo with living organisms. In one example, a direct correlation was reported between amyloid-β deposits, the primary constituent of senile plaques in Alzheimer's disease, and free radical production in vivo in live transgenic mouse used as models for Alzheimer's disease and in analogous ex vivo experiments in human Alzheimer tissue.[627] In another case, two-photon emission imaging microscopy using inert platinum complexes for the labeling of biological samples revealed the preferential localization of the complexes in intracellular nucleic acid structures, in particular the nucleoli.[628] Recently, several inorganic nanomaterials directly excitable by near-infrared radiation, including semiconductor quantum dots, single-walled carbon nanotubes, and up-conversion nanoparticles, have been developed for imaging applications using single-photon NIR processes.[629]

Several approaches have been developed to overcome the resolution limit intrinsic to optical microscopy in order to follow the behavior of individual molecules on liquid/solid interfaces. One methodology that has become quite common in biological studies is flow cytometry, a technique where the separation, counting, and examination of individual elements within biological samples such as cells or chromosomes is done by tagging them with specific fluorophores, suspending them in a stream of fluid, and detecting (and sometimes separating) them as they flow past one or several laser excitation sources.[630−636] By using multiple fluorophores with different characteristic fluorescence patterns, it is possible to carry out multiparametric analysis of the physical and/or chemical characteristics of up to thousands of particles per second.[637−641] The use of microbeads derivatized with the samples of interest has extended the use of flow cytometry to systems other than cells and other self-sustained particles.[642] The key in all these experiments is the ability to derivatize the desired functionalities in the membranes, cells, or other biological samples with the appropriate fluorescent tags. It should be said that it is the chemical specificity of the tagging process that is used to separate the individual objects of the sample by florescence detection, not the other way around. In other words, no additional chemical information is learned from the fluorescence measurements.

Perhaps a more straightforward way to isolate single chemical events at liquid/solid interfaces is by lowering the density of the reacting species at that interface to sufficiently low values to be able to expect only one reacting site in the area being imaged. In fact, by combining this single-molecule fluorescence microscopy detection scheme with the use of pulsed lasers, time resolution can be added to chemical characterization studies. Single-molecule time-resolved fluorescence microscopy has been used repeatedly to characterize the chemistry of enzymes.[643] In one early example, enzymatic turnovers of single cholesterol oxidase molecules were observed in real time by monitoring the emission from the enzyme's fluorescent active site, flavin adenine dinucleotide.[644] By probing the fluorescence lifetime of single flavins, variations in flavin-tyrosine distance could be inferred over time, and with that a mean force potential between the flavin and the tyrosine could be extracted and used to estimate conformational fluctuation at multiple time scales.[645] Similar conformational dynamics in other immobilized enzymes[646−649] and DNA strands[650−657] have been studied this way. Fluorescence lifetime images have also been reported in connection with dynamic neurobiological applications.[658] In a nonbiological application of this approach, the slip between deionized water and a smooth glass surface was shown, by imaging the flow of suspended submicrometer fluorescent particles, to be minimal at low shear rates on hydrophilic surface but to increase as the shear rate increases; surface hydrophobicity was determined to induce a small slip velocity.[659]

Time resolution is also commonly used in experiments based on Förster (or fluorescence) resonance energy transfer (FRET) and fluorescence lifetime imaging (FLIM). These approaches are commonly used to follow details related to the activity of proteins, including their conformational dynamics upon their interaction with the associated enzymes.[660−664] FRET in particular, where the excitation is transferred between two optical centers, is used directly to quantify the proximity between fluorophores (the efficiency of FRET is proportional to the inverse of the sixth power of their distance), and can be helpful to investigate cellular structure and function.[665] Many elegant FRET-based experiments related to biological studies have been published already where two functionalities are tagged with complementary fluorophores and the FRET activity between them measured versus time and/or imaged.[666−668] As an example, FRET studies on the size of lipid-dependent organization of glycosyl-phosphatidylinositol-anchored proteins in live cells revealed the extensive formation of monomers together with a smaller fraction of nanoscaled (<5 nm) cholesterol-sensitive clusters composed of at most four molecules.[669,670] In another

study, the conformational changes in RNA caused by the binding of the ribosomal protein S15 protein could be monitored in a single assay by using three fluorophores.[671] Yet another example of the use of FRET in the characterization of biological responses is that of the study of the conformational changes of the Ca^{2+} regulatory site of the $Na^{+}-Ca^{2+}$ exchanger, a plasma membrane protein expressed at high levels in cardiomyocytes, upon addition of Ca^{2+} ions.[672] In that case the FRET signal was obtained by linking yellow and cyan fluorescent proteins to the NH_2- and COOH-termini of the exchanger Ca^{2+} binding domain; expression of this construct in myocytes was found to generate changes in FRET associated with contraction, suggesting that the exchanger is regulated by Ca^{2+} on a beat-to-beat basis during excitation-contraction coupling. A final example concerns the use of FLIM for the imaging of the complexation between protein kinase C α and the actin binding protein ezrin in MCF-7 breast carcinoma cells believed to be involved in the control of cell migration and cancer cell metastasis.[673] The data from that study, shown in Figure 19, point to a significant decrease in the donor fluorescence lifetime, indicating appreciable FRET and therefore protein−protein interaction, at the plasma membrane and cell cortex beneath the membrane; the FRET interaction is a reflection of high cell motility. Note that, thanks to the sharp dependence of FRET on distance, with significant signals being observable for distances of a few nanometers at most, spatial resolution information for chemical interactions can be extracted in these experiments at a molecular level in spite of the much poorer resolution of the optical microscopes used for fluorescence detection.

Although much less commonly, fluorescence microscopy has also been applied to studies in materials science and catalysis.[674] An interesting example of this is given in Figure 20, which shows the quantitation of the kinetics of diffusion of bulky substrates inside a mesoporous material.[675] Another elegant study on diffusion combined time-resolved single-molecule fluorescence microscopy images with transmission electron microscopy (TEM) pictures of the material to establish diffusion patterns in mesoporous materials.[676] Several fluorescence microscopy studies have addressed the identification of catalytic sites as well. For instance, Tachikawa et al. used fluorescence imaging to locate single photocatalytically active sites on TiO_2 nanoparticles.[677,678] Roeffaers and co-workers reported spatially resolved images of catalysis where individual turnover events could be counted, allowing them to establish a clear dependence of activity on crystal face.[679] Similar reaction site identification was carried out by Shen et al. via single-molecule optical imaging of single-walled carbon nanotubes during electrocatalysis.[680] The suitability of a time-resolved single-molecule approach has also recently been proven for following catalytic and electrocatalytic reactions with single-reaction temporal resolution on individual nanoparticles and carbon nanotubes.[681,682]

7.2. Raman Microscopy

Raman spectroscopy can be implemented in microscopy mode as well. The signals in regular, nonenhanced Raman are typically too weak to provide meaningful, vibrational-differentiated, images, but a few examples can nevertheless been found of experiments carried out this way.[683,684] In one example, photomicrographs based on intensities in binned frequency ranges were obtained of a human osteogenic sarcoma cell in situ in its medium, and full Raman spectra then taken at specific points for the identification of the appropriate chemical compounds.[685]

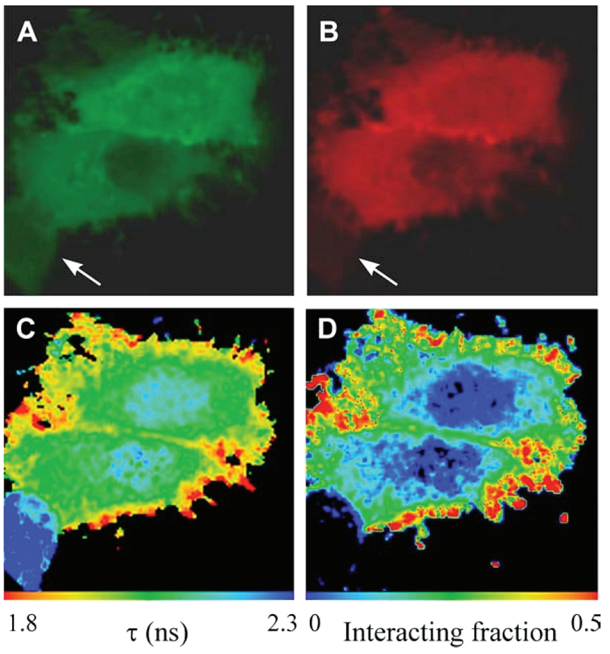

Figure 19. Example of the use of time resolution in Förster resonance energy transfer (FRET) experiments for fluorescence lifetime imaging microscopy (FLIM). Shown here are images from multiphoton FLIM experiments with MCF-7 breast carcinoma cells transfected with both a protein kinase C (PKC) α (aminoacids 1−337)-green fluorescence protein (GFP) and an ezrin-vesicular stomatitis virus glycoprotein construct stained with a Cy3-labeled antibody (IgG).[673] Panels A an B: Intensity images for the fluorescently labeled proteins PKCα-GFP and ezrin-fluorophore Cy3-IgG, respectively. Panel C: GFP fluorescence lifetime image. Panel D: Population map for the interacting species. High levels of interaction, manifested by a decrease in the donor fluorescence lifetime because of increase FRET, is seen at the plasma membrane and cell cortex beneath the membrane. Reproduced from ref. 673 with permission. Copyright 2004 Portland Press Limited.

Although the spatial resolution of the images were of the order of one micrometer, it was sufficient to identify standard DNA in B conformation from the nucleic acid, protein bands from the cytoplasm, lipids and cholesterol from the cell membrane, and the carotenoid compounds present in several bacterial strains. As with the majority of the imaging examples presented in this section, however, the emphasis in these studies was on mapping the distribution of compounds and functionalities across the samples being imaged, not on identifying any specific liquid/solid chemistry.

More popular is the use of coherent anti-Stokes Raman scattering (CARS) microscopy to obtain spatial resolution on the vibrational information of solid samples, typically cells, other biological systems, or self-assembled layers, immersed in liquid media.[686,687] In this approach, a specific frequency can be used to collect the spatial distribution of specific chemical groups. CARS microscopy is different from CARS spectroscopy in that it uses tightly focused beams in a collinear geometry to fulfill the phase-matching condition; the tight focus reduces the excitation volume and permits three-dimensional CARS imaging with submicrometer resolution.[688,689] The main drawback of the technique is that the signal of interest needs to be detected on top of a nonresonant background, although that background may be suppressed by using polarized light.[688,690] One example of this use of CARS microscopy is the selective imaging reported for

dx.doi.org/10.1021/cr2002068 |*Chem. Rev.* 2012, 112, 2920–2986

neutral lipid droplets in unstained live fibroblast cells used to monitor the 3T3-L1 cell differentiation process, which relied on the detection of the signal from aliphatic C−H vibrations.[691] That study revealed a clearance of lipid droplets at the early stages of differentiation followed by an unsynchronized reaccumulation in the cytoplasm. In another case, the resonant CARS signals from the CH_2 and H_2O stretch vibrations were used to characterize the molecular organization inside myelin figures of various surfactants, and light polarization was employed to analyze the orientation of the CH_2 groups and the H_2O molecules.[692] The resulting CARS images suggested that the myelin adopts a concentric lamellar structure with alternating surfactant bilayers and partially ordered water layers, with no sizable water core. CARS was also used to establish the ordered orientation of the hydration water at the surface of phospholipid bilayers with negatively charged 1-palmitoyl-2-oleoyl-sn-glycero-3-phospho-L-serine and neutral 1-palmitoyl-2-oleoyl-sn-glycero-3-phosphocholine dispersed in deuterated dodecane, aligned with the symmetry axis along the direction normal to the bilayer and displaying less hydrogen-bonding than bulk water.[693]

The signals from surfaces in either regular Raman or CARS microscopies can be enhanced by using silver or gold in the form of nanoparticles or other rough surfaces, taking advantage of the same SERS effect discussed in Section 3.1. In one example, this type of enhanced surface sensitivity was used to identify and determine the oxidation state of the flavin components associated with the envelope of the cells of different bacterial species.[694] SERS-CARS microscopy has also been used to monitor biological molecules such as deoxyguanosine monophosphate and deoxyadenosine monophosphate at the single-molecule level.[695] Biocompatible and nontoxic nanoparticles based on either pegylated gold[696] or single-wall carbon nanotubes nanoparticles[697,698] have been developed for in vivo SERS tumor targeting and detection.

Raman microscopy has been used occasionally to image chemistry in nonbiological systems, in particular chemistry that take place at the interface of nanoparticles suspended in liquids or on self-assembly layers.[699] For instance, the kinetics of the chemical reactions on single, optically trapped, (3-aminopropyl)-trimethoxysilane-primed silica microparticles in dimethylformamide (used in solid-phase peptide synthesis) have been measured by following frequency- and time-resolved Raman spectra (obtained using an inverted confocal Raman microscope).[700] Rates were quantified as the molecular species bind to or cleave from the particle surface in the two sequential steps that take place in this system, the fluorenylmethyloxycarbonyl-phenylalanine addition to a propylamine-primed silica surface and the deprotection of the phenylalanine by removal of the fluorenylmethyloxycarbonyl group (Figure 21). SERS microscopy, using the Raman peak of the hydroxyl bond of water, has also been employed to follow temperature in situ during the patterning of liquid-suspended gold nanoparticles using the same laser beam employed for Raman to enhance aggregation.[701] In an application related to chromatography, the accumulation of organic modifiers and the composition and solvation environment of a C_{18}-functionalized silica-microbead stationary phase was investigated using confocal Raman microscopy, by tuning to the nitrile-stretching frequency of acetonitrile.[702] Three different acetonitrile environments were identified within a single chromatographic particle, bonded to the interparticle mobile phase, attached to the C_{18} chain, and present in the residual surface silanols. Other in situ investigations of the adsorption of surfactants on individual nanoparticles have been carried out by using a SERS microprobe as well.[96,703]

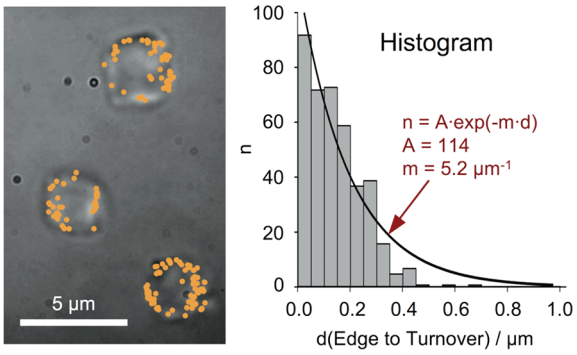

Figure 20. Use of fluorescence microscopy to follow catalytic reactions in situ on a mesoporous solid immerse in a liquid solution. The epoxidation of phenylbutadienyl-substituted boron dipyrromethene difluoride in n-butanol using tert-butyl hydroperoxide as the oxidant was followed by the shift in fluorescence of the reactant from red to yellow upon oxidation of one of the double bonds in the butadienyl bridge.[675] Left: Transmission image of three Ti-MCM-41 particles on which the positions where reactions were observed over a time span of 140 s are highlighted by yellow marks. Right: Histogram of the number of reaction events recorded versus depth of penetration into the mesoporous material. The mean penetration depth before reaction could be extracted from these results. Courtesy of Maarten B. J. Roeffaers. Adapted from ref. 675 with permission. Copyright 2010 Elsevier.

Finally, Raman microscopy has been used to identify heterogeneities in electrodes. For instance, in situ images of the Raman signal due to carbon taken for an industrial button battery cell during cycling indicated that lithium does not intercalate into the individual graphite particles in a homogeneous manner.[704] Other in situ Raman microscopy investigations in electrochemistry include studies on the inhibition of iron corrosion by benzotriazole, which was estimated to involve the cleavage of a N−H bond,[705] and on the electrooxidation of C_1 molecules on roughened Rh electrodes (following C−O vibrational modes).[706] The spatial resolution of the images in all these studies, about one micrometer, is orders of magnitude away from molecular dimensions, but in many instances comparable to the dimensions of the objects (nanoparticles, rough electrodes) being studied. The power of Raman-based microscopy is that the vibrational resolution of the images provides exquisite chemical discrimination not available with other optical microscopies.

7.3. Other Nonlinear Optical Microscopies

Imaging of surfaces can also be accomplished by using other nonlinear optical spectroscopies, sometimes in conjunction with CARS.[707−712] As with CARS, such images can be obtained either all at once by using regular microscopy optics or by rastering the laser beam used for excitation. For instance, a recent report has shown how the detection of SHG signals from membrane-bound chromophores can be used to image the spatial distribution of the membrane potentials in neurons.[713] Using the polarization sensitivity of the SHG signal, a ∼36° tilt angle of the chromophore to the membrane normal was determined. This example also shows how contrast can be enhanced and site specificity can be added in SHG-based images of biological systems by immobilizing optically active fluorophores such as quantum dots[714] or porphyrins[715] on the surfaces of interest. The simultaneous use of several nonlinear optical imaging techniques (CARS, SHG, SFG) can also afford the visualization of different structures in complex biological systems at the same time.[716] As with the other imaging approaches discussed in this section, though, the main use of these

microscopies has been to characterize biological samples,[717−720] not the details of any specific liquid/solid chemistry.

Like with Raman, microscopy using SFG can add significant chemical specificity, by selectively collecting the signal from a specific vibrational energy.[721] A nice nonbiological example of this approach can be seen in the study of the spatial distribution of the corrosion of gold surfaces by cyanide, in which SFG images for the distribution of individual cyanide adsorbates were recorded by using different IR laser wavelengths.[164] It was found that a linearly bound cyanide species forms on the gold surface during the initial stages of adsorption but higher-coordinated gold-cyanide complexes develop afterward. SFG microscopy can also be used to investigate the structure and orientation of adsorbates, as in the case of alkanethiolate monolayers on gold surfaces, which were characterized by following the average orientation of the terminal methyl groups.[722] The presence of film defects was also estimated in that case by measuring the CH_2/CH_3 intensity ratios. In another example, SFG microscopy was used to examine the spatial distribution of the composition of mixed self-assembled alkanethiolate monolayers on a gold substrate.[723] SFG microscopy can even be set up to map chirality (because chiral objects are noncentrosymmetric, as require for SFG generation), as in the case of the reported optically active images of chiral 1,1′-bi-2-naphthol solutions.[724] No liquid/solid interactions were identified in that case, but a glass spacer was used to separate one enantiomer from a racemic mixture, showing that unique chemistry could potentially be identified at the corresponding interfaces in similar systems. SFG microscopy is not yet a widely used technique; the examples of its use for the characterization of liquid/solid interfaces in nonbiological applications have to date come mostly from the Baldelli group.

7.4. Infrared and X-ray Microscopies

Most of the microscopies reviewed in the previous paragraphs rely on the use of visible or UV light, but other ranges of the electromagnetic spectrum can be used for this purpose as well. In particular, infrared absorption spectroscopy can be implemented with spatial resolution by using the appropriate optics.[725,726] One powerful advantage of infrared microscopy is that images can be recorded using the signal of specific vibrational features (like with Raman or SFG), an approach that provides great chemical selectivity at a molecular level.[727] On the negative side, although IR microscopy can in principle be carried out with conventional IR spectrometers and light sources, tunable light sources with high intensities in the infrared region, typically synchrotron facilities, are usually needed to obtain high spatial and spectroscopic resolution simultaneously. Also, sample preparation is an issue: many IR microscopy experiments have been geared to the study of biological samples, and those often need to be carried out by using frozen or partially dried tissues, or samples embedded in a matrix[728−730] (although conditions have been used in some instances compatible with living organisms[731]). IR microscopy can be hindered by extensive infrared absorption due to the solvent (water in many cases). Finally, the spatial resolution of IR microscopy is quite poor, in the micrometer range at best, and therefore the information extracted from such studies does not often address specific issues related to chemistry at liquid/solid interfaces but rather map out the spatial distribution of the different components in cells and other biological systems.

There are not many examples of the in situ characterization of liquid/solid interfaces with IR microscopy; only a couple will be cited here. In one instance, the intracellular water concentration

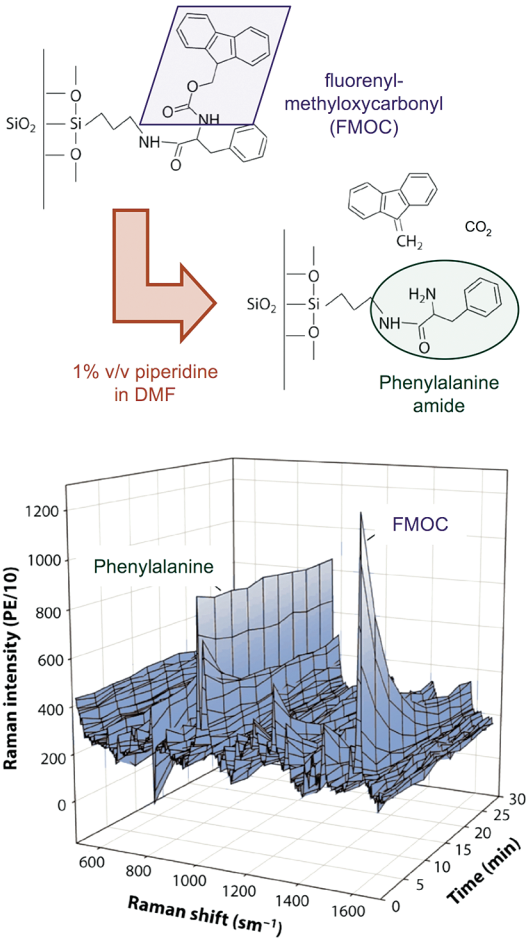

Figure 21. Example of the use of Raman microscopy for the study of chemical reactions at the liquid/solid interface. In this case, individual 5 μm silica nanoparticles were optical trapped within the focused beam of an inverted confocal Raman microscope in order to characterize their chemical conversion as a function of time.[700] The silica nanoparticles had been previously derivatized via the sequential attachment of (3-aminopropyl)trimethoxysilane and fluorenylmethyloxycarbonyl (FMOC)-phenylalanine. The deprotection of the phenylalanine by removal of the FMOC group using piperidine, the reaction indicated at the top, was followed. The time-dependent Raman spectra at the bottom show that while the aromatic C═C in-plane stretching mode of the FMOC group at 1609 cm^{-1} decreases with time, an indication of his removal from the surface, the intensity of the symmetric ring-breathing mode of phenylalanine at 1007 cm^{-1} remains constant throughout the reaction, showing that there is no loss of that group from the silica surface. Courtesy of Joel M. Harris. Reprinted from ref. 700 with permission. Copyright 2002 American Chemical Society.

in living liver cells was quantitatively imaged by following the water IR absorption bands using a diode laser tunable within the 1530−1570 nm range.[732] In another case, the spatial distribution of the composition of a living Micrasterias sp. algal cell was imaged in situ in the presence of a flowing liquid by mapping the IR signal for different frequency ranges corresponding to specific organic groups: CH_n, phospholipids, amide, and carbohydrates (Figure 22).[733] In a nonbiological application, near-infrared microscopy of fluid inclusions hosted by ore minerals that are opaque to visible light (pyrite, enargite, and quartz) was used to obtain compositional information such as Cs/(Na + K) and Cu/(Na + K) ratios on ore-precipitating fluids.[734] In a study on the effect of solid surfaces on the thermal toughening mechanism of

dx.doi.org/10.1021/cr2002068 |Chem. Rev. 2012, 112, 2920–2986

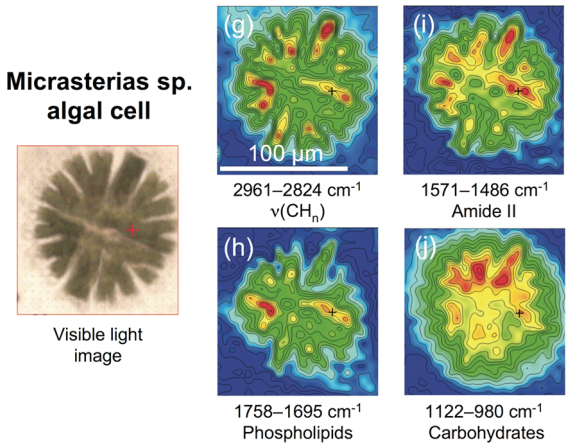

Figure 22. In situ visible (left) and mid-infrared images of a *Micrasterias* sp. cell in a flow chamber.[733] The infrared images were obtained by integration of the indicated frequency ranges to map out the distribution of different chemical groups within the cell: (g) 2961−2824 cm^{-1}, corresponding to the stretching frequencies on CH_n groups; (h) 1758−1695 cm^{-1}, for the detection of phospholipids; (i) 1767−1723 cm^{-1}, a range associated with the so-called amide II band; and (j) 1122−980 cm^{-1}, to image carbohydrates. Courtesy of Carol J. Hirschmugl, reproduced from ref. 733 with permission. Copyright 2009 The Society for Applied Spectroscopy.

dehydrated castor oil films, infrared absorption line scans taken across the depth of a thermally oxidized oil-on-steel film identified a new toughening mechanism in the layers closer to the steel surface based on cross-linking reactions.[735] Finally, the efficiency of intergranular esterification in waxy maize starch reacted with octenyl succinic anhydride in a slurry was monitored by imaging the signal for the carbonyl band at 1723 cm^{-1}.[736]

At the other end of the spectrum, images of systems that include liquid/solid interfaces can be obtained using X-rays.[737,738] Typical radiology images are common in medical analysis but are rarely used to look into specific chemical issues at liquid/solid interfaces. Chemical information can be obtained by using specific radioisotopically labeled compounds; the visualization of the incorporation of those labels into living organisms, predominantly cells, is the basis of the so-called radioautography technique.[739] However, molecular-level X-ray microscopy studies in chemistry and biology require higher spatial resolution, and are commonly performed using tunable X-rays from synchrotron sources. The need to use focused X-rays does add significant complexity to those experiments; high-resolution X-ray microscopy is often achieved by using zone plates, circular transmission gratings with radially increasing line density, as X-ray optics.[740] Interference from the solvent is in general less of an obstacle than with other types of radiation,[741−744] but X-ray-induced damage of the sample can be a problem, in particular in biological systems; cryo-treatments are often used to help preserve the sample during X-ray exposures.[745]

Chemical contrast enhancement agents are often required to better view the distribution of specific sites such as cellular structures.[742,746] However, natural contrast may also be optimized by taking advantage of the tunability of the X-ray energy in synchrotron sources. For instance, by utilizing the natural absorption contrast between protein and water at photon energies of about 0.52 keV, cell structures as small as 25 nm in size could be resolved in X-ray microscope images.[747] In a different example, metal 2p absorption edge signals were used to obtain spatially resolved images of metal speciation in microbial biofilms cultivated from river water, and comparisons made with biochemical characterization of the same spatial region using images recorded at the C 1s and O 1s edges.[747]

Only a few examples are available for the use of X-ray microscopy in the characterization of the chemistry of liquid/solid interfaces in materials science. In one case, X-ray microscopy was used to observe in situ and in real-time the changes in the shape of the liquid/solid interface induced by either particles or void spaces during melting of metallic systems.[748] The images in that work were of relatively poor resolution, showing features of dimensions close to one millimeter. In a more recent study, scanning transmission X-ray microscopy was used to image the results from the noncovalent assembly of lyotropic chromonic liquid crystals into aggregates and to show the ensuing orientational and positional ordering and the segregation of the components into nontrivial morphologies coexisting with the isotropic melt.[749] Elemental discrimination was added to the images by tuning the excitation source to specific NEXAFS features in the sample. An in situ investigation of an operating fuel cell using synchrotron X-ray radiography has been used to identify and follow the time evolution of the primary spots of liquid water formation.[750,751] In all these examples, the lateral resolution of the images was only in the submillimeter range. A different setup was used for scanning transmission X-ray microscopy in situ studies on the morphological changes induced by water uptake and release in mixed ammonium sulfate-adipic acid nanoparticles.[752] Although not strictly a liquid/solid system, layers of adsorbed water could be built up on those hygroscopic nanoparticles by increasing the relative humidity, at which point it was found that adipic acid forms a separate phase of complex morphology partially enclosed by the ammonium sulfate solution. X-ray microscopy images have also been obtained for the uptake of water on other hygroscopic samples via similar control of the relative humidity.[753,754] Resolutions below the 100 nm range were demonstrated, and chemical sensitivity added by NEXAFS measurements.

8. MICROSCOPIES. B. SCANNING

To obtain images of liquid/solid interfaces with atomic resolution, the most promising approach is the use of scanning microscopies (Figure 23). A sharp solid tip is rastered across the interface in a controlled fashion, in subnanometer steps, by using piezoelectric drivers. In scanning tunneling microscopy (STM), a map of the electronic structure of the interface at a given energy is obtained by biasing the tip with respect to the surface and recording the tunneling current as a function of the position of the tip (Figure 23, left).[755,756] STM is typically carried out in one of two modalities, in constant height mode, where the tunneling current is recorded as the tip is rastered at a fix distance from the interface, or in constant current mode, in which case the tip position is adjusted to keep the tunneling current constant and recorded in topographic maps. A serious limitation of STM is that in does not image atoms directly, only their associated electronic structure, a distinction that is often forgotten in the literature. Moreover, STM does not provide chemical information in the way as other spectroscopy do. Additional local electronic and vibrational information can in principle be obtained by scanning the bias voltage at specific points on the interface,[757] but this is not done often, and has virtually not been applied to liquid/solid interfaces to date.

In atomic force microscopy (AFM), the interaction force between the tip and the surface is followed instead, the changes

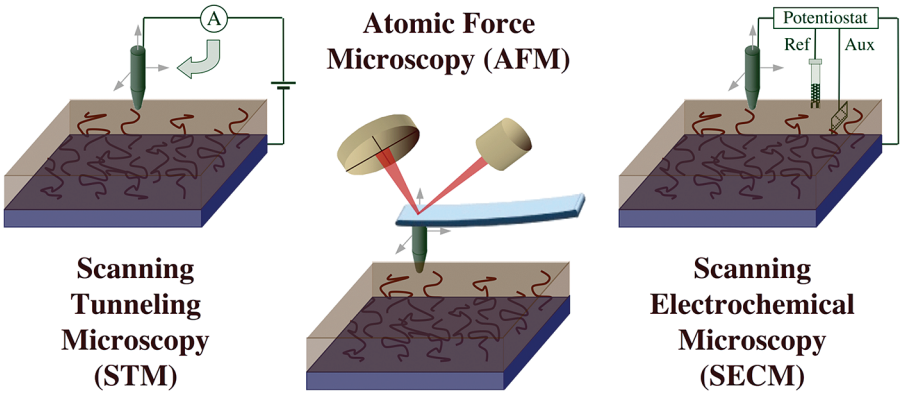

Figure 23. Schematic diagrams of the typical experimental setups used in scanning microscopy. Left: arrangement for scanning tunneling microscopy (STM), where a sharp tip is rastered across the liquid/solid interface using piezoelectrics as its height is either kept constant, in which case the tunneling current is mapped versus position, or adjusted to keep the current constant. Center: Analogous arrangement for atomic force microscopy (AFM), a technique where topographic images are obtained by following the deformation of the cantilever that supports the probing tip, typically by following the deflection of a laser beam off the top of the lever. Right: Setup for scanning electrochemical microscopy (SECM), where electrochemical reactions can be carried out and recorded locally by using the tip as an electrode.

of which are measured by following the deflection of a laser spot reflected from the top surface of the cantilever (used to support the tip) with an array of photodiodes (Figure 23, center). Like STM, AFM can be performed in two general modalities, constant height or constant force, and also used to quantify the interacting forces. For constant force imaging, AFM is typically operated in static (also called contact) mode, where the force between the tip and the surface is kept constant during scanning by maintaining a constant deflection and a topographic image of the surface is recorded. A variety of dynamic (noncontact) modes, where the cantilever is vibrated, are used to obtain additional information on the forces at play, and is usually preferred because of the lower risk of damaging the sample. As is the case with STM, AFM does not image chemical structures directly, but can in some instances provide information on atomic-level forces.[758]

The use of scanning microscopies has blossomed over the last couple of decades.[759−763] They have the advantage of not requiring a vacuum environment to operate (as oppose to electron microscopies); that makes them ideally suited for gas/solid and liquid/solid interface characterization. On the other hand, these scanning microscopies typically require the use of flat samples. Also, atomic resolution in liquid/solid interfaces is difficult to achieve, in particular in AFM. STM also requires the use of a conducting surface, and preferably nonpolar liquids, since the currents originating from the flow of polar molecules or dissolved ions can be large enough to prevent detection of the tunneling current. The latter effect may be minimized by coating the tip with an insulating material, a common practice in electrochemical STM studies.

8.1. Scanning Tunneling Microscopy (STM)

STM has long been used to probe in situ the structural details of the layers formed by physisorption of organic molecules at liquid/solid interfaces, typically on graphite, gold, or molybdenum disulfide substrates. In the early years, extensive work was dedicated to the study of the ordering adopted by liquid crystals upon interaction with the solid. Those studies often showed an increase in order with respect to the bulk phases and strong conformity to the structure of the surface.[764,765] In situ STM studies on the physisorption of long-chain hydrocarbons at liquid/solid interfaces have provided similar interesting information in connection with surface−adsorbate interactions and the effect of both the chemical nature of the solvent and the underlying structure of the solid surface on the rearrangement and bonding of adsorbates.[766−768] Already in the first study of this type, on the adsorption of *n*-alkane layers at the liquid/graphite interface, it was determined that the resulting layers possess a high degree of two-dimensional ordering and that the atomic structure of the images is dominated by features associated with the substrate.[769] Additional in situ STM studies on the adsorption of long-chain alkanes, alcohols, fatty acids, and dialkylbenzene from organic solutions onto the basal plane of graphite revealed a high degree of organization in lamellae. However, it was shown that whereas the extended alkyl chains of those molecules are always oriented parallel to a lattice axis within the basal plane of graphite, the planes of the carbon skeletons can be oriented either perpendicular or parallel to the substrate plane.[770] The growth of a second layer, rotated by 60° with respect to the first layer, was identified at the interface between a solution of hexatriacontane in decane and the basal plane of graphite.[771] Phase separation was observed on a graphite surface upon adsorption of triacontane/triacontanol mixtures from solution, and significant differences were identified in those phases in terms of the mobility and sticking probability of the molecules on the surface depending on the nature of the solvent.[772] Similar conclusions have been reached from studies on the adsorption of fatty acids and cholesterol,[773,774] thiols,[323,775] and porphyrins.[776]

Considerable attention has been focused recently on the study of the formation of molecular and supramolecular networks on surfaces via self-assembly. However, most of the STM work in this area has been carried out under UHV conditions, and little is known about the effect of the solvent in helping create the organized molecular patterns ultimately formed on the solid surface.[777,778] It has become clear, though, that both the nature of the solvent used and the concentration of solutes in the liquid phase play defining roles.[779,780] In one report, for instance, the two-dimensional pattern formed by physisorbed dehydrobenzoannulene molecules on a graphite surface were shown to transition from linear to honeycomb polymorphs with their concentration in solution.[781] Another in situ STM study showed that up to five two-dimensional networks of rhombic-shaped fused dehydrobenzo[12]annulenes can be formed at the 1,2,4-trichlorobenzene/graphite interface depending on the alkyl-chain length

dx.doi.org/10.1021/cr2002068 |*Chem. Rev.* 2012, 112, 2920–2986

and the solute concentration.[782] Similarly, independent alteration of the concentrations of two different carboxylic acids, benzenetribenzoic acid and trimesic acid, in binary solutions in two different solvents, heptanoic and nonanoic acid, resulted in six packed monolayer phases with different structures and stoichiometries on the same graphite surface, all stabilized by intermolecular hydrogen bonding between the carboxylic acid functional groups.[783] Multiple crystalline phases at the liquid/solid interface were also observed with an amide amphiphile containing a C_{18} alkyl chain, formed via noncovalent interactions.[784] The formation of these multiple phases has been explained as the result of a balance between kinetic and thermodynamic forces.[785]

More complex self-assembled patterns have also been imaged in situ by STM on liquid/solid interfaces by adding specific guest molecules to the porous supramolecular structures discussed above. One example of this can be seen in the case of the addition of coronene molecules to the two-dimensional molecular template of 1,3,5-benzenetricarboxylic acid that forms on a highly oriented pyrolytic graphite surface upon adsorption, in which case the guest molecules were seen to rotate inside their molecular bearing.[786] In a related study, coronene was shown capable of inducing the formation of a hydrogen-bonded isophthalic acid supramolecular macrocycle; the resulting heterocluster then forces an alkoxylated dehydrobenzo[12]annulene to form a van-der-Waals-stabilized honeycomb lattice to finally yield a three-component two-dimensional crystal containing nine molecules in the unit cell.[787] Even four-component self-assembled layers can be built this way.[788] Figure 24 shows another case in which C_{60} was seen to adsorb inside the cavity exposed by calix[8]arene molecules self-assembled on Au(111).[789] The selective accommodation of fullerenes in a two-dimensional hydrogen-bonded porous network formed by an azobenzene derivative, which contained two different types of cavities, was shown to be driven by the relative size of the void spaces in the host and guest molecules.[790] Either chemical markers within the molecules being self-assembled[791] or small probe molecules[792] can also be used as "flags" for the identification of interfacial structures, to determine, for example, the absolute chirality of optically active molecules self-assembled on solid surfaces.[793,794] Another possibility is to obtain spin-contrasted STM signals from the paramagnetic and diamagnetic parts of molecules, as demonstrated in a study on the self-assembly of 2-(14-carboxytetradecyl)-2-ethyl-4,4-dimethyl-3-oxazolidinyloxy adsorbed from a 1-phenyloctane solution onto a highly ordered pyrolytic graphite.[795]

In situ STM imaging can also be used to follow the dynamics of self-assembly and of adsorption on the resulting surface suprastructures. In general terms, it has been shown that the presence of the solvent helps with the reversible transition among the different two-dimensional phases that may form at the interface.[793] For instance, in one study, STM was used to document the reversible assembly and reassembly of two ordered supramolecular guanine motifs at a liquid water/graphite interface.[796] The kinetics of Ostwald ripening, that is, the coarsening of surface nanocrystals in two dimensions, was also observed in situ by STM for alkylated anthraquinone and oligothiophene.[797] Reversible phase transitions have been reported between different self-assembled structures of 1,3,5-tris(4-carboxyphenyl)benzene at the carboxylic acid/graphite interface.[798] In cases of adsorption of guest molecules on templates of host suprastructures, time-resolved STM experiments have been used to reveal that diffusion of the guest may proceed through thermally activated channeling or hoping between individual hosts.[799,800] In most of these examples, the dynamic processes

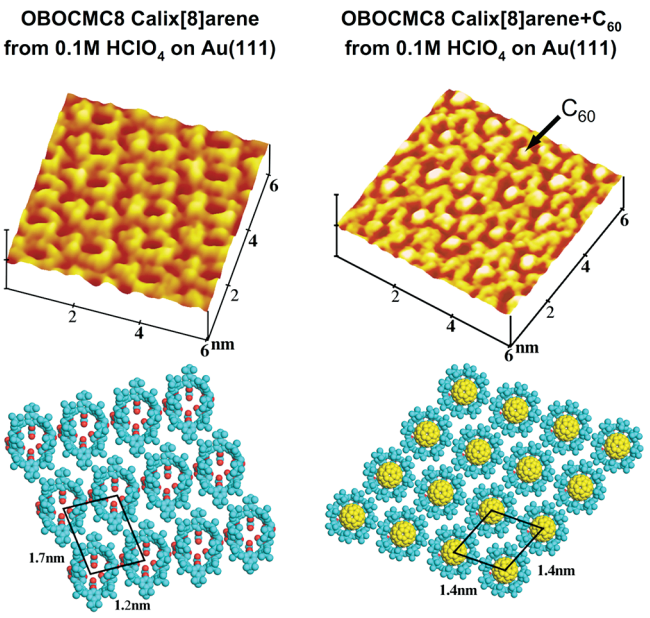

Figure 24. Illustration of the use of STM to characterize chemical processes in liquid/solid interfaces, in this case with monolayers of OBOCMC8, a calix[8]arene derivative, adsorbed from 0.1 M $HClO_4$ solutions onto a Au(111) surface.[789] Images are shown for adsorption of the calix[8]arene alone (left) and mixed with C_{60} (right). Schematic representations of the corresponding ordered arrays are shown at the bottom. The images suggest that the C_{60} buckyballs insert themselves into the calyx structure of OBOCMC8. Courtesy of Li-Jun Wan and Ge-Bo Pan. Reproduced from ref. 789 with permission. Copyright 2003 Wiley-VCH, Verlag GmbH & Co. KGaA.

described were identified by recording full images on a sector of the surface, and therefore could only be followed in a time scale in the order of seconds.

Some reports can also be found on the use of STM to characterize electrochemical processes. Indeed, such application of STM has more than a decade of history already, and has yielded information on the structures of adsorbed anions, the adsorption of organic molecules, the electrochemical dissolution of metals and semiconductors, and even the energetics of formation of adsorbed layers.[801−803] The majority of the studies in this area have focused on the characterization of the deposition of halide on the surface of single-crystal electrode surfaces, where complex ordered layers are often observed, sometimes changing with applied voltage.[804] It has also been shown that the ordered halide overlayers can be used as templates for the ordered deposition of a second layer of metallo-supramolecular cations.[805] In a case involving nonhalide anions, Taranovskyy et al. quantified the diffusion of sulfur atoms on a Cu(100) single-crystal electrode surface immersed in an HCl solution by recording the statistics of pairwise distances between adsorbates, and from that calculated the appropriate pairwise potentials.[806] An in situ STM study on the initial stages of oxidation of a Cu(111) surface in a basic solution showed that Cu_2O formation starts reversibly and preferentially at the upper-terrace side of step edges, with oxygen adsorption leading to a decrease in the mobility of the Cu atoms along the step edges.[807] In connection with cases of corrosion, an in situ STM study of Cu(100) electrode surfaces revealed that the initial stages of anodic Cu dissolution is accompanied by strong fluctuations in the step positions and an increase in step roughness in H_2SO_4 but involves step stabilization by a $c(2 \times 2)$ Cl adlayer and copper dissolution in complete atomic

rows with HCl.[808] Complex step dynamics under electrochemical conditions has been found to be common, and key in understanding the behavior of those surfaces.[809−811]

STM has also been used to look at the interfaces between solids and ionic liquids under electrochemical conditions. For instance, in situ STM images have highlighted the formation of ordered PF_6^- adsorbed layers from a 1-butyl-3-methylimidazolium hexafluorophosphate ionic liquid onto an electrified Au(111) interface.[812] Another in situ STM study showed that the electrodeposition of Ga on Au(111) from $GaCl_3$ in the ionic liquid 1-butyl-1-methylpyrrolidinium bis(trifluoromethylsulfonyl)-amide is initiated by the formation of islands.[813] Another in situ STM study has proven that ionic liquids may induce surface reconstruction in gold electrodes when an electric potential is applied.[814−817] A final, more unique, example here is the report of the use of 1-butyl-3-methylimidazolium hexafluorophosphate as an electrochemical gate in a STM configuration.[818]

In situ studies of the liquid/solid interfaces in catalysis using STM are quite scarce. One interesting example is that where single-molecule real-time imaging was performed on a manganese porphyrin oxidation catalysts adsorbed from a n-tetradecane liquid phase onto a Au(111) single-crystal.[819,820] It was determined that the oxygen atoms from molecular O_2 bind to adjacent porphyrin adsorbates on the surface before they react with the alkene substrate. In another report, the corrosion of platinum deposited onto a graphite surface, a model catalyst for the catalytic oxidation of L-sorbose to 2-keto-L-gulonic acid, in a neutral aqueous solution was shown by STM to occur within a few hours.[821] To note here is the fact that the conclusions in these examples were derived indirectly via imaging of the evolution of the surface during catalysis; we are not aware of any report of in situ STM studies of actual catalytic processes involving liquid/solid interfaces to date.

The tip in STM instruments can also be used to manipulate adsorbates and trigger specific surface chemistry, and a few examples of such operation in liquid/solid interfaces are already available in the literature. For instance, a C_{60} molecule has been transferred between adjacent cavities in the two-dimensional architecture built out of trimesic acid molecules adsorbed on a graphite substrate this way.[822] In another case, the group of Weiss recently reported on the manipulation and grafting of double-decker porphyrin molecules on graphite submerged under a 1-phenyloctane solvent.[823] Single "sandwich" naphthalocyanine-letetium-octaethylporphyrin molecules were adsorbed on the graphene and then decomposed with voltage pulses from the STM tip; afterward, the top octaethylporphyrin ligand was removed, so the bottom naphthalocyanine ligand was left on the surface. This approach allows for the nanopatterning of surfaces (Figure 25). The STM tip can be used to initiate polymerization reactions on solid surfaces as well.[824] For instance, it has been shown that chain polymerizations of the topmost surface layers from substituted diacetylene multilayer films deposited from phenyloctane solutions onto graphite substrates can be initiated by applying a pulsed voltage between the STM tip and the substrate.[825,826] In a more detailed study on the STM-tip-induced chain polymerization of 10,12-tricosadiynoic acid in a self-organized monolayer at the interface between a solution of the monomer and a highly oriented pyrolytic graphite, it was shown that oligomers could be produced by applying a short voltage pulse between the STM tip and the sample, with a probability that depends on the length of the applied pulse.[827] In that study, it was also proven that the polymerization could be confined to well-defined nanometer-sized areas by using molecular "corrals".

8.2. Scanning Electrochemical Microscopy (SECM)

The tip used in STM can also be used as an electrode to carry out scanning electrochemical microscopy (SECM), to add reactivity to the study of electrochemical systems (Figure 23, right panel). This technique was introduced by Bard in the late 1980s to investigate biological processes.[828−830] The small size of the tip adds a number of advantages in terms of the electrochemical studies, in particular the fact that those minimize the charging current, uncompensated resistance, and convection effects typically seen with conventional electrodes.[831,832] On the other hand, the electrochemical currents may interfere with the tunneling currents used in STM. In general, the tip in SECM is coated except for the very end in order to minimize contact with the liquid phase.

New advances in the use of SECM include the study of charge transport in thin films and membranes, electrocatalytic activity, the mapping of the local properties and reactivity of metals, insulators, and semiconductors, and the characterization of biological systems such as ion transport across channels in single cells and cellular and enzymatic activity.[833,834] In terms of problems related to energy generation, this technique has been used to study the deposition of metal nanoparticles, the chemical reactivity of noble metal nanoparticles for hydrogen and oxygen evolution, and electrocatalytic processes driven by enzymes for uses in biofuel cells.[833,835] In the next couple of paragraphs, we cite a few selected examples of the use of SECM to problems in different areas of chemistry, materials science, and biology.

In research related to corrosion, SECM has helped characterize the early stages of localized corrosion, the electroactive defect sites in passive films, the local initiation of pits, and the degradation of coating properties on steels.[836] For instance, in situ SCEM images of 304 stainless steel in a chloride solution at the open-circuit corrosion potential were used to locate the sites for the oxidation of Fe^{2+} emanating from metastable pits.[837] SECM was also used to identify localized electron-transfer activity at aluminum surfaces covered by their native oxide film in acetonitrile solutions, using the nitrobenzene/nitrobenzene-radical-anion couple as redox mediator.[838] In conjunction with AFM, SECM studies showed the superior properties of a newly developed Al−Mn−Si−Zr alloy for use as fin or tube material in heat exchangers for automobiles; that alloy displayed lower corrosion activity and smaller tunnel-like pits than the well-known EN AW-3003 material.[839]

In biological applications, SECM has been used to image individual cells on the basis of their activity in photosynthesis, respiration, electron transfer, single vesicular exocytosis, and membrane transport.[840−842] In-vivo SECM images of the oxygen evolution above single stomata in *Brassica juncea* showed a clear pore structure for the oxygen produced, and a decreased oxygen evolution in response to cadmium addition attributed to a lower photosynthetic yield.[843] Figure 26 shows images from a similar experiment with PC12 cells, a model cell type for studying neuronal function; a topographic image was correlated with an electrochemical image for oxygen reduction, obtained at a probe potential of −0.50 V versus a Ag/AgCl reference electrode, and the spatial distribution of the SECM signals was used, in conjunction with diffusion theory, to estimate the respiration rate of the PC12 cell.[844] SECM has also been employed to probe the redox properties of individual mammalian cells by measuring the rate of mediator regeneration by the cell, and to evaluate the several factors that determine the rates of the different steps of the process, including intracellular concentration of redox centers, mixed redox potential inside the cell, and the rate of

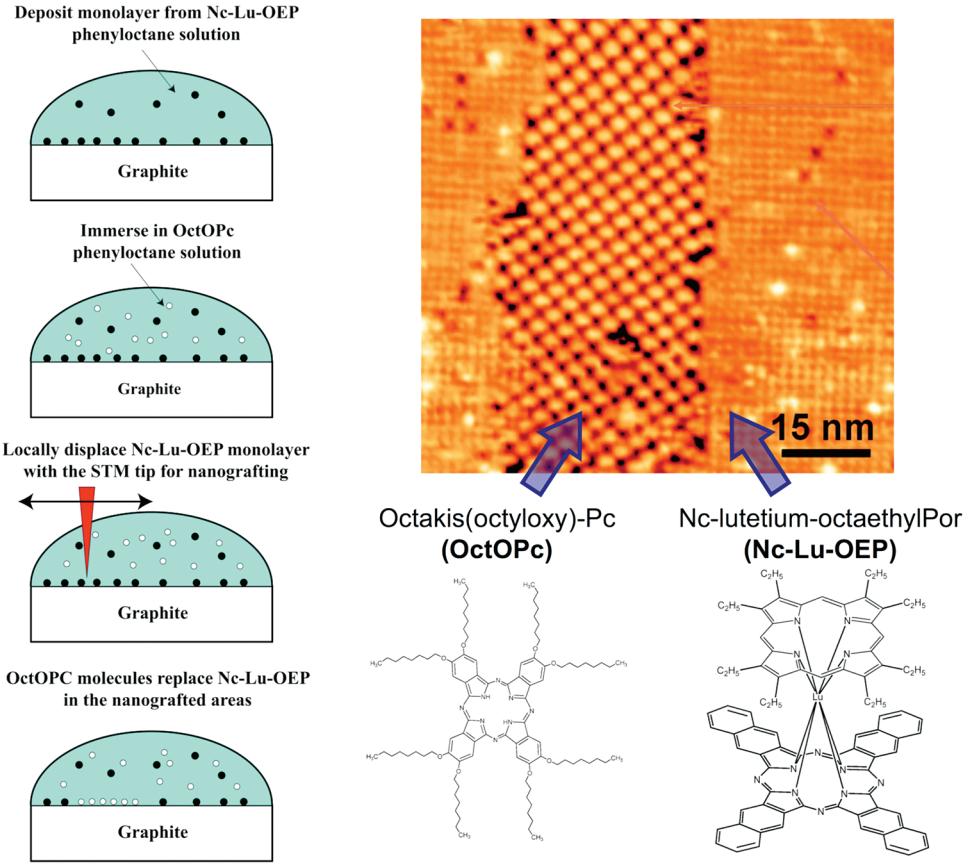

Figure 25. Example of the use of STM for the manipulation of molecules adsorbed at liquid/solid interfaces.[823] Left: Schematic representation of the nanografting procedure followed for the preparation of mixed layers of octakis(octyloxy)phthalocyanine (OctOPc) and naphtalocyanine-lutetium-octaethylporphyrin (Nc-Lu-OEP) onto a graphite surface from a 1-phenyloctane solution. Right: Resulting STM images. The smother surfaces seen on the sides correspond to the Nc-Lu-OEP double-decker molecules initially deposited on the surface, whereas the more corrugated center strip is associated with the bottom naphthalocyanine species that remains after removal of the top octaethylporphyrin ligand by applying voltage pulses with the STM tip. Courtesy of Paul S. Weiss, Tomohide Takami, Jianzhuang Jiang, and Bala Krishna Pathem. Reprinted from ref. 823 with permission. Copyright 2010 American Chemical Society.

membrane permeation by mediator species.[845] In a SECM study with living PC12 cells, six biocompatible redox mediators were identified and used for imaging of the cells before and after exposure to nerve growth factor.[846] In an example of studies of transport across membranes, the cytotoxicity of menadione on hepatocytes was studied with SECM by detecting the menadione-*S*-glutathione conjugate (thiodione) that is formed during the cellular detoxication process and is exported from the cell by an ATP-dependent pump.[847] Visualization of immobilized antibodies can also be achieved with SECM, since the tip current reflects the density of active binding sites in the immobilized antibody layer.[848]

Other heterogeneous systems amenable to studies by SECM include self-assembled layers, thin films, sensors, conductive polymers, modified electrodes, batteries, and electrocatalysts.[849] In one example, scanning probes were used to show that enantiopure metallo-supramolecular rhombs self-assemble from solution onto a Cu(100) electrode surface precovered by a tetragonal pattern of chloride anions through coordination of bispyridyl-substituted ligands.[850] In a study involving polymers, SECM has been used to image the ejection of $Os(bpy)_3^{2+}$ counterions from Nafion coatings on electrodes during their electrochemical oxidation to $Os(bpy)_3^{9+}$.[851] In another study, on the electrochemical reactivity of a Cu(100) single-crystal electrode surface covered with a free-base porphyrin, the formation of a well-ordered self-assembled layer of the reduced porphyrin after the first two-electron reduction step was revealed, and also the dissolution of copper starting at step edges coincidentally with the preferential oxidation of reduced porphyrin species at the same sites.[852] In a case associated with corrosion, a scanning vibrating electrode technique was added to SECM to investigate microscopic aspects of the electrochemistry of the iron−zinc galvanic couple immersed in aqueous sodium chloride solution to obtain information on the distribution of ionic currents arising from the metal surface, adding to the SECM measurements of the concentration of chemical species relevant to the corrosion processes.[853] In electrocatalysis, SECM has been used for the characterization of thin film combinatorial libraries for fuel cell electrode applications.[854]

SECM is ideal for measuring the kinetics of charge transfer locally at specific sites within liquid/solid interfaces.[855] Indeed, SECM has been used to measure rates of electron transfer across a variety of self-assembled molecular monolayers, to estimate rates for the direct transfer through the film, for transfers in bimolecular reactions between attached and dissolved redox species, and for electron transfers mediated by monolayer-attached redox moieties. Examples include cases as diverse as ferrocene/alkanethiol pairs, $Ru(NH_3)_6^{3+}$ through alkanethiol molecules,[856] and cytochrome c electrostatically immobilized onto a COOH-terminated alkanethiol self-assembled monolayer,[857] all supported on gold electrodes,

dx.doi.org/10.1021/cr2002068 |*Chem. Rev.* 2012, 112, 2920–2986

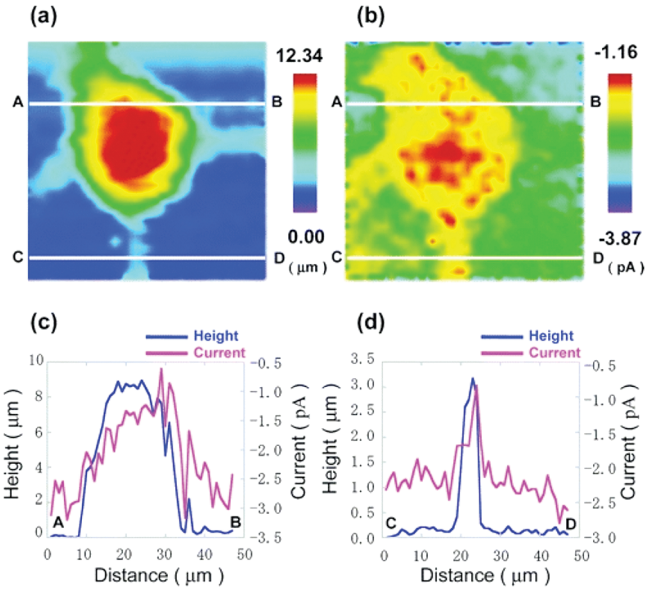

Figure 26. Example of the use of SCEM to correlate topographic information with specific electrochemical activity. In this case, images are provided for a single PC12 cell in aqueous solution.[844] Topographic (a) and electrochemical (b) two-dimensional contour maps are provided, the latter by using a probe potential of −0.50 V versus a Ag/AgCl reference electrode to promote reduction to O_2. Height and current profiles are also shown, in panels (c) and (d), for the two cross sections indicated by the white lines in the images above. Clear enhanced oxygen production activity is seen at the center of the cell, and an oxygen profile defined by diffusion of the product to the exterior of the cell. These data were used to estimate the respiration rate of the cell. Reprinted from ref. 844 with permission. Copyright 2006 American Chemical Society.

Cd^{2+} adsorbed on ω-mercaptoalkanoic acid self-assembled monolayers,[858] ferrocenyl-functionalized poly(propylenimine) dendrimers immobilized at monolayers of β-cyclodextrin on glass,[859] gold nanoparticles supported on a silanized glass substrate[860] or on polymer multilayers,[861] and glucose dehydrogenase immobilized on a hydrophobic surface,[862] to mention a few.

8.3. Atomic Force Microscopy (AFM)

Atomic force microscopy (AFM) is complementary to STM in that it is also useful to spatially image properties in liquid/solid interfaces.[758,863] The difference is that, in AFM, forces instead of tunneling currents are used to obtain topographic views of solid surfaces (Figure 23, center panel). It has been, in general, much more difficult to obtain atomic resolution with AFM than with STM, but that is starting to change thanks to new developments such as the introduction of tapping and intermittent contact modes and of frequency-modulation AFM, which reduces the magnitude of interfering lateral forces.[864,865] A number of complications do need to be addressed when dealing with liquid/solid interfaces beyond those intrinsic to all AFM experiments, including the softness of the interface, the presence of new van der Waals interactions, and the addition of capillary forces.[866] Another limitation is the low quality factor of the cantilever resonance in liquid environments, which leads to high noise levels and poor resolution; this problem can be minimized by using stiff cantilevers and/or reducing the amplitude of the oscillations.[867−873] On the positive side, AFM can be used not only to obtain topographic images, but also to measure forces down to the magnitude of individual molecular interactions.[874]

AFM has been extensively used to investigate systems of biological interest.[875−878] In terms of imaging, AFM affords the detailing of specific features within isolated cell membranes adsorbed onto flat supports with subnanometer resolution, and spatial resolution on the order of 10 nm on corrugated cell surfaces is possible as well. Much work is available in the literature on the use of AFM in situ for the imaging of live cells,[879] starting with the first reported AFM image, that of a plant cell imaged in water.[880] In the early years there was some fear that AFM would not be viable for the study of living cells because of the potential to rupture the delicate membranes, but in fact many images were soon obtained of living cells even in contact mode.[881−885] In one case, AFM was used to reveal that the rhodopsin in mouse disk membranes forms paracrystalline arrays of dimers.[886] Most of the early work on AFM imaging of cells focused on mammalian cells, mainly because those generally adhere well to surfaces and are therefore not easily removed by the scanning tip, but smaller bacterial and yeast cells can now be immobilized on surfaces before imaging by various techniques such as entrapment in membrane filters[887−889] and tethering via surface modifications.[890,891] AFM is also becoming a useful tool to image viruses,[892] and to study systems of pharmacological interest such as drug delivery.[893]

AFM imaging has been often used to identify changes in living systems, either intrinsic or generated upon the application of external stimuli. An interesting example from such AFM studies is the identification of 14 subunits arranged in a cylindrical ring in the turbine of ATP synthase from leaf chloroplasts, the smallest rotary motor in biology.[894] In another study, AFM images of individual tubulin protofilaments showed that taxol stabilizes microtubules, which exist in dynamic equilibrium growing and shrinking by the addition or loss of tubulin dimers from the ends of the protofilaments, by straightening the guanosine diphosphate protofilament and slowing down the transition of protofilaments from straight to a curved configuration.[895] There is also a report of AFM images of the cytoplasmic domains of the gap junction surface form a hexameric pore protruding from the membrane bilayer, which were shown to have significant intrinsic flexibility and to undergo a reversible conformational change upon injection of Ca^{2+} ions into the buffer solution.[896] AFM of freshly isolated outer mitochondrial membranes were used to demonstrate the existence of voltage-dependent anion channels in several forms, from monomers to hexamers and higher oligomers.[897] AFM has also provided some insight into the evolution of photosynthetic membranes of a bacterium in response to light, indicating that the local environment of core complexes remains unaltered while specialized paracrystalline light-harvesting antenna domains grow under low-light conditions.[898]

AFM can be used not only to image cells but also to measure forces within specific regions of those cells. In an early report, adhesive interaction forces measured in Madin−Darby canine kidney and RS cells by AFM were attributed to either the rupture of individual hydrogen bonds or interaction with ordered water layers near the surface.[899] In a subsequent study, an AFM mapping of the relative elasticity of mouse F9 embryonic carcinoma cells showed a correlation with magnetometer measurements that suggested promotion of cell adhesion by vinculin.[900] The turgor pressure of magnetotactic bacteria of the species Magnetospirillum was quantified with AFM by measuring the deformability of the wall.[901] AFM in force-mapping mode was used to track the dynamic changes in the stiffness of the cortex of adherent cultured cells associated with cell division, to show that cortical stiffening occurs over the equatorial region before any furrow appears, that the

stiffening increases as the furrow starts, and that polar relaxation of cells does not seem to be required for cell division to occur.[902]

AFM has also been used to measure the interaction forces between pairs of biomolecules, by functionalizing the AFM tip appropriately with one of the molecules of interest. Several examples of this use address interactions between DNA strands. In one report, by first attaching the oligonucleotides covalently to both a spherical probe and a flat surface, those forces were measured and correlated with the number of base pairs involved in the interchain interactions.[903] In another study, using self-assembled purines and pyrimidines on planar gold surfaces and on gold-coated AFM tips under water, directional hydrogen-bonding interaction between the tip molecules and the surface molecules could be detected and measured only when opposite base-pair coatings were used.[904] The AFM tip functionalization approach has also been used to probe receptor−ligand binding. For instance, specific and discrete forces have been identified using AFM between biotin, attached to the cantilever, and either avidin or streptavidin, anchored to the flat surface.[905,906] Another elegant example is that of the use of a chiral acylated phenylglycine-coated tip to distinguish between the two enantiomers of mandelic acid arrayed on a surface through differences in both the adhesion and the frictional forces measured by the probe.[907] A third example involving selective AFM probing on whole cells is the case of the imaging of the affinity of red blood cells to an AFM tip functionalized with *Helix pomatia* lectin as a way to differentiate between A and O types: the high specificity of the lectin for the N-acetylgalactosamine-terminated glycolipids present in the membrane of group A red blood cells afforded the discrimination between the two cell populations (Figure 27).[908] Measurements have been carried out on the forces required to unravel certain biomolecules as well. Examples of this include the unfolding of individual Titin[909] or tenascin[910] immunoglobulin domains, and the unzipping of an entire bacterial pore from an isolated membrane surface of *Deinococcus radiodurans*.[911]

Some reports are also available on the use of AFM to image liquid/solid interfaces in situ in nonbiological systems. In connection with the behavior of mineral surfaces, one of the earliest reports focused on the structure of freshly cleaved calcite under water.[912] Later, high-resolution in situ AFM of calcite surfaces showed low kink density and weak step edge fluctuations, a result that contradicts the classical terrace-ledge-kink model of crystal growth used to interpret mineral formation.[913] AFM has also been used to measure the force of interaction between a SiO_2 glass sphere and a TiO_2 crystal in an aqueous medium as a function of pH.[914] In a problem of electrochemistry, an in situ electrochemical AFM study proved that the inhibition of copper corrosion by linear sodium heptanoate is due to the formation of a layer of copper heptanoate, the morphology of which changes as a function of several electrochemical parameters.[915]

Liquid/solid AFM has also had some impact in colloid and polymer sciences.[916] For instance, AFM images of an asymmetric cationic Gemini surfactant adsorbed from an aqueous solution onto a mica surface indicate the formation of complete micelles with a hexagonal structure.[917] In more general terms, the different AFM images obtained for quaternary ammonium surfactant aggregates formed from aqueous solutions onto different solids indicate the balance that must exist between the natural free curvature as defined by intermolecular interactions and the constraints imposed by specific surfactant-surface interactions.[918] AFM has been used to prove phase separation in Langmuir−Blodgett films,[919] and also to directly measure the interaction forces between colloidal particles as a function of surface separation.[920] In an AFM study on the adsorption of charged latex particles onto a mica substrate, a high degree of short-range order was found when the surface coverage approached saturation, and a reduction in the range of ordering due to double-layer screening of interparticle repulsions was also observed.[921] AFM studies with different surfactants have shown how they adsorb and self-assemble at liquid/solid interfaces, and how mixtures of surface-active materials can show synergistic interactions that can be manifested as enhanced surface activity, spreading, foaming, and detergency.[922] Even the contact line tension of a solid (perfluorinated alkylsilane-covered glass)−liquid (water)−vapor (air) three-phase system could be determined from the liquid surface topography data obtained with scanning force microscopy.[923] Finally, in connection with polymer science, an in situ AFM study of the conformations of poly(2-vinylpyridine) at the liquid/solid interface as a function of pH indicated that the highly protonated poly(2-vinylpyridine) chains adopt a two-dimensional equilibrated random coil conformation, whereas at low degree of protonation they exist as strongly compressed three-dimensional coils.[924] Another report showed that the "reptational" movements of isolated isotactic poly(methylmethacrylate) polymer chains on a mica substrate can be accelerated by the addition of water.[925] Progress during the redox-driven cycle of individual neutral and oxidized poly ferrocenyldimethylsilane macromolecules was followed by AFM, where reversible motion could be controlled in situ by adjusting the electrochemical potential.[926]

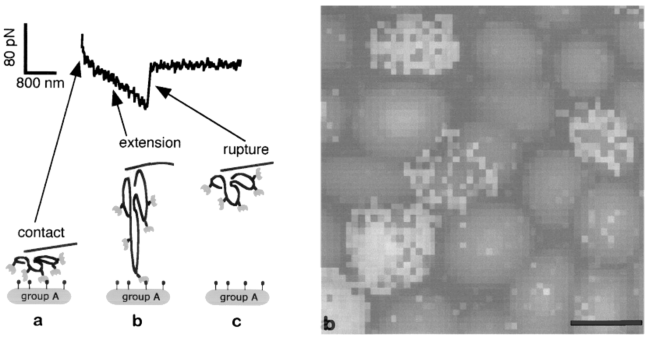

Figure 27. Illustration of the use of AFM in situ in a liquid environment to obtain a spatial mapping of specific chemical groups. In this case, a mixture of groups A and O red blood cells were probed with AFM by using a lectin-funtionalized tip, to take advantage of the selective affinity to lectin by the sugar moieties at the A (but not the O) cells.[908] Left: Typical force curve recorded on group A cells, showing the three main events in these experiments: (a) the approach of the tip into contact with the cell surface; (b) the stretching of the lectin as the AFM tip is moved away, because of its binding to the cell; and (c) the rupture of the lectin-sugar molecular bridge. Right: Superimposed topographic (light gray) and adhesion (sharper contrast, highly pixelated) images of mixed layer of group A and O red blood cells spread on a polylysine-coated glass surface. The adhesion forces at each image pixel were calculated from the last rupture peak of the retract curve (step c), whereas the height image was calculated from the piezo elongation at the contact point (step a). The selective chemistry between the lectin and sugar species was used here to discriminate between the two red blood cell groups: the bright regions in this image correspond to the group A cells. Adapted from ref. 908 with permission. Copyright 2000 SAGE Publications.

9. MICROSCOPIES. C. OPTICAL SCANNING

Close to atomic resolution in microscopy can also be obtained by optical means by placing the probe, typically a microscopic tip, very close to the liquid/solid interface in order to go beyond the

resolution limit imposed by the wavelength of the light. This approach is known as scanning near-field optical microscopy (SNOM, or NSOM).[927,928] In this case, the measurement of optical properties relies on the evanescent waves generated between the tip and the surface, and the resolution of the image is limited by the size of the detector aperture and the distance between the probe and the surface, which can be as small as a few nanometers, not by the wavelength of the illuminating light. To obtain spatial images of the sample, the tip is typically scanned by using piezoelectrics, in a similar way as in STM and AFM. Several spectroscopic methods can be coupled with SNOM, from which the most common is fluorescence detection. SNOM can be set up in a number of modes, roughly grouped as aperture and apertureless depending on the type of tip used, either a fiber optic, to allow light to travel in or out of the area being probed, or an opaque tip used as antenna for the collection and amplification of light coming from an outside source.

The main advantage of SNOM is that spectroscopic information can be added to the high spatial resolution possible with scanning microscopies. Atomic resolution is near impossible in this case, but resolution down to a few tens of nanometers has been possible in some instances, sufficiently high to identify single features in many biological systems. On the other hand, SNOM faces the same limitations of other scanning spectroscopies. One of the most critical when liquid/solid interfaces are involved is the ability to control the position of the tip, to avoid damaging the surface.[929−931] In addition, the optical signals are typically weak, especially when using apertured optical fibers, and that often leads to low signal-to-noise ratios, in particular if specific chemical information is desired.[932] Because of the need to combine two sophisticated sets of techniques, optical spectroscopies and scanning microscopies, SNOM is also quite difficult to implement. Nevertheless, many recent developments have help overcome the limitations of SNOM and achieve increasingly better spatial[933,934] and temporal[935,936] resolution in the imaging of liquid/solid interfaces.

Most SNOM studies of liquid/solid interfaces up to date have been directed at the characterization of biological systems and have often relied on the apertured fluorescence approach (after cloning appropriate fluorescent molecules to the cells to be studied). Even in this area, though, the number of reports to date has been limited. In one case, SNOM was used to determine that orange-emitting fluorophores are not a major component in lipofuscin granules isolated from human retinal pigment epithelium cells.[937] In another study, the distribution of the *N*-methyl-D-aspartate receptor channels in the membrane of a rat cortical neuron were identified after tagging them with a carbocyanine dye through the use of antibodies.[938] SNOM images of a nuclear pore complex (a supramolecular protein complex embedded in the double membrane of a cell nucleus), labeled by using fluorescent-marked antibodies against one of its nucleoporins, were obtained with sufficient resolution to identify single nuclear pores in the nuclear envelope with a nearest neighbor distance of ∼120 nm.[939] SNOM was also used to directly visualize nanometric-sized domains of the transmembrane protein DC-SIGN on the membrane of dendritic cells in a liquid environment with a resolution of approximately 90 nm.[940] In a final example, fluorescence SNOM was used to image the orientation[941] and phase separation[942,943] of supported phospholipid bilayers used as models for natural membranes. In all these examples, SNOM was used mainly to image and locate specific functions within the biological samples studied, not to investigate chemistry occurring at the liquid/solid interface.

The use of other versions of SNOM, including infrared and Raman-based spectroscopies and apertureless setups, for the characterization of liquid/solid interfaces is still by and large in the future.[944−947] There are nevertheless some interesting reports on these new directions of research already. For instance, an interferometric SNOM setup was successfully tested for the imaging of oil droplets on a mica support at a resolution of 10 Å.[948] Midinfrared SNOM images of single motile fibroblasts living cells could be obtained under water by using the Stanford Free Electron Laser tuned to absorption peaks of both protein and lipid molecules; strong absorption from lipid molecules was seen in the motile fibroblasts.[949] An apertureless IR version of SNOM has been developed where an AFM probe is used as a temperature sensor to measure the absorption of IR radiation,[950] and an interesting recent report has proven the applicability of this technique to map the spatial distribution of specific chemical groups in living cells.[951] There has also been some interest in the development of tip-enhanced Raman spectroscopy (TERS) in recent years,[952] but to the best of our knowledge, no applications of TERS to liquid/solid interfaces have been reported yet. The effect of the liquid solvent on the electric fields on which that technique relies for signal enhancement has not, as far as we know, been tested; a theoretical study predicts not only a reduction in signal enhancement of up to several orders of magnitude but also the red shift of some signals.[953]

10. MICROSCOPIES. D. ELECTRON (SEM, TEM)

Electron microscopies, which rely on the use of electrons, are typically operated under vacuum conditions and are therefore not typically suitable for the study of liquid/solid interfaces. In this respect, they share the same limitations of XPS and other surface-sensitive techniques, as discussed in Section 6.1, although the fact that electrons with much higher energies are used for microscopy means that they can penetrate deeper through condensed phases. The use of electron microscopy is certainly pervasive in studies involving the imaging of biological samples.[954] However, in most of those applications, the samples are prepared to make them compatible with the vacuum environment, a process that often involves freezing or casting in a matrix of an appropriate material. The main purpose in those cases is to obtain images of the tissues under study, not to investigate any particular interfacial chemistry. One advantage of electron microscopy is that compositional analysis can be added to the collection of images by using energy-dispersive X-ray spectroscopy (EDX, EDAX, EDS) or electron energy loss spectroscopy (EELS).

The same as with XPS, "environmental" electron microscopy instrumentation has been developed recently to deal with nonvacuum systems, mainly to look at gas/solid interfaces, but, in some instances, at liquid/solid systems also. In fact, setups based on closed cells were designed some time ago where confinement of the nonvacuum environment is achieved by using electron-transparent windows.[955,956] The early designs were mostly operational under gas atmospheres, but more recent cells afford in situ transmission electron microscopy (TEM) imaging of living organisms and bioreactions in aqueous conditions.[957] One nonbiological example of the use of this closed-cell TEM approach is that of the dynamic recording of the nucleation and growth of nanoscale copper clusters during electrodeposition.[958] A more recent in situ TEM study, on the development of platinum nanocrystal in colloidal solutions, showed that nanocrystals can grow by both monomer attachment from solution and particle coalescence, and

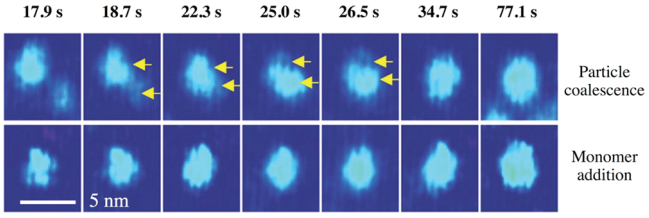

Figure 28. Example of the use of transmission electron microscopy (TEM) for the in situ characterization of reactions involving liquid/solid interfaces. The set of images in this figure corresponds to a time sequence during the growth of two platinum nanoparticles from Pt(acetylacetonate)$_2$ in a mixture of o-dichlorobenzene and oleylamine.[959] The two rows illustrate two growth mechanisms, via the coalescence of two smaller particles (top) and by stepwise growth one monomer at a time (bottom). Recrystallization was also observed during the coalescence of particles, as indicated by the contrast changes highlighted by the arrows. Courtesy of Paul Alivisatos and Haimei Zheng. Adapted from ref. 959 with permission. Copyright 2009 AAAS.

that the combination of the two processes helps narrow down an initially broad size distribution into a nearly monodisperse distribution (Figure 28).[959] Similar enclosed cells have been developed for use in scanning electron microscopy (SEM), mostly for biological uses.[960,961] In all these cases, though, it has become clear that a couple of problems may limit the usefulness of closed-cell arrangements: (1) the finite amount of liquid in the cell may skew the time evolution of the chemistry in the samples as the reactants in solution are consumed, and (2) bubbles may form via evaporation of the liquid by the electron beam. To avoid those problems, liquids may be introduced in electron microscopes via the use of microfluidic flow cells instead.[962−964] Such arrangements are quite new, and their usefulness for the study of liquid/solid interfaces is still to be proven.

TEM imaging can also be carried out in situ in cases where the vapor pressure of the liquid is low such as with some melts.[965,966] As an example, atomic-resolution TEM has been used to follow the melting of gold nanoparticles.[967,968] The impressive images from this study have provided clear evidence for frequent twinning of the crystalline nanoparticles at the onset of melting. High (15 ns) time resolution TEM was also used to follow the rapid solidification dynamics of 80 nm-thick Al thin films made by pulsed laser melting, and to determine the moving speed of the liquid/solid front.[969] In one case, by using a zeptoliter-size pipet, the crystallization of nanometer-sized fluid drops of $Au_{72}Ge_{28}$ was seen to avoid nucleation in the interior and to proceed via an initial liquid-state surface faceting instead.[970,971] Another research group carried out similar studies on the growth of Si and Ge nanowires promoted by Au−Si and Au−Ge catalysts, respectively, showing the liquid nature of the eutectic catalyst droplet; unexpected observations, including surface faceting and diffusion of the catalyst during growth, were reported.[972,973] TEM studies on the growth of solid silicon from liquid gold−silicon catalyst particles as a function of increasing silicon supersaturation indicated that the nucleation is heterogeneous, occurring consistently at the edge of the AuSi droplets regardless of particle size.[974−976] Another report provided electron microscopy evidence for the influence exerted by confined nanoscale geometries on the physical transformations of some materials.[977] It was shown that capillary pressure pushes the melt formed from heating a germanium nanowire attached to a gold nanocrystal into the cylindrical neck of the nanowire, and that gold diffusion is several orders of magnitude slower than in a bulk germanium crystal. The elemental concentrations and redistributions of different elements during crystals nucleation and growth with alloys has also been monitored in a transmission electron microscope by using energy-dispersive X-ray spectroscopy on partially molten Al−Si−Cu-Mg alloy particles during in situ heating.[978]

Finally, in situ TEM characterization of liquid/solid interfaces may also be possible with ionic liquids. In one report, the dimensions of the particles made during the synthesis of copper nanoparticles in ionic liquids using plasma electrochemical deposition were determined in situ by TEM.[979] Another in situ TEM study, on the structural evolution of the materials in a lithium ion battery during dynamic operation, indicated limited wetting of the ionic liquid used as the electrolyte on the surface of an SnO_2 electrode.[980] TEM has been used in situ to detect the nucleation of gold nanoparticles from tetrachloroauric acid catalyzed by rutile particles dissolved in a *N*,*N*,*N*-trimetyl-*N*-propylammonium-bis(trifluoromethanesulfonyl)imide ionic liquid upon radiation with UV light.[981]

11. CONCLUDING REMARKS

In this review, we have attempted to list and discuss the main spectroscopic techniques that have been developed or adapted for the study of the chemistry of liquid/solid interfaces at the molecular level. Clearly, the study of such interfaces is quite difficult, certainly more difficult that the characterization of vacuum/solid, or even gas/solid, interfaces. The fact that the surfaces of interest are buried in between two condensed, high-density, phases is an impediment for the use of most of the surface-sensitive techniques developed in the past decades, many of which rely on the use of particles such as electrons, ions, or atoms. Only in a very few instances, such as in the cases where special setups have been developed in conjunction with XPS (Section 6.1) and electron microscopies (Section 10), this difficulty has been circumvented.

The most promising alternative for probing liquid/solid interfaces is the use of analytical techniques based on electromagnetic radiation (light). The main problem with those is that most of them are not intrinsically surface-sensitive, and that it is therefore not easy to extract the signals due to the few atoms at the interface from those originating from the much more abundant bulk phases. This is perhaps the main reason why optical spectroscopies have not, until recently, been used much for the characterization of chemistry at any interfaces. Nevertheless, a good number of approaches have now been developed for the spectroscopic study of liquid/solid interfaces that take advantage of special spectroscopy rules only applicable to surfaces or rely on the uniqueness of the chemistry that occurs at the interface. In this review, we have surveyed the multiple ways in which infrared, visible, UV, and X-ray radiation is being used to probe liquid/solid interfaces. Some techniques, such as SHG, SPR, and ellipsometry, only provide average information on the properties of the surface and can be used mainly to follow surface coverages and film thicknesses, but other do provide detailed molecular knowledge: infrared absorption spectroscopy, SERS, and SFG yield valuable vibrational details, and X-ray absorption and scattering techniques can be used to extract both electronic and structural data from these systems. The microscopies surveyed in Sections 7−10 also provide spatial information on heterogeneous interfaces. Taking all these techniques together, it can be said that a reasonable tool set is already available to interrogate liquid/solid interfaces. On the other hand, there is much room for improvement still.

Several considerations need to be taken into account when selecting the appropriate technique for the study of a particular

liquid/solid interface. It should be noted, for one, that several of the techniques mentioned in this review are expensive or difficult to implement. X-ray absorption, scattering, and diffraction techniques, for instance, require the use of synchrotron radiation, neutron sources are even more difficult to come by, and even Raman, SFG, and SHG demand the use of lasers and complex optics. In addition, many techniques have often proven particularly apt for the study of very specific systems. To provide just one example, SPR, ellipsometry, and QCM have all been used mainly to follow the uptake of large molecules, surfactants and biologically relevant species (DNA, proteins). This compartmentalization of the use of a given technique for a specific family of systems is in some instances the result of a lack of communication between different fields of science, though. For instance, RAIRS was long ago adapted for the study of liquid/solid interfaces by the electrochemistry community but has not been used much in the characterization of other liquid/solid systems. SPR and QCM have been particularly popular in the design of bioassays but are not as commonly employed in other areas where adsorption isotherms and kinetics are relevant. Most of the STM work published to date involving liquid/solid interfaces focuses on supramolecular self-assembled monolayers. X-ray absorption spectroscopies have been mainly used to characterize the chemistry of catalysts, mineral samples, and nanoparticles, whereas X-ray scattering and diffraction techniques, which require similar synchrotron sources, have been employed mostly for studies in self-assembly and biological systems. Some of these preferences may be justified in terms of the specific information required in each case, but it is still curious that there is such minimal cross-use of spectroscopies among different fields of science. In this respect, we hope that our review helps break such barriers by providing a broad overview of the different options available to interrogate liquid/solid interfaces.

Beyond any biases originating from historical practices in particular fields of chemistry, materials science, or biology, the selection of the appropriate technique to be used to address a specific issue involving liquid/solid interfaces requires a few additional basic considerations. First and foremost, that selection is heavily dependent on the type of information being sought. For instance, vibrational spectroscopies provide very specific molecular-level knowledge and are typically used to learn something about the chemistry of adsorbates, and sometimes also about molecular orientations at the liquid/solid interface. Spectroscopies based on the use of UV−vis and X-ray radiation, by contrast, probe electronic properties, and may in many instances be used to probe not only adsorbates but also the solid surface. Many of the techniques discussed above, including ellipsometry and QCM, provide average information about the interface, and are not particularly helpful in unraveling chemical details but are rather useful to follow overall interface coverages. X-ray scattering and X-ray diffraction experiments require some degree of long-range ordering, and are used to extract structural information. Less common is the characterization of the liquid phase just above the liquid/solid interface even if that is of great importance in studies in electrochemistry and phase changes (to mention a couple of examples), but that can also be accomplished with some optical spectroscopies, as illustrated throughout our review.

There are also more practical issues to consider. Evidently, cost and availability are significant decision-making factors, as mentioned above. Many techniques are quite specialized, and are not commercially available; their development is in itself the central objective of many research efforts. Moreover, the nature of the sample may limit the use of some techniques. For instance, techniques with poor signals or large nonzero backgrounds originating from the bulk phases are mainly suitable for the characterization of samples with high interfacial areas such as nanoparticles, porous materials, and micelles and other self-assemblies. Examples here include not only NMR and ESR but also some vibrational spectroscopies. One way to compensate for poor signals is to use intense light sources, but that risks damaging the sample, in particular with biological systems; only robust solids are amenable to some X-ray based studies. At the other end, scanning microscopies and some optical spectroscopies requiring reflective surfaces typically operate on flat surfaces, and are therefore not useful for the study of systems where the topography of the interface is rough or difficult to control. Some spectroscopies also involve special sample preparation: surface-enhanced Raman often requires rough silver or gold surfaces, SPR relies on the excitation of the plasmons in gold substrates, ESR only works with paramagnetic samples, and fluorescence emission spectroscopies demand the addition of appropriate fluorophores.

Another consideration is the potential need to obtain information on the spatial distribution of the different chemistries that may take place within the liquid/solid interface of a given system. Most spectroscopies provide only an average of those, or at best an indication of the presence of all without any spatial information of their distribution. This issue may be addressed by using any of the microscopies discussed above, but in that case the level of spatial resolution required becomes an additional deciding factor. As explained above, regular optical microscopies offer resolution much lower that what is need to address chemical issues in liquid/solid interfaces at the molecular level unless additional arrangements are made to operate in "single-molecule" mode, for instance by diluting the sample or by using separation techniques such as flow cytometry. Even in those cases, it may be possible to follow individual chemical events but still not obtain atomic-level information. To achieve imaging at the molecular level, scanning microscopies are the best alternative available to date, but there the limitations are in the type of samples amenable for those studies, typically flat substrates. Also, most scanning microscopies offer only limited chemical information, and often require quantum mechanics simulations or much speculation for their interpretation. Of course, there are possible ways to address these limitations, most notably the use of scanning tunneling spectroscopy in STM to extract more chemical information on specific features imaged at the interface. It would also be desirable to be able to carry out electron microscopy experiments to investigate liquid/solid interfaces, but that, by and large, is not yet feasible.

One nice feature of the optical spectroscopies available for liquid/solid interface characterization that rely on the use of lasers or synchrotron sources is that they provide the opportunity to add a temporal dimension to most experiments if required. Pulsed lasers are particularly suitable for the study of dynamics with time resolution down to the picosecond, or even femtosecond, time domain. Synchrotron radiation is also intrinsically pulsed, although not much control can be exercised there in terms of pulse length or frequency. For kinetic studies in longer timeframes, for events occurring in milliseconds or longer times, most techniques described above can be used; the issue becomes one of signal-to-noise levels, as signal averaging is given up for the sake of time resolution. Fast-scan and step-scan FTIR instruments are certainly available for such kinetic studies, but have

seldom been used in studies of liquid/solid interfaces to date. Phase shifts and other more sophisticated approaches can also be used with many optical spectroscopies to extract temporal information.

Overall, it is worth reiterating that, although there is a battery of techniques available already for the investigation of liquid/solid interfaces, once the specific considerations discussed above are taken into consideration, many limitations remain. Some future directions can be suggested to improve on this situation. First, some techniques that are well-known in many other fields of research have not yet been exploited to their fullest potential when it comes to their use for the characterization of liquid/solid problems. The particular example of NMR comes to mind. Second, some spectroscopies are already reasonably well developed for the characterization of liquid/solid interfaces, yet have not been fully exploited for the study of chemistry at those interfaces. SERS in particular has been repeatedly used to analyze bulk samples, using the surface only as a way to enhance the Raman surface, but has seldom been applied to characterize the chemical nature of species at the liquid/solid interface itself. Third, techniques commonly used to study liquid/solid interfaces in one particular field of research have not been exploited for studies in other areas. There is a particularly deep divide between the way studies of biological versus nonbiological liquid/solid interfaces are approached. Finally, there is clearly plenty of room to adapt existing surface-sensitive techniques or develop new ones to operate at liquid/solid interfaces. The initial advances seen in this direction with XPS and electron microscopy should be continued, and extended to other techniques. It is our hope that this review may entice expert spectroscopists not working with liquid/solid interfaces to adapt their techniques for such uses. The research areas that require the characterization of liquid/solid interfaces have made much progress already, but there is much room for growth yet.

AUTHOR INFORMATION

Corresponding Author

*E-mail: zaera@ucr.edu.

BIOGRAPHY

Francisco Zaera received his Licenciate degree in Chemistry from the Simón Bolívar University in Caracas, Venezuela (1979), and his Ph.D. from the University of California, Berkeley (1984). He held an Assistant Chemist position at the National Synchrotron Light Source of Brookhaven National Laboratory, in a joint appointment with Exxon Research Laboratories, until 1986, after which he became a faculty member at the University of California, Riverside. Presently, he is a Distinguished Professor of Chemistry at UCR. Prof. Zaera has been awarded the 1994 and 1995 Union Carbide Innovation Recognition Program Award, the 2001 ACS George A. Olah Award in Hydrocarbon or Petroleum Chemistry, the 2003 Paul H. Emmett Award of the North American Catalysis Society, a 2004 Humboldt Research Award for Senior U.S. Scientist, and the 2008 ACS Arthur W. Adamson Award for Distinguished Service in the Advancement of Surface Chemistry. He is a Fellow of the American Vacuum Society, the American Association for the Advancement of Science, and the American Chemical Society. He has held several editorial positions, and is currently Senior Editor of The Journal of Physical Chemistry. He has also held several professional offices, including those of Treasurer (1997, 1998), Vice Chair (2005), Chair-Elect (2006), and Chair (2007) of the Colloids and Surface Chemistry Division of the American Chemical Society, and Treasurer-Secretary and President of the California Catalysis Society (1990-1992). Prof. Zaera has published close to 300 publications in scientific journals. His research interests are in surface and materials chemistry and in heterogeneous catalysis. More information about Prof. Zaera can be found at his web site, http://chem.ucr.edu/Zaera/lab.html.

ACKNOWLEDGMENT

We acknowledge financial support from the U.S. National Science Foundation and by the U.S. Department of Energy.

REFERENCES

(1) Zaera, F. *Surf. Sci.* **2011**, *605*, 1141.
(2) Woodruff, D. P.; Delchar, T. A. *Modern Techniques of Surface Science*, 2nd ed.; Cambridge University Press: Cambridge, U.K., 1994.
(3) Zaera, F. *Prog. Surf. Sci.* **2001**, *69*, 1.
(4) Somorjai, G. A. *Introduction to Surface Chemistry and Catalysis*, 2nd ed.; John Wiley & Sons: New York, 2010.
(5) Goodman, D. W. *Chem. Rev.* **1995**, *95*, 523.
(6) Somorjai, G. A.; Park, J. Y. *Chem. Soc. Rev.* **2008**, *37*, 2155.
(7) Griffiths, P. R.; de Haseth, J. A. *Fourier Transform Infrared Spectrometry*; John Wiley & Sons: New York, 1986.
(8) Hair, M. L. *Infrared Spectroscopy in Surface Chemistry*; Marcel Dekker: New York, 1967.
(9) Socrates, G. *Infrared Characteristic Group Frequencies: Tables and Charts*, 2nd ed.; Wiley: Chichester, U.K, 1994.
(10) McQuillan, A. J. *Adv. Mater. (Weinheim, Fed. Repub. Ger.)* **2001**, *13*, 1034.
(11) Hind, A. R.; Bhargava, S. K.; McKinnon, A. *Adv. Colloid Interface Sci.* **2001**, *93*, 91.
(12) Andanson, J.-M.; Baiker, A. *Chem. Soc. Rev.* **2010**, *39*, 4571.
(13) Gun, J.; Sagiv, J. *J. Colloid Interface Sci.* **1986**, *112*, 457.
(14) Sperline, R. P.; Muralidharan, S.; Freiser, H. *Langmuir* **1987**, *3*, 198.
(15) Rivera, D.; Poston, P. E.; Uibel, R. H.; Harris, J. M. *Anal. Chem.* **2000**, *72*, 1543.
(16) Greener, J.; Abbasi, B.; Kumacheva, E. *Lab Chip* **2010**, *10*, 1561.
(17) Häbich, A.; Qiao, G. G.; Ducker, W. *Langmuir* **2010**, *26*, 13944.
(18) Yoshida, M.; Yamakata, A.; Takanabe, K.; Kubota, J.; Osawa, M.; Domen, K. *J. Am. Chem. Soc.* **2009**, *131*, 13218.
(19) Cheng, Y. L.; Batchelder, D. N.; Evans, S. D.; Henderson, J. R. *J. Phys. Chem. B* **1998**, *102*, 5309.
(20) Greenler, R. G. *J. Chem. Phys.* **1966**, *44*, 310.
(21) Hoffmann, F. M. *Surf. Sci. Rep.* **1983**, *3*, 107.
(22) Chabal, Y. J. *Surf. Sci. Rep.* **1988**, *8*, 211.
(23) Zaera, F. *Int. Rev. Phys. Chem.* **2002**, *21*, 433.

(24) Neivandt, D. J.; Gee, M. L.; Hair, M. L.; Tripp, C. P. *J. Phys. Chem. B* **1998**, *102*, 5107.
(25) Singh, P. K.; Adler, J. J.; Rabinovich, Y. I.; Moudgil, B. M. *Langmuir* **2000**, *17*, 468.
(26) Cwiertny, D. M.; Hunter, G. J.; Pettibone, J. M.; Scherer, M. M.; Grassian, V. H. *J. Phys. Chem. C* **2008**, *113*, 2175.
(27) Bhandari, N.; Hausner, D. B.; Kubicki, J. D.; Strongin, D. R. *Langmuir* **2010**, *26*, 16246.
(28) Lefèvre, G. *Adv. Colloid Interface Sci.* **2004**, *107*, 109.
(29) Roddick-Lanzilotta, A. D.; McQuillan, A. J. *J. Colloid Interface Sci.* **2000**, *227*, 48.
(30) McClellan, S. J.; Franses, E. I. *Colloids Surf., A* **2005**, *260*, 265.
(31) Wei, T.; Kaewtathip, S.; Shing, K. *J. Phys. Chem. C* **2009**, *113*, 2053.
(32) Hofmann, M. P.; Young, A. M.; Gbureck, U.; Nazhat, S. N.; Barralet, J. E. *J. Mater. Chem.* **2006**, *16*, 3199.
(33) Rodes, A.; Rueda, M.; Prieto, F.; Prado, C.; Feliu, J. M.; Aldaz, A. *J. Phys. Chem. C* **2009**, *113*, 18784.
(34) Yajima, T.; Uchida, H.; Watanabe, M. *J. Phys. Chem. B* **2004**, *108*, 2654.
(35) Shao, M. H.; Adzic, R. R. *Electrochim. Acta* **2005**, *50*, 2415.
(36) Ortiz-Hernandez, I.; Williams, C. T. *Langmuir* **2003**, *19*, 2956.
(37) Ortiz-Hernandez, I.; Williams, C. T. *Langmuir* **2007**, *23*, 3172.
(38) Grunwaldt, J.-D.; Baiker, A. *Phys. Chem. Chem. Phys.* **2005**, *7*, 3526.
(39) Bürgi, T.; Baiker, A. In *Advances in Catalysis*; Bruce, C. G., Helmut, K., Eds.; Academic Press: San Diego, California, 2006; Vol. 50, p 227.
(40) Mojet, B. L.; Ebbesen, S. D.; Lefferts, L. *Chem. Soc. Rev.* **2010**, *39*, 4643.
(41) Ebbesen, S. D.; Mojet, B. L.; Lefferts, L. *J. Phys. Chem. C* **2009**, *113*, 2503.
(42) Ferri, D.; Baiker, A. *Top. Catal.* **2009**, *52*, 1323.
(43) Bürgi, T.; Baiker, A. *J. Phys. Chem. B* **2002**, *106*, 10649.
(44) Mul, G.; Hamminga, G. M.; Moulijn, J. A. *Vib. Spectrosc.* **2004**, *34*, 109.
(45) Watanabe, S. *Surf. Sci.* **1995**, *341*, 304.
(46) Niwano, M. *Surf. Sci.* **1999**, *427*−*428*, 199.
(47) Queeney, K. T.; Fukidome, H.; Chaban, E. E.; Chabal, Y. J. *J. Phys. Chem. B* **2001**, *105*, 3903.
(48) Roy, D.; Fendler, J. *Adv. Mater.* **2004**, *16*, 479.
(49) Dowrey, A. E.; Marcott, C. *Appl. Spectrosc.* **1982**, *36*, 414.
(50) Ishida, H.; Ishino, Y.; Buijs, H.; Tripp, C.; Dignam, M. J. *Appl. Spectrosc.* **1987**, *41*, 1288.
(51) Hoffmann, H.; Wright, N. A.; Zaera, F.; Griffiths, P. R. *Talanta* **1989**, *36*, 125.
(52) Barner, B. J.; Green, M. J.; Sáez, E. I.; Corn, R. M. *Anal. Chem.* **1991**, *63*, 55.
(53) Bewick, A.; Pons, S. In *Advances in Infrared and Raman Spectroscopy*; Clark, R. J. H., Hester, R. E., Eds.; Wiley Heyden: New York, 1985; Vol. 12, pp 1.
(54) Bard, A. J.; Abruna, H. D.; Chidsey, C. E.; Faulkner, L. R.; Feldberg, S. W.; Itaya, K.; Majda, M.; Melroy, O.; Murray, R. W. *J. Phys. Chem.* **1993**, *97*, 7147.
(55) Weaver, M. J.; Zou, S. *Adv. Spectrosc.* **1998**, *26*, 219.
(56) Jackson, R.; Zamlynny, V. *Electrochim. Acta* **2008**, *53*, 6768.
(57) Iwasita, T.; Nart, F. C. *Prog. Surf. Sci.* **1997**, *55*, 271.
(58) Korzeniewski, C. *Crit. Rev. Anal. Chem.* **1997**, *27*, 81.
(59) Chang, S. C.; Weaver, M. J. *J. Phys. Chem.* **1991**, *95*, 5391.
(60) Villegas, I.; Weaver, M. J. *J. Chem. Phys.* **1994**, *101*, 1648.
(61) Golden, W. G.; Dunn, D. S.; Overend, J. *J. Catal.* **1981**, *71*, 395.
(62) Bewick, A.; Kunimatsu, K.; Stanley Pons, B. *Electrochim. Acta* **1980**, *25*, 465.
(63) Marković, N. M.; Ross, P. N., Jr. *Surf. Sci. Rep.* **2002**, *45*, 117.
(64) Fang, X.; Wang, L.; Shen, P. K.; Cui, G.; Bianchini, C. *J. Power Sources* **2010**, *195*, 1375.
(65) Xia, X. H.; Iwasita, T.; Ge, F.; Vielstich, W. *Electrochim. Acta* **1996**, *41*, 711.
(66) Iwasita, T. *Electrochim. Acta* **2002**, *47*, 3663.
(67) Salavagione, H. J.; Arias, J.; Garcés, P.; Morallón, E.; Barbero, C.; Vázquez, J. L. *J. Electroanal. Chem.* **2004**, *565*, 375.
(68) Salavagione, H. J.; Arias-Pardilla, J.; Pérez, J. M.; Vázquez, J. L.; Morallón, E.; Miras, M. C.; Barbero, C. *J. Electroanal. Chem.* **2005**, *576*, 139.
(69) Bae, I. T.; Sandifer, M.; Lee, Y. W.; Tryk, D. A.; Sukenik, C. N.; Scherson, D. A. *Anal. Chem.* **1995**, *67*, 4508.
(70) Vigier, F.; Coutanceau, C.; Hahn, F.; Belgsir, E. M.; Lamy, C. *J. Electroanal. Chem.* **2004**, *563*, 81.
(71) Faguy, P. W.; Markovic, N.; Adzic, R. R.; Fierro, C. A.; Yeager, E. B. *J. Electroanal. Chem. Interfacial Electrochem.* **1990**, *289*, 245.
(72) Aurbach, D.; Chusid, O.; Weissman, I.; Dan, P. *Electrochim. Acta* **1996**, *41*, 747.
(73) Aurbach, D.; Markovsky, B.; Levi, M. D.; Levi, E.; Schechter, A.; Moshkovich, M.; Cohen, Y. *J. Power Sources* **1999**, *81*−*82*, 95.
(74) Dima, G. E.; Beltramo, G. L.; Koper, M. T. M. *Electrochim. Acta* **2005**, *50*, 4318.
(75) Bjerke, A. E.; Griffiths, P. R.; Theiss, W. *Anal. Chem.* **1999**, *71*, 1967.
(76) Ye, S.; Kondo, T.; Hoshi, N.; Inukai, J.; Soichiro, Y.; Osawa, M.; Itaya, K. *Electrochem.* **2009**, *77*, 2.
(77) Hartstein, A.; Kirtley, J. R.; Tsang, J. C. *Phys. Rev. Lett.* **1980**, *45*, 201.
(78) Hatta, A.; Chiba, Y.; SuÎtaka, W. *Surf. Sci.* **1985**, *158*, 616.
(79) Ayato, Y.; Kunimatsu, K.; Osawa, M.; Okada, T. *J. Electrochem. Soc.* **2006**, *153*, A203.
(80) Meier, D. M.; Urakawa, A.; Baiker, A. *J. Phys. Chem. C* **2009**, *113*, 21849.
(81) Kubota, J.; Ma, Z.; Zaera, F. *Langmuir* **2003**, *19*, 3371.
(82) Ma, Z.; Lee, I.; Kubota, J.; Zaera, F. *J. Mol. Catal. A* **2004**, *216*, 199.
(83) Kubota, J.; Zaera, F. *J. Am. Chem. Soc.* **2001**, *123*, 11115.
(84) Chu, W.; LeBlanc, R. J.; Williams, C. T.; Kubota, J.; Zaera, F. *J. Phys. Chem. B* **2003**, *107*, 14365.
(85) Ma, Z.; Lee, I.; Zaera, F. *J. Am. Chem. Soc.* **2007**, *129*, 16083.
(86) Lai, J.; Ma, Z.; Mink, L.; Mueller, L. J.; Zaera, F. *J. Phys. Chem. B* **2009**, *113*, 11696.
(87) Ma, Z.; Kubota, J.; Zaera, F. *J. Catal.* **2003**, *219*, 404.
(88) Ma, Z.; Zaera, F. *J. Phys. Chem. B* **2005**, *109*, 406.
(89) Ma, Z.; Zaera, F. *J. Am. Chem. Soc.* **2006**, *128*, 16414.
(90) Krejcik, M.; Danek, M.; Hartl, F. *J. Electroanal. Chem. Interfacial Electrochem.* **1991**, *317*, 179.
(91) Schneider, M. S.; Grunwaldt, J. D.; Burgi, T.; Baiker, A. *Rev. Sci. Instrum.* **2003**, *74*, 4121.
(92) Poliakoff, M.; Howdle, S. M.; Kazarian, S. G. *Angew. Chem., Int. Ed.* **1995**, *34*, 1275.
(93) Albiter, M. A.; Crooks, R. M.; Zaera, F. *J. Phys. Chem. Lett.* **2010**, *1*, 38.
(94) Gao, P.; Weaver, M. J. *J. Phys. Chem.* **1985**, *89*, 5040.
(95) Campion, A.; Kambhampati, P. *Chem. Soc. Rev.* **1998**, *27*, 241.
(96) Koglin, E.; Kreisig, S.; Copitzky, T. In *Horizons 2000—Aspects of Colloid and Interface Science at the Turn of the Millenium*; Lagaly, G., Ed.; Springer: Berlin/Heidelberg, 1998; Vol. 109, pp 232.
(97) Tian, Z.-Q.; Ren, B. *Annu. Rev. Phys. Chem.* **2004**, *55*, 197.
(98) Lin, X.-M.; Cui, Y.; Xu, Y.-H.; Ren, B.; Tian, Z.-Q. *Anal. Bioanal. Chem.* **2009**, *394*, 1729.
(99) Zou, S.; Weaver, M. J. *Anal. Chem.* **1998**, *70*, 2387.
(100) Zou, S.; Williams, C. T.; Chen, E. K. Y.; Weaver, M. J. *J. Am. Chem. Soc.* **1998**, *120*, 3811.
(101) Stiles, P. L.; Dieringer, J. A.; Shah, N. C.; Van Duyne, R. P. *Annu. Rev. Anal. Chem.* **2008**, *1*, 601.
(102) Torres, E. L.; Winefordner, J. D. *Anal. Chem.* **1987**, *59*, 1626.
(103) Yonzon, C. R.; Stuart, D. A.; Zhang, X.; McFarland, A. D.; Haynes, C. L.; Van Duyne, R. P. *Talanta* **2005**, *67*, 438.
(104) Hering, K.; Cialla, D.; Ackermann, K.; Dörfer, T.; Möller, R.; Schneidewind, H.; Mattheis, R.; Fritzsche, W.; Rösch, P.; Popp, J. *Anal. Bioanal. Chem.* **2008**, *390*, 113.
(105) Kudelski, A. *Talanta* **2008**, *76*, 1.

(106) Han, X.; Zhao, B.; Ozaki, Y. *Anal. Bioanal. Chem.* **2009**, *394*, 1719.
(107) Halvorson, R. A.; Vikesland, P. J. *Environ. Sci. Technol.* **2010**, *44*, 7749.
(108) Willets, K. *Anal. Bioanal. Chem.* **2009**, *394*, 85.
(109) Wachsmann-Hogiu, S.; Weeks, T.; Huser, T. *Curr. Opin. Biotechnol.* **2009**, *20*, 63.
(110) Kneipp, J.; Kneipp, H.; Wittig, B.; Kneipp, K. *Nanomed. Nanotechnol.* **2010**, *6*, 214.
(111) Souza, G. R.; Levin, C. S.; Hajitou, A.; Pasqualini, R.; Arap, W.; Miller, J. H. *Anal. Chem.* **2006**, *78*, 6232.
(112) Schlücker, S. *ChemPhysChem* **2009**, *10*, 1344.
(113) Gu, B.; Tio, J.; Wang, W.; Ku, Y.-K.; Dai, S. *Appl. Spectrosc.* **2004**, *58*, 741.
(114) Baker, G. A.; Moore, D. S. *Anal. Bioanal. Chem.* **2005**, *382*, 1751.
(115) Gouveia, V. J. P.; Gutz, I. G.; Rubim, J. C. *J. Electroanal. Chem.* **1994**, *371*, 37.
(116) He, L.; Natan, M. J.; Keating, C. D. *Anal. Chem.* **2000**, *72*, 5348.
(117) Farquharson, S.; Maksymiuk, P. *Appl. Spectrosc.* **2003**, *57*, 479.
(118) Brosseau, C. L.; Gambardella, A.; Casadio, F.; Grzywacz, C. M.; Wouters, J.; Van Duyne, R. P. *Anal. Chem.* **2009**, *81*, 3056.
(119) Keir, R.; Igata, E.; Arundell, M.; Smith, W. E.; Graham, D.; McHugh, C.; Cooper, J. M. *Anal. Chem.* **2002**, *74*, 1503.
(120) Weaver, M. J.; Zou, S.; Chan, H. Y. H. *Anal. Chem.* **2000**, *72*, 38 A.
(121) Tian, Z.-Q.; Ren, B.; Wu, D.-Y. *J. Phys. Chem. B* **2002**, *106*, 9463.
(122) Pemberton, J. E.; Buck, R. P. *Anal. Chem.* **1981**, *53*, 2263.
(123) Shi, C.; Zhang, W.; Birke, R. L.; Lombardi, J. R. *J. Phys. Chem.* **1990**, *94*, 4766.
(124) Tian, Z. Q.; Li, W. H.; Mao, B. W.; Gao, J. S. *J. Electroanal. Chem.* **1994**, *379*, 271.
(125) Gao, P.; Gosztola, D.; Weaver, M. J. *J. Phys. Chem.* **1988**, *92*, 7122.
(126) Yamamoto, Y.; Nishihara, H.; Aramaki, K. *J. Electrochem. Soc.* **1993**, *140*, 436.
(127) Szafranski, C. A.; Tanner, W.; Laibinis, P. E.; Garrell, R. L. *Langmuir* **1998**, *14*, 3570.
(128) Baldwin, J. A.; Vlčková, B.; Andrews, M. P.; Butler, I. S. *Langmuir* **1997**, *13*, 3744.
(129) Maeda, Y.; Yamamoto, H.; Kitano, H. *J. Phys. Chem.* **1995**, *99*, 4837.
(130) Smulevich, G.; Spiro, T. G. *J. Phys. Chem.* **1985**, *89*, 5168.
(131) Podstawka, E.; Ozaki, Y.; Proniewicz, L. M. *Appl. Spectrosc.* **2004**, *58*, 570.
(132) Brolo, A. G.; Germain, P.; Hager, G. *J. Phys. Chem. B* **2002**, *106*, 5982.
(133) Cañamares, M. V.; Garcia-Ramos, J. V.; Domingo, C.; Sanchez-Cortes, S. *J. Raman Spectrosc.* **2004**, *35*, 921.
(134) Cao, P.; Sun, Y.; Gu, R. *J. Raman Spectrosc.* **2005**, *36*, 725.
(135) Feilchenfeld, H.; Chumanov, G.; Cotton, T. M. *J. Phys. Chem.* **1996**, *100*, 4937.
(136) Zou, S.; Weaver, M. J. *J. Phys. Chem. B* **1999**, *103*, 2323.
(137) Quagliano, L. G. *J. Am. Chem. Soc.* **2004**, *126*, 7393.
(138) Heck, K. N.; Janesko, B. G.; Scuseria, G. E.; Halas, N. J.; Wong, M. S. *J. Am. Chem. Soc.* **2008**, *130*, 16592.
(139) Stemmet, C. P.; Schouten, J. C.; Nijhuis, T. A. *Ind. Eng. Chem. Res.* **2009**, *48*, 8205.
(140) Kim, H.; Kosuda, K. M.; Van Duyne, R. P.; Stair, P. C. *Chem. Soc. Rev.* **2010**, *39*, 4820.
(141) Bergner, G.; Chatzipapadopoulos, S.; Akimov, D.; Dietzek, B.; Malsch, D.; Henkel, T.; Schlücker, S.; Popp, J. *Small* **2009**, *5*, 2816.
(142) Djaker, N.; Lenne, P.-F.; Marguet, D.; Colonna, A.; Hadjur, C.; Rigneault, H. *Nucl. Instrum. Methods Phys. Res., Sect. A* **2007**, *571*, 177.
(143) Le, T.; Huff, T.; Cheng, J.-X. *BMC Cancer* **2009**, *9*, 42.
(144) Namboodiri, V.; Namboodiri, M.; Diaz, G. I. C.; Oppermann, M.; Flachenecker, G.; Materny, A. *Vib. Spectrosc.* **2011**, DOI: 10.1016/j.vibspec.2010.08.005.
(145) Bain, C. D. *Curr. Opin. Colloid Interface Sci.* **1998**, *3*, 287.
(146) Miranda, P. B.; Shen, Y. R. *J. Phys. Chem. B* **1999**, *103*, 3292.
(147) Verreault, D.; Kurz, V.; Howell, C.; Koelsch, P. *Rev. Sci. Instrum.* **2010**, 81.
(148) Buchbinder, A. M.; Weitz, E.; Geiger, F. M. *J. Phys. Chem. C* **2009**, *114*, 554.
(149) Buchbinder, A. M.; Weitz, E.; Geiger, F. M. *J. Am. Chem. Soc.* **2010**, *132*, 14661.
(150) Du, Q.; Freysz, E.; Shen, Y. R. *Phys. Rev. Lett.* **1994**, *72*, 238.
(151) Yeganeh, M. S.; Dougal, S. M.; Pink, H. S. *Phys. Rev. Lett.* **1999**, *83*, 1179.
(152) Noguchi, H.; Okada, T.; Uosaki, K. *Electrochim. Acta* **2008**, *53*, 6841.
(153) Yang, Z.; Li, Q.; Chou, K. C. *J. Phys. Chem. C* **2009**, *113*, 8201.
(154) Jena, K. C.; Hore, D. K. *Phys. Chem. Chem. Phys.* **2010**, *12*, 14383.
(155) Jena, K. C.; Hore, D. K. *J. Phys. Chem. C* **2009**, *113*, 15364.
(156) Simon, S.; Geraldine, L. R. *J. Phys. D: Appl. Phys.* **2008**, *41*, 033001.
(157) Hatch, S. R.; Polizzotti, R. S.; Dougal, S.; Rabinowitz, P. *Chem. Phys. Lett.* **1992**, *196*, 97.
(158) Ding, F.; Hu, Z.; Zhong, Q.; Manfred, K.; Gattass, R. R.; Brindza, M. R.; Fourkas, J. T.; Walker, R. A.; Weeks, J. D. *J. Phys. Chem. C* **2010**, *114*, 17651.
(159) Kurian, A.; Prasad, S.; Dhinojwala, A. *Langmuir* **2010**, *26*, 17804.
(160) Tadjeddine, A.; Peremans, A.; Guyot-Sionnest, P. *Surf. Sci.* **1995**, *335*, 210.
(161) Bozzini, B.; De Gaudenzi, G. P.; Busson, B.; Humbert, C.; Six, C.; Gayral, A.; Tadjeddine, A. *J. Power Sources* **2010**, *195*, 4119.
(162) Chou, K. C.; Kim, J.; Baldelli, S.; Somorjai, G. A. *J. Electroanal. Chem.* **2003**, *554−555*, 253.
(163) Leygraf, C. *Rev. Metal. (Madrid, Spain)* **2009**, *45*, 223.
(164) Cimatu, K.; Baldelli, S. *J. Am. Chem. Soc.* **2008**, *130*, 8030.
(165) Schultz, Z. D.; Biggin, M. E.; White, J. O.; Gewirth, A. A. *Anal. Chem.* **2003**, *76*, 604.
(166) Baldelli, S. *J. Phys. Chem. B* **2005**, *109*, 13049.
(167) Baldelli, S. *Acc. Chem. Res.* **2008**, *41*, 421.
(168) Jeon, Y.; Sung, J.; Bu, W.; Vaknin, D.; Ouchi, Y.; Kim, D. *J. Phys. Chem. C* **2008**, *112*, 19649.
(169) Zhou, W.; Inoue, S.; Iwahashi, T.; Kanai, K.; Seki, K.; Miyamae, T.; Kim, D.; Katayama, Y.; Ouchi, Y. *Electrochem. Commun.* **2010**, *12*, 672.
(170) Guyot-Sionnest, P.; Superfine, R.; Hunt, J. H.; Shen, Y. R. *Chem. Phys. Lett.* **1988**, *144*, 1.
(171) Miranda, P. B.; Pflumio, V.; Saijo, H.; Shen, Y. R. *Chem. Phys. Lett.* **1997**, *264*, 387.
(172) Kim, J.; Kim, G.; Cremer, P. S. *J. Am. Chem. Soc.* **2002**, *124*, 8751.
(173) Ye, S.; Noda, H.; Nishida, T.; Morita, S.; Osawa, M. *Langmuir* **2003**, *20*, 357.
(174) Lahann, J.; Mitragotri, S.; Tran, T.-N.; Kaido, H.; Sundaram, J.; Choi, I. S.; Hoffer, S.; Somorjai, G. A.; Langer, R. *Science* **2003**, *299*, 371.
(175) Roke, S. *ChemPhysChem* **2009**, *10*, 1380.
(176) Sovago, M.; Wurpel, G. W. H.; Smits, M.; Müller, M.; Bonn, M. *J. Am. Chem. Soc.* **2007**, *129*, 11079.
(177) Roke, S.; Roeterdink, W. G.; Wijnhoven, J. E. G. J.; Petukhov, A. V.; Kleyn, A. W.; Bonn, M. *Phys. Rev. Lett.* **2003**, *91*, 2583021.
(178) Roke, S.; Bonn, M.; Petukhov, A. V. *Phys. Rev. B* **2004**, *70*, 115106.
(179) Pászti, Z.; Guczi, L. *Vib. Spectrosc.* **2009**, *50*, 48.
(180) Chen, X.; Wang, J.; Sniadecki, J. J.; Even, M. A.; Chen, Z. *Langmuir* **2005**, *21*, 2662.
(181) Ye, S.; Nguyen, K. T.; Boughton, A. P.; Mello, C. M.; Chen, Z. *Langmuir* **2009**, *26*, 6471.

(182) Mermut, O.; Phillips, D. C.; York, R. L.; McCrea, K. R.; Ward, R. S.; Somorjai, G. A. *J. Am. Chem. Soc.* **2006**, *128*, 3598.
(183) York, R. L.; Holinga, G. J.; Somorjai, G. A. *Langmuir* **2009**, *25*, 9369.
(184) Weidner, T.; Breen, N. F.; Li, K.; Drobny, G. P.; Castner, D. G. *Proc. Natl. Acad. Sci. U. S. A.* **2010**, *107*, 13288.
(185) Wang, J.; Chen, X.; Clarke, M. L.; Chen, Z. *Proc. Natl. Acad. Sci. U. S. A.* **2005**, *102*, 4978.
(186) Arnolds, H.; Bonn, M. *Surf. Sci. Rep.* **2010**, *65*, 45.
(187) Matranga, C.; Guyot-Sionnest, P. *J. Chem. Phys.* **2000**, *112*, 7615.
(188) McGuire, J. A.; Shen, Y. R. *Science* **2006**, *313*, 1945.
(189) Smits, M.; Ghosh, A.; Bredenbeck, J.; Yamamoto, S.; Müller, M.; Bonn, M. *New J. Phys.* **2007**, *9*, 390/1.
(190) Zhou, W.; Ye, S.; Abe, M.; Nishida, T.; Uosaki, K.; Osawa, M.; Sasaki, Y. *Chem.—Eur. J.* **2005**, *11*, 5040.
(191) Decher, G.; Hong, J. D.; Schmitt, J. *Thin Solid Films* **1992**, *210−211*, 831.
(192) Raposo, M.; Pontes, R. S.; Mattoso, L. H. C.; Oliveira, O. N. *Macromolecules* **1997**, *30*, 6095.
(193) Hao, E.; Lian, T. *Langmuir* **2000**, *16*, 7879.
(194) Zhou, Y.; Li, Z.; Hu, N.; Zeng, Y.; Rusling, J. F. *Langmuir* **2002**, *18*, 8573.
(195) Feng, J.-J.; Xu, J.-J.; Chen, H.-Y. *Biosens. Bioelectron.* **2007**, *22*, 1618.
(196) Lei, C.; Wollenberger, U.; Jung, C.; Scheller, F. W. *Biochem. Biophys. Res. Commun.* **2000**, *268*, 740.
(197) Weissmahr, K. W.; Haderlein, S. B.; Schwarzenbach, R. P.; Hany, R.; Nüesch, R. *Environ. Sci. Technol.* **1996**, *31*, 240.
(198) Chernia, Z.; Gill, D. *Langmuir* **1999**, *15*, 1625.
(199) Gautier, C.; Bürgi, T. *J. Am. Chem. Soc.* **2006**, *128*, 11079.
(200) Murakoshi, K.; Kano, G.; Wada, Y.; Yanagida, S.; Miyazaki, H.; Matsumoto, M.; Murasawa, S. *J. Electroanal. Chem.* **1995**, *396*, 27.
(201) Pérez León, C.; Kador, L.; Peng, B.; Thelakkat, M. *J. Phys. Chem. B* **2006**, *110*, 8723.
(202) Ma, T.; Inoue, K.; Noma, H.; Yao, K.; Abe, E. *J. Photochem. Photobiol., A* **2002**, *152*, 207.
(203) Martini, I.; Hodak, J. H.; Hartland, G. V. *J. Phys. Chem. B* **1998**, *102*, 607.
(204) Misra, P.; Somasundaran, P. In *Interfacial Processes and Molecular Aggregation of Surfactants*; Narayanan, R., Ed.; Springer: Berlin/Heidelberg, 2008; Vol. 218, pp 143.
(205) Das, D.; Ismail, K. *J. Colloid Interface Sci.* **2008**, *327*, 198.
(206) Torrens, F.; Castellano, G.; Campos, A.; Abad, C. *J. Mol. Struct.* **2009**, *924−926*, 274.
(207) Zhang, J.; Hadlock, T.; Gent, A.; Strichartz, G. R. *Biophys. J.* **2007**, *92*, 3988.
(208) Serrano, A. G.; Cabré, E. J.; Oviedo, J. M.; Cruz, A.; González, B.; Palacios, A.; Estrada, P.; Pérez-Gil, J. *Biochim. Biophys. Acta, Biomembr.* **2006**, *1758*, 1621.
(209) Model, M. A.; Healy, K. E. *J. Biomed. Mater. Res.* **2000**, *50*, 90.
(210) Xie, X. S.; Choi, P. J.; Li, G.-W.; Lee, N. K.; Lia, G. *Annu. Rev. Biophys.* **2008**, *37*, 417.
(211) Karlsson, M.; Carlsson, U. *Biophys. J.* **2005**, *88*, 3536.
(212) Chalfie, M.; Tu, Y.; Euskirchen, G.; Ward, W. W.; Prasher, D. C. *Science* **1994**, *263*, 802.
(213) Tsien, R. Y. *Annu. Rev. Biochem.* **1998**, *67*, 509.
(214) Dickson, R. M.; Cubitt, A. B.; Tsien, R. Y.; Moerner, W. E. *Nature* **1997**, *388*, 355.
(215) Holzer, W.; Pichlmaier, M.; Penzkofer, A.; Bradley, D. D. C.; Blau, W. J. *Chem. Phys.* **1999**, *246*, 445.
(216) Matthews, L. R.; Knobbe, E. T. *Chem. Mater.* **1993**, *5*, 1697.
(217) Kramer, G.; Somasundaran, P. *Langmuir* **2002**, *18*, 9357.
(218) de Halleux, V.; Calbert, J. P.; Brocorens, P.; Cornil, J.; Declercq, J. P.; Brédas, J. L.; Geerts, Y. *Adv. Funct. Mater.* **2004**, *14*, 649.
(219) Cao, Z.; Xie, Q.; Li, M.; Yao, S. *J. Electroanal. Chem.* **2004**, *568*, 343.
(220) Krupadam, R. J.; Bhagat, B.; Wate, S. R.; Bodhe, G. L.; Sellergren, B.; Anjaneyulu, Y. *Environ. Sci. Technol.* **2009**, *43*, 2871.
(221) Li, L.; Huang, Y.; Wang, Y.; Wang, W. *Anal. Chim. Acta* **2009**, *631*, 182.
(222) Oroszlan, P.; Blanco, R.; Lu, X.-M.; Yarmush, D.; Karger, B. L. *J. Chromatogr. A* **1990**, *500*, 481.
(223) Grate, J. W.; Zhang, C.; Wietsma, T. W.; Warner, M. G.; Anheier, N. C., Jr.; Bernacki, B. E.; Orr, G.; Oostrom, M. *Water Resour. Res.* **2010**, *46*, W11602.
(224) Sanders, A.; Jennissen, H. P. *J. Mol. Recognit.* **1996**, *9*, 503.
(225) Hansen, R. L.; Harris, J. M. *Anal. Chem.* **1998**, *70*, 4247.
(226) Daly, S. M.; Przybycien, T. M.; Tilton, R. D. *Langmuir* **2003**, *19*, 3848.
(227) Zhang, C.; Allotta, P. M.; Xiong, G.; Stair, P. C. *J. Phys. Chem. C* **2008**, *112*, 14501.
(228) Williams, C. T.; Beattie, D. A. *Surf. Sci.* **2001**, *500*, 545.
(229) Geiger, F. M. *Annu. Rev. Phys. Chem.* **2009**, *60*, 61.
(230) Malin, J. N.; Hayes, P. L.; Geiger, F. M. *J. Phys. Chem. C* **2008**, *113*, 2041.
(231) Chen, E. H.; Hayes, P. L.; Nguyen, S. T.; Geiger, F. M. *J. Phys. Chem. C* **2010**, *114*, 19483.
(232) Thom, I.; Buck, M. *Surf. Sci.* **2005**, *581*, 33.
(233) Uchida, T.; Yamaguchi, A.; Ina, T.; Teramae, N. *J. Phys. Chem. B* **2000**, *104*, 12091.
(234) Buck, M.; Dannenberger, O.; Wolff, J. J. *Thin Solid Films* **1996**, *284−285*, 396.
(235) Konek, C. T.; Musorrafiti, M. J.; Al-Abadleh, H. A.; Bertin, P. A.; Nguyen, S. T.; Geiger, F. M. *J. Am. Chem. Soc.* **2004**, *126*, 11754.
(236) Fitts, J. P.; Machesky, M. L.; Wesolowski, D. J.; Shang, X.; Kubicki, J. D.; Flynn, G. W.; Heinz, T. F.; Eisenthal, K. B. *Chem. Phys. Lett.* **2005**, *411*, 399.
(237) Fitts, J. P.; Shang, X.; Flynn, G. W.; Heinz, T. F.; Eisenthal, K. B. *J. Phys. Chem. B* **2005**, *109*, 7981.
(238) Stack, A. G.; Higgins, S. R.; Eggleston, C. M. *Geochim. Cosmochim. Acta* **2001**, *65*, 3055.
(239) Xu, Z.; Dong, Y. *Surf. Sci.* **2000**, *445*, L65.
(240) Pettinger, B.; Lipkowski, J.; Mirwald, S.; Friedrich, A. *J. Electroanal. Chem.* **1992**, *329*, 289.
(241) Pettinger, B.; Lipkowski, J.; Mirwald, S.; Friedrich, A. *Surf. Sci.* **1992**, *269−270*, 377.
(242) Lovell, M. A.; Roy, D. *Appl. Surf. Sci.* **1998**, *135*, 46.
(243) Corn, R. M.; Higgins, D. A. *Chem. Rev.* **1994**, *94*, 107.
(244) Akemann, W.; Friedrich, K. A.; Linke, U.; Stimming, U. *Surf. Sci.* **1998**, *402−404*, 571.
(245) Siler, A.; Brindza, M.; Walker, R. *Anal. Bioanal. Chem.* **2009**, *395*, 1063.
(246) Zhang, X.; Cunningham, M. M.; Walker, R. A. *J. Phys. Chem. B* **2003**, *107*, 3183.
(247) Brindza, M. R.; Walker, R. A. *J. Am. Chem. Soc.* **2009**, *131*, 6207.
(248) Heinz, T. F.; Tom, H. W. K.; Shen, Y. R. *Phys. Rev. A* **1983**, *28*, 1883.
(249) Kautek, W.; Sorg, N.; Krüger, J. *Electrochim. Acta* **1994**, *39*, 1245.
(250) Lazarescu, V.; Lazarescu, M. F.; Santos, E.; Schmickler, W. *Electrochim. Acta* **2004**, *49*, 4231.
(251) Hicks, J. M.; Petralli-Mallow, T. *Appl. Phys. B: Lasers Opt.* **1999**, *68*, 589.
(252) Han, S. H.; Ji, N.; Belkin, M. A.; Shen, Y. R. *Phys. Rev. B* **2002**, *66*, 165415.
(253) Kriech, M. A.; Conboy, J. C. *J. Opt. Soc. Am. B: Opt. Phys.* **2004**, *21*, 1013.
(254) Polizzi, M. A.; Plocinik, R. M.; Simpson, G. J. *J. Am. Chem. Soc.* **2004**, *126*, 5001.
(255) Eisenthal, K. B. *Chem. Rev.* **2006**, *106*, 1462.
(256) Jen, S.-H.; Dai, H.-L. *J. Phys. Chem. B* **2006**, *110*, 23000.
(257) Schneider, L.; Schmid, H. J.; Peukert, W. *Appl. Phys. B: Lasers Opt.* **2007**, *87*, 333.

(258) Campen, R. K.; Zheng, D.-s.; Wang, H.-f.; Borguet, E. *J. Phys. Chem. C* **2007**, *111*, 8805.
(259) Wang, H.-f.; Troxler, T.; Yeh, A.-g.; Dai, H.-l. *J. Phys. Chem. C* **2007**, *111*, 8708.
(260) Haber, L. H.; Kwok, S. J. J.; Semeraro, M.; Eisenthal, K. B. *Chem. Phys. Lett.* **2011**, *507*, 11.
(261) Subir, M.; Liu, J.; Eisenthal, K. B. *J. Phys. Chem. C* **2008**, *112*, 15809.
(262) Vance, F. W.; Lemon, B. I.; Hupp, J. T. *J. Phys. Chem. B* **1998**, *102*, 10091.
(263) Ong, S.; Zhao, X.; Eisenthal, K. B. *Chem. Phys. Lett.* **1992**, *191*, 327.
(264) Yan, E. C. Y.; Eisenthal, K. B. *J. Phys. Chem. B* **1999**, *103*, 6056.
(265) Liu, Y.; Dadap, J. I.; Zimdars, D.; Eisenthal, K. B. *J. Phys. Chem. B* **1999**, *103*, 2480.
(266) Eckenrode, H. M.; Dai, H.-L. *Langmuir* **2004**, *20*, 9202.
(267) Shang, X.; Benderskii, A. V.; Eisenthal, K. B. *J. Phys. Chem. B* **2001**, *105*, 11578.
(268) Mishina, E. D.; Ohta, N.; Yu, Q. K.; Nakabayashi, S. *Surf. Sci.* **2001**, *494*, L748.
(269) Yamada, K.; Yonemura, H.; Matsuo, T.; Yamada, S. *J. Photochem. Photobiol., A* **1998**, *114*, 163.
(270) Liu, Y.; Yan, E. C. Y.; Eisenthal, K. B. *Biophys. J.* **2001**, *80*, 1004.
(271) Moreaux, L.; Sandre, O.; Charpak, S.; Blanchard-Desce, M.; Mertz, J. *Biophys. J.* **2001**, *80*, 1568.
(272) Liu, J.; Subir, M.; Nguyen, K.; Eisenthal, K. B. *J. Phys. Chem. B* **2008**, *112*, 15263.
(273) Wang, H.; Troxler, T.; Yeh, A.-G.; Dai, H.-L. *Langmuir* **2000**, *16*, 2475.
(274) Yui, H.; Hirose, Y.; Sawada, T. *Anal. Sci.* **2004**, *20*, 1493.
(275) Schürer, B.; Peukert, W. *Part. Sci. Technol.* **2010**, *28*, 458.
(276) Phillips, K.; Cheng, Q. *Anal. Bioanal. Chem.* **2007**, *387*, 1831.
(277) Cooke, S. J.; Roberts, G. G. *Thin Solid Films* **1992**, *210−211*, 685.
(278) Yang, X. L.; Dutta, P.; Wong, G. K.; Ketterson, J. B. *Thin Solid Films* **1992**, *219*, 210.
(279) Advincula, R.; Aust, E.; Meyer, W.; Knoll, W. *Langmuir* **1996**, *12*, 3536.
(280) Schuck, P. *Annu. Rev. Biophys. Biomol. Struct.* **1997**, *26*, 541.
(281) Homola, J. *Chem. Rev.* **2008**, *108*, 462.
(282) Brockman, J. M.; Nelson, B. P.; Corn, R. M. *Annu. Rev. Phys. Chem.* **2000**, *51*, 41.
(283) Hoa, X. D.; Kirk, A. G.; Tabrizian, M. *Biosens. Bioelectron.* **2007**, *23*, 151.
(284) Lee, H. J.; Wark, A. W.; Corn, R. M. *Langmuir* **2006**, *22*, 5241.
(285) McDonnell, J. M. *Curr. Opin. Chem. Biol.* **2001**, *5*, 572.
(286) Rich, R. L.; Myszka, D. G. *Curr. Opin. Biotechnol.* **2000**, *11*, 54.
(287) Boozer, C.; Kim, G.; Cong, S.; Guan, H.; Londergan, T. *Curr. Opin. Biotechnol.* **2006**, *17*, 400.
(288) Tanious, F. A.; Nguyen, B.; Wilson, W. D. In *Methods in Cell Biology*; John, J. C., Detrich, H. W., III, Eds.; Academic Press: Amsterdam, 2008; Vol. 84, pp 53.
(289) Rich, R. L.; Myszka, D. G. *J. Mol. Recognit.* **2010**, *23*, 1.
(290) Mozsolits, H.; Aguilar, M.-I. *Pept. Sci.* **2002**, *66*, 3.
(291) Besenicar, M.; Macek, P.; Lakey, J. H.; Anderluh, G. *Chem. Phys. Lipids* **2006**, *141*, 169.
(292) Schmitt, F. J.; Häussling, L.; Ringsdorf, H.; Knoll, W. *Thin Solid Films* **1992**, *210−211*, 815.
(293) Sigal, G. B.; Bamdad, C.; Barberis, A.; Strominger, J.; Whitesides, G. M. *Anal. Chem.* **1996**, *68*, 490.
(294) Mrksich, M.; Sigal, G. B.; Whitesides, G. M. *Langmuir* **1995**, *11*, 4383.
(295) Sigal, G. B.; Mrksich, M.; Whitesides, G. M. *Langmuir* **1997**, *13*, 2749.
(296) Nelson, B. P.; Grimsrud, T. E.; Liles, M. R.; Goodman, R. M.; Corn, R. M. *Anal. Chem.* **2000**, *73*, 1.
(297) Kanda, V.; Kariuki, J. K.; Harrison, D. J.; McDermott, M. T. *Anal. Chem.* **2004**, *76*, 7257.
(298) Homola, J.; Vaisocherov, H.; Dost·lek, J.; Piliarik, M. *Methods* **2005**, *37*, 26.
(299) Nikitin, P. I.; Grigorenko, A. N.; Beloglazov, A. A.; Valeiko, M. V.; Savchuk, A. I.; Savchuk, O. A.; Steiner, G.; Kuhne, C.; Huebner, A.; Salzer, R. *Sens. Actuators, A* **2000**, *85*, 189.
(300) Green, R. J.; Frazier, R. A.; Shakesheff, K. M.; Davies, M. C.; Roberts, C. J.; Tendler, S. J. B. *Biomaterials* **2000**, *21*, 1823.
(301) Frazier, R. A.; Matthijs, G.; Davies, M. C.; Roberts, C. J.; Schacht, E.; Tendler, S. J. B. *Biomaterials* **2000**, *21*, 957.
(302) Malmqvist, M. *Nature* **1993**, *361*, 186.
(303) Liedberg, B.; Lundström, I.; Stenberg, E. *Sens. Actuators, B* **1993**, *11*, 63.
(304) Silin, V.; Weetall, H.; Vanderah, D. J. *J. Colloid Interface Sci.* **1997**, *185*, 94.
(305) Huber, W.; Hurst, J.; Schlatter, D.; Barner, R.; Hübscher, J.; Kouns, W. C.; Steiner, B. *Eur. J. Biochem.* **1995**, *227*, 647.
(306) Jung, L. S.; Campbell, C. T. *J. Phys. Chem. B* **2000**, *104*, 11168.
(307) Peterlinz, K. A.; Georgiadis, R. *Langmuir* **1996**, *12*, 4731.
(308) Green, R. J.; Corneillie, S.; Davies, J.; Davies, M. C.; Roberts, C. J.; Schacht, E.; Tendler, S. J. B.; Williams, P. M. *Langmuir* **2000**, *16*, 2744.
(309) Bailey, L. E.; Kambhampati, D.; Kanazawa, K. K.; Knoll, W.; Frank, C. W. *Langmuir* **2001**, *18*, 479.
(310) Huang, M.; Shao, Y.; Sun, X.; Chen, H.; Liu, B.; Dong, S. *Langmuir* **2004**, *21*, 323.
(311) Linnert, T.; Mulvaney, P.; Henglein, A. *J. Phys. Chem.* **1993**, *97*, 679.
(312) Haes, A. J.; Hall, W. P.; Chang, L.; Klein, W. L.; Van Duyne, R. P. *Nano Lett.* **2004**, *4*, 1029.
(313) El-Sayed, I. H.; Huang, X.; El-Sayed, M. A. *Nano Lett.* **2005**, *5*, 829.
(314) Benjamins, J.-W.; Jönsson, B.; Thuresson, K.; Nylander, T. *Langmuir* **2002**, *18*, 6437.
(315) Tengvall, P.; Lundström, I.; Liedberg, B. *Biomaterials* **1998**, *19*, 407.
(316) Arwin, H. *Thin Solid Films* **2000**, *377−378*, 48.
(317) Tengvall, P.; Askendal, A.; Ingemar, L. *Biomaterials* **1996**, *17*, 1001.
(318) Cuypers, P. A.; Corsel, J. W.; Janssen, M. P.; Kop, J. M.; Hermens, W. T.; Hemker, H. C. *J. Biol. Chem.* **1983**, *258*, 2426.
(319) Cárdenas, M.; Campos-Terán, J.; Nylander, T.; Lindman, B. *Langmuir* **2004**, *20*, 8597.
(320) Cárdenas, M.; Elofsson, U.; Lindh, L. *Biomacromolecules* **2007**, *8*, 1149.
(321) Tiberg, F.; Joensson, B.; Tang, J.-a.; Lindman, B. *Langmuir* **1994**, *10*, 2294.
(322) Zhang, R.; Somasundaran, P. *Adv. Colloid Interface Sci.* **2006**, *123−126*, 213.
(323) Porter, M. D.; Bright, T. B.; Allara, D. L.; Chidsey, C. E. D. *J. Am. Chem. Soc.* **1987**, *109*, 3559.
(324) Ohtsuka, T.; Sato, Y.; Uosaki, K. *Langmuir* **1994**, *10*, 3658.
(325) Amador, S. M.; Pershan, P. S. *Phys. Rev. A* **1990**, *41*, 4326.
(326) Johnson, P. M.; Pankratz, S.; Mach, P.; Nguyen, H. T.; Huang, C. C. *Phys. Rev. Lett.* **1999**, *83*, 4073.
(327) Hsiung, H.; Rasing, T.; Shen, Y. R. *Phys. Rev. Lett.* **1986**, *57*, 3065.
(328) Hirosawa, I. *Jpn. J. Appl. Phys., Part 1* **1996**, *35*, 5873.
(329) Franquet, A.; De Laet, J.; Schram, T.; Terryn, H.; Subramanian, V.; van Ooij, W. J.; Vereecken, J. *Thin Solid Films* **2001**, *384*, 37.
(330) Franquet, A.; Terryn, H.; Vereecken, J. *Thin Solid Films* **2003**, *441*, 76.
(331) Vallant, T.; Simanko, W.; Brunner, H.; Mayer, U.; Hoffmann, H.; Schmid, R.; Kirchner, K.; Svagera, R.; Sch√°°gerl, G.; Ebel, M. *Organometallics* **1999**, *18*, 3744.
(332) Kim, Y. T.; Collins, R. W.; Vedam, K.; Allara, D. L. *J. Electrochem. Soc.* **1991**, *138*, 3266.
(333) Bohm, S.; Greef, R.; McMurray, H. N.; Powell, S. M.; Worsley, D. A. *J. Electrochem. Soc.* **2000**, *147*, 3286.

(334) Jin, G.; Jansson, R.; Arwin, H. *Rev. Sci. Instrum.* **1996**, *67*, 2930.
(335) Wang, Z. H.; Jin, G. *Anal. Chem.* **2003**, *75*, 6119.
(336) Keddie, J. L. *Curr. Opin. Colloid Interface Sci.* **2001**, *6*, 102.
(337) Hans, A. *Thin Solid Films* **2011**, *519*, 2589.
(338) Hinrichs, K.; Aulich, D.; Ionov, L.; Esser, N.; Eichhorn, K. J.; Motornov, M.; Stamm, M.; Minko, S. *Langmuir* **2009**, *25*, 10987.
(339) Nikonenko, N. A.; Bushnak, I. A.; Keddie, J. L. *Appl. Spectrosc.* **2009**, *63*, 889.
(340) Martin, S. J.; Granstaff, V. E.; Frye, G. C. *Anal. Chem.* **1991**, *63*, 2272.
(341) Arnau, A. *Sensors* **2008**, *8*, 370.
(342) Kanazawa, K.; Cho, N. J. *J. Sens.* **2009**, 2009.
(343) Koßlinger, C.; Uttenthaler, E.; Drost, S.; Aberl, F.; Wolf, H.; Brink, G.; Stanglmaier, A.; Sackmann, E. *Sens. Actuators, B* **1995**, *24*, 107.
(344) Kasemo, B. *Surf. Sci.* **2002**, *500*, 656.
(345) Okahata, Y.; Kawase, M.; Niikura, K.; Ohtake, F.; Furusawa, H.; Ebara, Y. *Anal. Chem.* **1998**, *70*, 1288.
(346) Janshoff, A.; Galla, H.-J.; Steinem, C. *Angew. Chem., Int. Ed.* **2000**, *39*, 4004.
(347) Andersson, M.; Sellborn, A.; Fant, C.; Gretzer, C.; Elwing, H. *J. Biomater. Sci., Polym. Ed.* **2002**, *13*, 907.
(348) Peh, W. Y. X.; Reimhult, E.; Teh, H. F.; Thomsen, J. S.; Su, X. *Biophys. J.* **2007**, *92*, 4415.
(349) Malmström, J.; Agheli, H.; Kingshott, P.; Sutherland, D. S. *Langmuir* **2007**, *23*, 9760.
(350) Chen, H.; Su, X.; Neoh, K.-G.; Choe, W.-S. *Langmuir* **2008**, *25*, 1588.
(351) Kurosawa, S.; Park, J.-W.; Aizawa, H.; Wakida, S.-I.; Tao, H.; Ishihara, K. *Biosens. Bioelectron.* **2006**, *22*, 473.
(352) Mannelli, I.; Minunni, M.; Tombelli, S.; Mascini, M. *Biosens. Bioelectron.* **2003**, *18*, 129.
(353) Jiang, X.; Li, D.; Xu, X.; Ying, Y.; Li, Y.; Ye, Z.; Wang, J. *Biosens. Bioelectron.* **2008**, *23*, 1577.
(354) March, C.; Manclús, J. J.; Jiménez, Y.; Arnau, A.; Montoya, A. *Talanta* **2009**, *78*, 827.
(355) Hao, R.; Wang, D.; Zhang, X. e.; Zuo, G.; Wei, H.; Yang, R.; Zhang, Z.; Cheng, Z.; Guo, Y.; Cui, Z.; Zhou, Y. *Biosens. Bioelectron.* **2009**, *24*, 1330.
(356) Fogel, R.; Mashazi, P.; Nyokong, T.; Limson, J. *Biosens. Bioelectron.* **2007**, *23*, 95.
(357) Schneider, T. W.; Buttry, D. A. *J. Am. Chem. Soc.* **1993**, *115*, 12391.
(358) Wang, J.; Frostman, L. M.; Ward, M. D. *J. Phys. Chem.* **1992**, *96*, 5224.
(359) Kawaguchi, T.; Yasuda, H.; Shimazu, K.; Porter, M. D. *Langmuir* **2000**, *16*, 9830.
(360) Cho, N.-J.; Cho, S.-J.; Cheong, K. H.; Glenn, J. S.; Frank, C. W. *J. Am. Chem. Soc.* **2007**, *129*, 10050.
(361) Keller, C. A.; Kasemo, B. *Biophys. J.* **1998**, *75*, 1397.
(362) Keller, C. A.; Glasmästar, K.; Zhdanov, V. P.; Kasemo, B. *Phys. Rev. Lett.* **2000**, *84*, 5443.
(363) Caruso, F.; Serizawa, T.; Furlong, D. N.; Okahata, Y. *Langmuir* **1995**, *11*, 1546.
(364) Evans, K. O.; Biresaw, G. *Thin Solid Films* **2010**, *519*, 900.
(365) Marx, K. A. *Biomacromolecules* **2003**, *4*, 1099.
(366) Wudy, F.; Multerer, M.; Stock, C.; Schmeer, G.; Gores, H. J. *Electrochim. Acta* **2008**, *53*, 6568.
(367) Bruckenstein, S.; Shay, M. *Electrochim. Acta* **1985**, *30*, 1295.
(368) Zhang, H.; Huang, X.; Fan, L. Z.; Nin, B.; Wu, Y. Q.; Zheng, L. P.; Cao, Y. *J. Appl. Polym. Sci.* **2006**, *100*, 3634.
(369) Wehrens-Dijksma, M.; Notten, P. H. L. *Electrochim. Acta* **2006**, *51*, 3609.
(370) Vicente, F.; Gregori, J.; García-Jareño, J.; Giménez-Romero, D. *J. Solid State Electrochem.* **2005**, *9*, 684.
(371) Cho, N.-J.; Kanazawa, K. K.; Glenn, J. S.; Frank, C. W. *Anal. Chem.* **2007**, *79*, 7027.
(372) Ferreira, G. N. M.; da-Silva, A.-C.; Tomé, B. *Trends Biotechnol.* **2009**, *27*, 689.
(373) Ozeki, T.; Morita, M.; Yoshimine, H.; Furusawa, H.; Okahata, Y. *Anal. Chem.* **2006**, *79*, 79.
(374) *X-ray Absorption: Principles, Applications, Techniques of EXAFS, SEXAFS, and XANES*; Koningsberger, D. C., Prins, R., Eds.; Wiley-Interscience: New York, 1988; Vol. 92.
(375) Stöhr, J. *NEXAFS Spectroscopy*; Springer-Verlag: Berlin, 1992.
(376) *X-ray Absorption Fine Structure for Catalysts and Surfaces*; Iwasawa, Y., Ed.; World Scientific: Singapore, 1996; Vol. 2.
(377) Shannon, I. J.; Maschmeyer, T.; Sankar, G.; Thomas, J. M.; Oldroyd, R. D.; Sheehy, M.; Madill, D.; Waller, A. M.; Townsend, R. P. *Catal. Lett.* **1997**, *44*, 23.
(378) Grunwaldt, J. D.; Caravati, M.; Hannemann, S.; Baiker, A. *Phys. Chem. Chem. Phys.* **2004**, *6*, 3037.
(379) Zaera, F.; Fischer, D. A.; Shen, S.; Gland, J. L. *Surf. Sci.* **1988**, *194*, 205.
(380) Haider, P.; Grunwaldt, J.-D.; Seidel, R.; Baiker, A. *J. Catal.* **2007**, *250*, 313.
(381) Lützenkirchen-Hecht, D.; Frahm, R. *Phys. B (Amsterdam, Neth.)* **2005**, *357*, 213.
(382) Edelmann, A.; Schießer, W.; Vinek, H.; Jentys, A. *Catal. Lett.* **2000**, *69*, 11.
(383) Beier, M. J.; Hansen, T. W.; Grunwaldt, J.-D. *J. Catal.* **2009**, *266*, 320.
(384) Grunwaldt, J. D.; Caravati, M.; Baiker, A. *J. Phys. Chem. B* **2006**, *110*, 9916.
(385) Lee, A. F.; Wilson, K. *Green Chem.* **2004**, *6*, 37.
(386) Sordelli, L.; Psaro, R.; Vlaic, G.; Cepparo, A.; Recchia, S.; Dossi, C.; Fusi, A.; Zanoni, R. *J. Catal.* **1999**, *182*, 186.
(387) Reimann, S.; Stötzel, J.; Frahm, R.; Kleist, W.; Grunwaldt, J.-D.; Baiker, A. *J. Am. Chem. Soc.* **2011**, *133*, 3921.
(388) Ramaker, D. E.; Koningsberger, D. C. *Phys. Chem. Chem. Phys.* **2010**, *12*, 5514.
(389) Nagy, Z. *J. Solid State Electrochem.* **2010**, 1.
(390) Melke, J.; Schoekel, A.; Dixon, D.; Cremers, C.; Ramaker, D. E.; Roth, C. *J. Phys. Chem. C* **2010**, *114*, 5914.
(391) Croze, V.; Ettingshausen, F.; Melke, J.; Soehn, M.; Stuermer, D.; Roth, C. *J. Appl. Electrochem.* **2010**, *40*, 877.
(392) Shao, M. H.; Sasaki, K.; Liu, P.; Adzic, R. R. *Z. Phys. Chem. (Munich)* **2007**, *221*, 1175.
(393) Pereira, L. G. S.; Paganin, V. A.; Ticianelli, E. A. *Electrochim. Acta* **2009**, *54*, 1992.
(394) Imai, H.; Izumi, K.; Matsumoto, M.; Kubo, Y.; Kato, K.; Imai, Y. *J. Am. Chem. Soc.* **2009**, *131*, 6293.
(395) Stoupin, S.; Rivera, H.; Li, Z.; Segre, C. U.; Korzeniewski, C.; Casadonte, J. D. J.; Inoue, H.; Smotkin, E. S. *Phys. Chem. Chem. Phys.* **2008**, *10*, 6430.
(396) Jiang, P.; Chen, J.-L.; Borondics, F.; Glans, P.-A.; West, M. W.; Chang, C.-L.; Salmeron, M.; Guo, J. *Electrochem. Commun.* **2010**, *12*, 820.
(397) Adriaens, A.; Dowsett, M.; Jones, G.; Leyssens, K.; Nikitenko, S. *J. Anal. At. Spectrom.* **2009**, *24*, 62.
(398) Lee, K.-T.; Lee, J.-F.; Wu, N.-L. *Electrochim. Acta* **2009**, *54*, 6148.
(399) Modiano, S.; Carreño, J. A. V.; Fugivara, C. S.; Torresi, R. M.; Vivier, V.; Benedetti, A. V.; Mattos, O. R. *Electrochim. Acta* **2008**, *53*, 3670.
(400) Tamura, K.; Oyanagi, H.; Kondo, T.; Koinuma, M.; Uosaki, K. *J. Phys. Chem. B* **2000**, *104*, 9017.
(401) Brown, G. E., Jr.; Sturchio, N. C. *Rev. Mineral. Geochem.* **2002**, *49*, 1.
(402) Hayes, K. F.; Roe, A. L.; Gordon, E. B.; Hodgson, K. O.; Leckie, J. O.; Parks, G. A. *Science* **1987**, *238*, 783.
(403) Peak, D. *J. Colloid Interface Sci.* **2006**, *303*, 337.
(404) Pokrovski, G. S.; Roux, J.; Hazemann, J. L.; Borisova, A. Y.; Gonchar, A. A.; Lemeshko, M. P. *Mineral. Mag.* **2008**, *72*, 667.
(405) Testemale, D.; Dufaud, F.; Martinez, I.; Bénézeth, P.; Hazemann, J. L.; Schott, J.; Guyot, F. *Chem. Geol.* **2009**, *259*, 8.
(406) Daval, D.; Testemale, D.; Recham, N.; Tarascon, J.-M.; Siebert, J.; Martinez, I.; Guyot, F. *Chem. Geol.* **2010**, *275*, 161.

(407) Villinski, J. E.; O'Day, P. A.; Corley, T. L.; Conklin, M. H. *Environ. Sci. Technol.* **2001**, *35*, 1157.
(408) Ohyama, J.; Teramura, K.; Okuoka, S.-i.; Yamazoe, S.; Kato, K.; Shishido, T.; Tanaka, T. *Langmuir* **2010**, *26*, 13907.
(409) Liu, H.; Guo, J.; Yin, Y.; Augustsson, A.; Dong, C.; Nordgren, J.; Chang, C.; Alivisatos, P.; Thornton, G.; Ogletree, D. F.; Requejo, F. G.; de Groot, F.; Salmeron, M. *Nano Lett.* **2007**, *7*, 1919.
(410) Choy, J. H.; Yoon, J. B.; Park, J. H. *J. Synchrotron Radiat.* **2001**, *8*, 782.
(411) Michailovski, A.; Grunwaldt, J.-D.; Baiker, A.; Kiebach, R.; Bensch, W.; Patzke, G. R. *Angew. Chem., Int. Ed.* **2005**, *44*, 5643.
(412) Fonseca, G. S.; Machado, G.; Teixeira, S. R.; Fecher, G. H.; Morais, J.; Alves, M. C. M.; Dupont, J. *J. Colloid Interface Sci.* **2006**, *301*, 193.
(413) Taylor, R. W.; Shen, S.; Bleam, W. F.; Tu, S. I. *Clays Clay Miner.* **2000**, *48*, 648.
(414) Salmeron, M.; Schlögl, R. *Surf. Sci. Rep.* **2008**, *63*, 169.
(415) Kvashnina, K. O.; Butorin, S. M.; Modin, A.; Soroka, I.; Marcellini, M.; Guo, J.-H.; Werme, L.; Nordgren, J. *J. Phys.: Condens. Matter* **2007**, *19*, 226002/1.
(416) Hollmark, H. M.; Vegelius, J. R.; Kristiansen, P.; Werme, L.; Duda, L. C. *J. Electrochem. Soc.* **2011**, *158*, C1.
(417) Renaud, G.; Lazzari, R.; Leroy, F. *Surf. Sci. Rep.* **2009**, *64*, 255.
(418) Daillant, J. *Curr. Opin. Colloid Interface Sci.* **2009**, *14*, 396.
(419) Hamilton, W. A. *Curr. Opin. Colloid Interface Sci.* **2005**, *9*, 390.
(420) Gibaud, A.; Bardeau, J. F.; Dutreilh-Colas, M.; Bellour, M.; Balasubramanian, V. V.; Robert, A.; Mehdi, A.; Reye, C.; Corriu, R. J. *J. Mater. Chem.* **2004**, *14*, 1854.
(421) Seeck, O. H.; Kim, H.; Lee, D. R.; Shu, D.; Kaendler, I. D.; Basu, J. K.; Sinha, S. K. *Europhys. Lett.* **2002**, *60*, 376.
(422) Fukuto, M.; Heilmann, R. K.; Pershan, P. S.; Badia, A.; Lennox, R. B. *J. Chem. Phys.* **2004**, *120*, 3446.
(423) Erokhina, S.; Berzina, T.; Cristofolini, L.; Erokhin, V.; Folli, C.; Konovalov, O.; Marino, I.-G.; Fontana, M. P. *Langmuir* **2008**, *24*, 12093.
(424) Jensen, T. R.; Balashev, K.; Bjørnholm, T.; Kjaer, K. *Biochimie* **2001**, *83*, 399.
(425) Brotons, G.; Salditt, T.; Dubois, M.; Zemb, T. *Langmuir* **2003**, *19*, 8235.
(426) Miller, C. E.; Majewski, J.; Kuhl, T. L. *Colloids Surf., A* **2006**, *284*−*285*, 434.
(427) Schubert, T.; Seitz, P. C.; Schneck, E.; Nakamura, M.; Shibakami, M.; Funari, S. S.; Konovalov, O.; Tanaka, M. *J. Phys. Chem. B* **2008**, *112*, 10041.
(428) Amenitsch, H.; Rappolt, M.; Teixeira, C. V.; Majerowicz, M.; Laggner, P. *Langmuir* **2004**, *20*, 4621.
(429) Spaar, A.; Münster, C.; Salditt, T. *Biophys. J.* **2004**, *87*, 396.
(430) Douarche, C.; Cortès, R.; Roser, S. J.; Sikorav, J.-L.; Braslau, A. *J. Phys. Chem. B* **2008**, *112*, 13676.
(431) Chi, E. Y.; Ege, C.; Winans, A.; Majewski, J.; Wu, G.; Kjaer, K.; Lee, K. Y. C. *Proteins: Struct., Funct., Bioinf.* **2008**, *72*, 1.
(432) Horton, M. R.; Reich, C.; Gast, A. P.; Rädler, J. O.; Nickel, B. *Langmuir* **2007**, *23*, 6263.
(433) Fenter, P.; Sturchio, N. C. *Prog. Surf. Sci.* **2004**, *77*, 171.
(434) Catalano, J. G. *Geochim. Cosmochim. Acta* **2011**, *75*, 2062.
(435) Machesky, M. L.; Předota, M.; Wesolowski, D. J.; Vlcek, L.; Cummings, P. T.; Rosenqvist, J.; Ridley, M. K.; Kubicki, J. D.; Bandura, A. V.; Kumar, N.; Sofo, J. O. *Langmuir* **2008**, *24*, 12331.
(436) Zhang, Z.; Fenter, P.; Cheng, L.; Sturchio, N. C.; Bedzyk, M. J.; Předota, M.; Bandura, A.; Kubicki, J. D.; Lvov, S. N.; Cummings, P. T.; Chialvo, A. A.; Ridley, M. K.; Bénézeth, P.; Anovitz, L.; Palmer, D. A.; Machesky, M. L.; Wesolowski, D. J. *Langmuir* **2004**, *20*, 4954.
(437) Valtiner, M.; Torrelles, X.; Pareek, A.; Borodin, S.; Gies, H.; Grundmeier, G. *J. Phys. Chem. C* **2010**, *114*, 15440.
(438) Fenter, P.; Park, C.; Nagy, K. L.; Sturchio, N. C. *Thin Solid Films* **2007**, *515*, 5654.
(439) Mo, H.; Evmenenko, G.; Dutta, P. *Chem. Phys. Lett.* **2005**, *415*, 106.
(440) Mezger, M.; Schröder, H.; Reichert, H.; Schramm, S.; Okasinski, J. S.; Schöder, S.; Honkimäki, V.; Deutsch, M.; Ocko, B. M.; Ralston, J.; Rohwerder, M.; Stratmann, M.; Dosch, H. *Science* **2008**, *322*, 424.
(441) De Marco, R.; Veder, J.-P. *TrAC, Trends Anal. Chem.* **2010**, *29*, 528.
(442) You, H.; Zurawski, D. J.; Nagy, Z.; Yonco, R. M. *J. Chem. Phys.* **1994**, *100*, 4699.
(443) Nagy, Z. n.; You, H. *Electrochim. Acta* **2002**, *47*, 3037.
(444) Marković, N. M.; Grgur, B. N.; Lucas, C. A.; Ross, P. N. *J. Phys. Chem. B* **1999**, *103*, 487.
(445) Tolmachev, Y. V.; Menzel, A.; Tkachuk, A. V.; Chu, Y. S.; You, H. *Electrochemical and Solid-State Letters* **2004**, *7*, E23.
(446) Gallagher, M. E.; Blizanac, B. B.; Lucas, C. A.; Ross, P. N.; Marković, N. M. *Surf. Sci.* **2005**, *582*, 215.
(447) Doshi, D. A.; Gibaud, A.; Goletto, V.; Lu, M.; Gerung, H.; Ocko, B.; Han, S. M.; Brinker, C. J. *J. Am. Chem. Soc.* **2003**, *125*, 11646.
(448) Sanyal, M. K.; Agrawal, V. V.; Bera, M. K.; Kalyanikutty, K. P.; Daillant, J.; Blot, C.; Kubowicz, S.; Konovalov, O.; Rao, C. N. R. *J. Phys. Chem. C* **2008**, *112*, 1739.
(449) Als-Nielsen, J.; Jacquemain, D.; Kjaer, K.; Leveiller, F.; Lahav, M.; Leiserowitz, L. *Phys. Rep.* **1994**, *246*, 251.
(450) Rapaport, H.; Kuzmenko, I.; Berfeld, M.; Kjaer, K.; Als-Nielsen, J.; Popovitz-Biro, R.; Weissbuch, I.; Lahav, M.; Leiserowitz, L. *J. Phys. Chem. B* **2000**, *104*, 1399.
(451) Hąc-Wydro, K.; Flasiński, M.; Broniatowski, M.; Dynarowicz-Łątka, P.; Majewski, J. *J. Phys. Chem. B* **2010**, *114*, 6866.
(452) Etienne, F.; Roche, Y.; Peretti, P.; Bernard, S. *Chem. Phys. Lipids* **2008**, *152*, 13.
(453) Lösche, M. In *Current Topics in Membranes*; Sidney, A., Simon, T. J. M., Ed.; Academic Press: San Diego, California, 2002; Vol. Vol. 52, pp 117.
(454) Salditt, T.; Li, C.; Spaar, A. *Biochim. Biophys. Acta, Biomembr.* **2006**, *1758*, 1483.
(455) Neville, F.; Ivankin, A.; Konovalov, O.; Gidalevitz, D. *Biochim. Biophys. Acta, Biomembr.* **2010**, *1798*, 851.
(456) Wang, X.; He, Q.; Zheng, S.; Brezesinski, G.; Möhwald, H.; Li, J. *J. Phys. Chem. B* **2004**, *108*, 14171.
(457) Sakamoto, K.; Hirayama, M.; Sonoyama, N.; Mori, D.; Yamada, A.; Tamura, K.; Mizuki, J. i.; Kanno, R. *Chem. Mater.* **2009**, *21*, 2632.
(458) Bramnik, N. N.; Trots, D. M.; Hofmann, H. J.; Ehrenberg, H. *Phys. Chem. Chem. Phys.* **2009**, *11*, 3271.
(459) Rosciano, F.; Holzapfel, M.; Kaiser, H.; Scheifele, W.; Ruch, P.; Hahn, M.; K√∂tz, R.; Nov√°k, P. *J. Synchrotron Radiat.* **2007**, *14*, 487.
(460) Renner, F. U.; Kageyama, H.; Siroma, Z.; Shikano, M.; Schöder, S.; Gründer, Y.; Sakata, O. *Electrochim. Acta* **2008**, *53*, 6064.
(461) Ruch, P. W.; Hahn, M.; Rosciano, F.; Holzapfel, M.; Kaiser, H.; Scheifele, W.; Schmitt, B.; Novák, P.; Kötz, R.; Wokaun, A. *Electrochim. Acta* **2007**, *53*, 1074.
(462) Keller, H.; Saracino, M.; Nguyen, H. M. T.; Broekmann, P. *Phys. Rev. B* **2010**, *82*, 245425.
(463) Herrero, E.; Glazier, S.; Buller, L. J.; AbruÒa, H. D. *J. Electroanal. Chem.* **1999**, *461*, 121.
(464) Grelet, E.; Dardel, S.; Bock, H.; Goldmann, M.; Lacaze, E.; Nallet, F. *Eur. Phys. J. E: Soft Matter Biol. Phys.* **2010**, *31*, 343.
(465) Dröge, S.; Al Khalifah, M. S.; O'Neill, M.; Thomas, H. E.; Simmonds, H. S.; Macdonald, J. E.; Aldred, M. P.; Vlachos, P.; Kitney, S. P.; Löbbert, A.; Kelly, S. M. *J. Phys. Chem. B* **2008**, *113*, 49.
(466) Volkmer, D.; Fricke, M.; Vollhardt, D.; Siegel, S. *J. Chem. Soc., Dalton Trans.* **2002**, 4547.
(467) Shah, I. A.; Nguyen, Q. D.; Philipsen, H. G. G.; van der Wolf, B. M. A.; Algra, R. G.; Tinnemans, P.; Koekkoek, A. J.; Panina, N.; van den Bruele, F. J. M.; van Enckevort, W. J. P.; Vlieg, E. *Surf. Sci.* **2011**, *605*, 1027.
(468) Fong, D. D.; Lucas, C. A.; Richard, M. I.; Toney, M. F. *MRS Bull.* **2010**, *35*, 504.
(469) Golks, F.; Krug, K.; Gründer, Y.; Zegenhagen, J.; Stettner, J.; Magnussen, O. M. *J. Am. Chem. Soc.* **2011**, *133*, 3772.

(470) Stamenković, V. R.; Arenz, M.; Lucas, C. A.; Gallagher, M. E.; Ross, P. N.; Marković, N. M. *J. Am. Chem. Soc.* **2003**, *125*, 2736.
(471) Caminiti, R.; Caracciolo, G.; Pisani, M. *Appl. Phys. Lett.* **2005**, *86*, 253902.
(472) Jelassi, J.; Grosz, T.; Bako, I.; Bellissent-Funel, M. C.; Dore, J. C.; Castricum, H. L.; Sridi-Dorbez, R. *J. Chem. Phys.* **2011**, *134*, 064509.
(473) Penfold, J.; Richardson, R. M.; Zarbakhsh, A.; Webster, J. R. P.; Bucknall, D. G.; Rennie, A. R.; Jones, R. A. L.; Cosgrove, T.; Thomas, R. K.; Higgins, J. S.; Fletcher, P. D. I.; Dickinson, E.; Roser, S. J.; McLure, I. A.; Hillman, A. R.; Richards, R. W.; Staples, E. J.; Burgess, A. N.; Simister, E. A.; White, J. W. *J. Chem. Soc., Faraday Trans.* **1997**, *93*, 3899.
(474) Majewski, J.; Kuhl, T. L.; Wong, J. Y.; Smith, G. S. *Rev. Mol. Biotechnol.* **2000**, *74*, 207.
(475) Torikai, N.; Yamada, N. L.; Noro, A.; Harada, M.; Kawaguchi, D.; Takano, A.; Matsushita, Y. *Polym. J.* **2007**, *39*, 1238.
(476) Lu, J. R.; Marrocco, A.; Su, T. J.; Thomas, R. K.; Penfold, J. *J. Colloid Interface Sci.* **1993**, *158*, 303.
(477) Turner, S. F.; Clarke, S. M.; Rennie, A. R.; Thirtle, P. N.; Cooke, D. J.; Li, Z. X.; Thomas, R. K. *Langmuir* **1999**, *15*, 1017.
(478) Salditt, T. *J. Phys.: Condens. Matter* **2005**, *17*, R287.
(479) Thirtle, P. N.; Li, Z. X.; Thomas, R. K.; Rennie, A. R.; Satija, S. K.; Sung, L. P. *Langmuir* **1997**, *13*, 5451.
(480) Lee, E. M.; Thomas, R. K.; Cummins, P. G.; Staples, E. J.; Penfold, J.; Rennie, A. R. *Chem. Phys. Lett.* **1989**, *162*, 196.
(481) McGillivray, D. J.; Thomas, R. K.; Rennie, A. R.; Penfold, J.; Sivia, D. S. *Langmuir* **2003**, *19*, 7719.
(482) Hamilton, W. A.; Porcar, L.; Butler, P. D.; Warr, G. G. *J. Chem. Phys.* **2002**, *116*, 8533.
(483) Kreuzer, M.; Kaltofen, T.; Steitz, R.; Zehnder, B. H.; Dahint, R. *Rev. Sci. Instrum.* **2011**, *82*, 023902.
(484) Smith, H. L.; Howland, M. C.; Szmodis, A. W.; Li, Q.; Daemen, L. L.; Parikh, A. N.; Majewski, J. *J. Am. Chem. Soc.* **2009**, *131*, 3631.
(485) Gutberlet, T.; Klösgen, B.; Krastev, R.; Steitz, R. *Adv. Eng. Mater.* **2004**, *6*, 832.
(486) Dubey, M.; Jablin, M. S.; Smith, H.; Majewski, J. *Acta Crystallogr., Sect. D: Biol. Crystallogr.* **2010**, *66*, 1237.
(487) Wu, J.-C.; Lin, T.-L.; Jeng, U. S.; Torikai, N. *Phys. B (Amsterdam, Neth.)* **2006**, *385*−*386*, 838.
(488) Vandoolaeghe, P.; Rennie, A. R.; Campbell, R. A.; Thomas, R. K.; Hook, F.; Fragneto, G.; Tiberg, F.; Nylander, T. *Soft Matter* **2008**, *4*, 2267.
(489) Majewski, J.; Smith, G. S.; Burgess, I.; Zamlynny, V.; Szymanski, G.; Lipkowski, J.; Satija, S. *Appl. Phys. A: Mater. Sci. Process.* **2002** *74*, s364.
(490) Schmidt, I.; Novales, B.; Boué, F.; Axelos, M. A. V. *J. Colloid Interface Sci.* **2010**, *345*, 316.
(491) He, L.; Smith, H. L.; Majewski, J.; Fujimoto, C. H.; Cornelius, C. J.; Perahia, D. *Macromolecules* **2009**, *42*, 5745.
(492) Gutfreund, P.; Wolff, M.; Maccarini, M.; Gerth, S.; Ankner, J. F.; Browning, J.; Halbert, C. E.; Wacklin, H.; Zabel, H. *J. Chem. Phys.* **2011**, *134*, 064711.
(493) Hickner, M. A.; Siegel, N. P.; Chen, K. S.; Hussey, D. S.; Jacobson, D. L.; Arif, M. *J. Electrochem. Soc.* **2008**, *155*, B427.
(494) Winn, A. J.; Derby, B.; Webster, J. R. P.; Holt, S. *J. Am. Ceram. Soc.* **2004**, *87*, 279.
(495) Edwards, R.; Derby, B.; Webster, J.; Xlao, P. *J. Phys. D: Appl. Phys.* **1999**, *32*, 2319.
(496) Prabhu, V. M.; Kang, S.; VanderHart, D. L.; Satija, S. K.; Lin, E. K.; Wu, W.-l. *Adv. Mater.* **2011**, *23*, 388.
(497) Wolff, M.; Scholz, U.; Hock, R.; Magerl, A.; Leiner, V.; Zabel, H. *Phys. Rev. Lett.* **2004**, *92*, 255501.
(498) Polak, E.; Munn, J.; Barnes, P.; Tarling, S. E.; Ritter, C. *J. Appl. Crystallogr.* **1990**, *23*, 258.
(499) Watson, J. N.; Iton, L. E.; White, J. W. *Chem. Commun.* **1996**, 2767.
(500) Walton, R. I.; Millange, F.; Smith, R. I.; Hansen, T. C.; O'Hare, D. *J. Am. Chem. Soc.* **2001**, *123*, 12547.
(501) Whittaker, A. G.; Harrison, A.; Oakley, G. S.; Youngson, I. D.; Heenan, R. K.; King, S. M. *Rev. Sci. Instrum.* **2001**, *72*, 173.
(502) Hoinkis, E. *Adv. Colloid Interface Sci.* **1998**, *76*−*77*, 39.
(503) *Handbook of X-ray and Ultraviolet Photoelectron Spectroscopy*; Briggs, D., Ed.; Heyden: London, 1978.
(504) Ogletree, D. F.; Bluhm, H.; Lebedev, G.; Fadley, C. S.; Hussain, Z.; Salmeron, M. *Rev. Sci. Instrum.* **2002**, *73*, 3872.
(505) Teschner, D.; Pestryakov, A.; Kleimenov, E.; Hävecker, M.; Bluhm, H.; Sauer, H.; Knop-Gericke, A.; Schlögl, R. *J. Catal.* **2005**, *230*, 186.
(506) Kolb, D. M.; Rath, D. L.; Wille, R.; Hansen, W. N. *Ber. Bunsen-Ges. Phys. Chem.* **1983**, *87*, 1108.
(507) D'Agostino, A. T.; Hansen, W. N. *Surf. Sci.* **1986**, *165*, 268.
(508) Kötz, E. R.; Neff, H.; Müller, K. *J. Electroanal. Chem. Interfacial Electrochem.* **1986**, *215*, 331.
(509) Zhou, W.; Kolb, D. M. *Surf. Sci.* **2004**, *573*, 176.
(510) Weingarth, D.; Foelske-Schmitz, A.; Wokaun, A.; Kötz, R. *Electrochem. Commun.* **2011**, DOI: 10.1016/j.elecom.2011.03.027.
(511) Cardenas, J.; Sjöberg, S. *Surf. Sci.* **2003**, *532*−*535*, 1104.
(512) Zemlyanov, D.; Weinberg, G.; Wild, U.; Schlögl, R. *Catal. Lett.* **2000**, *64*, 113.
(513) Kondoh, K.; Kimura, A.; Watanabe, R. *J. Jpn. Soc. Powder Powder Metall.* **1999**, *46*, 1141.
(514) Halka, V.; Freyland, W. *J. Chem. Phys.* **2007**, *127*, 034702/1.
(515) Aliaga, C.; Santos, C. S.; Baldelli, S. *Phys. Chem. Chem. Phys.* **2007**, *9*, 3683.
(516) Lovelock, K. R. J.; Villar-Garcia, I. J.; Maier, F.; Steinrück, H.-P.; Licence, P. *Chem. Rev.* **2010**, *110*, 5158.
(517) Bovio, S.; Podestà, A.; Lenardi, C.; Milani, P. *J. Phys. Chem. B* **2009**, *113*, 6600.
(518) Cremer, T.; Killian, M.; Gottfried, J. M.; Paape, N.; Wasserscheid, P.; Maier, F.; Steinrück, H.-P. *ChemPhysChem* **2008**, *9*, 2185.
(519) Cremer, T.; Stark, M.; Deyko, A.; Steinrück, H. P.; Maier, F. *Langmuir* **2011**, *27*, 3662.
(520) Taylor, A. W.; Qiu, F.; Villar-Garcia, I. J.; Licence, P. *Chem. Commun.* **2009**, 5817.
(521) Johnston, M.; Lee, J.-J.; Chottiner, G. S.; Miller, B.; Tsuda, T.; Hussey, C. L.; Scherson, D. A. *J. Phys. Chem. B* **2005**, *109*, 11296.
(522) Chang, J.-K.; Lee, M.-T.; Tsai, W.-T.; Deng, M.-J.; Sun, I. W. *Chem. Mater.* **2009**, *21*, 2688.
(523) Wang, M.; Schneider, A.; NiedziÛlka-Ĵnsson, J.; Marcon, L.; Ghodbane, S.; Steinmller-Nethl, D.; Li, M.; Boukherroub, R.; Szunerits, S. *Electrochim. Acta* **2010**, *55*, 1582.
(524) Chi, Y. S.; Lee, J. K.; Lee, S.-g.; Choi, I. S. *Langmuir* **2004**, *20*, 3024.
(525) Chi, Y. S.; Hwang, S.; Lee, B. S.; Kwak, J.; Choi, I. S.; Lee, S.-g. *Langmuir* **2005**, *21*, 4268.
(526) Qiu, F.; Taylor, A. W.; Men, S.; Villar-Garcia, I. J.; Licence, P. *Phys. Chem. Chem. Phys.* **2010**, *12*, 1982.
(527) Du, P.; Liu, S.; Wu, P.; Cai, C. *Electrochim. Acta* **2007**, *52*, 6534.
(528) Shigeyasu, M.; Murayama, H.; Tanaka, H. *Chem. Phys. Lett.* **2008**, *463*, 373.
(529) Bernardi, F.; Scholten, J. D.; Fecher, G. H.; Dupont, J.; Morais, J. *Chem. Phys. Lett.* **2009**, *479*, 113.
(530) Sobota, M.; Schmid, M.; Happel, M.; Amende, M.; Maier, F.; Steinruck, H.-P.; Paape, N.; Wasserscheid, P.; Laurin, M.; Gottfried, J. M.; Libuda, J. *Phys. Chem. Chem. Phys.* **2010**, *12*, 10610.
(531) Zhang, H.; Cui, H. *Langmuir* **2009**, *25*, 2604.
(532) Coman, S. M.; Florea, M.; Parvulescu, V. I.; David, V.; Medvedovici, A.; De Vos, D.; Jacobs, P. A.; Poncelet, G.; Grange, P. *J. Catal.* **2007**, *249*, 359.
(533) Yu, B.; Zhou, F.; Liu, G.; Liang, Y.; Huck, W. T. S.; Liu, W. *Chem. Commun.* **2006**, 2356.
(534) Wang, Z.; Zhang, Q.; Kuehner, D.; Xu, X.; Ivaska, A.; Niu, L. *Carbon* **2008**, *46*, 1687.

(535) Ghosal, S.; Hemminger, J. C.; Bluhm, H.; Mun, B. S.; Hebenstreit, E. L. D.; Ketteler, G.; Ogletree, D. F.; Requejo, F. G.; Salmeron, M. *Science* **2005**, *307*, 563.
(536) Nebel, C. E.; Shin, D.; Takeuchi, D.; Yamamoto, T.; Watanabe, H.; Nakamura, T. *Langmuir* **2006**, *22*, 5645.
(537) Derome, A. E. *Modern NMR Techniques for Chemistry Research*; Pergamon Press: New York, 1987.
(538) Keeler, J. *Understanding NMR Spectroscopy*; 2nd ed.; John Wiley & Sons: Chichester, 2010.
(539) Foster, A. J.; Lobo, R. F. *Chem. Soc. Rev.* **2010**, *39*, 4783.
(540) Shelimov, B.; Lambert, J.-F.; Che, M.; Didillon, B. *J. Am. Chem. Soc.* **1999**, *121*, 545.
(541) Kramer, J.; Koch, K. R. *Inorg. Chem.* **2006**, *45*, 7843.
(542) Okamura, E.; Yoshii, N. *J. Chem. Phys.* **2008**, *129*, 215102.
(543) Turov, V. V.; Leboda, R. *Adv. Colloid Interface Sci.* **1999**, *79*, 173.
(544) Webber, J. B. W. *Prog. Nucl. Magn. Reson. Spectrosc.* **2010**, *56*, 78.
(545) Mitchell, J.; Webber, J. B. W.; Strange, J. H. *Phys. Rep.* **2008**, *461*, 1.
(546) Letellier, M.; Tinet, D.; Maggion, R.; Fripiat, J. *Magn. Reson. Imag.* **1991**, *9*, 709.
(547) Wang, K.; Xing, B. *J. Environ. Qual.* **2005**, *34*, 342.
(548) Kudryavtsev, A. B.; Kouznetsova, T. V.; Linert, W.; Hunter, G. *Cem. Concr. Res.* **1997**, *27*, 501.
(549) Gilpin, R. K. *J. Chromatogr. A* **1993**, *656*, 217.
(550) Sentell, K. B. *J. Chromatogr. A* **1993**, *656*, 231.
(551) Zhang, B.; Yan, B. *Anal. Bioanal. Chem.* **2010**, *396*, 973.
(552) Sachleben, J. R.; Colvin, V.; Emsley, L.; Wooten, E. W.; Alivisatos, A. P. *J. Phys. Chem. B* **1998**, *102*, 10117.
(553) Diaz, D.; Rivera, M.; Ni, T.; Rodriguez, J.-C.; Castillo-Blum, S.-E.; Nagesha, D.; Robles, J.; Alvarez-Fregoso, O.-J.; Kotov, N. A. *J. Phys. Chem. B* **1999**, *103*, 9854.
(554) Majetich, S. A.; Carter, A. C.; Belot, J.; McCullough, R. D. *J. Phys. Chem.* **1994**, *98*, 13705.
(555) Holland, G. P.; Sharma, R.; Agola, J. O.; Amin, S.; Solomon, V. C.; Singh, P.; Buttry, D. A.; Yarger, J. L. *Chem. Mater.* **2007**, *19*, 2519.
(556) Willis, A. L.; Turro, N. J.; O'Brien, S. *Chem. Mater.* **2005**, *17*, 5970.
(557) Wang, H.; Shao, Z.; Wang, W.; Wang, F. *e-Polym.* **2010**, *116*, 1.
(558) Terrill, R. H.; Postlethwaite, T. A.; Chen, C.-h.; Poon, C.-D.; Terzis, A.; Chen, A.; Hutchison, J. E.; Clark, M. R.; Wignall, G. *J. Am. Chem. Soc.* **1995**, *117*, 12537.
(559) Badia, A.; Singh, S.; Demers, L.; Cuccia, L.; Brown, G. R.; Lennox, R. B. *Chem.—Eur. J.* **1996**, *2*, 359.
(560) Badia, A.; Gao, W.; Singh, S.; Demers, L.; Cuccia, L.; Reven, L. *Langmuir* **1996**, *12*, 1262.
(561) Schmitt, H.; Badia, A.; Dickinson, L.; Reven, L.; Lennox, R. B. *Adv. Mater.* **1998**, *10*, 475.
(562) Song, Y.; Harper, A. S.; Murray, R. W. *Langmuir* **2005**, *21*, 5492.
(563) Zelakiewicz, B. S.; de Dios, A. C.; Tong, Y. *J. Am. Chem. Soc.* **2002**, *125*, 18.
(564) Fleming, D. A.; Thode, C. J.; Williams, M. E. *Chem. Mater.* **2006**, *18*, 2327.
(565) Fremgen, D. E.; Smotkin, E. S.; Gerald, R. E.; Klingler, R. J.; Rathke, J. W. *J. Supercrit. Fluids* **2001**, *19*, 287.
(566) Xu, B.; Lynn, G. W.; Guo, J.; Melnichenko, Y. B.; Wignall, G. D.; McClain, J. B.; DeSimone, J. M.; Johnson, C. S. *J. Phys. Chem. B* **2005**, *109*, 10261.
(567) Engelhardt, G.; Michel, D. *High-Resolution Soli-State NMR of Silicates and Zeolites*; John Wiley & Sons: Chichester, U.K., 1987.
(568) Hughes, C. E.; Harris, K. D. M. *J. Phys. Chem. A* **2008**, *112*, 6808.
(569) Senker, J.; Sehnert, J.; Correll, S. *J. Am. Chem. Soc.* **2004**, *127*, 337.
(570) Shi, J.; Anderson, M. W.; Carr, S. W. *Chem. Mater.* **1996**, *8*, 369.
(571) Frasch, J.; Lebeau, B.; Soulard, M.; Patarin, J.; Zana, R. *Langmuir* **2000**, *16*, 9049.
(572) Flodström, K.; Wennerström, H.; Alfredsson, V. *Langmuir* **2003**, *20*, 680.
(573) Egger, C. C.; Anderson, M. W.; Tiddy, G. J. T.; Casci, J. L. *Phys. Chem. Chem. Phys.* **2005**, *7*, 1845.
(574) Haouas, M.; Gérardin, C.; Taulelle, F.; Estournes, C.; Loiseau, T.; Ferey, G. *J. Chim. Phys.* **1998**, *95*, 302.
(575) Vistad, Ø. B.; Akporiaye, D. E.; Taulelle, F.; Lillerud, K. P. *Chem. Mater.* **2003**, *15*, 1639.
(576) Luca, S.; White, J. F.; Sohal, A. K.; Filippov, D. V.; Van Boom, J. H.; Grisshammer, R.; Baldus, M. *Proc. Natl. Acad. Sci. U. S. A.* **2003**, *100*, 10706.
(577) Cady, S. D.; Schmidt-Rohr, K.; Wang, J.; Soto, C. S.; Degrado, W. F.; Hong, M. *Nature* **2010**, *463*, 689.
(578) Ghassemzadeh, L.; Kreuer, K.-D.; Maier, J.; Müller, K. *J. Phys. Chem. C* **2010**, *114*, 14635.
(579) Lai, J.; Niks, D.; Wang, Y.; Domratcheva, T.; Barends, T. R. M.; Schwarz, F.; Olsen, R. A.; Elliott, D. W.; Fatmi, M. Q.; Chang, C. E. A.; Schlichting, I.; Dunn, M. F.; Mueller, L. J. *J. Am. Chem. Soc.* **2011**, *133*, 4.
(580) Lysova, A. A.; Koptyug, I. V. *Chem. Soc. Rev.* **2010**, *39*, 4585.
(581) Chen, V.; Li, H.; Fane, A. G. *J. Membr. Sci.* **2004**, *241*, 23.
(582) Rieger, P. H. *Electron Spin Resonance: Analysis and Interpretation*; Royal Society of Chemistry: Cambridge, U.K., 2007.
(583) Lund, A.; Shiotani, M.; Shimada, S. *Principles and Applications of ESR Spectroscopy*; 1st ed.; Springer: New York, 2011.
(584) Robb, I. D.; Smith, R. *Polymer* **1977**, *18*, 500.
(585) Cohen Stuart, M. A.; Fleer, G. J.; Bijsterbosch, B. H. *J. Colloid Interface Sci.* **1982**, *90*, 321.
(586) Amiel, C.; Sebille, B.; Hommel, H.; Legrand, A. P. *J. Colloid Interface Sci.* **1994**, *165*, 236.
(587) Fox, K. K.; Robb, I. D.; Smith, R. *J. Chem. Soc. Faraday Trans. 1* **1974**, *70*, 1186.
(588) Hommel, H. *Adv. Colloid Interface Sci.* **2008**, *141*, 1.
(589) Belarbi, Z.; Sirlin, C.; Simon, J.; Andre, J. J. *J. Phys. Chem.* **1989**, *93*, 8105.
(590) Castellanos, S.; López-Calahorra, F.; Brillas, E.; Juliá, L.; Velasco, D. *Angew. Chem., Int. Ed.* **2009**, *48*, 6516.
(591) Wasserman, A.; Motyakin, M.; Yasina, L.; Zakharova, Y.; Matveenko, V.; Shulevich, Y.; Rogovina, L. *Appl. Magn. Reson.* **2010**, *38*, 117.
(592) Megli, F. M.; Russo, L.; Conte, E. *Biochim. Biophys. Acta, Biomembr.* **2009**, *1788*, 371.
(593) Ottaviani, M. F.; Leonardis, I.; Cappiello, A.; Cangiotti, M.; Mazzeo, R.; Trufelli, H.; Palma, P. *J. Colloid Interface Sci.* **2010**, *352*, 512.
(594) Wisniewska, A.; Subczynski, W. *Cell. Mol. Biol. Lett.* **2008**, *13*, 430.
(595) Bunge, A.; Kurz, A.; Windeck, A.-K.; Korte, T.; Flasche, W.; Liebscher, J.; Herrmann, A.; Huster, D. *Langmuir* **2007**, *23*, 4455.
(596) Ruthstein, S.; Schmidt, J.; Kesselman, E.; Popovitz-Biro, R.; Omer, L.; Frydman, V.; Talmon, Y.; Goldfarb, D. *Chem. Mater.* **2008**, *20*, 2779.
(597) Ottaviani, M. F.; Galarneau, A.; Desplantier-Giscard, D.; Di Renzo, F.; Fajula, F. *Microporous Mesoporous Mater.* **2001**, *44*−*45*, 1.
(598) Brik, M. E.; Titman, J. J.; Bayle, J. P.; Judeinstein, P. *J. Polym. Sci., Part B: Polym. Phys.* **1996**, *34*, 2533.
(599) Brückner, A. *Chem. Soc. Rev.* **2010**, *39*, 4673.
(600) Hou, Y.; Li, X.; Liu, P.; Zou, X.; Chen, G.; Yue, P.-L. *Sep. Purif. Technol.* **2009**, *67*, 135.
(601) Tudose, M.; Constantinescu, T.; Balaban, A. T.; Ionita, P. *Appl. Surf. Sci.* **2008**, *254*, 1904.
(602) Fubini, B.; Mollo, L.; Giamello, E. *Free Radical Res.* **1995**, *23*, 593.
(603) Dyrek, K.; Adamski, A.; Sojka, Z. *Spectrochim. Acta A* **1998**, *54*, 2337.
(604) DiCicco, M.; Compton, R.; Duong, T.; Jansen-Varnum, S. A. *J. Biomed. Mater. Res., Part B* **2005**, *75B*, 6.

(605) Navratil, M.; Mabbott, G. A.; Arriaga, E. A. *Anal. Chem.* **2006**, *78*, 4005.
(606) Lichtman, J. W.; Conchello, J.-A. *Nat. Meth.* **2005**, *2*, 910.
(607) Yeung, T.; Touret, N.; Grinstein, S. *Curr. Opin. Microbiol.* **2005**, *8*, 350.
(608) Sahai, E. *Nat. Rev. Cancer* **2007**, *7*, 737.
(609) Freites, J. A.; Ali, S.; Rosengarth, A.; Luecke, H.; Dennin, M. B. *Langmuir* **2004**, *20*, 11674.
(610) Price, A. D.; Schwartz, D. K. *J. Am. Chem. Soc.* **2008**, *130*, 8188.
(611) Fujimori, A.; Naito, H.; Miyazaki, T. *Artif. Organs* **1998**, *22*, 1014.
(612) Katano, K.; Safaei, R.; Samimi, G.; Holzer, A.; Tomioka, M.; Goodman, M.; Howell, S. B. *Clin. Cancer Res.* **2004**, *10*, 4578.
(613) Pozo, K.; Stephenson, F. A. *Biochem. Soc. Trans.* **2006**, *34*, 48.
(614) Burmeister, J. S.; Olivier, L. A.; Reichert, W. M.; Truskey, G. A. *Biomaterials* **1998**, *19*, 307.
(615) Toomre, D.; Manstein, D. J. *Trends Cell Biol.* **2001**, *11*, 298.
(616) Trache, A.; Meininger, G. A. *Total Internal Reflection Fluorescence (TIRF) Microscopy*; John Wiley & Sons, New York Inc., 2005.
(617) Martin, O.; Florian, S. *J. Phys. D: Appl. Phys.* **2005**, *38*, R185.
(618) Schneckenburger, H. *Curr. Opin. Biotechnol.* **2005**, *16*, 13.
(619) Hoover, D. K.; Lee, E.-J.; Yousaf, M. N. *Langmuir* **2009**, *25*, 2563.
(620) Lee, Y.; Sangmo, K.; Jin, S.; Yoo, J. Y. *Cell Commun. Adhesion* **2009**, *15*, 385.
(621) Arima, Y.; Iwata, H. *J. Mater. Chem.* **2007**, *17*, 4079.
(622) Shi, J.; Yang, T.; Kataoka, S.; Zhang, Y.; Diaz, A. J.; Cremer, P. S. *J. Am. Chem. Soc.* **2007**, *129*, 5954.
(623) Xu, C.; Zipfel, W.; Shear, J. B.; Williams, R. M.; Webb, W. W. *Proc. Natl. Acad. Sci. U. S. A.* **1996**, *93*, 10763.
(624) König, K. *J. Microsc.* **2000**, *200*, 83.
(625) Schenke-Layland, K.; Riemann, I.; Damour, O.; Stock, U. A.; König, K. *Adv. Drug Delivery Rev.* **2006**, *58*, 878.
(626) Koester, H. J.; Baur, D.; Uhl, R.; Hell, S. W. *Biophys. J.* **1999**, *77*, 2226.
(627) McLellan, M. E.; Kajdasz, S. T.; Hyman, B. T.; Bacskai, B. J. *J. Neurosci.* **2003**, *23*, 2212.
(628) Botchway, S. W.; Charnley, M.; Haycock, J. W.; Parker, A. W.; Rochester, D. L.; Weinstein, J. A.; Williams, J. A. G. *Proc. Natl. Acad. Sci. U. S. A.* **2008**, *105*, 16071.
(629) Liu, Z.; Peng, R. *Eur. J. Nucl. Med. Mol. Imaging* **2010**, *37*, S147.
(630) Davey, H. M.; Kell, D. B. *Microbiol. Rev.* **1996**, *60*, 641.
(631) Jennings, C. D.; Foon, K. A. *Blood* **1997**, *90*, 2863.
(632) Michelson, A. D. *Blood* **1996**, *87*, 4925.
(633) Vermes, I.; Haanen, C.; Reutelingsperger, C. *J. Immunol. Methods* **2000**, *243*, 167.
(634) Vives-Rego, J.; Lebaron, P.; Nebe-Von Caron, G. *FEMS Microbiol. Rev.* **2000**, *24*, 429.
(635) Krutzik, P. O.; Irish, J. M.; Nolan, G. P.; Perez, O. D. *Clin. Immunol.* **2004**, *110*, 206.
(636) Bolton, D. L.; Roederer, M. *Expert Rev. Vaccines* **2009**, *8*, 779.
(637) Baumgarth, N.; Roederer, M. *J. Immunol. Methods* **2000**, *243*, 77.
(638) De Rosa, S. C.; Brenchley, J. M.; Roederer, M. *Nat. Med.* **2003**, *9*, 112.
(639) Perfetto, S. P.; Chattopadhyay, P. K.; Roederer, M. *Nat. Rev. Immunol.* **2004**, *4*, 648.
(640) Edwards, B. S.; Oprea, T.; Prossnitz, E. R.; Sklar, L. A. *Curr. Opin. Chem. Biol.* **2004**, *8*, 392.
(641) Chattopadhyay, P. K.; Hogerkorp, C. M.; Roederer, M. *Immunology* **2008**, *125*, 441.
(642) Krishhan, V. V.; Khan, I. H.; Luciw, P. A. *Crit. Rev. Biotechnol.* **2009**, *29*, 29.
(643) Smiley, R. D.; Hammes, G. G. *Chem. Rev.* **2006**, *106*, 3080.
(644) Lu, H. P.; Xun, L.; Xie, X. S. *Science* **1998**, *282*, 1877.
(645) Yang, H.; Luo, G.; Karnchanaphanurach, P.; Louie, T.-M.; Rech, I.; Cova, S.; Xun, L.; Xie, X. S. *Science* **2003**, *302*, 262.
(646) Edman, L.; Földes-Papp, Z.; Wennmalm, S.; Rigler, R. *Chem. Phys.* **1999**, *247*, 11.
(647) Zhang, Z.; Rajagopalan, P. T. R.; Selzer, T.; Benkovic, S. J.; Hammes, G. G. *Proc. Natl. Acad. Sci. U. S. A.* **2004**, *101*, 2764.
(648) Brender, J. R.; Dertouzos, J.; Ballou, D. P.; Massey, V.; Palfey, B. A.; Entsch, B.; Steel, D. G.; Gafni, A. *J. Am. Chem. Soc.* **2005**, *127*, 18171.
(649) Flomenbom, O.; Velonia, K.; Loos, D.; Masuo, S.; Cotlet, M.; Engelborghs, Y.; Hofkens, J.; Rowan, A. E.; Nolte, R. J. M.; Van der Auweraer, M.; de Schryver, F. C.; Klafter, J. *Proc. Natl. Acad. Sci. U. S. A.* **2005**, *102*, 2368.
(650) John, R.; Davenport; Wuite, G. J. L.; Landick, R.; Bustamante, C. *Science* **2000**, *287*, 2497.
(651) Matsuura, S.-i.; Komatsu, J.; Hirano, K.; Yasuda, H.; Takashima, K.; Katsura, S.; Mizuno, A. *Nucleic Acids Res.* **2001**, *29*, e79.
(652) Bianco, P. R.; Brewer, L. R.; Corzett, M.; Balhorn, R.; Yeh, Y.; Kowalczykowski, S. C.; Baskin, R. J. *Nature* **2001**, *409*, 374.
(653) Dohoney, K. M.; Gelles, J. *Nature* **2001**, *409*, 370.
(654) Ha, T.; Rasnik, I.; Cheng, W.; Babcock, H. P.; Gauss, G. H.; Lohman, T. M.; Chu, S. *Nature* **2002**, *419*, 638.
(655) Perkins, T. T.; Dalal, R. V.; Mitsis, P. G.; Block, S. M. *Science* **2003**, *301*, 1914.
(656) Dessinges, M.-N.; Lionnet, T. e.; Xi, X. G.; Bensimon, D.; Croquette, V. *Proc. Natl. Acad. Sci. U. S. A.* **2004**, *101*, 6439.
(657) Zhang, Z.; Spiering, M. M.; Trakselis, M. A.; Ishmael, F. T.; Xi, J.; Benkovic, S. J.; Hammes, G. G. *Proc. Natl. Acad. Sci. U. S. A.* **2005**, *102*, 3254.
(658) Blandin, P.; Lévêque-Fort, S.; Lécart, S.; Cossec, J. C.; Potier, M. C.; Lenkei, Z.; Druon, F.; Georges, P. *Appl. Opt.* **2009**, *48*, 553.
(659) Huang, P.; Guasto, J. S.; Breuer, K. S. *J. Fluid Mech.* **2006**, *566*, 447.
(660) Ha, T.; Ting, A. Y.; Liang, J.; Caldwell, W. B.; Deniz, A. A.; Chemla, D. S.; Schultz, P. G.; Weiss, S. *Proc. Natl. Acad. Sci. U. S. A.* **1999**, *96*, 893.
(661) Bacskai, B. J.; Skoch, J.; Hickey, G. A.; Allen, R.; Hyman, B. T. *J. Biomed. Opt.* **2003**, *8*, 368.
(662) Krishnan, R. V.; Masuda, A.; Centonze, V. E.; Herman, B. *J. Biomed. Opt.* **2003**, *8*, 362.
(663) Antikainen, N. M.; Smiley, R. D.; Benkovic, S. J.; Hammes, G. G. *Biochemistry* **2005**, *44*, 16835.
(664) Wallrabe, H.; Periasamy, A. *Curr. Opin. Biotechnol.* **2005**, *16*, 19.
(665) Jares-Erijman, E. A.; Jovin, T. M. *Curr. Opin. Chem. Biol.* **2006**, *10*, 409.
(666) Giepmans, B. N. G.; Adams, S. R.; Ellisman, M. H.; Tsien, R. Y. *Science* **2006**, *312*, 217.
(667) Misgeld, T.; Kerschensteiner, M. *Nat. Rev. Neurosci.* **2006**, *7*, 449.
(668) Wang, Y.; Shyy, J. Y. J.; Chien, S. *Annu. Rev. Biomed. Eng.* **2008**, *10*, 1.
(669) Sharma, P.; Varma, R.; Sarasij, R. C.; Ira; Gousset, K.; Krishnamoorthy, G.; Rao, M.; Mayor, S. *Cell* **2004**, *116*, 577.
(670) Rao, M.; Mayor, S. *Biochim. Biophys. Acta, Mol. Cell Res.* **2005**, *1746*, 221.
(671) Klostermeier, D.; Sears, P.; Wong, C.-H.; Millar, D. P.; Williamson, J. R. *Nucleic Acids Res.* **2004**, *32*, 2707.
(672) Ottolia, M.; Philipson, K. D.; John, S. *Biophys. J.* **2004**, *87*, 899.
(673) Peter, M.; Ameer-Beg, S. M. *Biol. Cel* **2004**, *96*, 231.
(674) De Cremer, G.; Sels, B. F.; De Vos, D. E.; Hofkens, J.; Roeffaers, M. B. J. *Chem. Soc. Rev.* **2010**, *39*, 4703.
(675) De Cremer, G.; Bartholomeeusen, E.; Pescarmona, P. P.; Lin, K.; De Vos, D. E.; Hofkens, J.; Roeffaers, M. B. J.; Sels, B. F. *Catal. Today* **2010**, *157*, 236.
(676) Michaelis, J.; Brauchle, C. *Chem. Soc. Rev.* **2010**, *39*, 4731.
(677) Tachikawa, T.; Majima, T. *Langmuir* **2009**, *25*, 7791.
(678) Tachikawa, T.; Majima, T. *Chem. Soc. Rev.* **2010**, *39*, 4802.
(679) Roeffaers, M. B. J.; Sels, B. F.; Uji-i, H.; De Schryver, F. C.; Jacobs, P. A.; De Vos, D. E.; Hofkens, J. *Nature* **2006**, *439*, 572.
(680) Shen, H.; Xu, W.; Chen, P. *Phys. Chem. Chem. Phys.* **2010**, *12*, 6555.

(681) Roeffaers, M. B. J.; De Cremer, G.; Uji-i, H.; Muls, B.; Sels, B. F.; Jacobs, P. A.; De Schryver, F. C.; De Vos, D. E.; Hofkens, J. *Proc. Natl. Acad. Sci. U. S. A.* **2007**, *104*, 12603.
(682) Chen, P.; Zhou, X.; Shen, H.; Andoy, N. M.; Choudhary, E.; Han, K.-S.; Liu, G.; Meng, W. *Chem. Soc. Rev.* **2010**, *39*, 4560.
(683) Swain, R. J.; Stevens, M. M. *Biochem. Soc. Trans.* **2007**, *35*, 544.
(684) Sandt, C.; Smith-Palmer, T.; Pink, J.; Brennan, L.; Pink, D. *J. Appl. Microbiol.* **2007**, *103*, 1808.
(685) Krafft, C.; Knetschke, T.; Siegner, A.; Funk, R. H. W.; Salzer, R. *Vib. Spectrosc.* **2003**, *32*, 75.
(686) Baena, J. R.; Lendl, B. *Curr. Opin. Chem. Biol.* **2004**, *8*, 534.
(687) Rodriguez, L. G.; Lockett, S. J.; Holtom, G. R. *Cytometry Part A* **2006**, *69A*, 779.
(688) Cheng, J. X.; Xie, X. S. *J. Phys. Chem. B* **2004**, *108*, 827.
(689) Volkmer, A. *J. Phys. D: Appl. Phys.* **2005**, *38*, R59.
(690) Müller, M.; Zumbusch, A. *ChemPhysChem* **2007**, *8*, 2156.
(691) Nan, X.; Cheng, J.-X.; Xie, X. S. *J. Lipid Res.* **2003**, *44*, 2202.
(692) Kennedy, A. P.; Sutcliffe, J.; Cheng, J.-X. *Langmuir* **2005**, *21*, 6478.
(693) Cheng, J. X.; Pautot, S.; Weitz, D. A.; Xie, X. S. *Proc. Natl. Acad. Sci. U. S. A.* **2003**, *100*, 9826.
(694) Zeiri, L.; Bronk, B. V.; Shabtai, Y.; Eichler, J.; Efrima, S. *Appl. Spectrosc.* **2004**, *58*, 33.
(695) Koo, T. W.; Chan, S.; Berlin, A. A. *Opt. Lett.* **2005**, *30*, 1024.
(696) Qian, X.; Peng, X.-H.; Ansari, D. O.; Yin-Goen, Q.; Chen, G. Z.; Shin, D. M.; Yang, L.; Young, A. N.; Wang, M. D.; Nie, S. *Nat. Biotechnol.* **2008**, *26*, 83.
(697) Keren, S.; Zavaleta, C.; Cheng, Z.; de la Zerda, A.; Gheysens, O.; Gambhir, S. S. *Proc. Natl. Acad. Sci. U. S. A.* **2008**, *105*, 5844.
(698) Liu, Z.; Li, X.; Tabakman, S. M.; Jiang, K.; Fan, S.; Dai, H. *J. Am. Chem. Soc.* **2008**, *130*, 13540.
(699) Cherney, D. P.; Harris, J. M. *Annu. Rev. Anal. Chem.* **2010**, *3*, 277.
(700) Houlne, M. P.; Sjostrom, C. M.; Uibel, R. H.; Kleimeyer, J. A.; Harris, J. M. *Anal. Chem.* **2002**, *74*, 4311.
(701) Liu, Z.; Hung, W. H.; Aykol, M.; Valley, D.; Cronin, S. B. *Nanotechnol.* **2010**, 21.
(702) Gasser-Ramirez, J. L.; Harris, J. M. *Anal. Chem.* **2009**, *81*, 2869.
(703) Koglin, E.; Tarazona, A.; Kreisig, S.; Schwuger, M. J. *Colloids Surf., A* **1997**, *123−124*, 523.
(704) Migge, S.; Sandmann, G.; Rahner, D.; Dietz, H.; Plieth, W. *J. Solid State Electrochem.* **2005**, *9*, 132.
(705) Cao, P.; Gu, R.; Tian, Z. *Langmuir* **2002**, *18*, 7609.
(706) Lin, X. F.; Ren, B.; Tian, Z. Q. *J. Phys. Chem. B* **2004**, *108*, 981.
(707) Campagnola, P. J.; Wei, M.-d.; Lewis, A.; Loew, L. M. *Biophys. J.* **1999**, *77*, 3341.
(708) Schaller, R. D.; Johnson, J. C.; Wilson, K. R.; Lee, L. F.; Haber, L. H.; Saykally, R. J. *J. Phys. Chem. B* **2002**, *106*, 5143.
(709) Millard, A. C.; Campagnola, P. J.; Mohler, W.; Lewis, A.; Loew, L. M. In *Methods Enzymol.*; Gerard, M., Ian, P., Eds.; Academic Press: New York, 2003; Vol. 361, pp 47.
(710) Nadiarnykh, O.; LaComb, R.; Campagnola, P. J.; Mohler, W. A. *Optics Express* **2007**, *15*, 3348.
(711) Gualda, E. J.; Filippidis, G.; Voglis, G.; Mari, M.; Fotakis, C.; Tavernarakis, N. *J. Microsc.* **2008**, *229*, 141.
(712) Anisha Thayil, K. N.; Gualda, E. J.; Psilodimitrakopoulos, S.; Cormack, I. G.; Amat-RoldÁN, I.; Mathew, M.; Artigas, D.; Loza-Alvarez, P. *J. Microsc.* **2008**, *230*, 70.
(713) Jiang, J.; Eisenthal, K. B.; Yuste, R. *Biophys. J.* **2007**, *93*, L26.
(714) Pantazis, P.; Maloney, J.; Wu, D.; Fraser, S. E. *Proc. Natl. Acad. Sci. U. S. A.* **2010**, *107*, 14535.
(715) Reeve, J. E.; Collins, H. A.; Mey, K. D.; Kohl, M. M.; Thorley, K. J.; Paulsen, O.; Clays, K.; Anderson, H. L. *J. Am. Chem. Soc.* **2009**, *131*, 2758.
(716) Fu, Y.; Wang, H.; Shi, R.; Cheng, J.-X. *Biophys. J.* **2007**, *92*, 3251.
(717) Moreaux, L.; Sandre, O.; Mertz, J. *J. Opt. Soc. Am. B: Opt. Phys.* **2000**, *17*, 1685.
(718) Zoumi, A.; Yeh, A.; Tromberg, B. J. *Proc. Natl. Acad. Sci. U. S. A.* **2002**, *99*, 11014.
(719) Campagnola, P. J.; Millard, A. C.; Terasaki, M.; Hoppe, P. E.; Malone, C. J.; Mohler, W. A. *Biophys. J.* **2002**, *82*, 493.
(720) Zipfel, W. R.; Williams, R. M.; Christie, R.; Nikitin, A. Y.; Hyman, B. T.; Webb, W. W. *Proc. Natl. Acad. Sci. U. S. A.* **2003**, *100*, 7075.
(721) Cimatu, K. A.; Baldelli, S. *J. Phys. Chem. C* **2009**, *113*, 16575.
(722) Hernandez, M.; Chinwangso, P.; Cimatu, K.; Srisombat, L.-o.; Lee, T. R.; Baldelli, S. *J. Phys. Chem. C* **2011**, *115*, 4688.
(723) Kuhnke, K.; Hoffmann, D. M. P.; Wu, X. C.; Bittner, A. M.; Kern, K. *Appl. Phys. Lett.* **2003**, *83*, 3830.
(724) Ji, N.; Zhang, K.; Yang, H.; Shen, Y.-R. *J. Am. Chem. Soc.* **2006**, *128*, 3482.
(725) Wetzel, D. L.; LeVine, S. M. *Science* **1999**, *285*, 1224.
(726) Levin, I. W.; Bhargava, R. *Annu. Rev. Phys. Chem.* **2004**, *56*, 429.
(727) Miller, L. M.; Carr, G. L.; Jackson, M.; Dumas, P.; Williams, G. P. *Synch. Rad. News* **2000**, *13*, 31.
(728) Choo, L. P.; Wetzel, D. L.; Halliday, W. C.; Jackson, M.; LeVine, S. M.; Mantsch, H. H. *Biophys. J.* **1996**, *71*, 1672.
(729) Yu, P. *Br. J. Nutr.* **2004**, *92*, 869.
(730) Miller, L. M.; Dumas, P. *Biochim. Biophys. Acta, Biomembr.* **2006**, *1758*, 846.
(731) Jamin, N.; Dumas, P.; Moncuit, J.; Fridman, W.-H.; Teillaud, J.-L.; Carr, G. L.; Williams, G. P. *Proc. Natl. Acad. Sci. U. S. A.* **1998**, *95*, 4837.
(732) Brundermann, E.; Bergner, A.; Petrat, F.; Schiwon, R.; Wollny, G.; Kopf, I.; de Groot, H.; Havenith, M. *Analyst* **2004**, *129*, 893.
(733) Nasse, M. J.; Ratti, S.; Giordano, M.; Hirschmugl, C. J. *Appl. Spectrosc.* **2009**, *63*, 1181.
(734) Kouzmanov, K.; Pettke, T.; Heinrich, C. A. *Economic Geology* **2010**, *105*, 351.
(735) Doudin, K.; Al-Malaika, S.; Dole, H.; Stirling, T.; Sharples, M. *Polym. Degrad. Stab.* **2011**, *96*, 438.
(736) Wetzel, D. L.; Nasse, M. J. *Nucl. Instrum. Methods Phys. Res., Sect. A* **2011**, DOI: 10.1016/j.nima.2011.01.052.
(737) Schneider, G. *Anal. Bioanal .Chem.* **2003**, 558.
(738) Burkhard, K.; Thibault, P.; Gianoncelli, A.; Kiskinova, M. *J. Phys.: Condens. Matter* **2011**, *23*, 083002.
(739) Nagata, T. *Prog. Histochem. Cytochem.* **2002**, *37*, 59.
(740) Kirz, J.; Jacobsen, C.; Howells, M. *Q. Rev. Biophys.* **1995**, *28*, 33.
(741) Neuhäusler, U.; Jacobsen, C.; Schulze, D.; Stott, D.; Abend, S. *J. Synchrotron Radiat.* **2000**, *7*, 110.
(742) Meyer-Ilse, W.; Hamamoto, D.; Nair, A.; Lelièvre, S. A.; Denbeaux, G.; Johnson, L.; Pearson, A. L.; Yager, D.; Legros, M. A.; Larabell, C. A. *J. Microsc.* **2001**, *201*, 395.
(743) Takman, P. A. C.; Stollberg, H.; Johansson, G. A.; Holmberg, A.; Lindblom, M.; Hertz, H. M. *J. Microsc.* **2007**, *226*, 175.
(744) Ogura, T. *Biochem. Biophys. Res. Commun.* **2010**, *391*, 198.
(745) Schneider, G. *Ultramicroscopy* **1998**, *75*, 85.
(746) Vogt, S.; Schneider, G.; Steuernagel, A.; Lucchesi, J.; Schulze, E.; Rudolph, D.; Schmahl, G. *J. Struct. Biol.* **2000**, *132*, 123.
(747) Dynes, J. J.; Tyliszczak, T.; Araki, T.; Lawrence, J. R.; Swerhone, G. D. W.; Leppard, G. G.; Hitchcock, A. P. *Environ. Sci. Technol.* **2006**, *40*, 1556.
(748) Sen, S.; Curreri, P.; Kaukler, W.; Stefanescu, D. *Metall. Mater. Trans. A* **1997**, *28*, 2129.
(749) Tortora, L.; Park, H.-S.; Kang, S.-W.; Savaryn, V.; Hong, S.-H.; Kaznatcheev, K.; Finotello, D.; Sprunt, S.; Kumar, S.; Lavrentovich, O. D. *Soft Matter* **2010**, *6*, 4157.
(750) Manke, I.; Hartnig, C.; Grunerbel, M.; Lehnert, W.; Kardjilov, N.; Haibel, A.; Hilger, A.; Banhart, J.; Riesemeier, H. *Appl. Phys. Lett.* **2007**, *90*, 174105.
(751) Manke, I.; Hartnig, C.; Kardjilov, N.; Riesemeier, H.; Goebbels, J.; Kuhn, R.; Krüger, P.; Banhart, J. *Fuel Cells* **2010**, *10*, 26.
(752) Zelenay, V.; Ammann, M.; Křepelová, A.; Birrer, M.; Tzvetkov, G.; Vernooij, M. G. C.; Raabe, J.; Huthwelker, T. *J. Aerosol Sci.* **2011**, *42*, 38.

(753) Ghorai, S.; Tivanski, A. V. *Anal. Chem.* **2010**, *82*, 9289.
(754) Huthwelker, T.; Zelenay, V.; Birrer, M.; Krepelova, A.; Raabe, J.; Tzvetkov, G.; Vernooij, M. G. C.; Ammann, M. *Rev. Sci. Instrum.* **2010**, *81*, 113706.
(755) Chen, C. J. *Introduction to Scanning Tunneling Microscopy*, 2nd ed.; Oxford University Press: Oxford, U.K., 2008.
(756) *Scanning Tunneling Microscopy and Related Methods*; Behm, R. J.; García, N.; Rohrer, H., Eds.; Kluwer: Dordrecht, The Netherlands, 2010.
(757) Ho, W. *J. Chem. Phys.* **2002**, *117*, 11033.
(758) Barth, C.; Foster, A. S.; Henry, C. R.; Shluger, A. L. *Adv. Mater.* **2011**, *23*, 477.
(759) Binning, G.; Rohrer, H.; Gerber, C.; Weibel, E. *Phys. Rev. Lett.* **1982**, *49*, 57.
(760) Frommer, J. *Angew. Chem., Int. Ed.* **1992**, *31*, 1298.
(761) Hofer, W. A.; Foster, A. S.; Shluger, A. L. *Rev. Mod. Phys.* **2003**, *75*, 1287.
(762) Poggi, M. A.; Gadsby, E. D.; Bottomley, L. A.; King, W. P.; Oroudjev, E.; Hansma, H. *Anal. Chem.* **2004**, *76*, 3429.
(763) Otero, R.; Rosei, F.; Besenbacher, F. *Annu. Rev. Phys. Chem.* **2006**, *57*, 497.
(764) Foster, J. S.; Frommer, J. E. *Nature* **1988**, *333*, 542.
(765) Smith, D. P. E; Horber, J. K. H.; Binnig, G.; Nejoh, H. *Nature* **1990**, *344*, 641.
(766) Cincotti, S.; Rabe, J. P. *Appl. Phys. Lett.* **1993**, *62*, 3531.
(767) Rabe, J. P.; Buchholz, S.; Askadskaya, L. *Synth. Met.* **1993**, *54*, 339.
(768) Cyr, D. M.; Venkataraman, B.; Flynn, G. W. *Chem. Mater.* **1996**, *8*, 1600.
(769) McGonigal, G. C.; Bernhardt, R. H.; Thomson, D. J. *Appl. Phys. Lett.* **1990**, *57*, 28.
(770) Rabe, J. ú. P.; Buchholz, S. *Science* **1991**, *253*, 424.
(771) Watel, G.; Thibaudau, F.; Cousty, J. *Surf. Sci.* **1993**, *281*, L297.
(772) Venkataraman, B.; Breen, J. J.; Flynn, G. W. *J. Phys. Chem.* **1995**, *99*, 6608.
(773) Hibino, M.; Sumi, A.; Hatta, I. *Jpn. J. Appl. Phys.* **1995**, *34*, 3354.
(774) Stabel, A.; Dasaradhi, L.; O'Hagan, D.; Rabe, J. P. *Langmuir* **1995**, *11*, 1427.
(775) Venkataraman, B.; Flynn, G. W.; Wilbur, J. L.; Folkers, J. P.; Whitesides, G. M. *J. Phys. Chem.* **1995**, *99*, 8684.
(776) den Boer, D.; Habets, T.; Coenen, M. J. J.; van der Maas, M.; Peters, T. P. J; Crossley, M. J.; Khoury, T.; Rowan, A. E.; Nolte, R. J. M.; Speller, S.; Elemans, J. A. A. W. *Langmuir* **2011**, *27*, 2644.
(777) De Feyter, S.; De Schryver, F. C. *J. Phys. Chem. B* **2005**, *109*, 4290.
(778) Elemans, J. A. A. W.; Lei, S.; De Feyter, S. *Angew. Chem., Int. Ed.* **2009**, *48*, 7298.
(779) Yang, Y.; Wang, C. *Curr. Opin. Colloid Interface Sci.* **2009**, *14*, 135.
(780) Lei, S.; Tahara, K.; Tobe, Y.; De Feyter, S. *Chem. Commun.* **2010**, *46*, 9125.
(781) Lei, S.; Tahara, K.; De Schryver, F. C.; Van der Auweraer, M.; Tobe, Y.; De Feyter, S. *Angew. Chem., Int. Ed.* **2008**, *47*, 2964.
(782) Tahara, K.; Okuhata, S.; Adisoejoso, J.; Lei, S.; Fujita, T.; Feyter, S. D.; Tobe, Y. *J. Am. Chem. Soc.* **2009**, *131*, 17583.
(783) Kampschulte, L.; Werblowsky, T. L.; Kishore, R. S. K.; Schmittel, M.; Heckl, W. M.; Lackinger, M. *J. Am. Chem. Soc.* **2008**, *130*, 8502.
(784) Ahn, S.; Matzger, A. J. *J. Am. Chem. Soc.* **2010**, *132*, 11364.
(785) Kudernac, T.; Lei, S.; Elemans, J. A. A. W.; De Feyter, S. *Chem. Soc. Rev.* **2009**, *38*, 402.
(786) Griessl, S. J. H.; Lackinger, M.; Jamitzky, F.; Markert, T.; Hietschold, M.; Heckl, W. M. *Langmuir* **2004**, *20*, 9403.
(787) Lei, S.; Surin, M.; Tahara, K.; Adisoejoso, J.; Lazzaroni, R.; Tobe, Y.; Feyter, S. D. *Nano Lett.* **2008**, *8*, 2541.
(788) Adisoejoso, J.; Tahara, K.; Okuhata, S.; Lei, S.; Tobe, Y.; De Feyter, S. *Angew. Chem., Int. Ed.* **2009**, *48*, 7353.
(789) Pan, G.-B.; Liu, J.-M.; Zhang, H.-M.; Wan, L.-J.; Zheng, Q.-Y.; Bai, C.-L. *Angew. Chem., Int. Ed.* **2003**, *42*, 2747.
(790) Li, M.; Deng, K.; Lei, S.-B.; Yang, Y.-L.; Wang, T.-S.; Shen, Y.-T.; Wang, C.-R.; Zeng, Q.-D.; Wang, C. *Angew. Chem., Int. Ed.* **2008**, *47*, 6717.
(791) Giancarlo, L. C.; Flynn, G. W. *Acc. Chem. Res.* **2000**, *33*, 491.
(792) Hoeppener, S.; Chi, L.; Fuchs, H. *ChemPhysChem* **2003**, *4*, 494.
(793) De Feyter, S.; Gesquière, A.; Abdel-Mottaleb, M. M.; Grim, P. C. M.; De Schryver, F. C.; Meiners, C.; Sieffert, M.; Valiyaveettil, S.; Müllen, K. *Acc. Chem. Res.* **2000**, *33*, 520.
(794) Wei, Y.; Kannappan, K.; Flynn, G. W.; Zimmt, M. B. *J. Am. Chem. Soc.* **2004**, *126*, 5318.
(795) Krukowski, P.; Klusek, Z.; Olejniczak, W.; Klepaczko, R.; Puchalski, M.; Dabrowski, P.; Kowalczyk, P. J.; Gwozdzinski, K. *Appl. Surf. Sci.* **2009**, *255*, 8769.
(796) Ciesielski, A.; Lena, S.; Masiero, S.; Spada, G. P.; Samorì, P. *Angew. Chem., Int. Ed.* **2010**, *49*, 1963.
(797) Stabel, A.; Heinz, R.; De Schryver, F. C.; Rabe, J. P. *J. Phys. Chem.* **1995**, *99*, 505.
(798) Gutzler, R.; Sirtl, T.; Dienstmaier, J. F.; Mahata, K.; Heckl, W. M.; Schmittel, M.; Lackinger, M. *J. Am. Chem. Soc.* **2010**, *132*, 5084.
(799) Schull, G.; Douillard, L.; Fiorini-Debuisschert, C. l.; Charra, F.; Mathevet, F.; Kreher, D.; Attias, A.-J. *Nano Lett.* **2006**, *6*, 1360.
(800) Lei, S.; Tahara, K.; Feng, X.; Furukawa, S.; De Schryver, F. C.; Müllen, K.; Tobe, Y.; De Feyter, S. *J. Am. Chem. Soc.* **2008**, *130*, 7119.
(801) Itaya, K. *Prog. Surf. Sci.* **1998**, *58*, 121.
(802) Wilms, M.; Broekmann, P.; Stuhlmann, C.; Wandelt, K. *Surf. Sci.* **1998**, *416*, 121.
(803) Magnussen, O. M. *Chem. Rev.* **2002**, *102*, 679.
(804) Magnussen, O. M.; Ocko, B. M.; Wang, J. X.; Adzic, R. R. *J. Phys. Chem.* **1996**, *100*, 5500.
(805) Safarowsky, C.; Merz, L.; Rang, A.; Broekmann, P.; Hermann, B. A.; Schalley, C. A. *Angew. Chem., Int. Ed.* **2004**, *43*, 1291.
(806) Taranovskyy, A.; Tansel, T.; Magnussen, O. M. *Phys. Rev. Lett.* **2010**, *104*, 106101.
(807) Maurice, V.; Strehblow, H. H.; Marcus, P. *Surf. Sci.* **2000**, *458*, 185.
(808) Vogt, M. R.; Lachenwitzer, A.; Magnussen, O. M.; Behm, R. J. *Surf. Sci.* **1998**, *399*, 49.
(809) Ye, S.; Ishibashi, C.; Uosaki, K. *Langmuir* **1998**, *15*, 807.
(810) Magnussen, O. M.; Vogt, M. R. *Phys. Rev. Lett.* **2000**, *85*, 357.
(811) Giesen, M. *Prog. Surf. Sci.* **2001**, *68*, 1.
(812) Pan, G.-B.; Freyland, W. *Chem. Phys. Lett.* **2006**, *427*, 96.
(813) Gasparotto, L. H. S.; Borisenko, N.; Höfft, O.; Al-Salman, R.; Maus-Friedrichs, W.; Bocchi, N.; Zein El Abedin, S.; Endres, F. *Electrochim. Acta* **2009**, *55*, 218.
(814) Lin, L. G.; Wang, Y.; Yan, J. W.; Yuan, Y. Z.; Xiang, J.; Mao, B. W. *Electrochem. Commun.* **2003**, *5*, 995.
(815) Kubo, K.; Hirai, N.; Tanaka, T.; Hara, S. *Surf. Sci.* **2004**, *565*, L271.
(816) Hirai, N.; Yokogawa, T.; Tanaka, T. *Jpn. J. Appl. Phys.* **2006**, *45*, 2295.
(817) Borisenko, N.; Zein El Abedin, S.; Endres, F. *J. Phys. Chem. B* **2006**, *110*, 6250.
(818) Albrecht, T.; Moth-Poulsen, K.; Christensen, J. r. B.; Hjelm, J.; Bj√∏rnholm, T.; Ulstrup, J. *J. Am. Chem. Soc.* **2006**, *128*, 6574.
(819) Hulsken, B.; Van Hameren, R.; Gerritsen, J. W.; Khoury, T.; Thordarson, P.; Crossley, M. J.; Rowan, A. E.; Nolte, R. J. M.; Elemans, J. A. A. W.; Speller, S. *Nat. Nano* **2007**, *2*, 285.
(820) Hulsken, B.; Elemans, J. A. A. W.; Gerritsen, J. W.; Khoury, T.; Crossley, M. J.; Rowan, A. E.; Nolte, R. J. M.; Speller, S. *New J. Phys.* **2009**, 11.
(821) Bakos, I.; Mallat, T.; Baiker, A. *Catal. Lett.* **1997**, *43*, 201.
(822) Griessl, S. J. H.; Lackinger, M.; Jamitzky, F.; Markert, T.; Hietschold, M.; Heckl, W. M. *J. Phys. Chem. B* **2004**, *108*, 11556.
(823) Takami, T.; Ye, T.; Pathem, B. K.; Arnold, D. P.; Sugiura, K.-i.; Bian, Y.; Jiang, J.; Weiss, P. S. *J. Am. Chem. Soc.* **2010**, *132*, 16460.
(824) Xie, R.; Song, Y.; Wan, L.; Yuan, H.; Li, P.; Xiao, X.; Liu, L.; Ye, S.; Lei, S.; Wang, L. *Anal. Sci.* **2011**, *27*, 129.

(825) Okawa, Y.; Aono, M. *Nature* **2001**, *409*, 683.
(826) Takajo, D.; Okawa, Y.; Hasegawa, T.; Aono, M. *Langmuir* **2007**, *23*, 5247.
(827) Sullivan, S. P.; Schnieders, A.; Mbugua, S. K.; Beebe, T. P. *Langmuir* **2004**, *21*, 1322.
(828) Bard, A. J.; Fan, F. R. F.; Kwak, J.; Lev, O. *Anal. Chem.* **1989**, *61*, 132.
(829) Lee, C.; Kwak, J.; Bard, A. J. *Proc. Natl. Acad. Sci. U. S. A.* **1990**, *87*, 1740.
(830) Pierce, D. T.; Bard, A. J. *Anal. Chem.* **1993**, *65*, 3598.
(831) Penner, R. M.; Heben, M. J.; Longin, T. L.; Lewis, N. S. *Science* **1990**, *250*, 1118.
(832) Bard, A. J.; Fan, F.-R. F.; Pierce, D. T.; Unwin, P. R.; Wipf, D. O.; Zhou, F. *Science* **1991**, *254*, 68.
(833) Sun, P.; Laforge, F. O.; Mirkin, M. V. *Phys. Chem. Chem. Phys.* **2007**, *9*, 802.
(834) Amemiya, S.; Bard, A. J.; Fan, F.-R. F.; Mirkin, M. V.; Unwin, P. R. *Annu. Rev. Anal. Chem.* **2008**, *1*, 95.
(835) Bertoncello, P. *Energy Environm. Sci.* **2010**, *3*, 1620.
(836) Niu, L.; Yin, Y.; Guo, W.; Lu, M.; Qin, R.; Chen, S. *J. Mater. Sci.* **2009**, *44*, 4511.
(837) González-García, Y.; Burstein, G. T.; González, S.; Souto, R. M. *Electrochem. Commun.* **2004**, *6*, 637.
(838) Serebrennikova, I.; White, H. S. *Electrochem. Solid-State Lett.* **2001**, *4*, B4.
(839) Davoodi, A.; Pan, J.; Leygraf, C.; Norgren, S. *Electrochim. Acta* **2007**, *52*, 7697.
(840) Gyurcsányi, R. E.; Jágerszki, G.; Kiss, G.; Tóth, K. *Bioelectrochemistry* **2004**, *63*, 207.
(841) Amemiya, S.; Guo, J.; Xiong, H.; Gross, D. *Anal. Bioanal. Chem.* **2006**, *386*, 458.
(842) Schulte, A.; Nebel, M.; Schuhmann, W. *Annu. Rev. Anal. Chem.* **2010**, *3*, 299.
(843) Zhu, R.; Macfie, S. M.; Ding, Z. *J. Exp. Bot.* **2005**, *56*, 2831.
(844) Takahashi, Y.; Hirano, Y.; Yasukawa, T.; Shiku, H.; Yamada, H.; Matsue, T. *Langmuir* **2006**, *22*, 10299.
(845) Liu, B.; Rotenberg, S. A.; Mirkin, M. V. *Anal. Chem.* **2002**, *74*, 6340.
(846) Liebetrau, J. M.; Miller, H. M.; Baur, J. E.; Takacs, S. A.; Anupunpisit, V.; Garris, P. A.; Wipf, D. O. *Anal. Chem.* **2002**, *75*, 563.
(847) Mauzeroll, J.; Bard, A. J.; Owhadian, O.; Monks, T. J. *Proc. Natl. Acad. Sci. U. S. A.* **2004**, *101*, 17582.
(848) Wittstock, G.; Yu, K. J.; Halsall, H. B.; Ridgway, T. H.; Heineman, W. R. *Anal. Chem.* **1995**, *67*, 3578.
(849) Mirkin, M. V.; Horrocks, B. R. *Anal. Chim. Acta* **2000**, *406*, 119.
(850) Jeong, K. S.; Kim, S. Y.; Shin, U.-S.; Kogej, M.; Hai, N. T. M.; Broekmann, P.; Jeong, N.; Kirchner, B.; Reiher, M.; Schalley, C. A. *J. Am. Chem. Soc.* **2005**, *127*, 17672.
(851) Lee, C.; Anson, F. C. *Anal. Chem.* **1992**, *64*, 528.
(852) Hai, N. T. M.; Furukawa, S.; Vosch, T.; De Feyter, S.; Broekmann, P.; Wandelt, K. *Phys. Chem. Chem. Phys.* **2009**, *11*, 5422.
(853) Simıes, A. M.; Bastos, A. C.; Ferreira, M. G.; Gonz·lez-GarcÌa, Y.; Gonz·lez, S.; Souto, R. M. *Corros. Sci.* **2007**, *49*, 726.
(854) Black, M.; *Meas. Sci. Technol.* **2005**, *16*, 174.
(855) Lu, X.; Wang, Q.; Liu, X. *Anal. Chim. Acta* **2007**, *601*, 10.
(856) Liu, B.; Bard, A. J.; Mirkin, M. V.; Creager, S. E. *J. Am. Chem. Soc.* **2004**, *126*, 1485.
(857) Holt, K. B. *Langmuir* **2006**, *22*, 4298.
(858) Burshtain, D.; Mandler, D. *J. Electroanal. Chem.* **2005**, *581*, 310.
(859) Nijhuis, C. A.; Sinha, J. K.; Wittstock, G.; Huskens, J.; Ravoo, B. J.; Reinhoudt, D. N. *Langmuir* **2006**, *22*, 9770.
(860) Zhang, J.; Lahtinen, R. M.; Kontturi, K.; Unwin, P. R.; Schiffrin, D. J. *Chem. Commun.* **2001**, 1818.
(861) Ruiz, V.; Liljeroth, P.; Quinn, B. M.; Kontturi, K. *Nano Lett.* **2003**, *3*, 1459.
(862) Zhao, C.; Wittstock, G. *Anal. Chem.* **2004**, *76*, 3145.
(863) McConney, M. E.; Singamaneni, S.; Tsukruk, V. V. *Polym. Rev.* **2010**, *50*, 235.
(864) Zhong, Q.; Inniss, D.; Kjoller, K.; Elings, V. B. *Surf. Sci.* **1993**, *290*, L688.
(865) Fukuma, T. *Jpn. J. Appl. Phys.* **2009**, 48.
(866) Radmacher, M.; Fritz, M.; Hansma, P. K. *Biophys. J.* **1995**, *69*, 264.
(867) Lavrik, N. V.; Sepaniak, M. J.; Datskos, P. G. *Rev. Sci. Instrum.* **2004**, *75*, 2229.
(868) Uchihashi, T.; Higgins, M. J.; Yasuda, S.; Jarvis, S. P.; Akita, S.; Nakayama, Y.; Sader, J. E. *Appl. Phys. Lett.* **2004**, *85*, 3575.
(869) Fukuma, T.; Kobayashi, K.; Matsushige, K.; Yamada, H. *Appl. Phys. Lett.* **2005**, *86*, 193108.
(870) Mullin, N.; Hobbs, J. *Appl. Phys. Lett.* **2008**, *92*, 053103/1.
(871) Lee, M.; Sung, B.; Hashemi, N.; Jhe, W. *Faraday Discuss.* **2009**, *141*, 415.
(872) Gan, Y. *Surf. Sci. Rep.* **2009**, *64*, 99.
(873) Voitchovsky, K.; Kuna, J. J.; Contera, S. A.; Tosatti, E.; Stellacci, F. *Nat. Nano* **2010**, *5*, 401.
(874) Butt, H.-J.; Cappella, B.; Kappl, M. *Surf. Sci. Rep.* **2005**, *59*, 1.
(875) Hörber, J. K. H.; Miles, M. J. *Science* **2003**, *302*, 1002.
(876) Gadegaard, N. *Biotech. Histochem.* **2006**, *81*, 87.
(877) Muller, D. J.; Dufrêne, Y. F. *Nat. Nano* **2008**, *3*, 261.
(878) Dorobantu, L. S.; Gray, M. R. *Scanning* **2010**, *32*, 74.
(879) Allison, D. P.; Mortensen, N. P.; Sullivan, C. J.; Doktycz, M. J. *Wiley Interdiscip. Rev.: Nanomed. Nanobiotechnol.* **2010**, *2*, 618.
(880) Butt, H. J.; Wolff, E. K.; Gould, S. A. C.; Dixon Northern, B.; Peterson, C. M.; Hansma, P. K. *J. Struct. Biol.* **1990**, *105*, 54.
(881) Haberle, W.; Horber, J. K. H.; Binnig, G. *J. Vac. Sci. Technol. B* **1991**, *9*, 1210.
(882) Radmacher, M.; Tillamnn, R. W.; Fritz, M.; Gaub, H. E. *Science* **1992**, *257*, 1900.
(883) Henderson, E.; Haydon, P. G.; Sakaguchi, D. S. *Science* **1992**, *257*, 1944.
(884) Hoh, J. H.; Schoenenberger, C. A. *J. Cell Sci.* **1994**, *107*, 1105.
(885) Fritz, M.; Radmacher, M.; Gaub, H. E. *Biophys. J.* **1994**, *66*, 1328.
(886) Fotiadis, D.; Liang, Y.; Filipek, S.; Saperstein, D. A.; Engel, A.; Palczewski, K. *Nature* **2003**, *421*, 127.
(887) Kasas, S.; Ikai, A. *Biophys. J.* **1995**, *68*, 1678.
(888) Touhami, A.; Jericho, M. H.; Beveridge, T. J. *J. Bacteriol.* **2004**, *186*, 3286.
(889) Méndez-Vilas, A.; Gallardo-Moreno, A. M.; González-Martín, M. L. *Microsc. Microanal.* **2007**, *13*, 55.
(890) Doktycz, M. J.; Sullivan, C. J.; Hoyt, P. R.; Pelletier, D. A.; Wu, S.; Allison, D. P. *Ultramicroscopy* **2003**, *97*, 209.
(891) Plomp, M.; Leighton, T. J.; Wheeler, K. E.; Hill, H. D.; Malkin, A. J. *Proc. Natl. Acad. Sci. U. S. A.* **2007**, *104*, 9644.
(892) Baclayon, M.; Wuite, G. J. L.; Roos, W. H. *Soft Matter* **2010**, *6*, 5273.
(893) Turner, Y. T. A.; Roberts, C. J.; Davies, M. C. *Adv. Drug Delivery Rev.* **2007**, *59*, 1453.
(894) Seelert, H.; Poetsch, A.; Dencher, N. A.; Engel, A.; Stahlberg, H.; Muller, D. J. *Nature* **2000**, *405*, 418.
(895) Elie-Caille, C.; Severin, F.; Helenius, J.; Howard, J.; Muller, D. J.; Hyman, A. A. *Curr. Biol.* **2007**, *17*, 1765.
(896) Muller, D. J.; Hand, G. M.; Engel, A.; Sosinsky, G. E. *EMBO J.* **2002**, *21*, 3598.
(897) Hoogenboom, B. W.; Suda, K.; Engel, A.; Fotiadis, D. *J. Mol. Biol.* **2007**, *370*, 246.
(898) Scheuring, S.; Sturgis, J. N. *Science* **2005**, *309*, 484.
(899) Hoh, J. H.; Cleveland, J. P.; Prater, C. B.; Revel, J. P.; Hansma, P. K. *J. Am. Chem. Soc.* **1992**, *114*, 4917.
(900) Goldmann, W. H.; Galneder, R.; Ludwig, M.; Xu, W.; Adamson, E. D.; Wang, N.; Ezzell, R. M. *Exp. Cell Res.* **1998**, *239*, 235.
(901) Arnoldi, M.; Fritz, M.; Bäuerlein, E.; Radmacher, M.; Sackmann, E.; Boulbitch, A. *Phys. Rev. E* **2000**, *62*, 1034.
(902) Matzke, R.; Jacobson, K.; Radmacher, M. *Nat. Cell Biol.* **2001**, *3*, 607.

(903) Lee, G. U.; Chrisey, L. A.; Colton, R. J. *Science* **1994**, *266*, 771.
(904) Boland, T.; Ratner, B. D. *Proc. Natl. Acad. Sci. U. S. A.* **1995**, *92*, 5297.
(905) Florin, E. L.; Moy, V. T.; Gaub, H. E. *Science* **1994**, *264*, 415.
(906) Lee, G. U.; Kidwell, D. A.; Colton, R. J. *Langmuir* **1994**, *10*, 354.
(907) McKendry, R.; Theoclitou, M.-E.; Rayment, T.; Abell, C. *Nature* **1998**, *391*, 566.
(908) Grandbois, M.; Dettmann, W.; Benoit, M.; Gaub, H. E. *J. Histochem. Cytochem.* **2000**, *48*, 719.
(909) Rief, M.; Gautel, M.; Oesterhelt, F.; Fernandez, J. M.; Gaub, H. E. *Science* **1997**, *276*, 1109.
(910) Oberhauser, A. F.; Marszalek, P. E.; Erickson, H. P.; Fernandez, J. M. *Nature* **1998**, *393*, 181.
(911) Müller, D. J.; Baumeister, W.; Engel, A. *Proc. Natl. Acad. Sci. U. S. A.* **1999**, *96*, 13170.
(912) Ohnesorge, F.; Binnig, G. *Science* **1993**, *260*, 1451.
(913) De Yoreo, J. J.; Zepeda-Ruiz, L. A.; Friddle, R. W.; Qiu, S. R.; Wasylenki, L. E.; Chernov, A. A.; Gilmer, G. H.; Dove, P. M. *Cryst. Growth Des.* **2009**, *9*, 5135.
(914) Larson, I.; Drummond, C. J.; Chan, D. Y. C.; Grieser, F. *J. Phys. Chem.* **1995**, *99*, 2114.
(915) Rocca, E.; Bertrand, G.; Rapin, C.; Labrune, J. C. *J. Electroanal. Chem.* **2001**, *503*, 133.
(916) Butt, H. J.; Berger, R.; Bonaccurso, E.; Chen, Y.; Wang, J. *Adv. Colloid Interface Sci.* **2007**, *133*, 91.
(917) Manne, S.; Schäffer, T. E.; Huo, Q.; Hansma, P. K.; Morse, D. E.; Stucky, G. D.; Aksay, I. A. *Langmuir* **1997**, *13*, 6382.
(918) Manne, S.; Gaub, H. E. *Science* **1995**, *270*, 1480.
(919) Chi, L. F.; Anders, M.; Fuchs, H.; Johnston, R. R.; Ringsdorf, H. *Science* **1993**, *259*, 213.
(920) Liang, Y.; Hilal, N.; Langston, P.; Starov, V. *Adv. Colloid Interface Sci.* **2007**, *134*−*135*, 151.
(921) Johnson, C. A.; Lenhoff, A. M. *J. Colloid Interface Sci.* **1996**, *179*, 587.
(922) Paria, S.; Khilar, K. C. *Adv. Colloid Interface Sci.* **2004**, *110*, 75.
(923) Pompe, T.; Herminghaus, S. *Phys. Rev. Lett.* **2000**, *85*, 1930.
(924) Roiter, Y.; Minko, S. *J. Am. Chem. Soc.* **2005**, *127*, 15688.
(925) Kumaki, J.; Kawauchi, T.; Yashima, E. *Macromolecules* **2006**, *39*, 1209.
(926) Zou, S.; Hempenius, M. A.; Schönherr, H.; Julius Vancso, G. *Macromol. Rapid Commun.* **2006**, *27*, 103.
(927) Lewis, A.; Taha, H.; Strinkovski, A.; Manevitch, A.; Khatchatouriants, A.; Dekhter, R.; Ammann, E. *Nat. Biotechnol.* **2003**, *21*, 1378.
(928) Rasmussen, A.; Deckert, V. *Anal. Bioanal. Chem.* **2005**, *381*, 165.
(929) Muramatsu, H.; Chiba, N.; Homma, K.; Nakajima, K.; Ataka, T.; Ohta, S.; Kusumi, A.; Fujihira, M. *Appl. Phys. Lett.* **1995**, *66*, 3245.
(930) Tsai, D. P.; Lu, Y. Y. *Appl. Phys. Lett.* **1998**, *73*, 2724.
(931) Koopman, M.; de Bakker, B. I.; Garcia-Parajo, M. F.; van Hulst, N. F. *Appl. Phys. Lett.* **2003**, *83*, 5083.
(932) Betzig, E.; Trautman, J. K. *Science* **1992**, *257*, 189.
(933) Lei, F. H.; Huang, L.; Piot, O.; Trussardi, A.; Manfait, M.; Shang, G.; Troyon, M. *J. Appl. Phys.* **2006**, *100*, 084317.
(934) Lei, F.; Manfait, M. *Surf. Interface Anal.* **2007**, *39*, 674.
(935) Micheletto, R.; Denyer, M.; Scholl, M.; Nakajima, K.; Offenhauser, A.; Hara, M.; Knoll, W. *Appl. Opt.* **1999**, *38*, 6648.
(936) Mensi, M.; Dukenbayev, K.; Sekatskii, S.; Dietler, G. *Laser Phys.* **2010**, *20*, 78.
(937) Clancy, C. M. R.; Krogmeier, J. R.; Pawlak, A.; Rozanowska, M.; Sarna, T.; Dunn, R. C.; Simon, J. D. *J. Phys. Chem. B* **2000**, *104*, 12098.
(938) Talley, C. E.; Cooksey, G. A.; Dunn, R. C. *Appl. Phys. Lett.* **1996**, *69*, 3809.
(939) Höppener, C.; Molenda, D.; Fuchs, H.; Naber, A. *J. Microsc.* **2003**, *210*, 288.
(940) Koopman, M.; Cambi, A.; de Bakker, B. I.; Joosten, B.; Figdor, C. G.; van Hulst, N. F.; Garcia-Parajo, M. F. *FEBS Lett.* **2004**, *573*, 6.
(941) Hollars, C. W.; Dunn, R. C. *J. Chem. Phys.* **2000**, *112*, 7822.
(942) Yuan, C.; Johnston, L. J. *J. Microsc.* **2002**, *205*, 136.
(943) Ianoul, A.; Burgos, P.; Lu, Z.; Taylor, R. S.; Johnston, L. J. *Langmuir* **2003**, *19*, 9246.
(944) Dragnea, B.; Leone, S. R. *Int. Rev. Phys. Chem.* **2001**, *20*, 59.
(945) Kopf, I.; Samson, J.-S.; Wollny, G.; Grunwald, C.; Bründermann, E.; Havenith, M. *J. Phys. Chem. C* **2007**, *111*, 8166.
(946) Tian, Z.-Q.; Ren, B.; Li, J.-F.; Yang, Z.-L. *Chem. Commun.* **2007**, 3514.
(947) Elfick, A.; Downes, A.; Mouras, R. *Anal. Bioanal. Chem.* **2010**, *396*, 45.
(948) Zenhausern, F.; Martin, Y.; Wickramasinghe, H. K. *Science* **1995**, *5227*, 1083.
(949) Hong, M. K.; Jeung, A. G.; Dokholyan, N. V.; Smith, T. I.; Schwettman, H. A.; Huie, P.; Erramilli, S. *Nucl. Instrum. Methods Phys. Res., Sect. B* **1998**, *144*, 246.
(950) Rice, J. H. *Nanoscale* **2010**, *2*, 660.
(951) Mayet, C.; Dazzi, A.; Prazeres, R.; Allot, F.; Glotin, F.; Ortega, J. M. *Opt. Lett.* **2008**, *33*, 1611.
(952) Stöckle, R. M.; Suh, Y. D.; Deckert, V.; Zenobi, R. *Chem. Phys. Lett.* **2000**, *318*, 131.
(953) Downes, A.; Salter, D.; Elfick, A. *J. Phys. Chem. B* **2006**, *110*, 6692.
(954) Nagata, T. *Prog. Histochem. Cytochem.* **2004**, *39*, 185.
(955) Fukami, A.; Fukushima, K.; Kohyama, N. In *Microstructure of Fine-Grained Sediments from Mud to Shale*; Bennett, R. H., Bryant, W. R., Hulbert, M. H., Eds.; Springer-Verlag: New York, 1991, pp 321.
(956) Zheng, H.; Claridge, S. A.; Minor, A. M.; Alivisatos, A. P.; Dahmen, U. *Nano Lett.* **2009**, *9*, 2460.
(957) Liu, K.-L.; Wu, C.-C.; Huang, Y.-J.; Peng, H.-L.; Chang, H.-Y.; Chang, P.; Hsu, L.; Yew, T.-R. *Lab Chip* **2008**, *8*, 1915.
(958) Williamson, M. J.; Tromp, R. M.; Vereecken, P. M.; Hull, R.; Ross, F. M. *Nat. Mater.* **2003**, *2*, 532.
(959) Zheng, H.; Smith, R. K.; Jun, Y.-w.; Kisielowski, C.; Dahmen, U.; Alivisatos, A. P. *Science* **2009**, *324*, 1309.
(960) Thiberge, S.; Nechushtan, A.; Sprinzak, D.; Gileadi, O.; Behar, V.; Zik, O.; Chowers, Y.; Michaeli, S.; Schlessinger, J.; Moses, E. *Proc. Natl. Acad. Sci. U. S. A.* **2004**, *101*, 3346.
(961) Nishiyama, H.; Suga, M.; Ogura, T.; Maruyama, Y.; Koizumi, M.; Mio, K.; Kitamura, S.; Sato, C. *J. Struct. Biol.* **2010**, *169*, 438.
(962) Jonge, N. d.; Peckys, D. B.; Kremers, G. J.; Piston, D. W. *Proc. Natl. Acad. Sci. U. S. A.* **2009**, *106*, 2159.
(963) Grogan, J. M.; Bau, H. H. *J. Microelectromech. Syst.* **2010**, *19*, 885.
(964) Klein, K. L.; Anderson, I. M.; De Jonge, N. *J. Microsc.* **2011**, *242*, 117.
(965) Howe, J. M.; Saka, H. *MRS Bull.* **2004**, *29*, 951.
(966) Saka, H.; Sasaki, K.; Tsukimoto, S.; Arai, S. *J. Mater. Res.* **2005**, *20*, 1629.
(967) Van Huis, M. A.; Young, N. P.; Pandraud, G.; Creemer, J. F.; Vanmaekelbergh, D.; Kirkland, A. I.; Zandbergen, H. W. *Adv. Mater.* **2009**, *21*, 4992.
(968) Young, N. P.; van Huis, M. A.; Zandbergen, H. W.; Xu, H.; Kirkland, A. I. *Ultramicroscopy* **2010**, *110*, 506.
(969) Kulovits, A.; Wiezorek, J. M. K.; Lagrange, T.; Reed, B. W.; Campbell, G. H. *Philos. Mag. Lett.* **2011**, *91*, 287.
(970) Sutter, P. W.; Sutter, E. A. *Nat. Mater.* **2007**, *6*, 363.
(971) Sutter, E. A.; Sutter, P. W. *ACS Nano* **2010**, *4*, 4943.
(972) Gai, P. L.; Sharma, R.; Ross, F. M. *MRS Bull.* **2008**, *33*, 107.
(973) Frances, M. R. *Rep. Prog. Phys.* **2010**, *73*, 114501.
(974) Kim, B. J.; Tersoff, J.; Kodambaka, S.; Reuter, M. C.; Stach, E. A.; Ross, F. M. *Science* **2008**, *322*, 1070.
(975) Bhatta, U. M.; Rath, A.; Dash, J. K.; Ghatak, J.; Yi-Feng, L.; Liu, C.-P.; Satyam, P. V. *Nanotechnol.* **2009**, *20*, 465601.
(976) Madras, P.; Dailey, E.; Drucker, J. *Nano Lett.* **2010**, *10*, 1759.
(977) Holmberg, V. C.; Panthani, M. G.; Korgel, B. A. *Science* **2009**, *326*, 405.
(978) Eswaramoorthy, S. K.; Howe, J. M.; Muralidharan, G. *Science* **2007**, *318*, 1437.

(979) Brettholle, M.; Hofft, O.; Klarhofer, L.; Mathes, S.; Maus-Friedrichs, W.; Zein El Abedin, S.; Krischok, S.; Janek, J.; Endres, F. *Phys. Chem. Chem. Phys.* **2010**, *12*, 1750.
(980) Wang, C. M.; Xu, W.; Liu, J.; Choi, D. W.; Arey, B.; Saraf, L. V.; Zhang, J. G.; Yang, Z. G.; Thevuthasan, S.; Baer, D. R.; Salmon, N. *J. Mater. Res.* **2010**, *25*, 1541.
(981) Yoshida, K.; Nozaki, T.; Hirayama, T.; Tanaka, N. *J. Electron Microsc.* **2007**, *56*, 177.
(982) Mifflin, A. L.; Gerth, K. A.; Weiss, B. M.; Geiger, F. M. *J. Phys. Chem. A* **2003**, *107*, 6212.
(983) Li, Y.; Lee, H. J.; Corn, R. M. *Anal. Chem.* **2007**, *79*, 1082.